ALMA MATER STUDIORUM
UNIVERSITÀ DEGLI STUDI DI BOLOGNA

FACOLTÀ DI SCIENZE MATEMATICHE, FISICHE E NATURALI

Dottorato di Ricerca in
Scienze Ambientali: Tutela e Gestione delle Risorse Naturali

Ciclo XXIV
Settore concorsuale di afferenza: 04/A1
Settore scientifico disciplinare: GEO/08 Geochimica e vulcanologia

EFFECTS OF RESOURCES EXPLOITATION ON WATER QUALITY: CASE STUDIES IN SALT WATER INTRUSION AND ACID MINE DRAINAGE

Tesi Presentata da: Dott. ssa Martina Kralj

Coordinatore Dottorato:
Prof. Enrico Dinelli

Tutore: Prof. Enrico Dinelli

Relatore: Dr. Massimo Marchesi

Esame finale anno 2012

INDEX

Preliminary remarks

Groundwater and surface water are the most used reservoirs by humans for water supply, especially because of their accessibility. Its vulnerability depends on a combination of natural landscape features, such as geology, topography, and soils; climate and atmospheric contributions; and human activities related to different land uses and land-management practices. The evaluation of the water quality, defined by its chemical, physical and biological characteristics in respect to its suitability for a particular purpose, require the identification of the interconnections among surface water and ground water, atmospheric contributions, natural landscape features, and human activities.

Throughout the world, pressures on water resources are increasing, mainly as a result of human activity. Urbanisation, population growth, increased living standards, growing competition for water, industrial development, agricultural activities and mining enterprises are some of the causes of water contamination.

Groundwater and surface water contrasts markedly in terms of the activities and compounds that cause pollution. In addition, there are completely different controls that govern the contaminant mobility and persistence in the two water systems' settings. Groundwater is less vulnerable to human impacts than surface water. However, once polluted, cleaning it up takes a relatively long time is more technically demanding and can be much more costly. Moreover, surface water is hydraulically connected to ground water in most of the cases, therefore it is important to consider ground water and surface water as a single resource.

The objective of this research is to characterize two different cases of water pollution: a saltwater intrusion contamination in a costal aquifer, and the impact of acid mine drainage on a river basin, considering surface and groundwater.

- The first chapter focus on the geochemical characterization of a shallow coastal aquifer affected by saltwater intrusion in the San Vitale pine forest near Ravenna (Italy). Many factors are responsible for the salinization of the area in particular the overexploitation of the aquifer for irrigation use and the subsidence of the examined area, attributed to natural (sediment compaction) and anthropic (natural gas exploitation) causes.

- The purpose of the second case study was the examination of the impact of acid mine drainage on the surface- and ground- waters in the San Juan de Sora Sora River basin in Bolivia. The characterization of waters and sediments was performed in order to determine the influence of a tin-extraction mine on water quality, in an area considered among the world richest in ore deposits.

Premessa

La struttura originale di questa tesi è dovuta al fatto che durante il periodo di ricerca, non avendo potuto usufruire di una borsa di studio che mi permettesse di intraprendere un cammino lineare, sono stata spinta a cercare progetti diversi, già attivi e con fondi disponibili, assieme ad altri finanziamenti personali. La borsa di studio Marco Polo mi ha permesso di partecipare a diversi progetti in Spagna, da cui poi è iniziato, grazie anche al finanziamento successivo, il programma Erasmus Mundus, il progetto svolto in Bolivia, apparentemente molto 'lontano` dal primo studio, una ricerca svolta invece nella provincia di Ravenna. Entrambe queste esperienze mi hanno permesso di entrare in contatto con realtà molto diverse e molto lontane fra loro, dalle quali ho cercato di ricavare un'unitarietà e un filone comune, in quanto tutte riconducenti al deterioro di una risorsa preziosa come l'acqua, quest'ultima senza confini.

Nella certezza dell'unicità di questo bene insostituibile, mi ritengo fortunata per avere avuto la possibilità di scoprire come questa risorsa venga vissuta in realtà così diverse dalla nostra quotidianità, e quanto sia prioritaria e importante la sua salvaguardia.

Questa premessa mi sembra indispensabile per capire l'analisi che propongo, nata al di fuori dei consueti percorsi previsti per una ricerca di dottorato.

Salt Water Intrusion (SWI)

Water quality for coastal aquifers is nowadays a global scale problem, since a large portion of the population uses this resource as supply of fresh water. Saltwater intrusion is the major concern commonly found in coastal areas, reducing the availability of groundwater resource. At present, many coastal aquifers in the world, especially the shallow ones, are affected by intensive saltwater intrusion caused both by natural and/or human-induced processes. The problem is intensified by the population growth, and by the increasing use of coastal areas, especially during summer, by tourism industry (70% of the world population occupies the coastal plain zones) (Vengos, 2003).

Saltwater intrusion is defined as an induced flow of seawater into freshwater aquifers, primarily caused by groundwater development near to the coast. When groundwater is pumped from aquifers in hydraulic connection with the sea, an induced gradient is generated, with a consequent migration of salt water from the sea toward the aquifer, and finally into the wells. Because fresh water is less dense than salt water, it tends to floats on top. The boundary between salt water and fresh water is not distinct; the zone of dispersion, transition zone, or salt-water interface is brackish with salt water and fresh water mixing.

Under normal conditions fresh water flows from inland aquifers and recharge areas, finally discharging to the sea, from the areas with higher water table (WT) level to areas with lower WT level. This natural movement of fresh water towards the sea prevents salt water intrusion in coastal aquifers (Barlow, 2003).

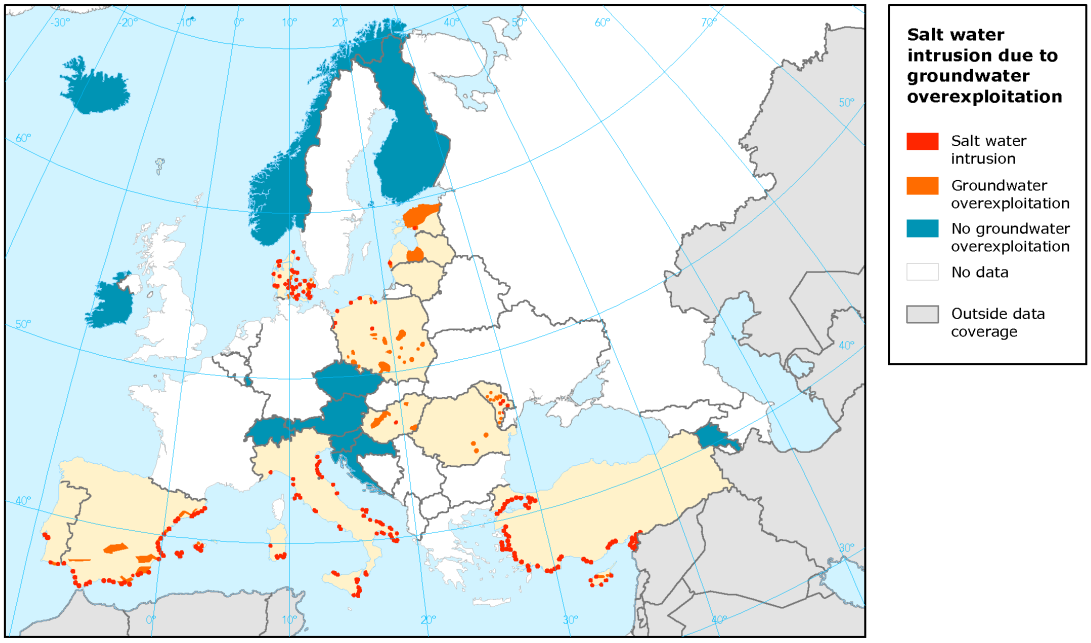

Figure 1: ground-water overexploitation and salt water intrusion in Europe (Source EEA, 1999).

Generally, saltwater intrusion into coastal aquifers is caused by two mechanisms:

- Lateral encroachment from the ocean due to excessive water withdrawals from coastal aquifers, or
- Upward movement from deeper saline zones due to upconing near coastal discharge/pumping wells.

Saltwater intrusion into freshwater aquifers is influenced also by factors such as tidal fluctuations, long-term climate and sea level changes, fractures in coastal rock formations, change of land use and land management practice, seasonal changes in evaporation and recharge rates (Barlow, 2003).

Saltwater has high concentrations of total dissolved solids and other inorganic constituents, becoming unfit for human consumption and many other anthropogenic uses. Saltwater intrusion reduces fresh ground-water storage and, in extreme cases, leads to the abandonment of supply wells when concentrations of dissolved ions exceed drinking-water standards (U.S. Geological Survey, 1999).

Remarkable is the difference between the chemical composition of the saline water, associated with salt-water intrusion, and the theoretical mixture of seawater with groundwater (Jones et al., 1999). These geochemical modifications for seawater intrusion have been attributed mainly to base-exchange reactions with the aquifer materials, typically, clay minerals, organic matter, oxy- hydroxides, and fine-grained rock materials (Vengos, 2003).

In order to manage coastal groundwater resources, the study of movement, mixing and interaction between freshwater and saltwater, as well as the parameters which influence these processes is necessary. Nowadays, detailed studies on saltwater intrusion have become necessary in designing and planning groundwater systems exploitation in coastal areas.

Acid Mine Drainage (AMD)

Human activities such as mining threaten the water sources on which we all depend. There is growing awareness of the environmental legacy of mining activities that have been undertaken with little concern for the environment. Mining consumes, diverts and can seriously pollute water resources through heavy use of water in processing ore, and through water pollution from discharged mine effluent and seepage from tailings and waste rock impoundments.

Acid Rock Drainage (ARD) is a natural process whereby acidity is produced when sulphides in rocks are exposed to air and water. Acid Mine Drainage (AMD) is essentially the same process, however greatly magnified. Although this process occurs naturally, mining can promote AMD generation through the mine tailings and waste rock product, which due to their smaller grain size, have much greater surface area than in-place geologic material (Jennings et al., 2008). Characterized by low pH and high concentrations of heavy metals and other toxic elements, AMD can severely contaminate surface and ground- water, and soils as well.

Generally the recovery of metals from sulphide-rich ore bodies proceeds through a series of steps from mining, crushing, and mineral recovery, followed typically by smelting of the sulphide ores, and thence to metal refining. Although the nature of the ore body dictates the processes used to extract metals from ore, each of these steps generates a waste stream. The oxidation of sulphide minerals in these waste materials (mostly pyrite and pyrrhotite) released elements such as aluminium, arsenic, cadmium, cobalt, copper, mercury, nickel, lead, and zinc to the water flowing through the mine waste (Blowes et al., 2003).

Metal contamination associated with AMD depends on the type and amount of sulphide mineral oxidized, as well as the type of minerals present in the rock. The acid generation is a complex process which requires the presence of:

- Sulphide materials
- Water or a humid atmosphere
- an oxidant, particularly oxygen from the atmosphere or from chemical sources

Additionally, bacteria in the majority of cases play a major role in accelerating the rate of acid generation (Akcil and Koldas, 2006). The acid will leach from the rock as long as its source rock is exposed to air and water and until all the available sulphides are leached out. This process can last hundreds, even thousands of years. Acid is carried off the mine site by rainwater or surface drainage and deposited into nearby streams, rivers, lakes and groundwater.

Despite the various options available for remediating, preventing is considered to be the better option. This is not feasible in many locations and in such cases, it is necessary to collect, treat, and discharge mine sediments. For a responsible management of the sediments, use of selective sequential extraction analysis is a developing tool, in the prediction of the potential effects of metal contamination in changing environmental conditions.

References

Akcila A., & Soner Koldas S. (2006). Acid Mine Drainage (AMD): causes, treatment and case studies, *Journal of Cleaner Production 14(12–13)*, 1139–1145.

Barlow, P. M. (2003). Groundwater in Freshwater-Saltwater Environments of the Atlantic Coast. *U.S. Geological Survey Circular: 1262*.

Blowes, D.W., Ptacek, C.J., Jambor, J.L., & Weisener, C.G. (2003). The geochemistry of acid mine drainage. *In: Lollar, B.S. (Ed.), Environmental Geochemistry. Treatise on Geochemistry,vol. 9*. Elservier–Pergamon, Oxford, 149–204.

EEA (1999). Groundwater quality and quantity in Europe. *Environmental assessment report No 3*. European Environment Agency. Copenhagen.

Jennings, S.R., Neuman, D.R., & Blicker, P.S. (2008). Acid Mine Drainage and Effects on Fish Health and Ecology: A Review. *Reclamation Research Group Publication*, Bozeman, MT.

Jones B. F. (1965). Geochemical evolution of closed basin water in the western Great Basin. *In Second Symposium on Salt (ed. J. L. Rau). Northern Ohio Geol. Soc. vol. 1*, 181–200.

Nordstrom, D.K. (1982). Aqueous pyrite oxidation and the consequent formation of secondary iron minerals, *In: Kittrick, J.A., Fanning, D.S. and Hossner, L.R., eds. Acid sulfate weathering. Soil Science Society of America*, 37-63.

Vengos A. (2003). Salinization and saline environment. In: Lollar, B.S. (Ed.), Environmental Geochemistry. Treatise on Geochemistry,vol. 9. Elservier–Pergamon, Oxford, 333–365

Abstract

Throughout the world, pressures on water resources are increasing, mainly as a result of human activity. Because of their accessibility, groundwater and surface water are the most used reservoirs. The evaluation of the water quality requires the identification of the interconnections among the water reservoirs, natural landscape features, human activities and aquatic health.

This study focuses on the estimation of the water pollution linked to two different environmental issues: salt water intrusion and acid mine drainage related to the exploitation of natural resources.

Effects of salt water intrusion occurring in the shallow aquifer north of Ravenna (Italy) was analysed through the study of ion- exchange occurring in the area and its variance throughout the year, applying a depth-specific sampling method. In the study area were identified ion exchange, calcite and dolomite precipitation, and gypsum dissolution and sulphate reduction as the main processes controlling the groundwater composition. High concentrations of arsenic detected only at specific depth indicate its connexion with the organic matter.

Acid mine drainage effects related to the tin extraction in the Bolivian Altiplano was studied, on water and sediment matrix. Water contamination results strictly dependent on the seasonal variation, on pH and redox conditions. During the dry season the strong evaporation and scarce water flow lead to low pH values, high concentrations of heavy metals in surface waters and precipitation of secondary minerals along the river, which could be released in oxidizing conditions as demonstrated through the sequential extraction analysis. The increase of the water flow during the wet season lead to an increase of pH values and a decrease in heavy metal concentrations, due to dilution effect and, as e.g. for the iron, to precipitation.

PART I

Groundwater chemistry and arsenic occurrence in the phreatic aquifer system of the San Vitale pine forest

Abstract

Groundwaters quality of the shallow phreatic aquifer of the San Vitale pine forest in Ravenna (Italy) is severely affected by coastal saline intrusion. Fifteen piezometers were sampled at various depths using a staddle parker system, during spring, summer and autumn seasons in order to understand the geochemical processes occurring close to the freshwater/saline interface and its variations during the year. Sea water fraction, ionic deltas and saturation index were investigated to characterize the hydrogeochemical features of the aquifer in the area. The Water table level lies mostly below sea level, consequently there is no natural freshwater hydraulic gradient contrasting the density gradient of the saltwater. The depletion on Na^{+} indicates a salinization process in the eastern part of the aquifer and in the deeper waters, confirmed by the Base EXchange index (BEX) calculated through the Stuyfzand method. Cation exchange, dolomitization, gypsum dissolution and sulphide reduction were identified as operating in the aquifer.

Additionally, the presence of Arsenic was investigated as most of the sampling wells exceeding the arsenic concentrations currently Italian legal maximum contaminant level (10 µg/l). The amounts of dissolved arsenic in the groundwater are related to a layer rich in organic matter, and correlate along the depth with the concentrations of Fe^{2+}, HCO_3^{-} and SO_4^{2-}, according to the reducing condition of the aquifer.

General context, materials and methods

Introduction

When considering the water resources in areas bordering seas, coastal aquifers are important sources of fresh water. Since groundwater systems in these areas are in contact with saline water, one of the major environmental problems might be saltwater intrusion, which can reduce the available fresh groundwater resources in coastal aquifers. At present, many coastal aquifers in the world, especially shallow ones, experience an intensive saltwater intrusion caused by both natural and human-induced processes. The European Environment Agency has recognized that the problem of saltwater intrusion due to groundwater over-exploitation is one of the major threats to coastal area freshwater resources in Europe, and Italy especially, with its 8500 km of coastline, has been indicated as one of the most critical countries (Scheidleger et al., 2004). Many studies in Italy shows that freshwater resources are becoming increasingly scarce from intense use, salinization and long periods of drought, not only for the loss of drinking water supply, but also for the effects on natural vegetation, ecosystems, wetlands and salinization of agricultural soils in the coastal zone (Antonellini et al., 2008; Barrocu et al., 2001; Cau et al., 2002; Capaccioni et al., 2005; De Luca et al., 2005; Doveri et al., 2010; Giambastiani et al., 2007; Polemio et al., 2010; Pranzini, 2002).
Costal aquifer salinization consists, from a geochemical perspective, of a high-salinity solution (seawater) mixing with a dilute solution (fresh water) in a medium that has especially reactive minerals. When this salt-water/fresh-water mixing occurs, processes like cation exchange contribute significantly to the final composition of the groundwater.

Outline and objectives of the study

The aims of this study were to:

- ✓ determine the influence of the water table on the salt water intrusion occurrence
- ✓ characterize geochemically the groundwaters of the pine forest and its variability in relation to the seasonality
- ✓ determine the intensity of the salinization processes
- ✓ study the water rock interactions related to the salinization/freshening of the aquifer
- ✓ analyse the arsenic occurrence

Study area

Background

The San Vitale pine forest is situated 3 to 5 km west of the Adriatic Sea on a dune belt system within the Po Plain in northern Italy. The area is particularly affected by several natural and anthropogenic features such as: land subsidence; saltwater intrusion in the phreatic aquifer and seawater encroachment inland along the rivers; direct contamination from water bodies open to the sea; destruction of coastal dunes and reduction of their barrier effect; land reclamation drainage systems; insufficient aquifer recharge and sea level rise.

The natural subsidence rate, due to the compaction of alluvial deposits, is approx. 1 mm/year (Selli and Ciabatti, 1977; Pieri and Groppi, 1981), however in the last century the main topographical variation of the area has been due to anthropogenic subsidence. Land settlement, dramatically increased the subsidence rate up to 110 mm/year after World War II, primarily due to groundwater pumping and, subordinately, gas winning from a number of deep on-shore and off-shore reservoirs (Teatini et al., 2006). Nowadays, subsidence rate has declined down to 1 cm/year. Land subsidence has dropped most of the territory below mean sea level, modifying the river and normal groundwater flow regimes. A drainage system is necessary primarily to lower the phreatic level and keep the agricultural land dry, together with keeping tree roots in the coastal areas above the watertable. However, the result of the drainage system management is an unstable phreatic level in the aquifer, which is not able to contrast saltwater intrusion and saline and brackish groundwater are intruding landwards. Therefore this consequence is far from helping to maintain the Pine forest ecosystem, which is very sensitive to salinity of the water.

The San Vitale pine forest represents an historical landmark in the Po River Plain. It extends north– south for 10 km, beginning north of Ravenna, over an area of about 16.6 km^2 (Figure 1). It is bounded by the Destra Reno Channel to the north, by the scolo Canala and Staggi to the south and by the Piallassa Baiona to the east. It is finally bounded by a complex system of drainage channels connected with the Via Cerba drainage-pumping machine on the west. The entire San Vitale area is part of the Delta Po natural park.

Planted by monastic communities between the 10th and 15th century (Giambastiani et al., 2007), the pine forest is nowadays a popular tourist's destination, especially for its historical value. The surrounding area underlies several economic interests; the urban area of Ravenna, industrial plants, agriculture, harbour activities and tourism.

San Vitale area is bordered in the northern part by a large swamp area, Punta Alberete, and by cropland to the south. Punte Alberete, for a total area of 189 ha, is protected by the Ramsar Convention being a valuable wetland and hosting rare bird species, which makes this place a famous tourist attraction for bird watching. The woodland established in this part is seasonally flooded by adjoining Lamone river (SEHUMED, 2000).

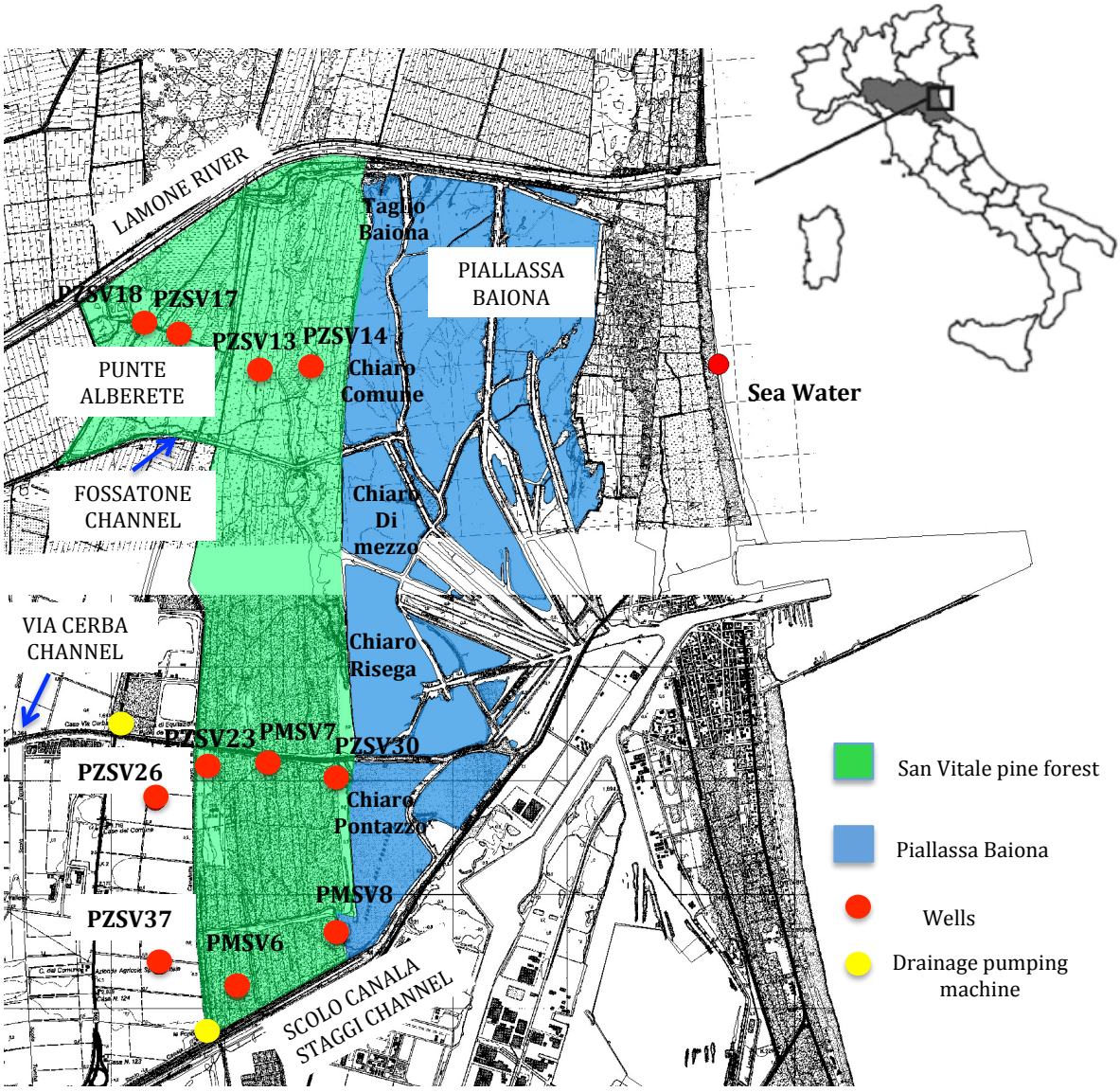

Figure 1: Location map of San Vitale pine forest and Punte Alberete swamp (green) and the Biallassa Baiona (blu) adjacent to the Adriatic coastline north of Ravenna (Po Plain, Italy). Red dots indicate the sampled wells and the yellow one the drainage pumping machines.

Geological setting

The Romagna coastal plain, where the San Vitale pine forest is located, comprises the southeastern part of the wider Po River Plain. The Po Plain covers an area of roughly 70,000 km^2 enclosed between the Alps to the north and Apennines to the south. These two chains supply the Po basin with continental sediments of heterogeneous composition. Those derived transported from by the Po River are a complex mixture of many rock types, with the important provenance signal of high contribution of ophiolitic rock (Amorosi et al., 2002). The contribution from the apenninic chain is dominated from contribution deriving from the erosion of the Marnoso-arenacea formation a thick flysch unit with abundant carbonate contribution. The uppermost aquifer is however related to a coastal environment of deposition, so contribution from other sources (especially to northern Adriatic ones enriched in dolomite) can be present. The Ravenna study area, as part of the southeasternmost Po Plain fill, underwent severe alterations in its depositional environment. The sedimentation dynamic in the coastal area was prevalently controlled by climatic and eustatic fluctuations. During last glacial maximum the relative sea level dropped about 100 to 120 m in the Adriatic epicontinental plain (Van Straaten, 1970), shifting the shoreline 250 km south compared to its present position and thus, forming an alluvial plain. Marine as well as continental deposits from Late Quaternary cover marine sediments of Pliocene to Middle Pleistocene age (Amorosi et al., 1999).

Therefore, Pleistocene accumulation was basically driven by continental sedimentation (Curzi et al., 2006) of 4th order lowstand alternating with short-term transgressive periods (Amorosi et al., 2004). The continental sedimentation induced the deposition of alluvial facies, represented in Figure 2, (Amorosi et al., 1999), which consist of subfacies composed of silt to silty sands tending to coarsen upwards (Amorosi et al., 1999). These facies indicate subaerial exposure and are interpreted as floodplain sediments, levee or channel-fill deposits. Back-barrier deposits, accumulated during Holocene transgression when sea level rose sharply between 18000 and 6,000 BP overlies the alluvial facies.

Initially (10500 to 9000 BP) still restricted to incised valleys, those transgressive sand and coastal plain deposits promoted the formation of shallow marine environments (Amorosi et al., 2002; 2003). During peak transgression (6000 to 5000 BP) these accumulations filled lagoons, swamps and marshlands further landward (Amorosi et al., 1999), as reflected by peats and muds enriched in organic carbon (Amorosi et al., 2002).

As Stefani and Vincenzi (2005) point out, the years 3500-3000 BP were characterized by warm climate and stability in the riverine system. Under Roman intervention a vast stable hydraulic system was established meanwhile the following cooler and moister period (approximately 1500 – 1300 BP) led to a distinct deposition as well as failures in the waterworks (Stefani and Vincenzi, 2005).

During the last 2000 years the fluctuations of the sea and the subsidence rates provoked movements of the coastline and the subsequent formation of beach ridges and submersion which create brackish marshes and lagoons in progradation with the littoral strip (Bondesan et al., 1995).

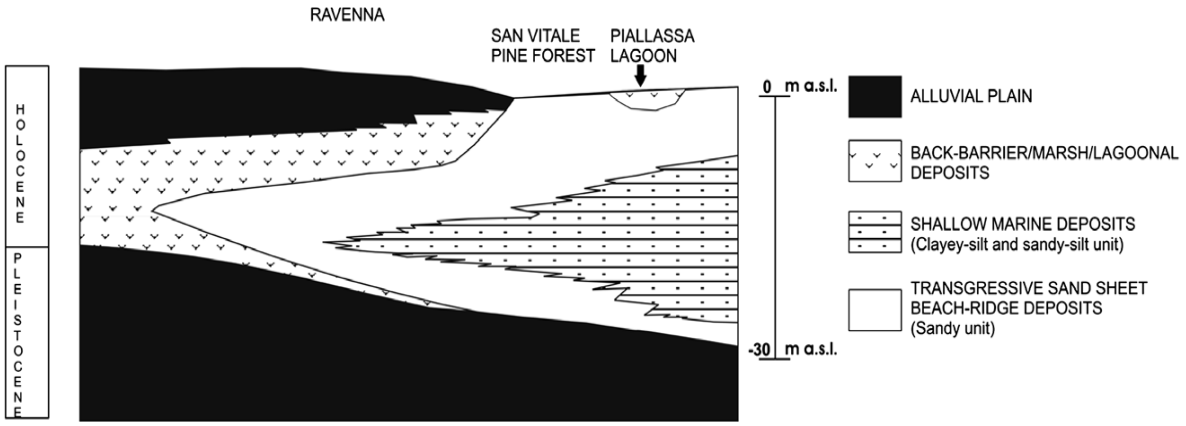

Figure 2: Stratigraphic cross-section of the coastal plain of Ravenna (Po plain, Italy), (Amorosi et al. 1999)

Hydrogeology

The aquifer system in the area is characterized by the stratigraphic architecture. Two prominent stratigraphic markers, corresponding to wedge-shaped coastal sand bodies, recorded between 0-30 m and 100-130 m borehole depths, are separated by a thick succession of mud-prone alluvial deposits (Figure 3). This sequence formed during the transgressive- regressive cycles of Quaternary sedimentation is characteristic of the entire Adriatic coastal plain and can be traced parallel to the shoreline (Amorosi, 2008). These sandy successions identify the coastal aquifers; marked as particular saltwater induced as they derive from prograding delta and beach deposits accumulated during sea level highstand.

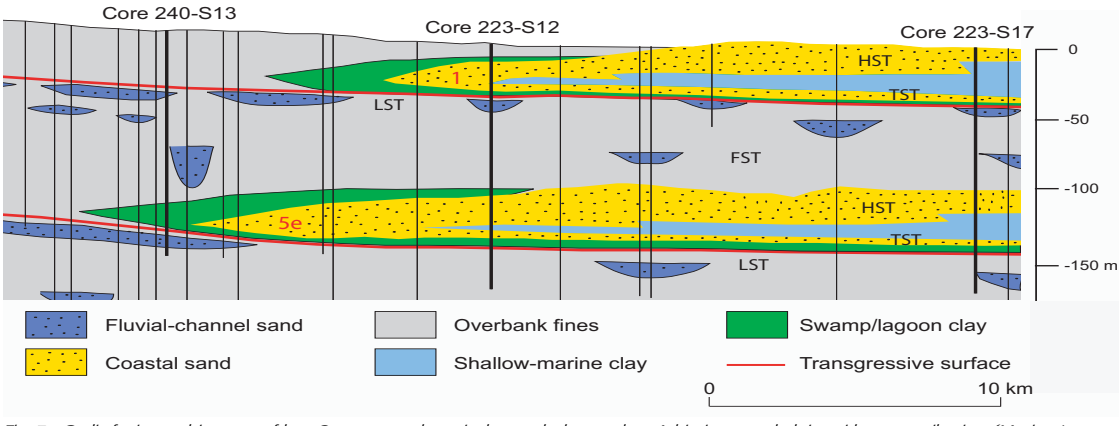

Figure 3: Cross-section of the coastal sedimentary succession defining the aquifers. TST: Transgressive Systems Tract, HST: Highstand Systems Tract, FST: Falling-stage systems Tract, LST: Lowstand systems Tract (Amorosi, 2008).

The San Vitale aquifer comprises an unconfined system based upon beach and dune sandy deposits. Some lenses of clay and peat alter the hydrological setting into confined zones, particularly in swamp areas as they occur in the northwestern part of the San Vitale pine forest and Punte Alberete wetland.

The upper aquifer subsystem A1 is formed by two layers: a relatively thick medium-grained sand shallow unit of 10 m (from 0 m to -10 m a.s.l.) and a lower fine-grained sand unit of a lesser thickness (from -21 m to -26 m a.s.l.) The two bodies are separated

by a clayey-silt and sandy-silt unit (from -10 m to -21 m a.s.l.). The Würmian continental silty-clay basement lies at a depth varying from -20 m in the western sector to -30 m at the present shoreline (Veggiani, 1971; 1974) (Figure 2). Since the sandy layer was deposited as dune and coastal sands its composition is relatively homogeneous and of high permeability. Antonellini et al. (2008) report hydraulic conductivities as high as 24.8 m/d for the San Vitale pine forest. The porosity varies from 0.15 to 0.35 (Giambastiani et al., 2007).

The climate of the area is characterized by moderate precipitation of 600-1000 mm/year (Figure 4) usually dominant during fall, with a maximum value in October and annual mean temperatures of 14.4°C. The aquifer is characterized by a low recharge rate of 14 mm/a due to the effect of high evaporation. The aquifer thickness varies between 3 m coastward up to 30 m in the most western part and it is on average 10 m. The amount of the aquifer volume is estimated as 60000 m^3/m shoreline (Antonellini et al., 2008).

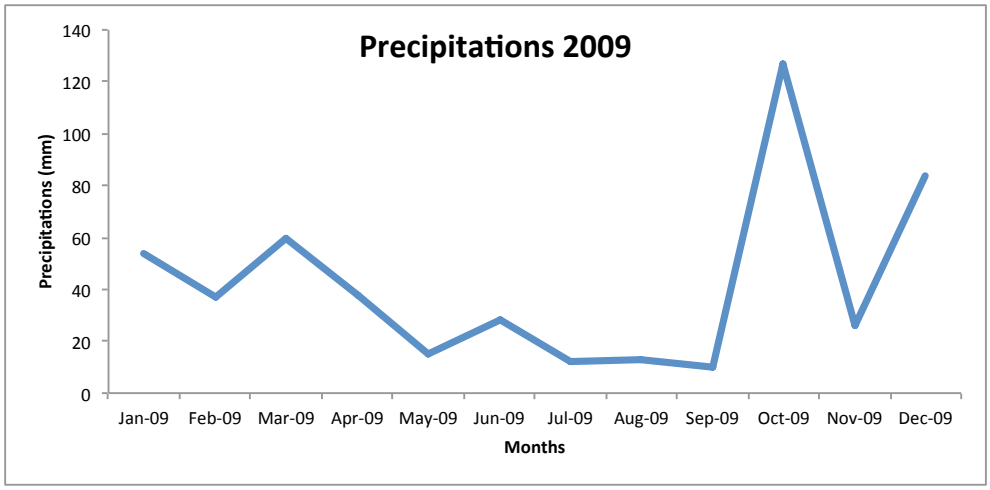

Figure 4: Precipitations in mm in the year 2009 in San Vitale pine forest.

The area is placed on low topography close or even below sea level and is further threatened by proceeding subsidence. The hydraulic heads are reported between -0.5 m and 3.5 m above sea level with hydraulic head gradients *i* of 0.005 seaward and 0.001 directed landwards in areas where the watertable lies below sea level (Antonellini et al., 2008). Artificial dykes and channels and drainage machines regulating the hydraulic head to prevent salt-water intrusion, leading to percolation into groundwater where required.

The seaside various channels are directly connected to the saline lagoon Piallassa and the Adriatic Sea. These channels divide the lagoon into sub-basins; to the north, the Taglio Baiona, Chiaro and Comune basins are subjected to drainage by Fossatone channel and Lamone River and they are isolated from the Adriatic Sea influence. On the contrary the central Chiaro Risega exchanges seawater during high and low tide and comprises brackish water. In the southern part (Chiaro di Pontazzo) it forms a closed basin shut off from the Adriatic Sea but highly influenced by saline waters.

Materials and methods

Sampling

To characterize the aquifer of the San Vitale pine forest and Punte Alberete swamp area, a total of 15 piezometers, subdivided in three transects, were selected (Figure 1). Sampling sites are quite perpendicular to the shore, from the Adriatic Sea landward into the studied area, over a distance from 3500 to 5800 m from the shoreline.

The transect at north is situated between Punte Alberete and the northern part of San Vitale pine forest; it consists of 4 iron cased piezometers, screened in the last metres and penetrate the aquifer to a depth of 6 metres.

The transect situated in the central part of the pine forest is oriented across the Cerba channel and include 5 piezometers cased of polyvinylchloride (PVC): 4 screened from 0.5 m down to 15 m, penetrating most of the upper aquifer while the other one is screened from 13.7 m to a depth of 27 m, so as to extract groundwater only by the lower aquifer. The transect comprises the dunes of San Vitale and cropland under fruit cultivation in the western part.

Finally, the transect in the southern part of the area under examination is composed by 5 PVC piezometers, three of them are fully screened while the other 2 are catching groundwater only by the lower aquifer. The hydrology of the area is eventually under the influence of the Staggi Channel to the south and to the pumping machine to the west, which drain adjacent agricultural field.

Groundwater sampling along the three transects was performed during three field-campaign: from May to December 2009. 45 groundwater samples from 15 piezometers were extracted in between May and July 2009. Further, 15 groundwater samples were collected in September from the central transect in order to examine the variation of its composition after the season of uppermost water demand. Finally, additional 20 groundwater samples were collected in December to determine the influence of the rainy period on the aquifer. A seawater sample was taken as a reference value from the Adriatic Sea at Lido di Marina to allow a comparison with the groundwater sample constitution. The Table 1 shows location and description of sampling points.

All the piezometers were sampled with a depth specific method by using the Packer system except for the piezometers PMSV6 and PMSV8 during spring, sampled with a depth integrated method, by flushing it completely; thus, deriving information about the entire water column.

Table 1: Sampling point location and description.

	X	Y	Distance from sea (m)	Altitude (m)	Depth (m)	Material	Transect	Screen (m)
PZSV17	757245	934153	4700	1.88	6	iron	Northern	full
PZSV18	755773	934520	5000	1.20	6	iron	Northern	full
PZSV13	756802	934118	4000	1.89	6	iron	Northern	full
PZSV14	757243	934140	3500	1.50	6	iron	Northern	full
PZSVS23	756350	930622	5100	0.65	15	PVC	Central	full
PZSVS30	757486	930511	4000	0.85	15	PVC	Central	full
PZSVS26	755886	930335	5600	0.66	15	PVC	Central	full
PMSV7	756882	930638	4600	0.44	15	PVC	Central	full
PMSV7 p	756882	930638	4600	0.38	27	PVC	Central	13.5-27
PZSV37	755920	928895	5800	0.42	15	PVC	Southern	full
PMSV 6	756605	928665	5200	0.62	15	PVC	Southern	full
PMSV 6 p	756589	928677	5200	0.66	27	PVC	Southern	13.5-30
PMSV 8	757484	929151	4200	1.00	15	PVC	Southern	full
PMSV 8 p	757484	929151	4200	1.05	27	PVC	Southern	13.5-31
Sea Water	760830	934159	0	0.00	-	-	-	-

Before groundwater collection a depth profile of the temperature, electrical conductivity (EC), and salinity from the water table to the piezometer's bottom was measured on-site (CTD-probe AquaTROLL®200). The water level from top of the piezometer down to the water table was measured applying an electrical water table indicator in order to allow a reference of the hydraulic head to sea level.

Samples were taken close to the water table and at the bottom of the piezometer. On the base of the EC results, one or two more sample depths were chosen where abrupt changes in EC occur as it may indicates the interface of fresh and saltwater.

Operating a straddle field packer system, with a resolution of 20 cm, the piezometers were flushed at the specific sampling window until achieving constant values of EC and salinity or three times the total volume. Flushing at moderate pumping rates by using a Solinst®410 Peristaltic Pump aims at displacing stagnant water from the piezometer and receiving a groundwater sample representative for in-situ conditions. The multi-level sampling technique allows a depth specific approach; it consists of isolating specific sections of the monitored well with inflatable packers (bladders) considering the groundwater's chemistry at the well-defined sampling window. A series of such samples allows the definition of the vertical distribution of water quality. Samples of the deeper aquifer collected during the first campaign, are subjected to a depth integrated method, i.e., the piezometer is fully flushed before extraction, thus mixing up bottom and top groundwater.

Non-filtered samples provided readings of pH, redox potential (Eh) and temperature utilizing a HANNA® HI 9026 pH meter. The accuracy lies in the range of ± 0.01 pH, ± 0.20 mV, ± 0.40°C. In order to prevent extended aerial exposure and the consequent risk of precipitation and flocculation, the measurements of sulphide, ferrous iron and total iron concentrations were conducted on-site by applying a HACH® DR/2010 Spectrophotometer. The Methylene Blue Method was applied for sulphide analysis, the FerroVer Method for total iron and 1,10 Phenanthroline Method for bivalent iron (detection limit 0.01 mg/l).

Subsamples of groundwater were filtered through a 0.45 μm cellulose filter and filled into 250 ml polyethylene (PE) bottles acidified with nitric acid (HNO_3^-) down to a pH < 2 for cation and trace element analysis, in order to prevent cation precipitation or biological uptake. Non-acidified samples for major anion analysis were left. Those bottles were filled completely and capped tightly before transporting them into the laboratory of the University of Bologna, where they were stored dark and refrigerated.
Total alkalinity was determined in the laboratory, on a filtered subsample, by the titration method with 0.02 HCl at pH of 4.5. Major nutrient (nitrate, nitrite, ammonia, phosphate) determination was performed on filtered non-acidified groundwater samples employing a HACH® DR/2010 Spectrophotometer. These analyses were implemented within 24 h after sampling to avoid biogeochemical alterations. Nitrate follows the Cadmium Reduction Method and is subjected to a precision of ± 0.01 mg/l N – NO_3^-. The Diazotization Method delivers readings of nitrite at accuracies of ± 0.0011 mg/l NO2 – N, meanwhile PO_4^{3-} - P, measured by Asorbic Acid Method, ± 1 mg/l. The Salicylate Method applied for the detection of NH_3-N counts with a precision of ± 0.015 mg/l.
For cation determination (Ca^{2+}, K^+, Mg^{2+}, Na^+) AAnalyst 100 Atomic Absorption Spectrometer was operated on acidified and filtered samples, detection limits are listed as 0.01 mg/l. Previously filtered samples for major anion (SO_4^{2-}, NO_3^-, F^-, Br^-, Cl^-) were analysed with ion-chromatography (IC) analysis (DIONEX®DS5 Detection Stabilizer, detection limits: 0.01 mg/l). Trace element analyses (As, Ni, Cu, Mn, Fe, Si, B) were performed on acidified groundwater samples with the inductively coupled plasma (ICP) method using an ICP 6000 Series ICP atomic emission Spectrometer (detection limits are 0.01 mg/l).

Results and discussion

Data from the sampling methods - depth specific and depth integrated - for PMSV8 are shown in Figure 5. Different conclusions on the process might be drawn according to the adopted sampling strategy since the results are completely different depending on the sampling system adopted. The depth-integrated approach leads to samples resembling seawater and assumes the same concentration for the entire piezometer depth, meanwhile depth specific collection discriminates between different water types occurring with decreasing level. The depth specific method using the packer system has been choose for this study to better define the chemical influx of the salt-water intrusion. Data obtained from all year round sampling are presented in the Annex 1.

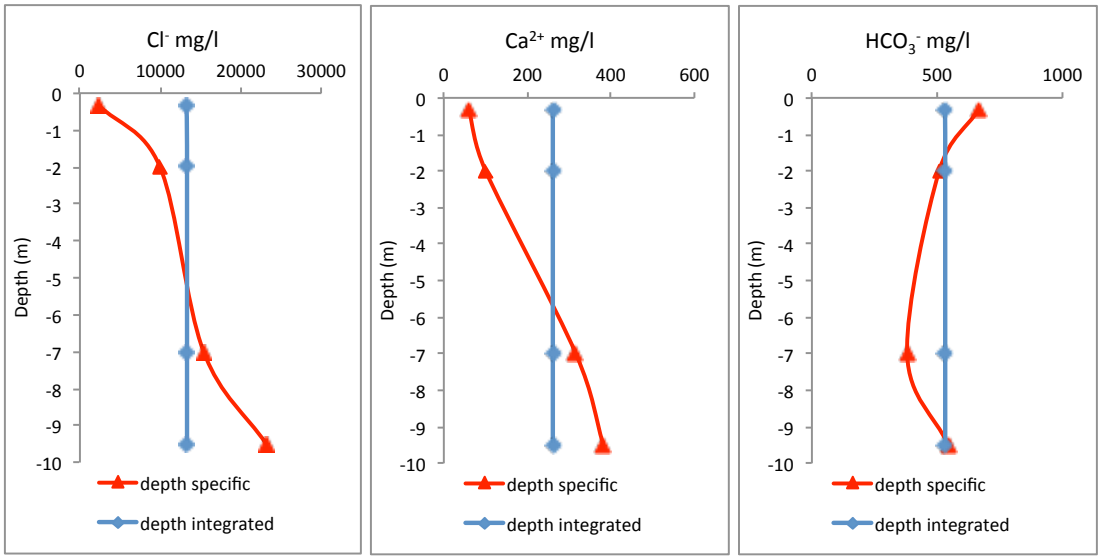

Figure 5: Comparison of different sampling methods applied to the same piezometer (PMSV8); depth integrated indicate a completely flushed sampling when fully screened; depth specific sampling indicates flushed only at sampling depth.

Water table and fresh- salt- water interface

The elevation of the sampled piezometers ranges between 0.42 and 1.89 m above mean sea level (a.msl) (Table 1), while the water table in between -1.80 and 0.76 (Table 2), which lies consistently below msl (b.msl) (Figure 2) in large parts of the study area (except the northern transect). The water table only surpasses msl (from c. 0.0 m up to c. 0.8 m) in the Punte Alberete area.

From spring to summer 2009 the water table significantly dropped up to 1 m within the wetlands of Punte Alberete. During autumn, the piezometric heads of the entire transect result above mean sea level. The water table results stable all year round in the middle of the central transect (Figure 2b) with a lower level recorded at PZSV23 (c. -1.3 m) and at PMSV7 that lies close to the mean sea level. A strong decrease in water table occurs during summer for PZSV30 and in the nearby agricultural fields at PZSV26. The water table of the southern transect (Figure 2c) lies close to the mean sea water level during spring, whereas the western part strongly dropped during the summer period. Data

concerning this transect during the autumn season are missing and the database is completed by data provided from the sampling campaign of December 2010 for the CSI (Coastal Saline Intrusion) project.

Table 2: Water table data and the calculated depth of the saline interface by Glover, 1964.

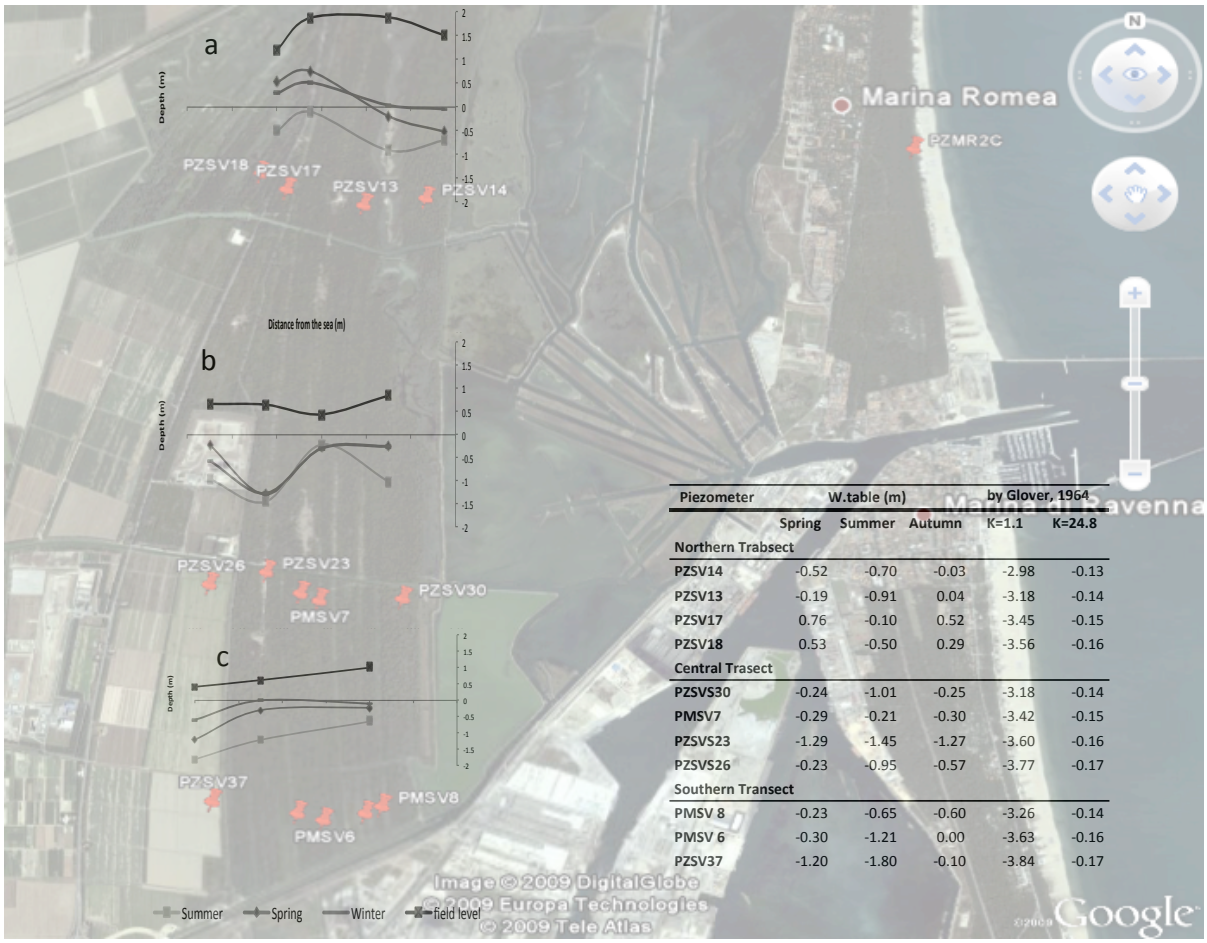

Piezometer	W.table (m)			by Glover, 1964	
	Spring	Summer	Autumn	K=1.1	K=24.8
Northern Trabsect					
PZSV14	-0.52	-0.70	-0.03	-2.98	-0.13
PZSV13	-0.19	-0.91	0.04	-3.18	-0.14
PZSV17	0.76	-0.10	0.52	-3.45	-0.15
PZSV18	0.53	-0.50	0.29	-3.56	-0.16
Central Trasect					
PZSVS30	-0.24	-1.01	-0.25	-3.18	-0.14
PMSV7	-0.29	-0.21	-0.30	-3.42	-0.15
PZSVS23	-1.29	-1.45	-1.27	-3.60	-0.16
PZSVS26	-0.23	-0.95	-0.57	-3.77	-0.17
Southern Transect					
PMSV 8	-0.23	-0.65	-0.60	-3.26	-0.14
PMSV 6	-0.30	-1.21	0.00	-3.63	-0.16
PZSV37	-1.20	-1.80	-0.10	-3.84	-0.17

Figure 6: Elevation and water table level data for the three sampling campaign in the studied area. In the Table 1 are indicated the main characteristics of the piezometers and the theoretical salt-water fresh-water interface (Glover, 1964).

To calculate the depth of the fresh-salt water interface (z), the Ghijben-Herzberg equation was used. The Ghijben-Herzberg equation (Equation 1) as a first estimation applies in particular for estimating freshwater lenses below an island. This principle assumes the position of hydraulic heads (h) to occur above mean sea level, thus allowing a natural down flow gradient to the sea. The two thicknesses h and z, are related by ρf and ρs where ρf is the density of freshwater and ρs is the density of saltwater.
According to this model, since the watertable in the studied area lies consistently below sea level, there is a strong landward gradient promoting seawater invasion into the aquifer.

$$z = \frac{\rho_f}{(\rho_s - \rho_f)} \times h$$

Equation 1

In the northern transect, according to the Ghijben- Herzberg principle, a freshwater lens till 32 m thickness b. msl is deduced for the Punte Alberete swamp. Extending the Ghijben-Herzberg model to the groundwater recharge (q') and the distance from the sea (x) as proposed by Glover (1964), the depth of the interface (z) is calculated by the Equation 2, *G* is presented by the density differences and K refers to the hydraulic conductivity

$$z = \frac{\sqrt{2q' \times G}}{K}$$

Equation 2

Antonellini et al. (2008) report for the San Vitale forest a recharge rate q'= 0.014 m/yr and the hydraulic conductivities vary from 1.1 m/d and 24.8 m/d. The depth (z) is then given for each point x in Table 2. According to the model the position of the interface is predicted between 2.98 m below msl in the eastern part (oriented to the sea) and 3.84 m b.msl landwards for a minimum hydraulic conductivity, given as K = 1.1 m/d. Considering the maximum hydraulic conductivity K = 24.8 m/d the seawater forms an interface in depths of 0.66 m b.msl seawards and 0.85 m b.msl landwards. Comparing the results obtained with the Glover equation with the field data, in autumn the interface depth (z) obtained with the higher K (24.8 m/d) is similar to the measured, which indicate the high hydraulic conductivity in the aquifer in this season. In summer, because of lower water table levels, also hydraulic conductivity decrease as well and the interface (z) is then characterized by an intermediate value between the two extreme values calculated by Antonellini et al. (2008)

Chemical characterization

The all rough data are presented in the Annex 1. The pH of the analysed samples ranged between 6.7 and 7.7 (Tables 3-4). During the sampling occurred in spring and summer, temperature vary between 14 and 24 °C, with a minimum recorded in the deeper aquifer whereas, and in between 12.5 and 16.2 °C in autumn, with a minimum on the surface. The conductivity ranges between 1.5 and 64 mS cm^{-1} with the maximum value in the deeper aquifer (PMSV8p) and a minimum on the surface (PZSV26) during spring (Tables 3-4).

The redox conditions indicate that the waters are oxygenated on the surface and characterized by an increase of reducing conditions with the depth.

Table 3: Physical parameters of the spring sampling campaign.

Spring - northern trasect			
northern trasect			
Wells	pH	Eh [mV]	T [°C]
PZSV17a	7.03	-137.60	19.2
PZSV17b	7.12	-152.20	17.5
PZSV17c	7.42	-168.90	17.3
PZSV18a	7.32	-80.50	24.0
PZSV18b	7.09	-136.90	17.7
PZSV18c	7.05	-158.60	20.4
PZSV13a	7.08	-58.80	20.0
PZSV13b	7.06	-87.00	18.8
PZSV13c	7.09	-103.90	17.5
PZSV14a	6.87	-150.80	16.9
PZSV14b	6.95	-159.00	16.5
PZSV14c	7.18	-142.70	16.3

Spring - central transect			
central transect			
Wells	pH	Eh [mV]	T [°C]
PZSVS23a	7.46	165.40	15.8
PZSVS23b	7.60	-127.90	14.8
PZSVS23c	7.63	-135.00	15.9
PZSVS23d	7.70	-158.60	16.0
PZSVS23e	7.37	-152.20	15.5
PZSVS30a	7.10	-5.30	15.6
PZSVS30b	7.10	-111.50	15.7
PZSVS30c	7.45	-110.00	16.0
PZSVS26a	7.28	-89.20	17.3
PZSVS26b	7.32	-135.00	17.3
PZSVS26c	7.17	-152.50	16.8
PZSVS26d	7.29	-77.90	17.8
PMSV7a	7.63	54.50	20.2
PMSV7b	7.66	68.40	18.2
PMSV7c	6.70	-7.00	18.8
PMSV7d	7.56	-146.70	18.6
PMSV7p a	7.55	-172.20	17.6

Spring - southern transect			
southern transect			
Wells	pH	Eh [mV]	T [°C]
PZSV37a	7.46	-161.40	18.4
PZSV37b	7.43	-182.40	19.0
PZSV37c	7.46	-134.00	17.4
PZSV37d	7.44	-146.70	17.0
PMSV 6	7.20	-113.80	15.9
PMSV 6p	7.56	-166.00	15.0
PMSV 6p	7.50	-133.50	15.9
PMSV 8p	7.41	-118.80	15.6
PMSV 8p	7.40	-133.20	15.1
PMSV8a	7.67	35.30	18.9
PMSV8b	7.45	-100.20	17.2
PMSV8c	7.25	-103.70	17.0
PMSV8d	7.22	-94.00	16.3
PMSV 8	7.15	-109.20	14.6

Table 4: Physical parameters of the summer and autumn sampling campaigns.

Summer - central transect			
central transect			
Piezometer	pH	Eh [mV]	T [°C]
PZSV 23 a	7.53	123.3	20.5
PZSV 23 b	7.46	60	18.1
PZSV 23 c	7.38	-66	17.4
PZSV 23 d	7.15	-102.1	16.9
PZSV 26 a	7.3	-49.7	17.7
PZSV 26 b	7.25	-101.5	15.5
PZSV 26 c	7.39	-104.5	16.4
PMSV7a	7.8	76	23.9
PMSV7b	7.89	17	21.7
PMSV7c	7.53	-98	19.8
PMSV7d	7.49	-144	16.8
PMSV7Pc	7.33	-145	17.3
PZSV 30a	7.23	-31.7	19.1
PZSV 30b	6.95	-93.1	14.9
PZSV 30c	7.05	-80.7	13.9

Autumn - northern trasect			
norther trasect			
Piezometer	pH	Eh [mV]	T [°C]
PZSV17a	7.45	-17.90	4.98
PZSV17b	7.32	-10.00	5.46
PZSV17c	7.46	-18.40	17.35
PZSV14a	7.24	-5.10	25.76
PZSV14b	7.22	-4.00	26.86
PZSV14c	7.34	-12.00	34.98
PZSV18a	7.35	-15	2.17
PZSV18b	7.46	-18.7	2.29
PZSV18c	7.46	-17.2	5.3
PZSV13a	7.41	-13.4	2.22
PZSV13c	7.53	-20.5	2.37

Autumn - central transect			
central transect			
Piezometer	pH	Eh [mV]	T [°C]
PZSV23a	7.5	-29.4	2.8
PZSV23b	7.66	-111.1	3.25
PZSV23c	7.73	-194.3	9
PZSV30a	6.8	4.6	30.72
PZSV30b	6.98	-45.3	53.37
PZSV30c	7.03	-106	59.32
PZPM7p	7.71	-156.7	36.55
PZSV26a	7.7	-86.7	3
PZSV26b	7.85	-160	7.28
PZSV26c	7.71	-152	15.95
PZSV26d	7.59	-150	28.17
PZPM7a	7.97	-53.5	5
PZPM7b	7.71	-98.8	26.53
PZPM7c	7.78	-105.7	47.58

The projection of the major ions composition in the Piper-type diagram shows that the majority of the samples vary between freshwater and seawater compositions. In freshwater, major cations are Ca^{2+} and Mg^{2+} and HCO_3^- is the major anion, while SO_4^{2-} and Cl^- are of minor importance. In a rough classification, the freshwater is of the Ca-HCO_3 type and saltwater of Na-Cl type. The analysed samples lie very close to the theoretical mixing line between these two water types and most of the waters are of the Na-Cl type.

The distribution of cation and anion mixing ratio from field samples as well as the theoretical freshwater-seawater mixing line are shown in Figure 7. This line was based on seawater and rainwater representative of the area. A rainwater sample was taken in the San Vitale pine forest (CSI, project 2010) and a seawater sample from the Adriatic Sea.

In the upper part of the Piper diagram the hydrogeochemical processes that are responsible for groundwater composition can be identified. The average composition of fresh water and seawater are shown and a straight line between the two indicates water composition due to conservative mixing. The groundwater samples displaced below and above the theoretical mixing line are subjected to cation exchange. Cation exchange reactions are often associated with water salinization processes, and explain the enrichment or depletion of cations in solution (Appelo and Postma, 2005).

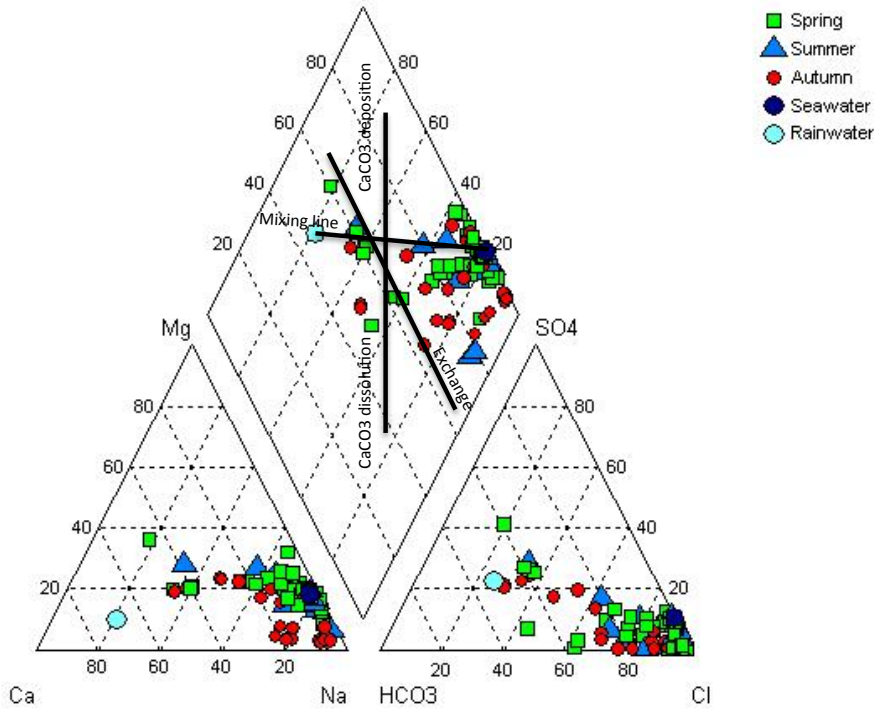

Figure 7: Groundwater composition of water samples represented by means of a Piper-type diagram, the black lines represents: the theoretical mixing line between rainwater composition (S.Vitale 2010) and seawater (Adriatic Sea 2009); calcite deposition above mixing line, precipitation below the mixing line; ion exchange processes.

In order to discuss further the processes driving the chemical compositions of groundwaters, molar ratios Na^+/Cl^- and SO_4^{2-}/Cl^- as function of Cl^- were calculated. In these diagrams (Figure 8) it is notable that a simple binary mixing between saltwater and freshwater can't explain the chemical composition of the groundwaters. In the saline and brackish waters the Na^+/Cl^- ratio is lower and in freshwaters higher than expected from a simple mixing. The SO_4^{2-}/Cl^- ratio display depletion of SO_4^{2-} in brackish and saline groundwater and indicate excess in some freshwater samples.

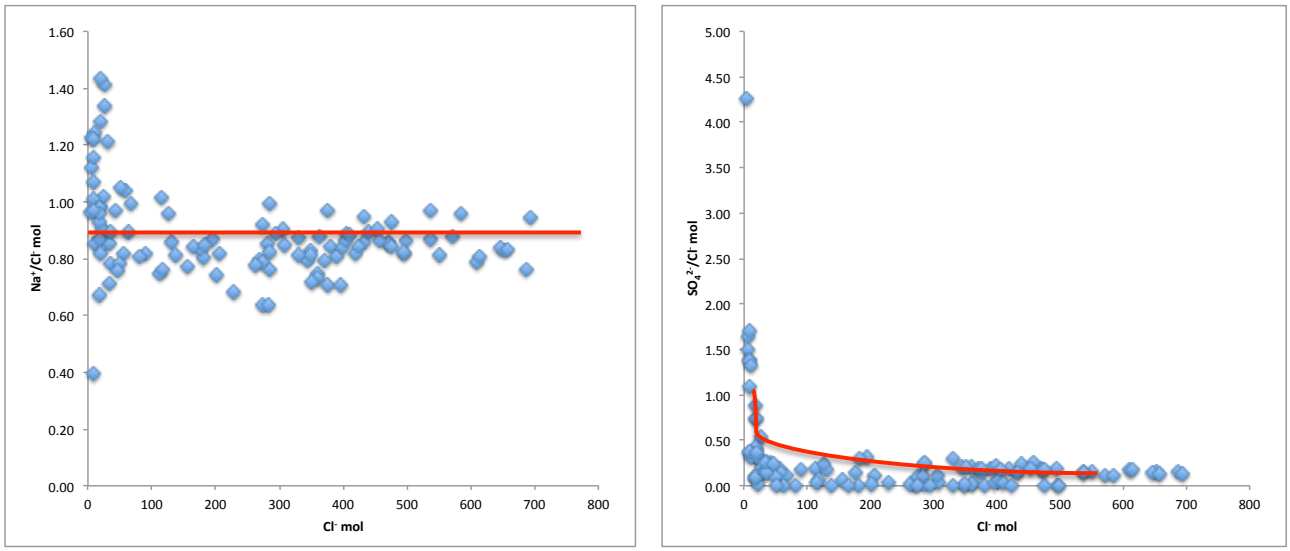

Figure 8: Molar ratios for Na+/Cl- and SO42-/Cl-, plotted versus Cl- for groundwaters. The red line indicate theoretical mixing curve between seawater and freshwater typical of the studied area.

Stuyfzand (1989) classification set on the basis of chloride concentration as shown in Table 5 was used in order to discern between the water types.

Table 5: Division in main types on the basis of chloride concentration (Stuyfzand, 1989).

Main Type	Code	Cl^- mg l^{-1}	Main Type	Code	Cl^- mg l^{-1}
very oligohaline	G	<5	brackish	B	$300\text{-}10^3$
ologohaline	g	5-30	brackish-salt	b	$10^3\text{-}10^4$
fresh	F	30-150	salt	S	$10^4\text{-}2.10^4$
fresh-brackish	f	150-300	hyperhaline	H	$>2.10^4$

The northern transect (Figure 10) is characterized by a freshwater lens in spring that penetrates the aquifer till the depth of 4 metres at a distance from the coastline of 4000 m (PZSV17). The most seaward location (PZSV14) is distinct from the brackish water at the water table and from saltwater at 4 m depth. Landward (PZSV18), brackish water reaches until watertable again. There is no data concerning the summer season. The freshwater lens become brackish in autumn and the seawater at the most seaward piezometer is detected at 2 m b.msl; an increase of the thickness of the brackish water is found landwards (PZSV18).

The seaward site (PZSV30) of the central transect (Figure 11) is all year round characterized by saline water up to the surface. This piezometer is characterized for its hyperhaline waters that reach values of 2.40^4 mg l^{-1}, at 5 m b.msl during spring, that raise 4 m b.msl during the summer whereas reach 5.7 m b.msl during the wintertime. The central part of the transect is distinguished from brackish waters on the surface, at a distance of 4000 m from the shoreline (PMSV7) decreasing landwards into the depth of 6 m, at a distance of 5600 m from the sea (PZSV26) during spring and summer.

No fresh water is detected in autumn and the entire water column is characterized by brackish water landwards. At 5100 m from the shoreline, there is an enlargement of the dispersion zone; in particular during the autumn season, this feature could be observed

at all transects. The piezometer (PMSV7p) catching in the lower aquifer indicates that the composition of the waters is almost constant all over the year, with a chloride content varying between 12300 and 12800 mg l^{-1}.
The brackish water reaches the watertable in the southern transect (Figure 12) and forms only a thin lens of 2m at 4200 m from the coastline (PMSV8) with its widest thickness of 2.7 m at a distance of 5200 m from sea (PZSV37). There is no data about the interface in the central part of this transect.

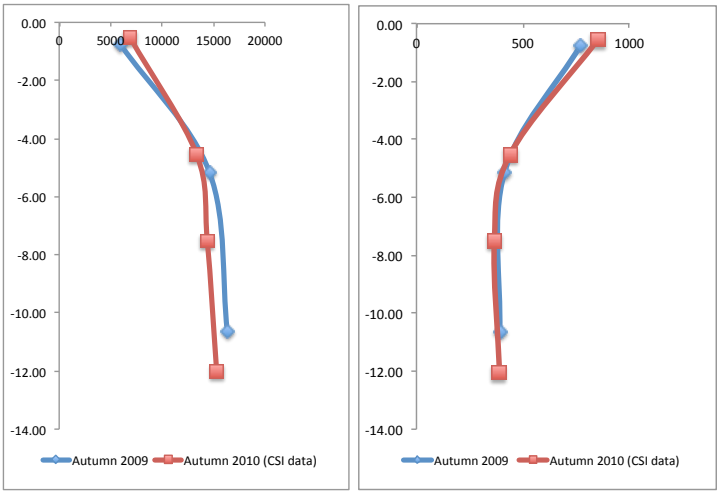

Figure 9: comparison of the chloride and calcium data between two different sampling campaign during autumn

In the autumn campaign the PMSV6 was the only sampled in the southern transect. In order to extend this study to the southern part, data of CSI project, sampled in autumn 2010 was used. The data of PMSV6 was processed to compare the situation in both different sampling campaigns and in order to reveal if the situation is comparable (Figure 9). On the basis of this consideration, it can be asserted that in autumn the entire transect is characterized by brackish water from the watertable like in spring. An enlarging of the thickness of the brackish waters up to the depth of 10 metres is recorded landwards (PZSV37). In the central part (PMSV6) the brackish-salty interface rise up to 3 metres and there is an enlarging of the dispersion zone as it occurs for the central transect. The seaward piezometer (PMSV8) is characterized by a brackish water lens reaching the depth of 6m and a thin transition zone. At the depth of 15 meters b.msl waters have hypersaline characteristics.

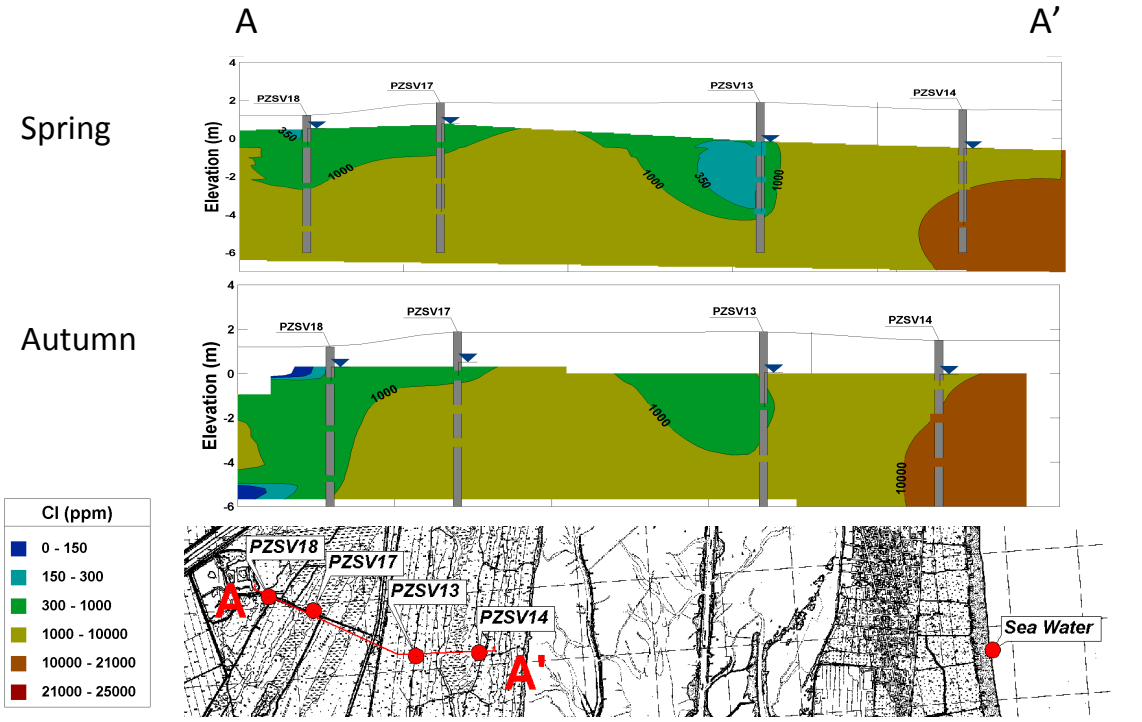

Figure 10: Northern transect chloride concentrations based on the Stuyfzand (1989) classification during spring and autumn.

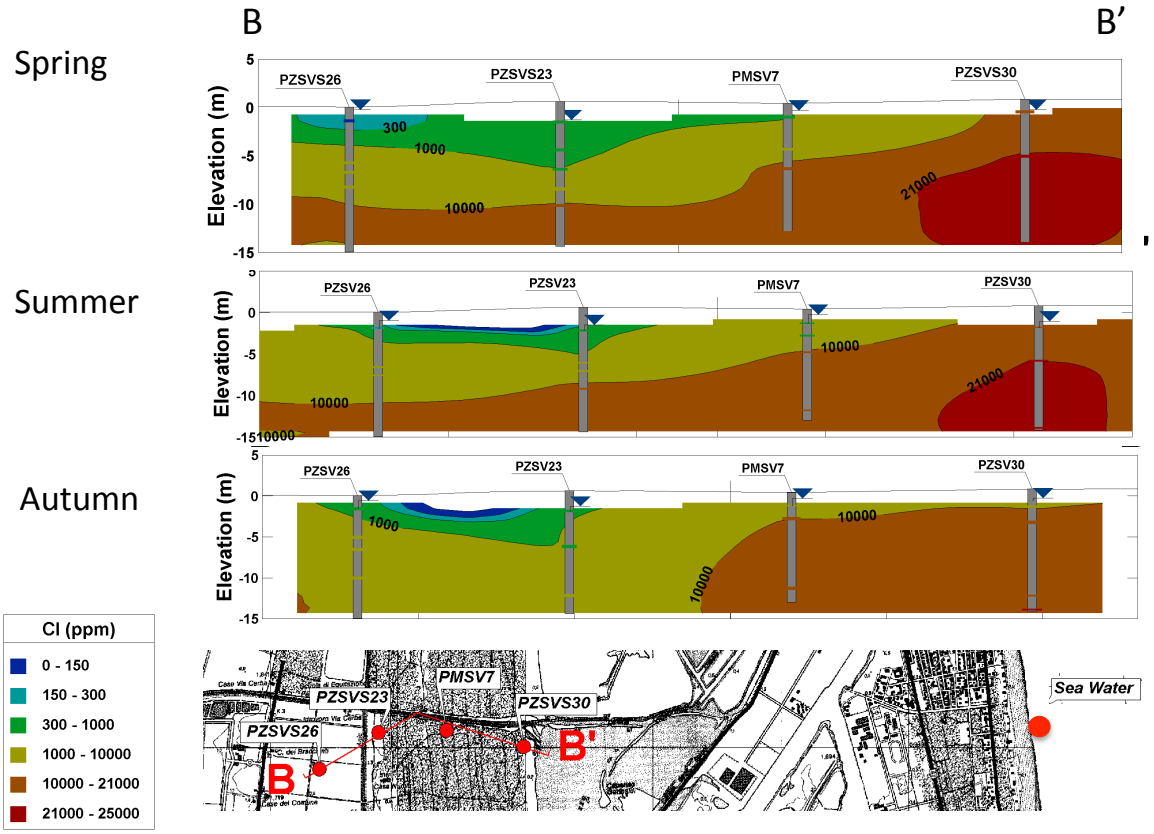

Figure 11: Central transect chloride concentrations based on the Stuyfzand (1989) classification during spring, summer and autumn.

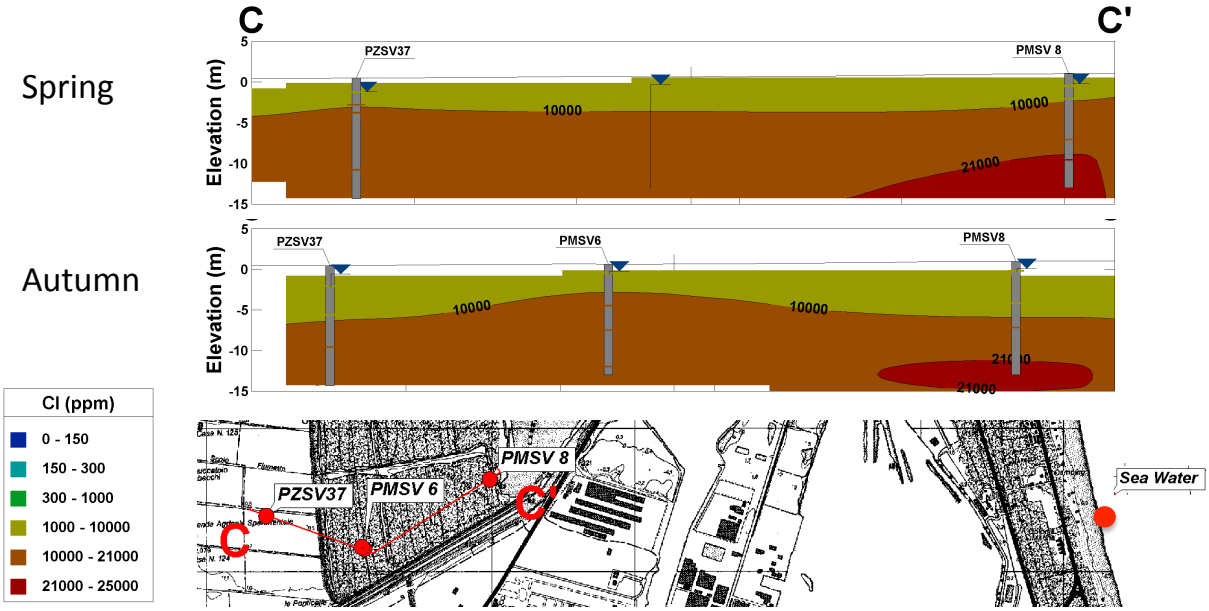

Figure 12: Southern transect chloride concentrations based on the Stuyfzand (1989) classification during spring and autumn.

Quantification of sea water intrusion

The fraction of seawater (f_{sea}) was computed by weighing the measured Cl^- ($m_{Cl^-,sample}$) concentration within the sample against a component derived from conservative mixing of fresh ($m_{Cl^-,fresh}$) and seawater ($m_{Cl^-,sea}$) following the Equation 3. Chloride is assumed to be a conservative parameter, the only inputs are from the salts in the aquifer matrix itself or from a salinization source, and it is not usually removed from the system due to its high solubility (Appelo and Postma, 2005).

$$f_{sea} = \frac{m_{Cl^-,\,sample} - m_{Cl^-,fresh}}{m_{Cl^-,\,sea} - m_{Cl^-,fresh}} \qquad \text{Equation 3}$$

The groundwater of the studied area has a seawater fraction that range between 0 and 156%, indicating the presence of fresh- and hyper saline waters types (Annex 1). The seawater fraction distribution of the area during the spring season is shown in Figure 13.

The figure 'a' represents the surface waters and indicates the presence of the fresh waters (0-25%) in the eastern part of the pine forest perpendicular to the seashore that extend to the southern part in the seaward direction. Fresh-brackish waters, formed by a 25-50% of seawaters characterize all the seaward part of the pine forest and the southern part landwards. In the central part seaward is yet present an area characterized by seawater (78-105%). Between 2 and 5 meters depth, the freshwater lens is replaced by waters with a content of seawater that range between 26 and 52% (Figure 7b). The waters from the central part (at the borderline with the Piallassa Baiona) have content in salts that exceed the seawater (105-157%).

Figure 13 'c' and 'd' respectively representing the depths of 5-7metres and 8-12 metres are only plotted in the southern part, as the piezometers sampled in the northern part reach a maximum depth of 5 metres. Below the depth of 5 metres brackish waters affect the entire pine forest, and the salty water bubble is enlarging seawards. After the depth of 8 metres most of the observed area is characterized by salty and hypersaline waters.

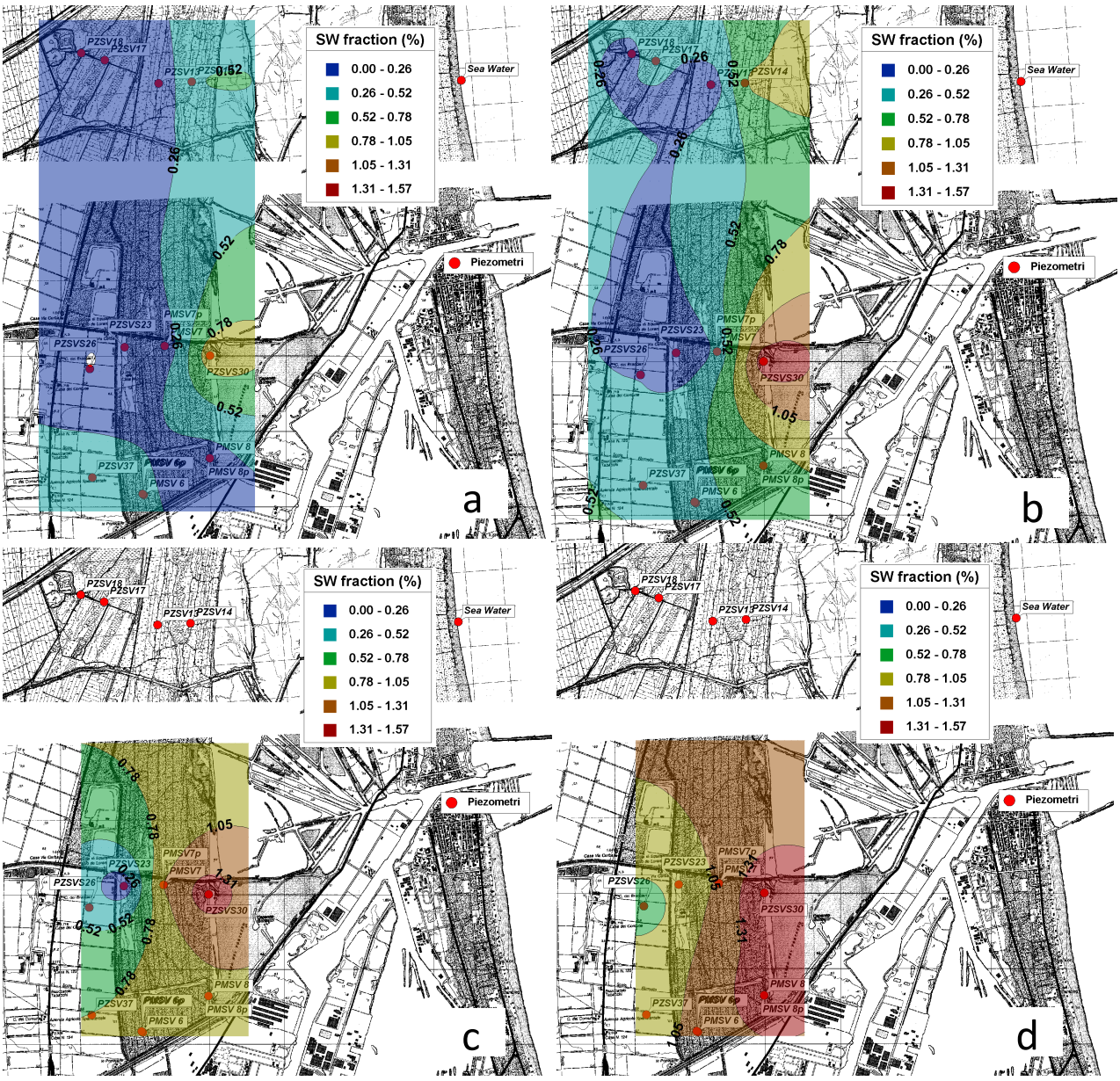

Figure 13: Salinity distribution in the surface (a), at depth between: 2 and 5 metres (b), 5-7 metres (c), 8-12 metres (d) in spring period 2009. Derived by EnviroInsite, Kriging.

Salinization/ freshening and related water rock interactions

Seawater intrusion is not the only process affecting hydrochemistry of groundwater in the study area. Water chemistry depends on chemical reactions occurring as consequence of the mixing processes. Ion-exchange, dissolution and precipitation are some of the most common processes related to salinization or freshening of an aquifer and explain the enrichment or depletion of ions in solution (Andersen et al., 2005; Cruz et al., 2011; Trabelsi et al., 2011). If exchange reactions are identified in field measurements in coastal areas, it could be considered an indication for a recent movement of the saltwater–freshwater interface. Many studies show patterns of exchange reactions all over the world (Anderson, 2004; Capaccioni et al., 2005; Russak and Sivan, 2010; de Montety et al., 2008; Pulido-Leboeuf 2004; Panteleit et al., 2003) caused by saline intrusion or freshening.

Ion exchange

In order to better understand the hydrochemical processes that take place in the aquifer of the San Vitale pine forest during the freshwater–seawater mixing, ionic concentration changes were calculated. These processes can be evaluated from the calculation of the expected composition based on conservative mixing of saline/seawater and fresh-water, and then comparing the results with the measured concentrations in the water sample. All the concentrations are expressed in mmol/l (Appelo and Postma, 2005).

The concentration of an ion *i,* by conservative mixing of seawater and freshwater is:

$$m_{i,\,mix} = f_{sea} \times m_{i,\,sea} + (1 - f_{sea}) \times m_{i,\,fresh} \qquad \text{Equation 4}$$

Where $m_{i,}$ represents the concentration of the ion, the subscripts $_{mix\ sea}$ and $_{fresh}$ indicate a conservative mixture, seawater and freshwater, respectively. The difference between the concentration within the sample measured and the $m_{i,\,mix}$ delivers the amount of depletion/enrichment by:

$$m_{i,\,react} = m_{i,\,sample} - m_{i,\,mix} \qquad \text{Equation 5}$$

A positive $m_{i,\,react}$ indicates the groundwater to be enriched for species *i* and a negative $m_{i,\,react}$ indicate depletion compared to plain mixing.
In the calculation of $m_{i,\,react}$ values, rain sample of Ravenna (CSI Project, 2011) and a seawater sample of the Adriatic coast were used as end-members. In Annex 1 are presented all the data obtained for the depletion/enrichment of Na^+, Ca^{2+}, Mg^{2+}, K^+, HCO_3^- and SO_4^{2-}.
The first thing to note is that the modifying processes in the mixing zone of this aquifer are complex and do not show a homogeneous pattern in either space or time. The aquifer is nearly in equilibrium in the landward part and the cation exchange increase

with depth and proximity of the sea.
As reported in Annex 1, Na_{react} ranges between 15.2 and -42.2 meq during the three seasons. In general, Na^+ depletion is accompanied by Mg^{2+} and SO_4^{2-} depletion and HCO_3^- enrichment.
Na_{react} is commonly negative in the deeper samples and in the highly saline water. The depletion of Na^+ could be explained with the cation exchange taking place between the negative charged surfaces in the sediment which release Ca^{2+} and/or Mg^{2+} to the solution and capture Na^+ from it (Appelo and Greinaert, 1991; Beekman and Appelo, 1991; Panteleit et al., 2003). The depletion of sulphate found in the majority of the samples is commonly observed in coastal seawater-freshwater mixing zones (Nadler et al., 1980; Magaritz and Luzier, 1985; Bishop and Lloyd, 1990; Stoessell et al., 1993; Barker et al., 1998; Cai et al., 2003, Andersen et al., 2005).
A decreasing Na^+ content in the analysed waters would be the result of the exchange of adsorbed Ca^{2+} through Na^+:

$$2Na^+ + Ca\text{-}X_2 \rightarrow 2Na\text{-}X + Ca^{2+} \qquad \text{Equation 6}$$

where X represents the negative charged exchanger site on the surface of the aquifer material. Since this exchange reaction affects the cation ratio in the water only, it would result in a shift of the sample projection in the Piper diamond parallel to the anion axis toward upper left (Figure 7). This process is typical in aquifer affected by saltwater intrusion. This must be reflected in lower Na^+/Cl^- as shown in the Figure 8.

Vice versa the Eqn. 7 could explain an increasing Na^{2+} content:

$$Ca^{2+} + 2Na\text{-}X \rightarrow Ca\text{-}X_2 + 2Na^+ \qquad \text{Equation 7}$$

where X symbolize the exchanger site. The increase in the Na^+ concentrations will shift the sample projection in the Piper diamond parallel to the anion axis toward the lower right (Figure 7). This process is characteristic of a freshening of the aquifer.
The saturation index (SI=log(IAP/K), where IAP is the ion activity product) for calcite, dolomite and gypsum was calculated using the geochemical code PHREEQC (Parkhurst and Appelo, 1999) in order to test the possibility that SO_4-reduction and dolomitization processes are taking place. The data are presented in Annex 1.
The saturation state for calcite is a complex function of the distribution of $CaCO_3$ in the sediment, coupling to redox reactions, interactions with ion exchange processes, and finally mixing between freshwater and seawater (Equation 8) (Bishop and Lloyd, 1990; Appelo, 1994; Melo et al., 1999). Interestingly in the study area the decrease in alkalinity in the transition zone corresponds to the zone of Na^+ depletion and Ca^{2+} enrichment, supporting the coupling of ion exchange and calcite precipitation.

$$CaCO_3 + H_2O \leftrightarrow Ca^{2+} + HCO_3^- + OH^- \qquad \text{Equation 8}$$

Besides calcite dissolution, the oxidation of organic carbon through sulphate reduction

is another source for HCO_3^- in the waters. The layers of organic matter in the investigated area (CSI, 2010), the suboxic conditions reflected in the low EH values and high-reduced iron concentrations of the samples (Annex1), the characteristic foul smell noticed during the sampling, giving a qualitative detection of the presence of H_2S, indicate that the system has the necessary conditions for bacterial sulphate reduction:

$$2CH_2O + SO_4^{2-} \rightarrow H_2S + 2HCO_3^- \qquad \text{Equation 9}$$

The oxidation of organic carbon though sulphate reduction affects the anion mixing ratios in the Piper diagram shifting the sample projection parallel to the cation axis toward lower left (Figure 7). The concentration of sulphide is consistently smaller than the amount of sulphate missing. Some of the sulphide may have precipitated in a number of metastable metal sulphide minerals as pyrite or iron-mono- sulphides and some hydrogen sulphide could also be lost from the upper- most groundwater by degassing (Andersen, 2001; Morse et al., 1987).
Despite the activities of sulphate and calcium in an aquifer are not high enough to reach the solubility product of gypsum, Gomis-Yagües et al., (2000) proved that in an area affected by saltwater intrusion conditions (increase in SO_4^{2-}) and ion exchange reactions (displacement of calcium ions from exchange sites) the depletion of SO_4^{2-} and Ca^{2+} in the aquifer could be attributed to the gypsum precipitation. In this scenario, during seawater intrusion, gypsum precipitation would take place in the zone close to the coast, and would explain the deficit of sulphate in water samples. The calculated SI for gypsum in the studied area is negative for all the samples, which support the SO_4^{2-} depletion due to bacterial reduction.
The explanation for the negative Mg_{react} would be dolomitization. This process can justify the observed deficiencies in Ca_{react} to balance Na_{react}.

Seasonal variations

Spring sampling

During the spring sampling campaign in the northern transect the surface values of all the piezometers, instead of the seaward result in equilibrium for Na^+ (Figure 14). The aquifer with the increasing of the depth result depleted in Na^+ and slightly enriched in Mg^{2+} and HCO_3^-. In the most seaward piezometer (PZSV14), the waters are strongly depleted in Na^+ and SO_4^{2-} and enriched in magnesium and calcium typical of ion exchange caused by the saltwater intrusion (Appelo and Postma, 2005; Cardona et al., 2004; de Montety et al., 2008; el Yaouti et al., 2009). The depletion of sulphate is probably caused by sulphate reduction processes.
In the western part of the central transect, piezometer PZSV26 is in equilibrium on the surface and there is a characteristic ion exchange due to the salinization of the area, with a depletion of Na^+ in deeper waters. The depletion of Mg^{2+} could be explained by cation exchange processes that take place in the seawater/freshwater interface until the exchange capacity of the exchanger is satisfied and the equilibrium restored (Custodio and Bruggeman, 1987). The saturation index, the depletion of Mg2+ and SO42- and the

high increase in HCO3-, indicates that various processes affect the waters. Sulphate reduction brings in solution bicarbonate, which leads to dolomite precipitation and a depletion in Mg^{2+}. The piezometer PZSV23 indicates equilibrium in the area up to 8 metres and salinization in the depth with the same characteristic of the landward piezometer. PZSV7 in the surface is the only site characterized by Na^{+} enrichment as index of freshening of the surface waters.

The negative Na_{react} values are characteristic of deep samples of the seaward piezometers PMSV7 and PZSV30. These waters are depleted in Mg^{2+} and SO_4^{2-} too. The SI indicates that the waters are in equilibrium for calcite and that a precipitation of dolomite occurs. A strong enrichment of Ca^{2+} in surface waters of PZSV30 accompanied by SO_4^{2-} equilibrium indicate the salinization of the area and its removal with the depth is typical of sulphate reduction and calcite precipitation.

In the southern transect the waters are characterized by high depletion of Na^{+}, Ca^{2+}, and Mg^{2+} contrarily to the surface sample of PMSV8, which is enriched in Na^{+} and in equilibrium for Ca^{2+}, Mg^{2+}, and SO_4^{2-}. The SI indicates that calcite is in equilibrium, dolomite precipitate and gypsum dissolve in all the samples.

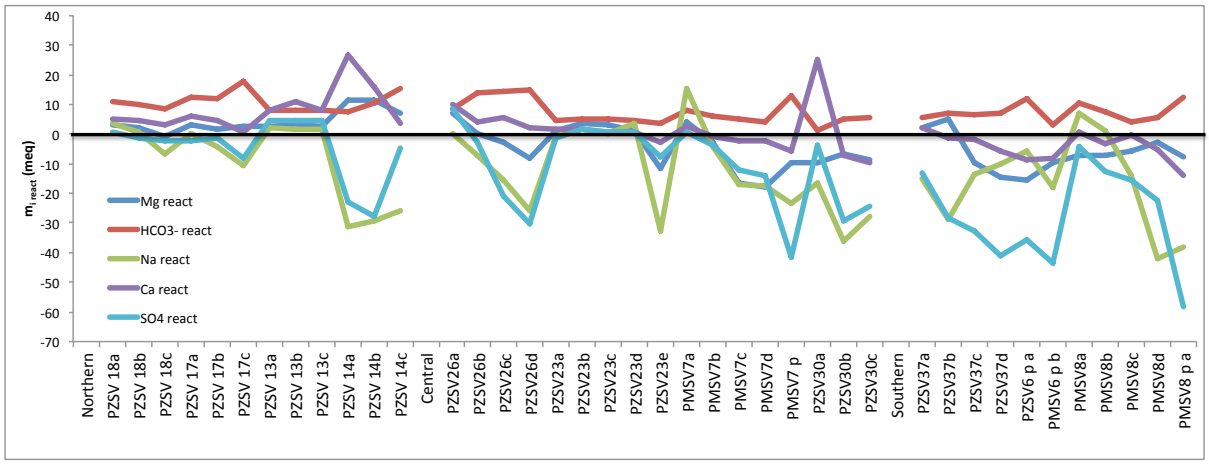

Figure 14: Ionic deltas, Na_{react}, $HCO_3^{-}{}_{react}$, Mg_{react}, Ca_{react} and $SO_4^{2-}{}_{react}$ of the samples taken in spring along the three transect.

Summer sampling

The $m_{i,\ react}$ values calculated for the summer sampling indicates that the aquifer has similar characteristics of the spring season. Surface waters of the western area are in equilibrium for all the analysed elements (Figure 15); the increasing depth enriches waters of Na^{+}, Mg^{2+}, whereas depletes them of SO_4^{2-}. The depletion of the cations indicates a thinning of the equilibrium area in the central aquifer (PZSV23) compared with the spring sampling. During the summer the surface waters of the seaward aquifer (PZSV30) are also enriched in calcium and appear in equilibrium with the sulphate. The SI indicates calcite in equilibrium, dolomite precipitation and gypsum dissolution instead for sample PZSV30 where should precipitate and gypsum is near equilibrium.

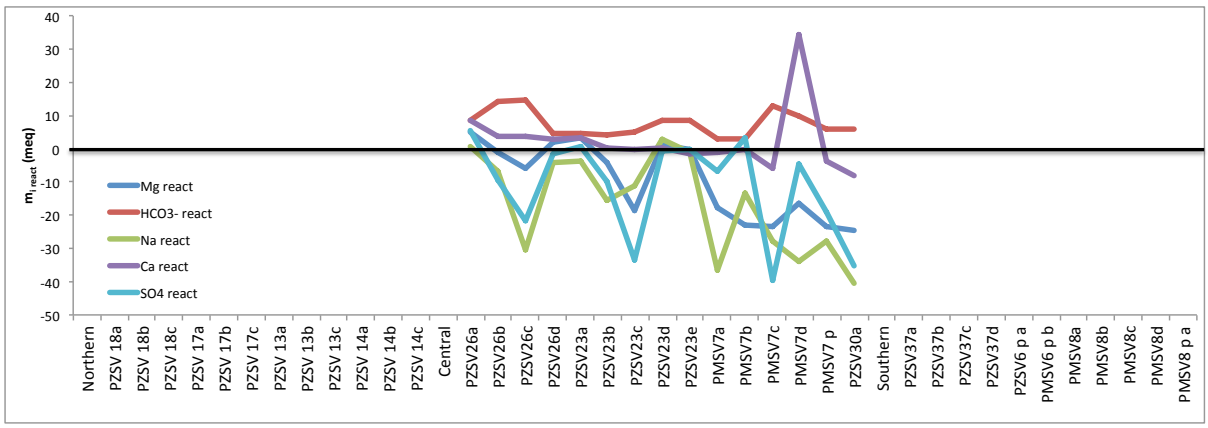

Figure 15: Ionic deltas, Na_{react}, $HCO_3^-{}_{react}$, Mg_{react}, Ca_{react} and $SO_4^{2-}{}_{react}$ of the samples taken in summer in the central transect.

Autumn sampling

In the northern transect the state of the aquifer is similar to the spring one, with an equilibrium on the surface and a progressive depletion of Na^+ and SO_4^{2-} with the depth (Figure 16). The waters located seawards, are strongly depleted in Na^+ and characterized by enrichment of Ca^{2+} and HCO_3^-, in the meantime depleted of Mg^{2+}. The positive calcite and dolomite SI indicate that precipitation occurs in the deeper samples.

The most particular data of the central transect correspond to both the piezometers PZSV23 and PMSV7 where waters are in equilibrium or enriched with Na^+ within the water column. These waters are in equilibrium for Ca^{2+} and Mg^{2+}. The enrichment of Na^+ in the deeper samples of PMSV7 is followed by the enrichment of Mg^{2+}, which may indicate that the Na^+/Mg^{2+} exchange is probably a subordinate process (Martinez and Bocanegra, 2002). The SI near zero for the piezometer PZSV23 indicates that these waters are in equilibrium for calcite whereas a dolomite precipitation occurs. Waters from the landward piezometer PZSV26 are in equilibrium on the surface up to 5 metres and are characterized by Na^+, Mg^{2+} and SO_4^{2-} depletion, and HCO_3^- enrichment. The SI indicates slight calcium precipitation in the water column and an increase of dolomite precipitation with increasing depth.

In the southern transect, most of the surface waters are nearly in equilibrium. The landward piezometer (PZSV37) is characterized by a balance on the surface; a strong depletion of SO_4^{2-} and enrichment in HCO_3^{2-} with the increasing depth, and by the increasing precipitation of dolomite. The surface waters of the PMSV6 are characterized by Na^+ depletion, strong Ca^{2+} and slight SO_4^{2-} enrichment. The most seaward waters are enriched with Na^+ and are strongly depleted in SO_4^{2-}.

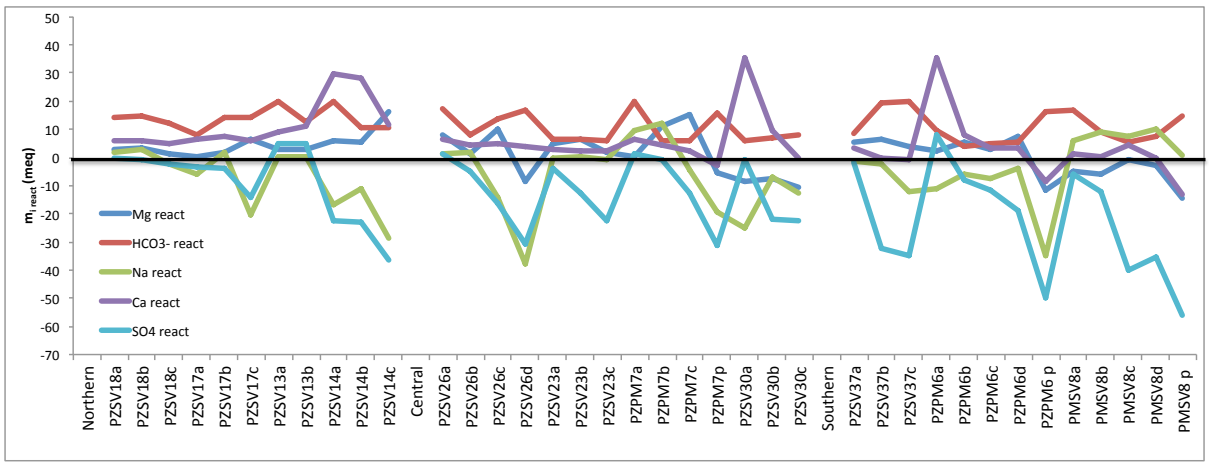

Figure 16: Ionic deltas, Na_{react}, $HCO_3^-{}_{react}$, Mg_{react}, Ca_{react} and $SO_4^{2-}{}_{react}$ of the samples taken in autumn along the three transect.

Deeper aquifer

Data from the deeper aquifer (Annex 1) indicate its subjection to ion –exchange all over the year. The waters result depleted in Na^+, Ca^{2+} and Mg^{2+} instead of the sample PMSV8p during autumn, that results in equilibrium respect to the Na_{react} concentrations. The enrichment in HCO_3^-, the strong depletion of SO_4^{2-} and the low Eh values, support the reduction of sulphate as the main process affecting the deep aquifer. The saturation index shows slight calcite and dolomite precipitation and gypsum dissolution.

Stuyfzand water classification

In order to better analyse the behaviour of the aquifer, Stuyfzand classification method has been used (Stuyfzand, 1986) subdividing the most important chemical water characteristics at 4 levels. The waters have been classified determining the:

- main type, based on the chloride concentration (Table 5);
- type, subdivided on the basis of an index of hardness (0-9)
- subtype, determined by the cation and anion which preponderate in the ion balance
- class, (BEX, Base EXchange Index) corrected for the occurrence of dolomite in the aquifer (Stuyfzand, 2008), calculated from $Na^+ + K^+ - 0.8768 * Cl^-$ in meq/L, to evaluate the tendency of the salinization processes.

The class indicates whether cation exchange has taken place and the nature of the exchange too; the consequent positive values can be related to freshwater encroachment, in contrast with the negative ones, linked to salinization, whereas BEX=0 designate a state of equilibrium.

The water types obtained with this classification are presented in Table 2 of Annex 1 and plotted in depth profiles in Figures 17-18-19. Data obtained with the BEX, correlate very well with the interpretation of the aquifer state analysed through the simple ion exchange and the depletion or enrichment of Na_{react} thus, indicating that salinization is taking place in the largest part of the studied area and that only few locations are subjected to geochemical evidences of freshening.

During spring CaMix and NaMix waters with a depth- increasing alkalinity characterize the northern and central part of the aquifer. The BEX indicates that this area is interested by surface freshening that reach depths up to 8 meters in PZSV23. Deeper and seaward waters are classified as brackish and saline- NaCl water type and the seaward as saline and hypersaline- NaCl waters. BEX indicate salinization in the seaward part of the aquifer contrarily to the southernmost one, which is characterized by surface freshening. In the landward part of the southern aquifer the thin transition zone and negative BEX at 4 meters could ascribe to the exploitation of the aquifer for agricultural use. The influence of the agriculture in the west area is supported by the high nitrate and phosphate found in the PZSV26 and PZSV37 samples (Annex 1).
With reference to the central transect, it is important to note that during the summer both the salinization of the central part of the aquifer and the persistence of the freshwater lens in the western part, are probably caused by irrigation of the agriculture fields as supported by the high phosphate levels recorded in Situ (10.4 mg/l).
The western part of the aquifer is subject to freshening in all the studied transects during autumn. The seaward part is in equilibrium in the north, subjected to salinization in the centre and to freshening in the southern part. The enlarging of the transition zone suggests that the salinization observed in the western part during spring is mostly caused by the overexploitation of the aquifer for irrigation uses.

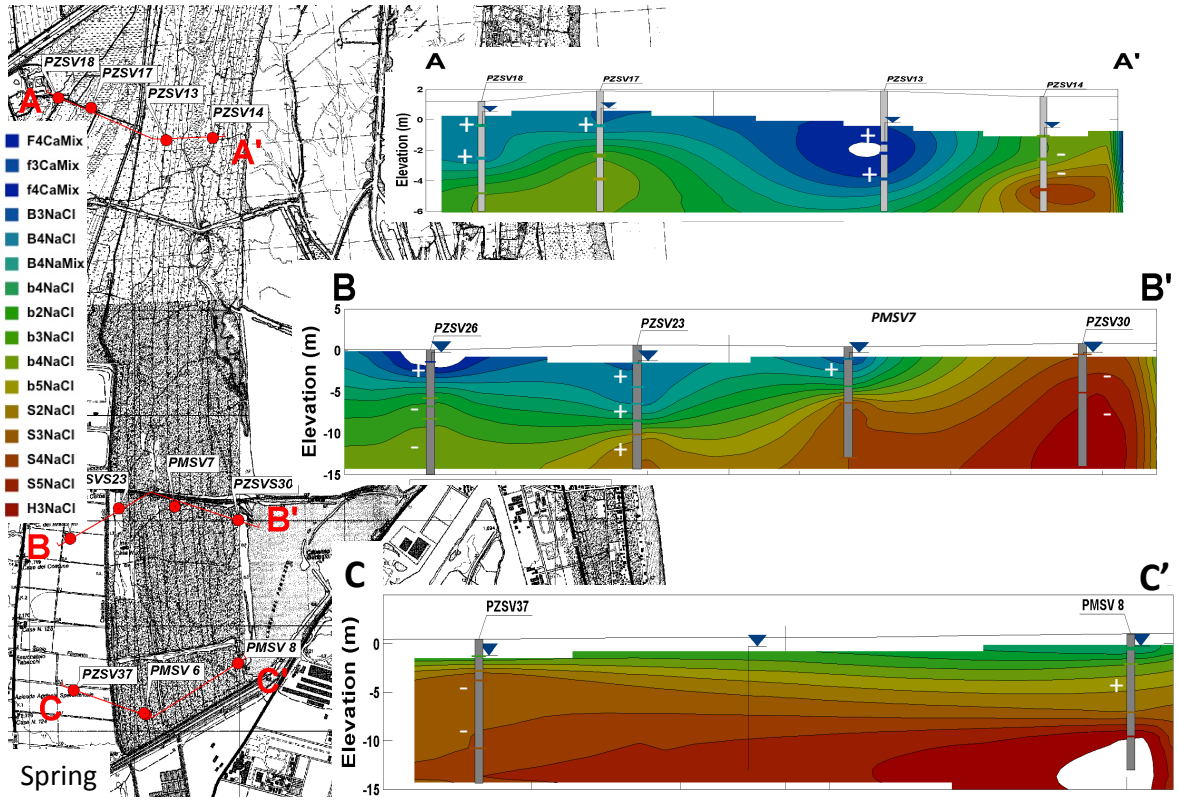

Figure 17: Depth profiles in spring representing the water types obtained with the Stuyfzand classification. The '+' indicate a positive BEX and means freshening of the waters, otherwise '-' indicate the negative BEX that mean salinization of the waters.

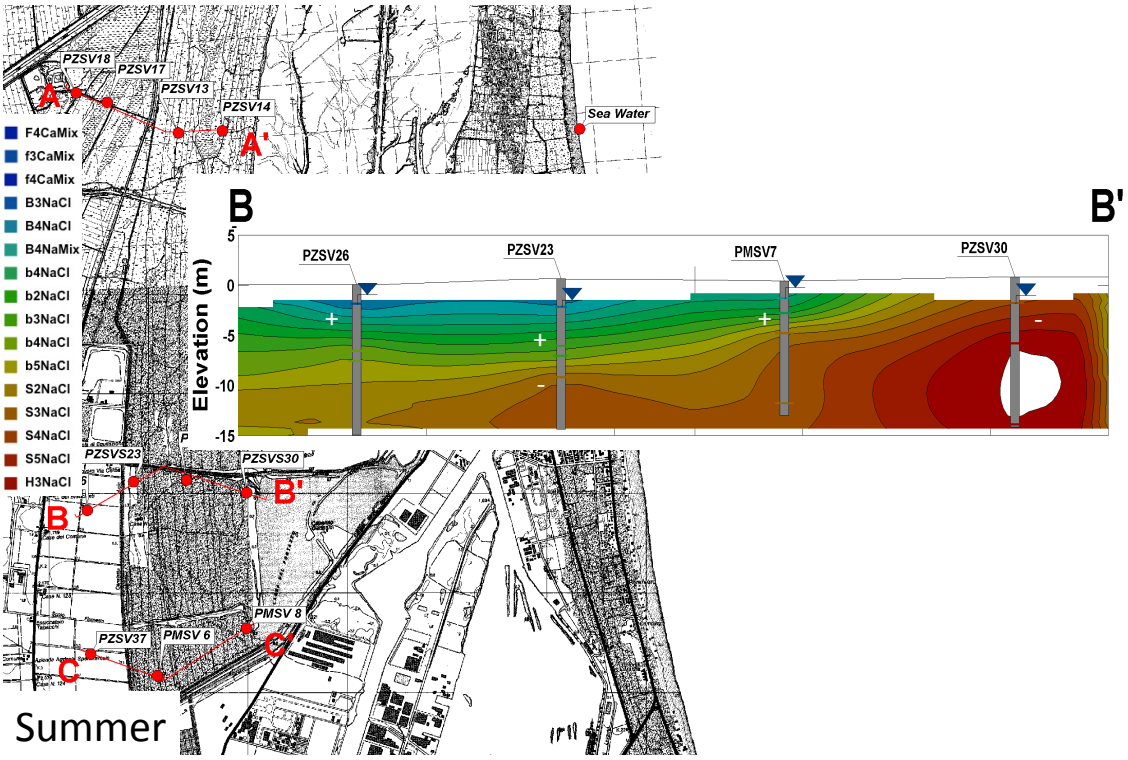

Figure 18: Depth profiles in summer representing the water types obtained with the Stuyfzand classification. The '+' indicate a positive BEX and means freshening of the waters, otherwise '-' indicate the negative BEX that mean salinization of the waters.

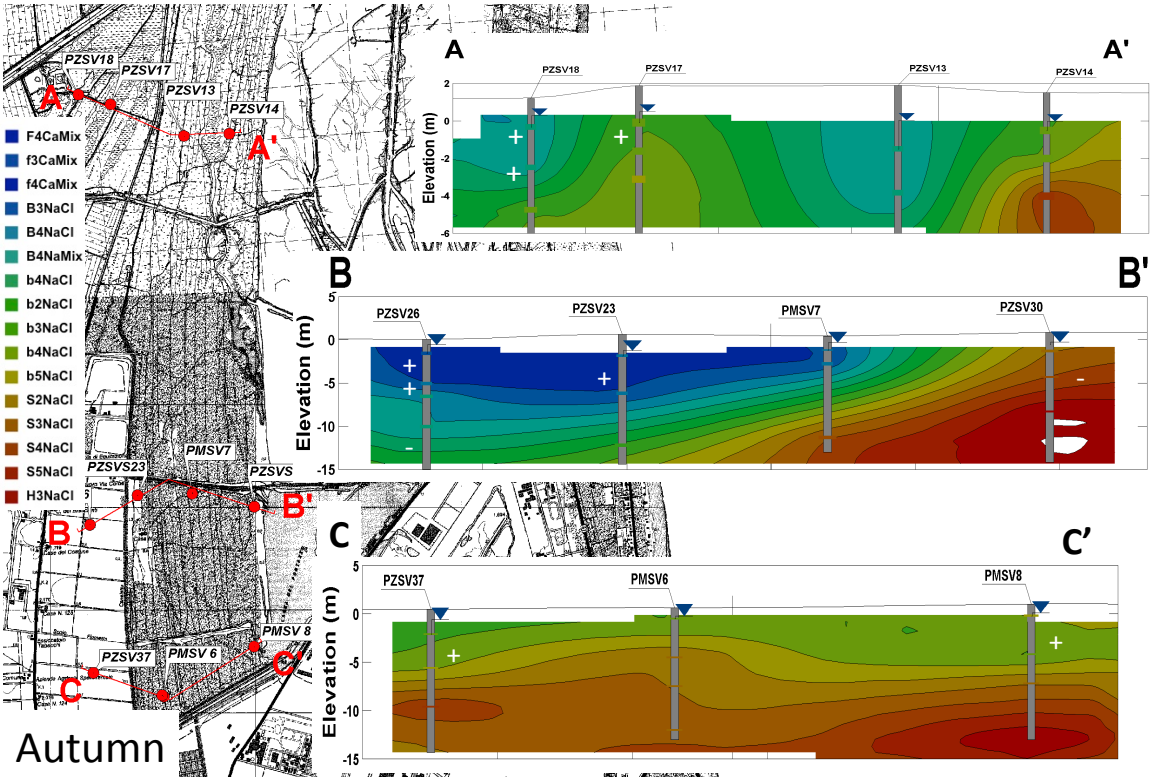

Figure 19: Depth profiles in autumn representing the water types obtained with the Stuyfzand classification. The '+' indicate a positive BEX and means freshening of the waters, otherwise '-' indicate the negative BEX that mean salinization of the waters.

Arsenic occurrence

The presence of arsenic in the area has been documented many years ago in deep groundwaters in the area. The regional agency for the environment (ARPA), which performs a three-monthly monitoring of the regional aquifer since 1987, reports the presence of this metalloid of natural origin, in concentrations up to 98 ppb in December 2003 (ARPA, e-water).

Arsenic analysis was performed on the spring and autumn samples in the central transect of the studied aquifer and on the spring samples in the southern transept only.

The determination of both presence and concentration of Arsenic along the water column was possible by means of the depth-specific method applied in this study. The Arsenic concentration show a heterogeneous distribution along the water column; the highest values correspond to depths ranging between 5 and 7 m b.msl whereas for the PMSV7, higher concentration is detected on the surface (Figures 13-14). A recent study of some cores of sediment in the pine forest and the contiguous agricultural field report that the sediment is characterized by a peat layer and sand mixed with organic matter at depth ranging between 4 and 7.5 m b.msl (Bonanni, 2011). High concentration of arsenic and heavy metals (Cr, Co, Ni, Zn and Pb) were found in correspondence of the peat layer in the sediments, probably adsorbed by organic matter (Du Laing et al., 2009) or precipitate with pyrite or sulphide, due to sulphate reduction (Dellwig et al., 2002).

A series of sediment experiments have demonstrated the roles of organic matter and Fe-hydroxides in releasing As into groundwater in reducing aquifer (Hasan et al., 2009; Banning et al., 2009; Selim Reza et al., 2010; Nickson et al., 2000; Bhattacharya et al., 2001; McArthur et al., 2004; Islam et al., 2005). Fe(III) and/or As(V) can be directly used by microbes as electron acceptors, converting As(V) to the potentially more mobile As(III) (Islam et al., 2005; Lear et al., 2007). In fact, As contamination results from a combination of microbial decomposition of organic matter and reductive dissolution of As-bearing Fe compounds hence, As contamination is spatially heterogeneous and strongly dependent on the geomorphology of the area.

Presence of arsenic in groundwater is well documented in association with high levels of other elements as Fe, increased concentration of HCO_3^- and depletion of NO_3^- and SO_4^{2-} through their reduction during the oxidation of organic matter (Appelo and Postma, 2005) thus invoked as inferring the presence of an As release mechanism and explaining As contamination of groundwater (Selim Reza et al., 2010; Berg et al., 2008; Bibi et al., 2008; Itai el al., 2008) However, such interpretations may be mistaken because these components may not behave conservatively in the aquifer (McArthur et al., 2001) and may be affected by other processes, like ion exchange, dissolution and release to groundwater or precipitation and removal. The occasional lack of correlation between As and Fe in the reducing groundwater (Nath et al., 2005, 2008; McArthur et al., 2001; Du Laing et al., 2009) suggests that multiple processes may affect As concentration in groundwater.

The concentration of the studied area derived from the central transect, vary between 0 and 120 ppb and between 0 and 40 ppb in the southern transect greatly exceeding the WHO guideline in drinking waters (10 ppb) (Figures 20-21). Through a careful

observation of the profiles it is important to notice that the maximum concentration of As doesn't correspond to the peak of the other related elements. Peak in Fe^{2+} and depletion in sulphate are shifted to the deeper sampling point for PZSV26, PZSV23 and PZSV37 during spring and summer. The decrease of the As concentration can be attributed to re-adsorption of the arsenic on remaining Fe oxides, as suggested by Appela and Postma, (2005) or more probably to the precipitation of As as sulphides or co-precipitated with pyrite, as supported by the strong depletion of sulphates (Du Laing et al., 2009; Dellwig et al., 2002). This is consistent with previous publications reporting decline in dissolved As concentration during microbial SO_4^{2-} reduction (Kirk et al., 2004; Haque and Johannesson, 2006; Keimowitz et al., 2007). The two seaward piezometers (PZSV30 and PMSV8) are characterized by a low concentration and by an increase in As related to the Fe^{2+} peak; sulphate concentration doesn't show consistent depletion as occurred for others samples even if the analysis of the $SO_4^{2-}{}_{react}$ (Annex 1) reports a strong depletion in the deeper samples.

Water from PMSV7 behaves differently with the maximum As concentration on the surface; this is probably due to the influence of the close channel, supposed to be reach in organic matter.

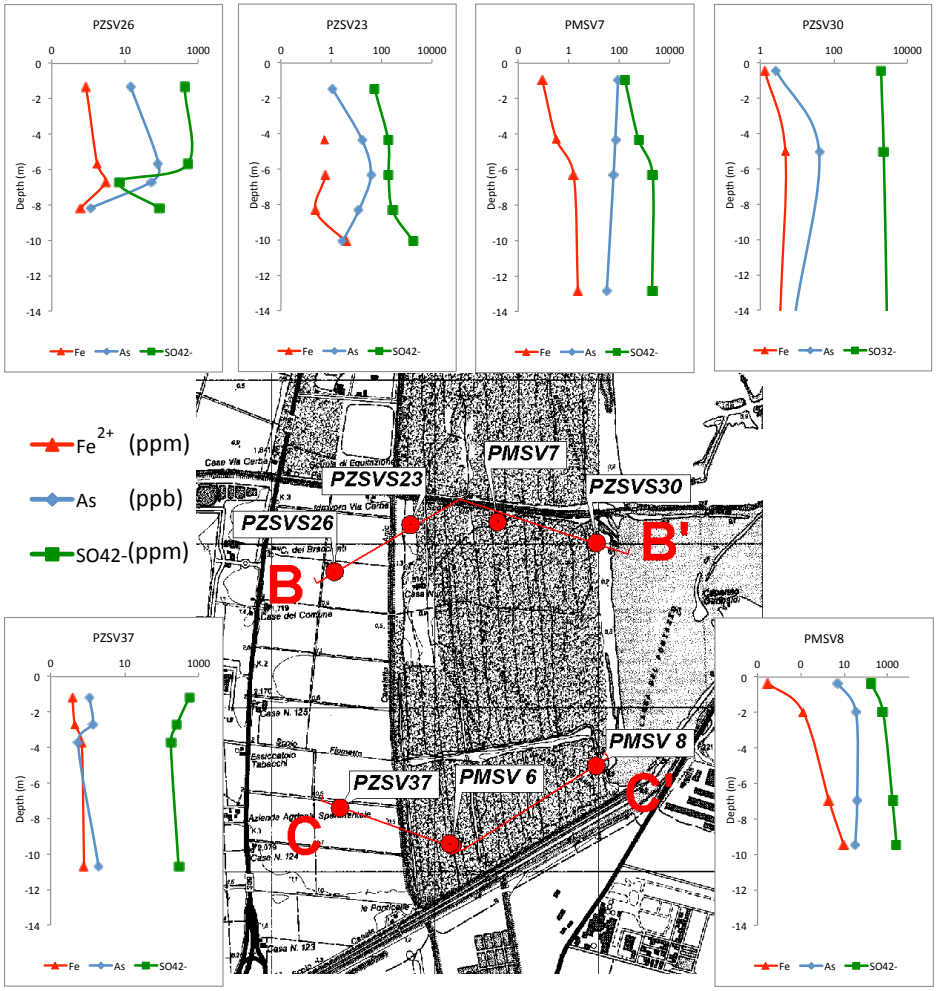

Figure 20: Depth profiles of arsenic, iron and sulphate during the spring sampling.

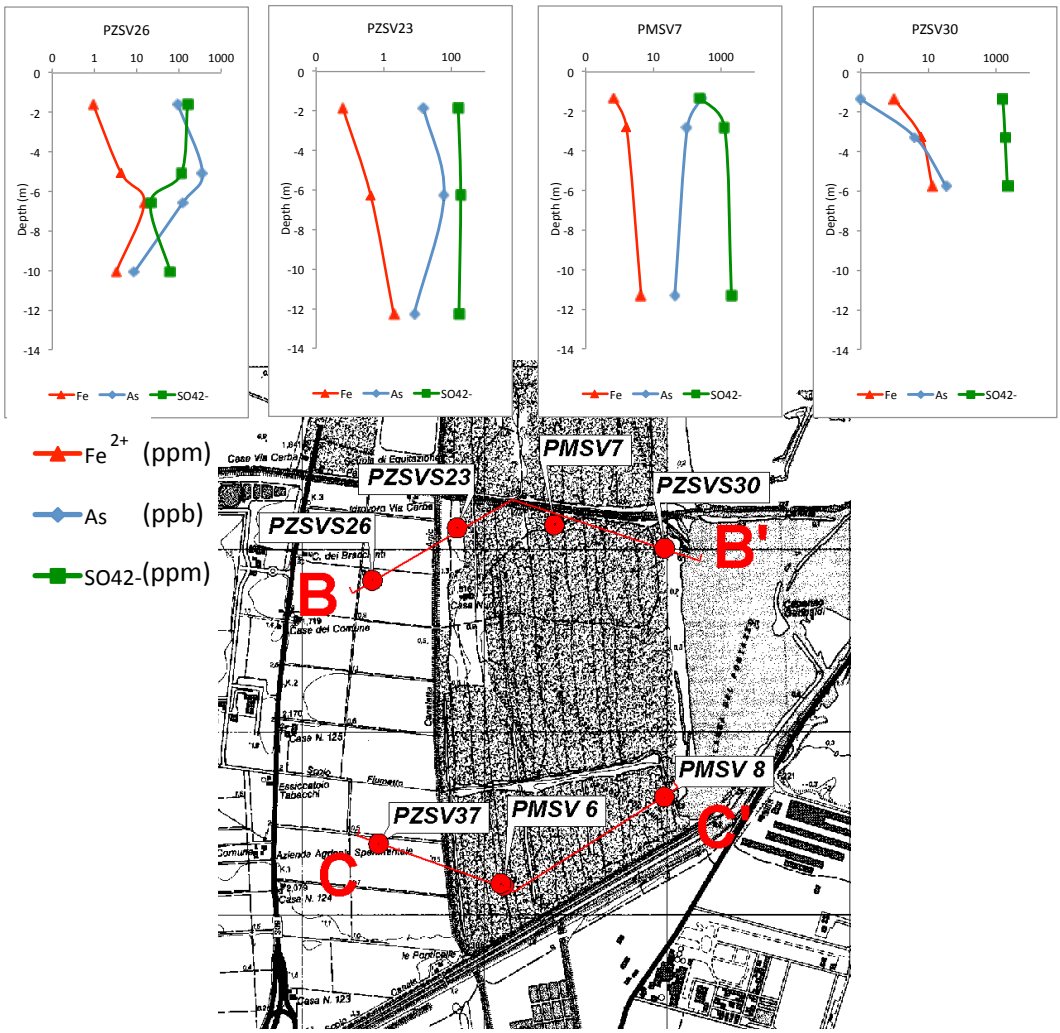

Figure 21: Depth profiles of arsenic, iron and sulphate during the autumn sampling.

Conclusions

This study contributes to a better understanding of the processes affecting the aquifer of the San Vitale pine forest due to the saltwater intrusion, establishing that the environment is governed mainly by geomorphology and human activities.

The depth of the water table is mostly below the mean sea level during all year, promoting the saltwater intrusion in the area except for Punte Alberete area during spring and winter. In agreement with what is expected, this phenomenon is even more pronounced during summerwhen the water table level is on average deeper than in winter.

The use of the depth specific method allows the determination of the evolution of geochemical characteristics along the whole aquifer thickness. Overall the southern part of the pine forest is more salinized than in the north and the seaward area is characterized by saline and hyperhaline waters. The thickness of the transition zone does not vary with the distance from the sea as expected. In the landward area there is a thinning of the mixing zone especially during spring and summer, probably due to the exploitation of the aquifer for irrigational use and the consequent lowering of the water table. In general the thickness of the mixing zone varies seasonally with an enlargement during winter and get thinner again in summer, which indicate the importance of the seasonality and the rain periods in the aquifer recharge.

The calculation of the seawater fraction and the enrichment and/or depletion of ions respect to the theoretical composition is a useful tool to determine the state of the aquifer, as confirmed by the comparison with the BEX calculated through the Stuyfzand method.

In the study area, seawater intrusion and freshening alternates, without having enough time to affect the whole aquifer. Moreover the inversion of the flow results in a series of transient states reflecting physical and chemical processes. The groundwater composition at the seawater/freshwater interface is controlled by the combined effects of ion exchange, calcite and dolomite precipitation, gypsum dissolution and sulphate reduction. This chemical processes are strictly linked each other and could be summarized as follows:

- Na^+ and Mg^{2+} from seawater displaced the freshwater cations Ca^{2+} from the exchanger complex;
- organic matter represents the main ion exchanger;
- degradation of organic matter and gypsum dissolution release ions HCO_3^- which affect the equilibrium of carbonate and dolomite and the ion exchange processes.

The calculated BEX indicate that the area is interested by saltwater intrusion in the eastern part of the pine forest and landward during spring. The surface waters are in equilibrium or subjected to freshening for a deep up to 8 meters in the middle part, parallel to the sea. During summer the deeper freshening zone of the middle part is substituted by salinization, probably due to the scarce recharge of the aquifer and the high evapotranspiration that characterize the summer season. In autumn the fresh/saline interface goes deeper and a freshwater lens in the middle part of the pine

forest characterizes the surface waters.

High concentrations of arsenic were detected in the central part of the pine forest. The observations indicate that its occurrence is limited to a restricted depth, which is probably related to the presence of organic matter. The correlation with Fe^{2+}, HCO_3^- and SO_4^{2-} is in conformity with the characteristics of a strongly reducing aquifer. The depletion of As and Fe^{2+} could be claimed to the precipitation of sulphides and pyrite. The unique high concentrations of As detected in surface reflect the water interchange with the near channel, probably very high in organic matter content.

References

Amorosi, A., Colalongo, M. L., Pasini, G., & Preti, D. (1999). Sedimentary response to Late Quaternary sea-level changes in the Romagna coastal plain (northern Italy). *Sedimentology 46*, 99–121.

Amorosi, A., Centineo, M. C., Dinelli, E., Lucchini, F., & Tateo, F. (2002). Geochemical and mineralogical variations as indicators of provenance changes in Late Quaternary deposits of SE Po Plain. *Sedimentary Geology 151*, 273-292.

Amorosi, A., Centineo, M. C., Colalongo, M. C., Pasini, G., Sarti, G. & Vaiani, S. C. (2003). Facies Architecture and Latest Pleistocene-Holocene Depositional History of the Po Delta (Comacchio Area), Italy. *Journal of Geology. 11*, 39-56.

Amorosi, A., Colalongo, M.L., Fiorinia, F., Fuscoa, F., Pasini, G., Vaiania, S.C., & Sartic, G. (2004), Palaeogeographic and palaeoclimatic evolution of the Po Plain from 150-ky core records, *Global and Planetary Change 40(55),* 55-78.

Amorosi, A. (2008). Delineating aquifer geometry within a sequence stratigraphic framework: Evidence from the Quaternary of the Po River Basin, Northern Italy. In: A. Amorosi, A., Haq B. U., Sabato, L. (Eds.). Advances in Application of Sequence Stratigraphy in Italy. *GeoActa. Special Publication 1*, 1-14.

Andersen, M. S. (2001). Geochemical processes at a seawater-freshwater interface. Ph.D. thesis, Technical University of Denmark, Kgs. Lyngby.

Andersen, M.S., Nyvang, V., Jakobsen, R., & Postma, D. L. (2005). Geochemical processes and solute transport at the seawater/freshwater interface of a sandy aquifer. Geochimica and Cosmochimica Acta 69:3979– 3994.

Antonellini, M., Mollema, P., Giambastiani, B. M. S., Bishop, K., Caruso, K., Minchio, A., Pellegrini, P., Sabia, M., Ulazzi, E., & Gabbianelli, G. (2008). Salt water intrusion in the coastal aquifer of the southern Po Plain, Italy. *Hydrogeology Journal 16*, 1541–1556

Appelo, C. A. J, & Greinaert, W. (1991) Processes accompanying the intrusion of salt water. *In: Breuck WD (ed) Hydrogeology of salt water intrusion - a selection of SWIM paper*s. Heise, Hannover, 291–303

Appelo, C. A. J. (1994). Cation and proton exchange, pH variations, and carbonate reactions in a freshening aquifer. *Water Resources Research, 30*(10), 2793-2805.

Appelo, C. A. J. & Postma, D. L. (2005). *Geochemistry, Groundwater and Pollution.* 2nd ed. Rotterdam. Balkema. 649 p.

ARPA, (Agenzia regionale prevenzione e ambiente dell' Emilia-Romagna)
http://www.arpa.emr.it/pubblicazioni/acqua/generale_675.asp

Banning, A., Coldewey, W.G., & Göbel, P. (2009). A procedure to identify natural arsenic sources, applied in an affected area in North Rhine-Westphalia, Germany. Environmental Geology 57 (4), 775-787 .

Barker, A. P., Newton, R. J., Bottrell, S. H., & Tellam J. H. (1998) Processes affecting groundwater chemistry in a zone of saline intrusion into an urban sandstone aquifer. *Applied Geochemistry* 13 (6), 735–749.

Barrocu, G., Muscas, L., & Sciabica, M. G. (2001). GIS and modeling for studying saltwater intrusion in the Capoterra Alluvial plain (Sardinia, Italy). *Proc. SWICA-M3, Essaouira, Morocco, April 2001.*

Beekman, H.E., & Appelo, C.A.J. (1991) Ion chromatography of fresh- and salt-water displacement: laboratory experiments and multicom- ponent transport modelling. *Journal of Contaminant Hydrology 7*, 21–37.

Berg, M., Pham, T.K.T., Stengel, C., Buschmann, J., Pham, H.V., Nguyen, V.D., Giger, W., & Stuben, D. (2008). Hydrological and sedimentary controls leading to arsenic contamination of groundwater in the Hanoi area, Vietnam: the impact of iron-arsenic ratios, peat, river bank deposits, and excessive groundwater abstraction. *Chemical Geology 249(1-2*), 91-112.

Bhattacharya P, Jacks G, Jana J, Sracek A., Gustafsson JP, Chatterjee D (2001) Geochemistry of the Holocene alluvial sediments of Bengal Delta Plain from West Bengal, India: implications on arsenic contamination in groundwater. In: *Groundwater arsenic contamination in the Bengal Delta Plain of Bangladesh,* Jacks G, Bhattacharya P, Khan AA (eds). KTH Special Publication TRITA-AMI Report 3084, 21–40.

Bibi, M.H., Ahmed, F.. & Ishiga, H. (2008). Geochemical study of arsenic concentrations in groundwater of the Meghna River Delta, Bangladesh. *Journal of Geochemical Exploration 97* (2-3), 43–58.

Bishop, P. K., & Lloyd, J. W. (1990). Chemical and isotopic evidence for hydrogeochemical processes occurring in the lincolnshire limestone. *Journal of Hydrology, 121*(1-4), 293-320.

Bonanni, G. M. (2010). Caratterizzazione geochimica dell'acquifero freatico costiero di Ravenna (area nord). Masterthesis in environmental geochemistry, Università di Bologna.

Bondesan, M., Favero, V., & Viñals, M. J. (1995). New evidence on the evolution of the Po-delta coastal plain during the Holocene. *Quaternaary International 29/30*, 105–110.

Cai ,W. J., Wang, Y., Krest, J., & Moore W. S. (2003). The geochemistry of dissolved inorganic carbon in a surficial groundwater aquifer in North Inlet, South Carolina and the carbon fluxes to the coastal ocean. *Geochimica and Cosmochimica. Acta* **67(4),** 631–637.

Capaccioni, B., Didero, M., Paletta, C., & Didero, L. (2005). Saline intrusion and refreshening in a multilayer coastal aquifer in the Catania Plain (Sicily, southern Italy): dynamics of degradation processes according to the hydrochemical characteristics of groundwater. *Journal of Hydrology 307*, 1–16.

Cardona, A., Carrillo-Rivera, J. J., Huizar-Álvarez, R., & Graniel-Castro, E. (2004). Salinization in coastal aquifers of arid zones: An example from santo domingo, baja california sur, mexico. *Environmental Geology, 45*(3), 350-366.

Cau, P., Lecca, G., Muscas, L., Barrocu, G. & Uras, G. (2002). Saltwater intrusion in the plain of Oristano (Sardinia), *17th Salt Water Intrusion Meeting, Delft, The Netherlands, 6–10 May 2002*, 435–444.

Cruz, J. V., Coutinho, R., Pacheco, D., Cymbron, R., Antunes, P., Freire, P., et al. (2011). Groundwater salinization in the azores archipelago (portugal). *Environmental Earth Sciences, 62*(6), 1273-1285.

Curzi, P.V., Dinelli, E., Ricci Lucchi, M., & Vaiani, S. C. (2006). Paleoenvironmental control on sediment composition and provenance in the late Quaternary deltaic successions: a case study from the Po delta area (Northern Italy). *Geological Journal 41*, 591-612.

Custodio, E. & Bruggeman, K.A., (1987). Groundwater Problems in Coastal Areas UNESCO, Paris.

CSI project, (2011). Rapporto Finale progetto Coastal Salt Intrusion. Convenzione tra ENI, Comune di Ravenna e Lab. IGRG.

De Luca, A., Preziosi, E., Giuliano, G., Mastroianni, D., & Falconi, F. (2005). First evaluation of the saltwater intrusion in the Tiber delta area (Rome, central Italy). *18th Salt Water Intrusion Meeting, Cartagena, Spain, 31 May–3 June 2004*, 34

de Montety, V., Radakovitch, O., Vallet-Coulomb, C., Blavoux, B., Hermitte, D., & Valles, V. (2008). Origin of groundwater salinity and hydrogeochemical processes in a confined coastal aquifer: Case of the Rhône delta (southern France). *Applied Geochemistry, 23*(8), 2337-2349.

Dellwig, O., Böttcher, M. E., Lipinski, M., & Brumsack, H. J. (2002). Trace metals in Holocene coastal peats and their relation to pyrite formation (NW Germany). *Chemical Geology 182 (2-4),* 423–442.

Doveri, M., Giannecchini, R., & Butteri, M. (2010). Seawater intrusion in the Versiliese-Pisan coastal aquifer system (north-western Tuscany): results from a hydrogeologic-hydrogeochemical study. *21th Salt Water Intrusion Meeting, Azores, Portugal, 21-26 June*, 150-153.

Du Laing, G., Chapagain, S. K., Dewispelaere, M., Meers, E., Kazama, F., Tack, F. M. G., Rinklebec, J. & Verlooa, M. G. (2009). Presence and mobility of arsenic in estuarine wetland soils of the Scheldt estuary (Belgium), *Journal of Environmental Monitoring 11(4)*, 873–881.

El Yaouti, F., El Mandour, A., Khattach, D., Benavente, J., & Kaufmann, O. (2009). Salinization processes in the unconfined aquifer of bou-areg (NE morocco): A geostatistical, geochemical, and tomographic study. *Applied Geochemistry, 24*(1), 16-31.

Giambastiani, B. M. S., Antonellini, M., Oude Essink, G. H. P., & Stuurmann, R. J. (2007). Saltwater intrusion in the unconfined coastal aquifer of Ravenna (Italy): A numerical model. *Journal of Hydrology 340*, 91-104.

Glover, R.E. (1964). The pattern of fresh-water flow in a coastal aquifer. *In: Sea water in coastal aquifers. US Geological Survey water Supply Paper. 1613-C*: 32-34.

Gomis-Yagües, V., Boluda-Botella, N., & Ruiz-Beviá, F. (2000). Gypsum precipitation/dissolution as an explanation of the decrease of sulphate concentration during seawater intrusion. *Journal of Hydrology, 228*(1-2), 48-55.

Haque, S.E., & Johannesson, K.H., (2006). Concentrations and speciation of arsenic along a groundwater flow-path in the upper floridan aquifer, Florida, USA. *Environmental Geology 50(2)*, 219–228.

Hasan, M., Brömssen, M., Bhattacharya, P., Ahmed, K., Sikder, A., , Jacks, G., & Sracek O. (2009). Geochemistry and mineralogy of shallow alluvial aquifers in Daudkandi upazila in the Meghna flood plain, Bangladesh. *Environmental Geology 57(3),* 499–511.

Islam, FS, Boothman, C, Gault, AG, Polya, DA, & Lloyd, JR (2005). Potential role of the Fe(III)-reducing bacteria Geobater and Geothrix in controlling arsenic solubility in Bengal delta sediments. *Mineralogical Magazine 69*, 865–875.

Itai, T., Masuda, H., Seddique, A.A., Mitamura, M., Maruoka, T., Li, X., Kusakabe, M., Dipak, B.K., Farooqi, A., Yamanaka, T., Nakaya, S., Matsuda, J-i., & Ahmed, K.M. (2008). Hydrological and geochemical constraints on the mechanism of formation of arsenic contaminated groundwater in Sonargaon, Bangladesh, *Applied Geochemistry, 23(11)*, 3155-3176.

Keimowitz, A.R., Mailloux, B.J., Cole, P., Stute, M., Simpson, H.J., & Chillrud, S.N., (2007). Laboratory investigations of enhanced sulfate reduction as a groundwater arsenic remediation strategy. *Environmental Science & Technology 41(19)*, 6718–6724.

Kirk, M.F., Holm, T.R., Park, J., Jin, Q., Sanford, R.A., Fouke, B.W., & Bethke, C.M., (2004). Bacterial sulfate reduction limits natural arsenic contamination in groundwater. *Geology 32(11)*, 953–956.

Lear, G., Polya, D. A., Song, B., Gault, A.G., & Lloyd, J.R., (2007). Molecular analysis of arsenate-reducing bacteria within Cambodian sediments following amendment with acetate. *Applyed and Environmental Microbiology 73(4)*, 1041-1048.

Magaritz M. & Luzier J. E. (1985). Water–rock interactions and seawater–freshwater mixing effects in the coastal dunes aquifer, Coos Bay, Oregon. Geochimica and Cosmochiica. Acta 49(12), 2515–2525.

Martinez, M.E., & Bocanegra, E.M. (2002). Hydrochemistry and cation- exchange processes in the coastal aquifer of Mar Del Plata, Argentinia. *Hydrogeol Journal 10*,393–408.

McArthur, J.M., Ravenscroft, P., Safiulla, S., & Thirlwall, M.F., (2001). Arsenic in groundwater: testing pollution mechanisms for sedimentary aquifers in Bangladesh. *Water Resources Research 37(1)*, 109–117.

McArthur, J.M., Banerjee, D.M., Hudson-Edwards, K.A., Mishra, R., Purohit, R., Ravenscroft, P., Cronin, A., Howarth, R.J., Chatterjee, A., Lowry, D., Houghton, S., & Chadha, D.K. (2004) Natural organic matter in sedimentary basins and its relation to arsenic in anoxic ground water: the example of West Bengal ant its worldwide implications. *Applied Geochemistry 19(8)*, 1255–1293.

Melo, M. T. C., Marques da Silva, M. A., & Edmunds, W. M. (1999). Hydrochemistry and flow modelling of the Aveiro Multilayer Cretaceous Aquifer. *Physics and Chemistry of the Earth* **24,** 331–336.

Morse, J. W., Millero, F. J., Cornwell, J. C., & Rickard, D. (1987). The chemistry of the hydrogen sulfide and iron sulfide systems in natural waters. *Earth Science Reviews, 24*(1), 1-42.

Nadler, A., Magaritz, M., & Mazor, E. (1980). Chemical reactions of seawater with rocks and freshwater: experimental and field observation on brackish waters in Israel. *Geochimica Cosmochimica Acta 44*, 879–886.

Nath, B., Berner, Z., Basu Mallik, S., Chatterjee, D., Charlet, L., & Stueben, D., (2005). Characterization of aquifers conducting groundwaters with low and high arsenic concentrations: a comparative case study from West Bengal, India. *Mineralogical Magazine. 69(5)*, 841–853.

Nath, B., Stueben, D., Basu Mallik, S., Chatterjee, D., & Charlet, L., (2008). Mobility of arsenic in West Bengal aquifers conducting low and high groundwater arsenic, part I: comparative hydrochemical and hydrogeological characteristics. *Applyed Geochemistry 23(5)*, 977-995.

Nickson, R.T., McArthura, J.M., Ravenscroftb, P., Burgessa, W.G., & Ahmedc, K.M. (2000). Mechanism of arsenic release to groundwater, Bangladesh and West Bengal. *Applied Geochemistry 15(4),* 403-413.

Panteleit, B., Kessels, W., & Schulz, H.D. (2003). Geochemical processes in the salt-freshwater transition zone—exchanger reactions in a 2D- sand-tank experiment. *In: Hadeler A, Schulz HD (eds) Geo- chemical Processes in soil and groundwater—measurement– modeling–upscaling*. Wiley VCH, Weinheim, 596–610

Parkhurst, D. L. & Appelo, C. A. J. (1999). User`s guide to PHREEQC (version 2) – a computer program for speciation, batch-reaction, one-dimensional transport, and inverse geochemical calculations*. U. S. Geological Survey Water Resources investigation report 99-4259*. 312.

Pieri, M. & Groppi, G., (1981). Subsurface geological structure of the Po Plain, Italy. *Progetto Finalizzato Geodinamica, C.N.R., Publ. 414*.

Polemio, M., Casarano, D., & Limoni, P. P., (2010). Apulian coastal aquifers and management criteria. *21th Salt Water Intrusion Meeting, Azores, Portugal, 21-26 June*, 203-206.

Pranzini, G. (2002). Groundwater salinization in Versilia (Italy). *17th Salt Water Intrusion Meeting, Delft, The Netherlands, 6–10 May 2002*, 412–421

Pulido-Leboeuf, P. (2004). Seawater intrusion and associated processes in a small coastal complex aquifer (Castell de Ferro, Spain). *Applied geochemistry* 19(10), 1517–1527.

Russak, A., & Sivan, O. (2010). Hydrogeochemical tool to identify salinization or freshening of coastal aquifers determined from combined field work, experiments, and modeling. *Environmental Science and Technology, 44*(11), 4096-4102.

Scheidleger, A., Grath, J., & Lindinger, H. (2004). Saltwater intrusion due to groundwater over-exploitation EEA inventory throughout Europe. *18th Saltwater Intrusion Meeting, Cartagena, Spain, 31 May–3 June 2004*, 125

SEHUMED, (2000). Mediterranean Wetlands Technical Data – Punte Alberete (Italy). SEHUMED. No. 15.09.2000.

Selim Reza, A.H.M., Jiin-Shuh, Jean, Ming-Kuo Lee, Huai-Jen Yang, Chia-Chuan Liu (2010) Arsenic enrichment and mobilization in the Holocene alluvial aquifers of the

Chapai-Nawabganj district, Bangladesh: A geochemical and statistical study. *Applied Geochemistry 25(8)*, 1280–1289.

Selli, R., & Ciabatti, M. (1977). L'abbassamento del suolo della zona litoranea ravennate. *Giornale di Geologia 42 (1)*, 1–47.

Stefani, M. & Vincenzi, S. (2005). The interplay of eustasy, climate and human activity in the late Quaternary depositional evolution and sedimentary architecture of the Po Delta system*. Marine Geology 222-223*, 19-48.

Stoessell, R. K., Moore, Y. H., & Coke, J. G. (1993). The occurrence and effect of sulfate reduction and sulfide oxidation on coastal limestone dissolution in Yucatan Cenotes. *Ground Water 31(4),* 566–575.

Stuyfzand, P. J. (1986). A new hydrogeochemical classification of watertypes: Principles and application to the coastal dunes aquifer system of the Netherlands. *Proceedings. 9th Salt Water Intrusion Meeting. Delft*. ,641-656

Stuyfzand, P. J. (1989). An accurate, relatively simple calculation of the Saturation Index of Calcite for Fresh to Salt Water*. Journal of Hydrology. 105*, 95-107.

Stuyfzand, P.J. (2008). Base exchange Indices as Indicators of salinization or Freshening of (Coastal) Aquifers. *20th Salt Water Intrusion Meeting. 23-27 June, Naples, USA*

Teatini, P., Ferronato, M., Gambolati, G., & Gonella, M. (2006). Groundwater pumping and land subsidence in the Emilia-Romagna coastland, Italy: modeling the past occurrence and the future trend. *Water Resources Research 42*, 1–19.

Trabelsi, R., Abid, K., Zouari, K., & Yahyaoui, H. (2011). Groundwater salinization processes in shallow coastal aquifer of djeffara plain of medenine, southeastern tunisia. *Environmental Earth Sciences,* , 1-13.

Van Straaten, L.M.J.U. (1970). Holocene and Late Pleistocene sedimentation in the Adriatic Sea. *Geologische Rundschau 60*, 106-131.

Veggiani, A. (1971). Inquadramento geologico dei sondaggi geotecnici nell'area antistante la costa adriatica ravennate. *Atti 2nd Conv. St. Probl. Geol. Appl.*, Genova, 1-7.

Veggiani, A. (1974). Le variazioni idrografiche del basso corso del fiume Po negli ultimi 3000 anni. *Padusa 1–2*, 39–60.

PART II

Aqueous and sediment geochemistry of acid mine drainage in the San Juan de Sora Sora basin (Bolivia)

Abstract

Water and sediment quality in the San Juan de Sora Sora river basin is affected by acid mine drainage (AMD) from three main mines (mainly on cassiterite deposits). The area, with a population over 50.000 inhabitants approx., is located in the Oruro department, Bolivia. Concentrations of trace metals and REE were determined in stream waters, groundwater wells, suspended materials and bedload sediments. Moreover, a BCR sequential extraction (four-stage) were applied in bedload and suspended sediment in order to better constrain mobility and relative sources of trace metals and REE.

The main stream and tributaries waters are characterized by strongly acidic conditions (pH 2.9-4.5), elevated SO42- concentrations (up to 2400 mg/L), and high metal contents (especially Fe, Zn, Cd, Ni, Pb). Hydrochemistry coupled to sequential extraction allow the characterization of the contribution of the three considered main mines. The decrease in trace metal concentrations in waters during the wet season are associated to the dilution effect, instead for iron, subject to precipitation. The presence of trace elements in some groundwater sample during the wet season reflect its connection with the surface waters.

The sequential extraction shows differences in partitioning and total concentration between suspended and bedload sediment, with higher metal concentrations and exchangeable fraction in the suspended material. Cd, Zn and Cu seem related to the oxidizable fraction.

General context, materials and methods

Introduction

Mine wastes are the largest volume of materials handled in the world. The generation of acidic drainage and the release of water containing high concentrations of dissolved metals from these wastes is an environmental problem of international scale (Blowes et al., 2003). Movement of contaminants in and near mining sites is a complex function of the geology, hydrology, geochemistry, pedology, meteorology, microbiology, and mining and mineral processing history (Nordstrom and Alpers, 1999a). At most sites, pyrite-rich ores are the main source of acid mine drainage (AMD), which may have adverse impacts on biota (Gray, 1997). Pyrite-rich ores in industrialized countries have been extensively investigated (Alpers et al., 2003; Audry et al., 2005; Sanchez España et al., 2005; Salvarredy-Araguren et al. 2008; Nordstrom and Alpers, 2000). However, in the last decades an important part of mining exploitation has been performed in the developing countries, where scientific investigations are less common.

In South America, studies dealing with mining contamination have mainly focused on contamination in Chile (Dittmar, 2004; Dold and Fontbote, 2002; Oyarzun et al., 2004; Romero et al., 2003; Smedley and Kinniburgh, 2002) and in Brasil (Lodenius and Malm, 1998; Pfeiffer et al., 1993; Wasserman et al., 2003).

In the last years some scientific studies have evaluated problems related to mining contamination in Bolivia (Bervoets et al., 1998; Espi et al., 1997; Oporto et al., 2007) and geochemical behavior at mine sites with the focus on trace metals in surface and groundwater and sediments (Quino 2006; Lilja and Linde 2006; Salvarredy-Aranguren, 2008; Maurice-Bourgoin et al., 2003; Miller et al. 2004; Smolders et al., 2003; 2004; Ramos Ramos et al., 2011; Rojas 2007; Selander and Svan 2007; Cáceres et al. 2004; Hudson-Edwards et al., 2001; Villaroel et al.2006; Oruro Pilot Project (PPO 1992, 1996a, b, c, 1997; Strosnider et al., 2011).

Bolivia has a long mining history dating back as far as 1000 AD, when the Tiwanaku and later the Inca civilizations started the mineral extraction (Abbott and Wolfe, 2003). With the Spanish colonization, extraction and processing ratio took different proportions. Since 1545 an intensive mining and processing of Ag, Sn, Pb and Zn ores have occurred in various locations and in the last century Bolivia became one of the largest producer of Sn in the world (Montes de Oca, 1982). Large and medium scale mining activities were intensively developed in several regions of the country resulting in significant environmental damage (Chatelain and Wittinton, 1992).

The Huanuni Basin is located at more than 4000 m above sea level (a.s.l.) in the Bolivian tin Belt. Mining is the main economic activity of the area. The rise of mineral prices in the period 2006-2008 revitalized this activity with the opening of abandoned mines and creation of workers cooperative that operate without any control over the consequent environmental and social impact. In the area a very large volume of sulfide-rich mine waste has been deposited and waste rock and mill tailings directly discharged into the rivers by different mining operations creating a permanent source of pollution (Miller et al., 2004; Reif et al., 1989; Smolders et al., 2003).

Surface- and ground- waters, stream sediments and soils are contaminated with various ecotoxic metals in the highly impacted rivers of Huanuni basin. Previous studies have documented trace metal contamination in sediments (Tapia et al., 2012) and in waters (Ny, 2009; Rosenberg 2010) without addressing specific sources. The AMD discharges identified in this study help to link downstream pollution to primary origins.

Outline and objectives of the study

The aims of this study were to:

- ✓ characterize the intensity and the sources of the mining contamination in the Huanuni basin, focusing on surface- and groundwaters, and bedload and suspended sediments;
- ✓ evaluate the importance of the seasonality in the contamination propagation;
- ✓ determine the geochemical and mineralogical processes involved in water and sediment water contamination;
- ✓ study the interactions between surface- and ground-waters, suspended sediment and stream waters in the contaminant behavior

Study Area

Geomorphologic framework

The study area is located in the Oruro department of Bolivia represented in Figure 1. It consists of two physiographic units: the Eastern Cordillera and the Altiplano. Eastern Cordillera consists of mountains ranges up to 4000-4500 m in altitude, separated by deep valleys. The Central Altiplano Plateau is a c. 200000 km^2 intermontane endorheic and tectonic basin which formed during the Pliocene and Early Pleistocene (some 3-2 My) stretching from Peru in the north to Chile in the south. This high plateau at above 3700 m a.s.l. lying between the western and eastern Andes Cordillears is filled with predominantly Quaternary continental deposits.

The two physiological units, the Eastern Cordillera and the Altiplano, have distinct morphological, structural and geological habits and are separated by the Poopó-Uyuni fault system (Troëng and Riera, 1996a; 1996b; 1998). Andean tectonism is the reason of most of the tectonic features in the area. The major processes of mountain formation in that area took place during the late Devonian, late Triassic, and throughout the late Tertiary and Quaternary. The bedrock in the area is dominated of folded Lower Palaeozoic marine clastic sediments and extensive Quaternary deposits cover the Altiplano, to the west of the fault. The Eastern Cordillera is a series of Paleozoic sediments from the Ordovician to the Devonian, a Mesozoic sequence from the Jurassic to the Cretaceous and some Tertiary sediment. Above the rocks Tertiary volcanic rocks have been deposited in different effusive volcanic fields (Troëng and Riera, 1996; Cunningham et al., 1991; Banks et al., 2004). The geology of the area is shown in Figure 2 and includes also the location of the study area.

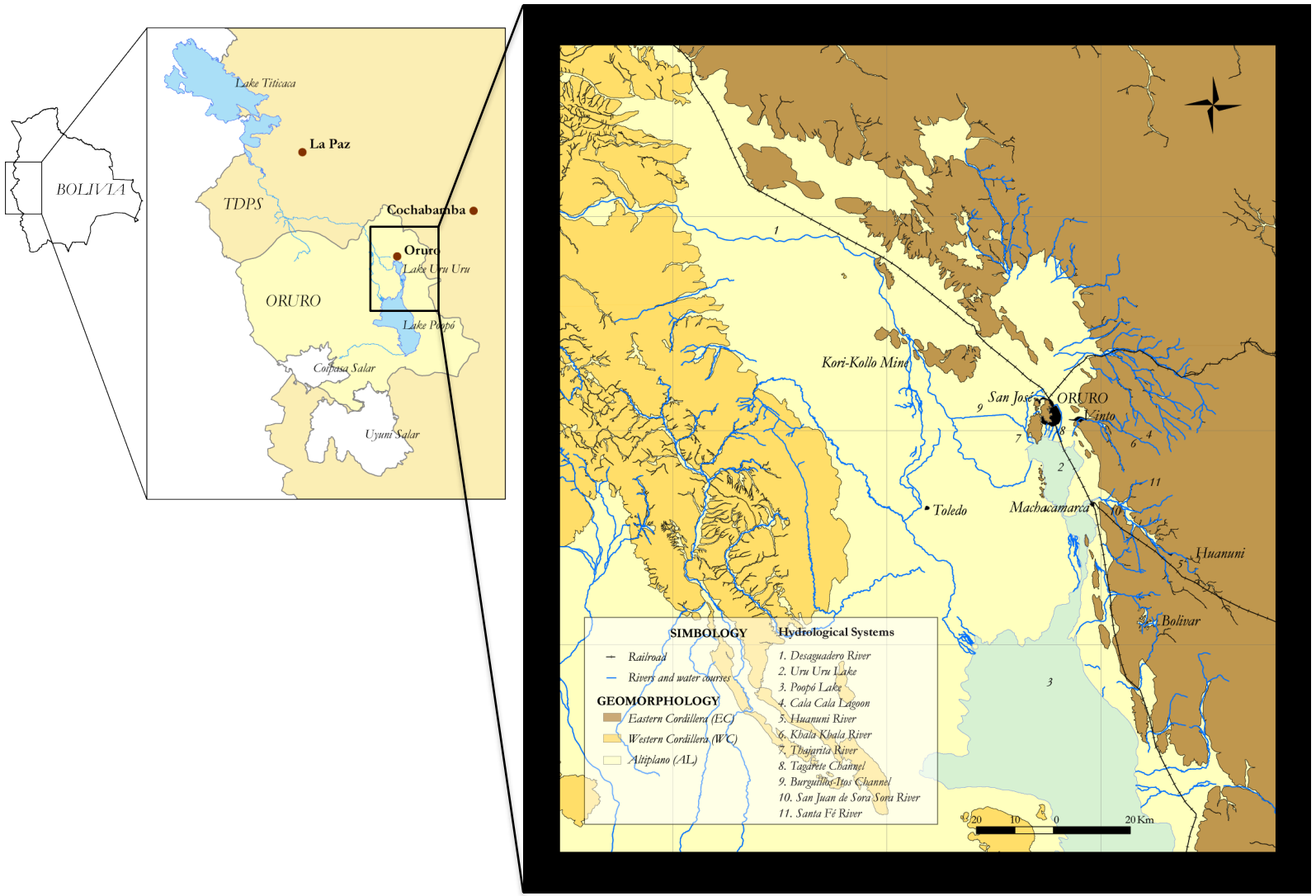

Figure 1: Geomorphologic setting of the study area, western Andes Cordillera, Altiplano and eastern Andes Cordillera (Tapia et al., 2012).

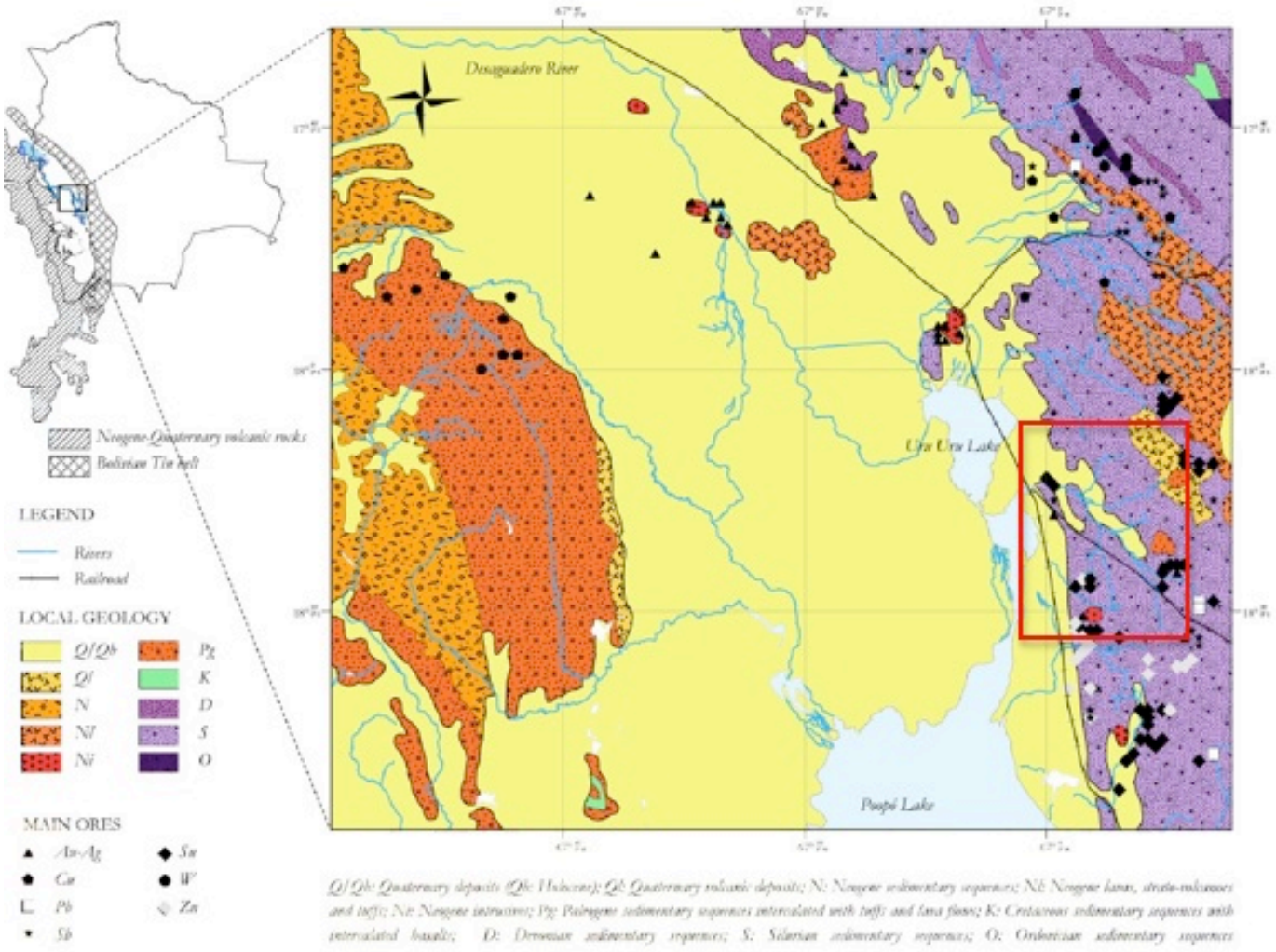

Figure 2: Geological setting of the Altiplano and Eastern Cordillera (Tapia et al., 2012). The red square indicate the study area.

Hydrology and climate

The hydrology of the area can be described by the endorheic TDPS-system (Lake Titicaca- Desaguadero River- Lake Popoo- Salar Coipasa) (Figure 1). Lake Titicaca corresponds to a large (c. 8000 km2), warm, monomictic lake at an altitude of c. 3800 m. It is located in the northern part of the Altiplano between Perú and Bolivia. The lake drains to the south via the Desaguadero River to Lake Poopó and Lake Uru Uru through two arms. Lakes Poopó and Uru Uru are located in the central Altiplano, both are shallow (< 6 m) and exhibit highly variable surface area varying between dry season (DS) and wet season (WS) depending on precipitation and evaporation. These lakes are highly correlated with the Desaguadero River discharges; therefore the volume and extension are associated to Lake Titicaca water level, governed by the El Niño Southern Oscillation (ENSO) events (Markgraf, 2001). Further south, Coipasa Salar is located in the topographic low of the southernmost central Altiplano. During rainy years this Salar connects Lake Poopó through Río Laca Jahuira yet most of the time both basins are not permanently linked (Risacher and Fritz, 1991).

The study area is part of the Poopó basin, a region characterized by an arid to semi-arid climate. The total annual precipitation has a mean of ~400 mm, with a remarkable difference between the rainy season (~250 mm) and the dry season (~11mm) (SENAMHI, 2011). The rainy season takes place during the austral summer, from December to March, and is characterized by an intense convective activity combined with moisture advection from the Amazon basin (Garreaud, 1999). During austral winter, the eastern moist flux is replaced by westerly winds, which provide dry air related to the atmospheric stability over the Pacific Ocean. In these conditions, rainfall events are due either to the northward motion of Pacific cold fronts or to polar air intrusion along Chile (cut-offs) (Vuille and Amman, 1997).

The precipitation over the area is sensitive to variations in the large-scale circulation patterns. These variations are expressed as inter-annual variability in the precipitation. The effects of El Niño-Southern Oscillation (ENSO) on the atmospheric circulation are observed as variations in the amount of precipitation in the Altiplano, so that El Niño years are related to below-normal precipitation and La Niña years to the opposite (Pillco Zolá and Bengtsson, 2006).

The mean temperature is 10°C, but it greatly varies during the day from -10°C to 14°C in the winter and from -2°C to 18°C in the summer (Rocha, 2002). The mean potential evaporation rate over the entire Altiplano is estimated at more than 1500 mm $year^{-1}$ (Roche et al., 1992). Precipitation and potential evapotranspiration are approximately equal in January and February. Potential monthly evapotranspiration greatly exceeds average rainfall from March to December and soils suffer a permanent moisture deficit and a consequent increase in salinity (Binford et al., 1997).

Ore geology

In Bolivia, more than 15 types of metallic mineral deposits have been recognized (Figure 3), demonstrating the great variety of metallic resources that characterize the most prolific geological and metallogenic environment of the continent (Arce Burgoa, 2009). The Bolivian Orogen can be divided into four metallogenic belts, the Polymetallic Belt of the Altiplano and Western Cordillera, the Tin Belt, the Gold-Antimony Belt, and the Lead-Zinc Belt (Arce-Burgoa 2009). In the Altiplano and the western Andes Cordillera Sedimentary-Rock Hosted Copper Deposits correspond to Miocene to Pliocene stratiform copper deposits scattered along the length of the Altiplano, while the Polymetallic Belt is mainly composed of epithermal Ag-Au-Pb-Zn-Cu deposits formed during the Middle-Late Miocene and Early Pliocene (Arce-Burgoa 2009).

The eastern Andes Cordillera is the host for most of the mineral resources of Oruro Department and includes the well-known Bolivian Tin Belt, the Gold-Antimony Belts and the Lead-Zinc Belt. The Bolivian tin belt is a 900 km long belt extending east-west throughout Bolivia from northernmost Argentina to southernmost Perù Argentina and shows great variations in type, age and mineral contents.

Mineralization in the southern part of Bolivian tin belt occurs as quartz-cassiterite-sulphide veins including the historically important silver-rich veins, many of which are presently mined for zinc with silver as a by-product (Grant et al., 1980). In the veins, cassiterite + quartz occur as an early 'oxide stage' of precipitation, followed by pyrrhotite + sphalerite + galena + chalcopyrite. Quartz, muscovite and tourmaline are the typical minerals of the altered wall rock bordering the cassiterite veins. Sericitization is especially common in altered igneous rocks. Fluorite and apatite are reported at Huanuni, and rare topaz occurs with tourmaline and quartz at Morococala. Boron (tourmaline) is a characteristic and very abundant component of the hydrothermal tin ore system (Müller et al., 2001).

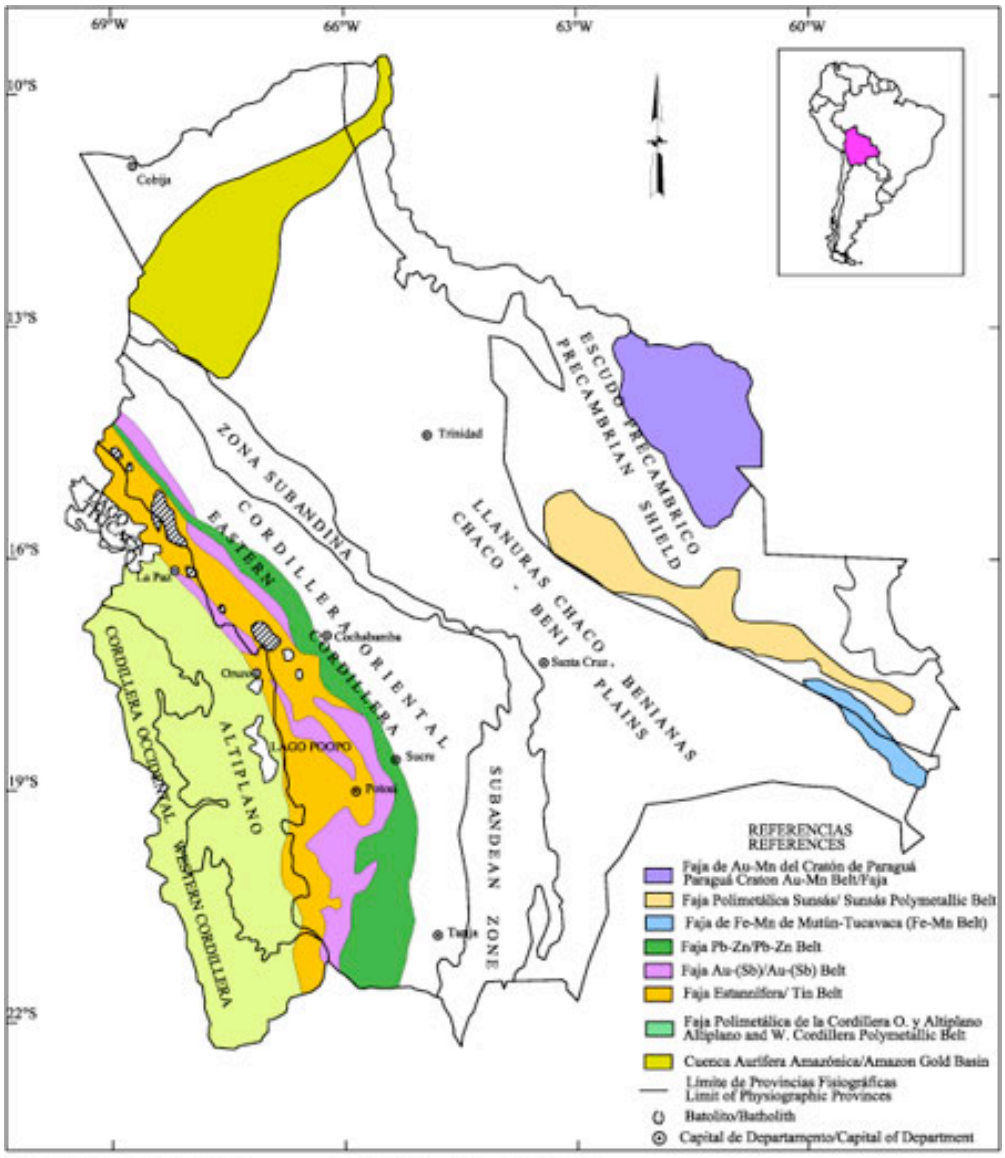

Figure 3: Metallogenic belts in Bolivia (Arce Burgoa, 2009).

Vegetation and land use

The vegetation in the Poopó area is typical for the Altiplano and is called Puna Seca, dry Andean highland, where perennial grasses cover most of the land. The vegetation in the area of Lake Poopó is strongly influenced by earlier uses of trees as fuel and for construction purposes, which have resulted in an eradication of all trees. On the hillsides in the Poopó basin the vegetation mostly consists of bushes and cactuses, adapted to high altitude and rocky ground. Many of the plants in the area are halophytes, which can manage in environments with high contents of salts (Rosenberg and Stålhammar)

Many small communities are present in the study area. The inhabitants of the Altiplano mainly earn their livings by breeding livestock primarily cattle and sheep. As most people in the area are dependent on the grazing of animals, the land is suffering from overgrazing (PPO 9608). To a lesser degree the soils are used for cultivation of potato, barley, quinoa, cañahua etc (Montes de Oca, 1982). The agriculture is sustained by

irrigation and seasonal rain. In the mountains the main activity, apart from livestock and agriculture, is mining which contribute to high pollution of minerals in lakes, rivers and soil. Wastewater from the mining activities is sometimes dumped into rivers without proper treatment, mainly from small-scale mining. This in addition to natural contamination and pollution from human activity and agriculture will result in high concentrations of pollutants in the water. Despite the pollutants and the high salinity, river water is used for irrigation and the groundwater is used for household needs such as cooking and drinking water for humans and animals (Pillco and Calizaya, 2008; Ny and Mikaelsson, 2010).

Mine activities in the area

The main mine activities extracting tin in the Huanuni basin are the 'Empresa Minera Huanuni' (EMH) and the mine corporation of Santa Fe, composed by the mines Japo and Morococala.

The EMH is located 47 km far from the city of Oruro, at an altitude of 3925 m in the Posokoni Mountain. The EMH, is actually the main mine centre of Bolivian country, regarding the exploitation volumes and the employers.

The ore deposit in the area was discovered in 1745 and during the years, many changes in the management of the mine occur. Nowadays the extraction processes are managed by the national corporation COMIBOL. In 2006, an important incorporation of the independent workers took place; that of the people used to re-mobilize the sediment after the mine discharge in order to recover the tin not extracted by the mine processing. The employees grew up from 700 to 4560 and the extraction volumes increase from 400 to 1000 ton/day (now rising to1400 ton/day). The average tin composition is 3.6 % in actual reserves, but reaches up to 30 % in certain ore shoots. The ore deposits mainly consist of the minerals cassiterites with sphalerites and sulfostannates (Sn, Zn, Ag) but minor deposits of sulfosalts-sphalerites-sulfostannates with galena (Ag, Sn, Zn, Pb), wolframite- ferberite with stibnite (W, Sb) and sphalerite-argentiferous galena (Zn, Pb, Ag) also exists (Troëng and Riera, 1996b).

The extracted mineral is processed in two plant; Santa Elena, part of the Huanuni mine complex, with a rating of 1200 ton/day and Machacamarca, located 15 km downstream, that processes nearly 200 ton/day. After the processing of the mineral the total extracted amount is 500-850 ton/month with a mean lay of 43%. These extracting processes use the 69% of the total amount of the surface waters. (López et al., 2010)

Ore deposits of the Santa Fe area are known since 1888. During the years, tin and Ag-Pb-Zn complex were extracted in the area. In the '80 the mines closed due to the economic crisis. In the last years, due to the increase in the tin economic value, some private workers reopened the existing mines and formed the Santa Fe Corporation. There is no data about the production quantities and the quality of the final product.

The main contamination sources of the area due to tin extraction are:

- mill tailing- (residual material, including sulphide gangue minerals, that is discharged to tailings impoundments, typically as a slurry of water and finely ground rock) directly discharged in the river

- the solid waste deposited over the years in many areas around the mines that undergoes leaching

Materials and methods

Sampling

Samples were collected during two sampling campaigns centered on the most extreme periods of the dry and wet seasons of one water-year. The first sampling was performed in the dry season in June 2009 and the second in March 2011 representing the wet season.

In both seasons, the sampling was performed at surface- and ground- waters, stream and bedload sediments. The sampling sites were chosen to represent the entire San Juan de Sora Sora basin, impacted mainly by three active mines Huanuni, Morococala and Japo, sparse small-scale mining and the re-processing activities of the river sediment.

Sampling was designed to assess the influence of the mining activities in the area (Figure 4), the sampling points were chosen along the major rivers of the area: the San Juan de Sora Sora River and its two major tributaries Huanuni and Santa Fe Rivers.

Along the Huanuni River 8 sites were chosen. The first HA-1 is located upstream the Huanuni mine, in order to determine the background characteristics of the area. The others sites are situated downstream the mine, HA-2 was sampled after the mine discharges, HA-3 in an area of river sediments re-processing, HA-4 near the discharge in the river of the Huanuni village sewage system, HA-5 at the confluence with the Ventaimedia river, HA-6, 7 and 8 along the large sediment valley till the confluence with the Santa Fe river. The H-8b sampling point is outcrop of different kind of water.

Two samples were taken along the Ventaimedia River, a tributary of Huanuni River, which is not impacted by mining extractions, in order to characterize an unpolluted area.

Santa Fe River carries waters coming from two mines, Japo and Morococala. The sample JAPO was taken in the Japo River, a tributary of Santa Fe, just below the Japo mine discharge, the same was done for the SF-1, taken downstream the Morococala mine. No possibility was found to sample upstream the mines, as both of them are located on the riverhead. Sample SF-2 was taken downstream the confluence of the two rivers (Japo and Santa Fe), characterized by high gradient and a stony riverbed, SF-3 was sampled in a sediment re-processing area and SF-4 in the valley before the confluence with the Huanuni River and the formation of the San Juan de Sora Sora River.

Along the San Juan de Sora Sora River 4 sites were sampled SSA-1, 2 in the valley, SSA-3 after the processing plant of Machacamarca and sample SSA-2b was taken from red coloured waters just before the Machacamarca village.

For all that points the sampling of stream waters, bedload sediments was performed.

Ground waters were sampled through 7 private wells, pumped with mechanic or manual peristaltic pumps. There is no data about the depth of the water table and some pH and temperature values of the first sampling campaign are missing.

Three sampling points W-1, 2 3 are located in the valley before the San Juan de Sora Sora River flow in the Uru Uru lake, other wells were sampled along the valley in distinct villages, W-4 in the Raelenga Village, W-5 in the Carbuyo Village, W-6 at res Pozos and W-7 in Pacopampa Villages.

The sampling points are shown in the Figure 4 and the Table1 presents the sampling points, the location in UTM coordinate system, the distance from the mine discharge in kilometres and the sampled matrix. W indicates surface waters, BS bedload sediments, SS suspended sediments and GW groundwaters.

Table 1: Location of the sampling points, distance from the mine discharge and sampled matrix (W= surface water, BS= bedload sediment, SS= suspended sediment, GW= groundwater).

Sampling point	X	Y	Location	mine discharge (km)	Sampled matrix
Ventaimedia River					
VA-1	726343	7976023	Ventaimedia village	no discharge	W-BS
VA-2	725207	7977970	Before the confluence with the Huanuni River	no discharge	W-BS
Huanuni River					
HA-1	731095	7976201	Upstream the Huanuni mine	-1	W-BS
HA-2	729209	7976787	Huanuni mine discharge	0	W-BS
HA-3	728191	7976775	River sediments re-processing site	2	W-BS-SS
HA-4	725258	7978660	Near the discharge in the river of the Huanuni village sewage system	6	W-BS
HA-5	724856	7978621	After the confluence with the Ventaimedia River	7	W-BS-SS
HA-6	722447	7982414	Along the large sediment valley	13	W-BS
HA-7	720188	7983960	Along the large sediment valley	15	W-BS
HA-8	717431	7987413	Along the large sediment valley	20	W-BS
San Juan de Sora Sora River					
SSA-1	715710	7989641	Confluence with the Santa Fe River	23	W-BS-SS
SSA-2	712969	7990335	Before the Machacamarca village	26	W-BS
SSA-3	708085	7989527	After Machacamarca village	31	W-BS
Japo ans Santa Fe River					
Japo-1	727561	7999777	Japo mine discharge	0	W-BS
SF-1	732370	7992766	Morococala mine discharge	0	W-BS
SF-2	726427	7989512	After the confluence with Japo River	7	W-BS
SF-3	723875	7988730	Along the Santa Fe River	10	W-BS
SF-4	717346	7988386	Before the confluence with San Juan de Sora Sora River	15	W-BS
Outcrops					
HA-8B	717576	7987350	Waters used for the Machacamarca plant and irrigation	20	W-BS
SSA-2B	712969	7990335	Red waters before Machacamarca village	26	W-BS
Wells					
W-1	706890	7993017	North of the San Juan de Sora Sora mouth		GW
W-2	708452	7993034	North of the San Juan de Sora Sora mouth		GW
W-3	710744	7992460	North of the San Juan de Sora Sora mouth		GW
W-4	713152	7991179	Raelenga Village		GW
W-5	716903	7989528	Carbuyo Village		GW
W-6	717569	7989159	Tres Pozos Village		GW
W-7	718079	7986615	Pacopampa Village		GW

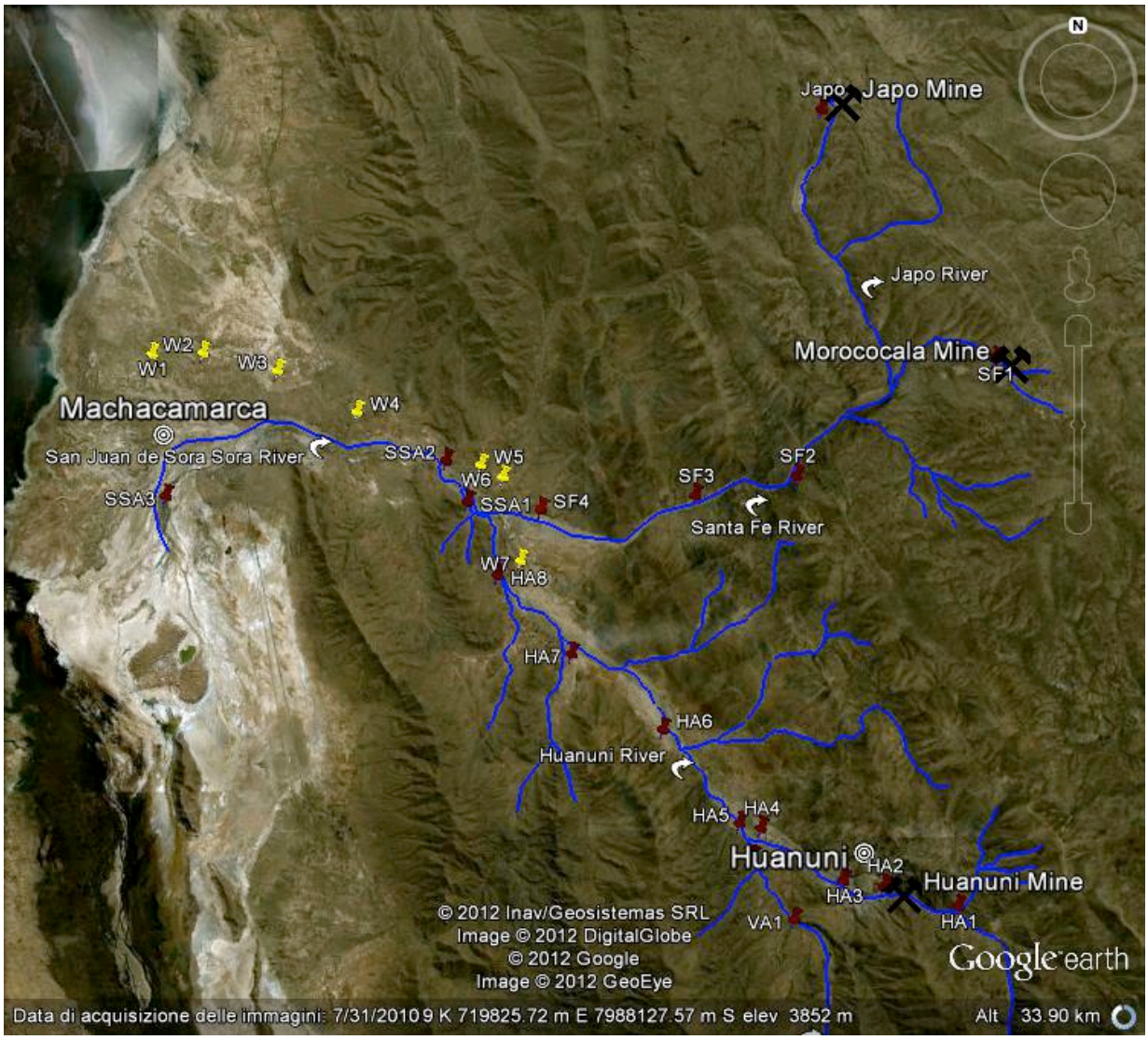

Figure 4: Map of the studied area. In yellow are presented the wells and in red the stream waters sampled.

Water samples

Approximately 250 ml of water samples was collected in polyethylene bottles and afterwards filtered at 0.45 µm using an electrical pump in the laboratory. The filtration wasn't performed in the filed as the waters were too turbid to allow filtration. The samples were stored in coolers and not exposed to light before shipment to Spain.

The water samples were analyzed for the physical parameters: pH, Eh, temperature, conductivity and TDS; and in the chemical composition by major ions, trace and heavy metals and rare earth elements (REE).

TDS and conductivity were measured in situ with a conductivity/TDS-meter (HACH Company model 44600) and temperature, pH and Eh, also in field, with a portable EC10 pH/mV/temperature-meter model 50058. Alkalinity was measured in the laboratories of the University of Oruro the same day by titrating 25 ml of sample with HCl 0.02 N till pH4, assuming that bicarbonate and carbonate account for all alkalinity.

Anions were measured with high performance liquid chromatography HPLC, (Waters 2690 Allianc) without any treatment, the detection limits for the anions are 0.1 ppm.

The samples were acidified with nitric acid at 1% to analyze cations and metals. The analyses of the cations were performed by ICP- OES (Perkin Elmer Optima 3200 RL) and the determination of trace elements in solution by ICP- MS (Perkin-Elmer Elan-6000), The analysis of the DS sampling campaign were performed with a semi quantitative method, which permit a large number of analysed elements but higher detection limits, determining a luck of information for some elements concentrations in the groundwaters.
All the chemical analyses for water samples were performed at the Scientific- Technical service of Barcelona (Spain).

Solid fraction

A total of 20 bedload sediment were collected in polyethylene containers and oven dried (50ºC) until complete dryness. Subsequently samples were homogenized with a manual agate mortar. Approximately 20g were stored in a plastic bag for XRF and DRX analysis and further 20 g for the speciation analysis and stored at room temperature till analysis.
Suspended sediment was sampled in 3 sampling points collecting a few litres of water, depending on turbidity. The suspended particulate was allowed to sediment for a few days. The sedimented material was oven dried and homogenized with a manual agate mortar at the same way of the bedload sediment.
- *Chemical composition* of the sampled bedload and suspended sediments was determined by X-ray fluorescence (XRF) using a Philips PW 2400 spectrometer. The major ions were determined by fussed samples and the trace elements by pressed pellets. Geological international reference samples were used to calibrate the instrument.
- *Mobility of heavy metals* was determined by SEP-BCR (Sequential extractions procedures-Community Bureau of Reference). This analysis was applied to 8 bedload and 3 suspended sediment samples. This sequential analysis aims at the subsequent destruction of specific phases of the sediment. In particular the solid material react with a number of extractants with increased reactivity, which causes the destruction of several components of the sediment and the release of metals with different mobility. The fractions extracted with the milder reagents are the most mobile and therefore more dangerous from an environmental perspective, because they represent the portion of the metal potentially more easily released from the solid material. (Figueiras et al., 2002).

The process consists in 4 steps described below.
Step 1: 40 ml of acetic acid 0.11 mol l^{-1} were added to 1 g of sediment in a centrifuge tube. Then the tube was then shaken for 16 h (overnight) at room temperature. The extract was separated from the solid residue by centrifugation at 3000 *g* for 20 min and the supernatant liquid was decanted into a polyethylene container and stored at 4°C until next analysis.

Step 2: 40 ml of hydroxylamine hydrochloride 0.5 mol l^{-1} (pH 1.5 with the addition of HNO_3 2 mol l^{-1}) were added to 3 the residue from step 1 in the centrifuge tube, and the extraction was performed as above.
Step 3: 10 ml of hydrogen peroxide 8.8 mol l^{-1} were added carefully, in small aliquots to avoid any loss due to violent reaction of the residue in the centrifuge tube. After that, the tube was covered loosely with a stopper and digestion was allowed to proceed for 1 h at room temperature with occasional manual shaking. The digestion continued by heating the covered tube for 1 h at 85°C in a water bath, and then the volume was reduced to few millilitres by further heating of the uncovered tube. A further aliquot of 10 ml of hydrogen peroxide was added to the residue. The tube was covered again and heated at 85°C for 1 h. Then, the stopper was removed and the volume reduced almost to dryness. After cooling, 50 ml of ammonium acetate 1.0 mol l^{-1} were added to the residue and the tube was shakened in for 16 h (overnight) at room temperature. The remaining operations for separation of the extract were as above.
Step 4*:* The residue from step 3 was transferred to a suitable digestion vessel and was digested with 'aqua regia' following a modification of the ISO 11466 protocol. (Sahuquillo et al., 2003) 3ml of HCl and 9ml of HNO_3 were added carefully at the residue. The mixture reacted in the microwaves according to the program of mineralization described in the Table2. Once cooled down, the solutions were filtered using an ash-free filter paper (Whatman no. 40) and their volume was made up to 50 ml by the addition of de-ionized water. These solutions were stored at 4°C in polypropylene bottles until analysis.

Table 2: program of mineralization in the microwaves for the digestion of the sediment samples

Program	**Power**	**Time**
1	250 W	10 min
2	450 W	10 min
3	600 W	10 min
4	250 W	5 min
5	Ventilation	10 min

The digestions of the sediments were executed at the Environmental Sciences Interdisciplinary Research Center (CIRSA) at the University of Bologna. The analyses were made at the Scientific- Technical service of Barcelona (Spain).

Results and discussion

Geochemical characterization of waters

Physical parameters

Physical parameters measured in the field for the stream waters in the dry season (DS, 20 sites) and in the wet season (WS, 17 sites) surveys and for the 7 sampled wells are presented in the Table 3. During the second sampling campaign few points (VA-2, SSA-1 and SSA-2b) were not sampled, because of the similar results with the closer sites during the first sampling campaign, in order to reduce the charge of analysis and fieldwork. The numbering of the samples indicates the increasing distances from the source of the spill.

- Ventaimedia and Huanuni

The pH and TDS values indicate a clear difference between pristine and mine impacted waters. The sampling points referring to the pH values can be subdivided in two groups, above and below pH 6. The sites VA-1, VA-2 and HA-1, sampled in areas not affected by mine activities have pH values ranging between 6.3 and 7.4. We will refer to the values of that samples as background values for the area of Huanuni mine. These waters are characterized by conductivity values varying between 78 to 320 μS and TDS values ranging between 78-163 mg l^{-1}. During the wet season all these parameters give lower values respect to the dry season.

The sites downstream the Huanuni mine (HA-2-8) are characterized by lower pH values ranging between 3.6-4.2 in the dry season and 4.0-5.3 in the wet season. Conductivity values show a great difference between the two seasons, ranging between 2405-1438 μS with a maximum value in the HA-4 in the dry season and between 366-1000 μS in the wet season. At HA-5 in the DS, after the confluence of the Huanuni and Ventaimedia rivers the conductivity is lower, probably due to dilution effects. After the confluence, in the valley, the values have constant values near 1500 μS. The TDS indicates the same behaviour with higher values in the DS.

- Santa Fe- Japo

Unfortunately it was impossible to sample upstream the mines of Morococala and Japo because the two mines lies on the head of the rivers. The pH values for that two rivers are under 4 in both seasons, with lover values in DS (2.9-3.1) and slightly higher in WS (3.3-3.9). The EC data shows high values in the Japo and SF-1 samples in both seasons and a dilution effect downstream.

- San Juan de Sora Sora

The physico-chemical values of the San Juan de Sora Sora River are characterized by the mixing of the waters of the two rivers, Huanuni and Santa Fe. The pH values increase downstream (3.4-4.5) in the DS and are constant in the WS. The EC and TDS values are rather constant downstream in both seasons.

- Outcrops

The outcrops samples are characterized by the same behaviour of the near samples for both seasons.

- Groundwaters

The pH values ranges between 6.1 and 7.1 without any variance between the two seasons. Temperature values are constant in the dry season and increase during the wet season. The wells W-1, W-3 and W-7 are characterized by high conductivity in DS with an increase in WS, up to 3618 μS. The TDS values reflect the conductivity with the higher values in the sample W-3.

Table 3: Physical characteristics, major ions and heavy metals in the surface and groundwaters of the investigated area. Heavy metals concentrations limits proposed on water guidelines of the World Health Organization* (WHO, 2011); **health-based guideline; * total iron (Linton 2007); **** New York State Department of Environmental Conservation (NYSDEC) and Quebec water quality standard for surface and ground water, (NYSDEC ,1986).**

		Ventaimedia		Huanuni river								Snta Fe- Japo river					S. Juan de Sora Sora river			Outcrops		Wells						
Sample		VA-1	VA-2	HA-1	HA-2	HA-3	HA-4	HA-5	HA-6	HA-7	HA-8	JAPO-1	SF-1	SF-2	SF-3	SF-4	SSA-1	SSA-2	SSA-3	HA-8b	SSA-2b	W-1	W-2	W-3	W-4	W-5	W-6	W-7
pH	DS	7.4	6.3	7.3	3.9	3.6	3.6	4.1	3.8	3.7	4.2	3.0	2.9	2.9	2.9	3.1	3.4	3.7	4.5	3.7	3.2	6.2	6.8	7.1	7.0	-	-	6.7
	WS	7.0	-	6.8	5.3	4.9	4.8	4.0	5.0	4.8	4.3	3.3	3.5	3.9	3.7	3.7	-	3.8	3.7	4.3	-	6.9	7.0	7.0	6.5	6.6	7.3	6.1
T°C	DS	11.3	12.3	7.1	10.6	11.6	12.9	13.2	13.2	12.6	12.8	10.6	15.5	7.9	8.2	11.4	11.0	11.1	12.9	12.2	8.5	11	10	10	10	-	-	-
	WS	17.0	-	13.1	10.2	11.7	12.8	12.0	10.2	11.0	15.0	14.8	14.8	15.0	16.2	15.9	-	12.9	12.4	19.0	-	16	15	17	-	15	18	15
EC (µS)	DS	318	320	187	2290	2367	2405	1532	1438	1535	1524	1800	2865	1481	1425	1310	1306	1545	1385	1471	2010	1726	948	2330	841	-	-	958
	WS	234	-	156	366	460	620	1000	502	608	1324	2030	2087	530	548	649	-	751	870	793	-	1751	872	3618	488	428	970	1355
TDS (mg l^{-1})	DS	158	162	93	1120	1200	1242	743	720	760	760	897	1434	759	726	663	659	675	697	760	1035	862	545	1150	419	-	-	469
	WS	116	-	78	188	228	311	499	252	300	655	1016	1026	264	276	324	-	374	435	392	-	875	434	1827	253	214	486	685
Cl (ppm)	DS	9.1	8.7	10.7	13.7	22.3	33.2	22.4	16.9	16.1	33.7	19.6	29.3	19.8	19.8	9.6	29.3	22.0	75.9	20.3	23.1	384	396	135	36	24	57	54
	WS	7.7	-	5.5	5.7	6.0	8.6	9.5	8.5	8.1	12.7	10.4	9.1	6.9	9.0	8.0	-	12.7	21.3	-	31.2	416	215	519	37	18	22	18
SO_4(ppm)	DS	92	94	44	1509	1889	1907	991	948	992	995	1326	2460	673	875	720	913	908	738	689	875	325	212	1252	317	91	85	478
	WS	79	-	31	221	240	361	643	345	284	494	1499	1810	233	295	335	-	527	601	-	949	301	330	1253	390	79	128	871
NO_3(ppm)	DS	<0.1	<0.1	<0.1	29.7	25.9	<0.1	<0.1	<0.1	<0.1	<0.1	<0.1	<0.1	<0.1	<0.1	<0.1	<0.1	<0.1	<0.1	<0.1	<0.1	<0.1	<0.1	<0.1	<0.1	<0.1	<0.1	<0.1
	WS	0.12	-	1.74	<0.1	4.3	3.1	2.8	3.0	2.3	5.0	1.6	5.5	1.9	3.0	2.0	-	3.3	3.1	-	5.5	<0.1	72.9	<0.1	<0.1	<0.1	3.3	<0.1
NO_2 (ppm)	DS	<0.1	<0.1	<0.1	<0.1	<0.1	<0.1	<0.1	<0.1	<0.1	<0.1	<0.1	<0.1	<0.1	<0.1	<0.1	<0.1	<0.1	<0.1	<0.1	<0.1	<0.1	<0.1	<0.1	<0.1	<0.1	<0.1	<0.1
	WS	0.25	-	0.25	<0.1	<0.1	<0.1	<0.1	<0.1	<0.1	<0.1	<0.1	<0.1	<0.1	<0.1	<0.1	0.1	<0.1	<0.1	<0.1	<0.1	0.1	<0.1	<0.1	<0.1	<0.1	<0.1	<0.1
Na^+ (ppm)	DS	17.1	16.0	12.3	18.9	27.8	36.4	28.3	25.7	24.4	38.0	4.2	26.7	13.2	16.8	19.6	33.7	29.5	70.8	25.6	32.0	287	312	250	59	43	93	65
	WS	12.2	-	9.1	9.7	10.0	13.2	13.7	13.3	11.7	18.1	7.2	19.0	11.7	14.0	12.4	-	17.9	24.2	-	42.9	278	150	389	50	41	144	33
Ca^{2+} (ppm)	DS	32.1	33.1	20.5	110.3	114.1	126.7	94.4	89.5	109.6	117.6	27.4	344.2	62.3	74.1	88.7	113.9	107.4	180.5	84.6	207.2	86	96	334	91	41	50	125
	WS	22.8	-	16.2	24.5	25.2	32.9	44.2	32.6	26.5	60.4	33.7	146.9	26.0	40.8	30.4	-	49.5	63.8	-	138.7	88	93	487	126	41	65	225
Mg^{2+} (ppm)	DS	15.4	15.2	9.5	34.5	47.7	49.4	39.2	45.3	53.4	52.8	18.4	105.2	27.6	28.1	42.0	52.3	55.5	68.2	39.3	92.8	36	45	105	36	17	16	54
	WS	10.6	-	6.7	8.9	9.8	13.7	21.8	15.1	8.6	28.0	25.4	41.0	8.3	19.1	10.6	-	21.3	25.9	-	64.4	35	34	144	44	15	23	94
K^+ (ppm)	DS	3.2	3.7	2.4	11.7	13.8	14.2	7.1	4.5	6.1	7.2	3.3	13.3	1.9	2.1	2.9	5.8	3.3	9.7	4.7	10.9	25	19	15	14	9	13	9
	WS	3.4	-	2.6	3.6	3.8	4.2	4.3	3.7	3.6	4.9	5.2	7.7	3.6	3.7	3.2	-	4.3	5.0	-	9.2	23	14	19	9	6	11	12
Zn (ppm), 3**	DS	0.03	0.05	0.04	129	141	124	52	39	44	44	51	85	33	30	28	39	29	64	25	29	0.09	0.05	0.03	0.04	0.01	0.02	0.25
	WS	0.11	-	0.07	11	15	17	24	11	6	15	41	43	6	13	7	-	12	16	26	-	0.12	0.12	0.08	0.11	0.10	0.09	4.97
Mn (ppm), 0.5*	DS	0.01	0.01	0.01	20	20	21	15	18	22	20	6	5	6	4	7	18	19	20	13	14	0.00	0.45	0.03	0.00	0.01	0.00	0.00
	WS	0.00	-	0.01	2	2	5	9	4	1.1	13	7	3	1	6	2	-	7	9	27	-	0.01	0.00	0.00	0.09	0.00	0.01	0.01
Fe (ppm), 1***	DS	0.00	0.00	0.00	525.5	580.0	527.0	135.5	76.5	65.5	58.0	293.3	335.8	133.2	101.7	9.4	36.0	8.6	62.3	0.03	19.6	0.05	0.01	0.00	0.01	0.01	0.00	0.02
	WS	0.00	-	0.00	1.5	3.4	9.3	76.2	2.6	2.7	2.8	352.3	204.6	2.6	3.2	2.8	-	2.8	4.7	0.4	-	0.29	0.03	0.02	0.04	0.01	0.00	0.01
Co (ppb),5 ****	DS	0.32	0.34	0.21	1442	1300	1259	570	453	521	487	254	120	162	99	154	399	295	361	6	312	< 0.2	< 0.2	< 0.2	< 0.2	< 0.2	< 0.2	< 0.2
	WS	0.07	-	0.09	133	130	179	240	126	23	207	233	69	24	150	33	-	132	152	114	-	0.40	0.18	0.86	1.27	0.27	0.31	0.44
Cu (ppb), 2000[4]	DS	5.70	2.66	6.73	2646	3479	4889	2896	1950	2022	1453	5653	260	2640	1460	761	1272	1198	2038	329	1040	< 2	< 2	< 2	< 2	3.54	< 2	< 2
	WS	1.52	-	1.79	552	900	881	1873	648	355	1198	8454	617	377	876	377	-	881	1089	1348	-	4.62	2.25	5.31	2.52	1.33	1.60	1.34
Cd (ppb), 3*	DS	0.49	0.56	< 0.2	3402	3349	3219	1273	812	1086	1068	6032	307	2500	1305	978	963	659	1058	589	722	1.29	1.69	0.90	< 0.2	< 0.2	< 0.2	4.62
	WS	0.64	-	0.35	759	528	545	623	332	183	427	3803	206	179	356	218	-	357	391	668	-	0.76	0.08	0.12	0.86	0.05	0.14	56.95
Pb (ppb), 10*	DS	169.45	181.71	488	2629	459	1634	196	112	118	84	44	21	19	34	5	78	12	1311	44	20	1.67	2.62	< 0.2	0.52	0.21	2.61	1.48
	WS	0.17	-	0.1	7	13	24	27	13	36	17	26	13	34	16	28	-	13	32	2	-	7.22	0.12	0.29	0.13	6.49	21.00	0.26

Chemical parameters

Major elements

The chemical composition of the waters for Cl, SO_4, HCO_3, Na+K, Ca, and Mg in the investigated area are presented in the Table 3. In Figure 5 are represented the data in Piper-type diagrams of the DS and WS respectively. In both seasons the waters have the same characteristics and distributions. Cation and anion distributions identify 2 different surface-water types; the background samples HA-1, VA-1 and VA-2 are classified as Ca-Mg-Na-HCO_3-SO_4 waters, and the others affected by mine extractions as Ca-Mg-SO4 waters.

Analysing the anion distributions in DS it is possible to separate the ground-waters in three groups; W-1, W-2 are chlorine waters, W-3, W-4 and W-7 are enriched in sulphate and W-5 and W-6 are HCO3-SO4 waters. In the WS the samples W-2 and W-7 are enriched in sulphate and W-3 in Cl and sulphate.

Considering the features of the surface- and ground- waters, wells 5 and 6 have the same characteristics of the surface background waters; samples W-3, W-4 and W-7 are found in a mixing line between the pristine and polluted samples in the dry season and shows an increase in sulphate and chlorine concentrations in the WS that indicate a mixing with the mine polluted waters.

Water from mining sector is characterized by a decrease in pH and an increase in sulphate concentrations due to oxidative dissolution of pyrite. High EC values in groundwater are linked to the presence of saline groundwater. Salt deposit of palaeolakes present in the region and evaporative enrichment of the dissolved solutes are responsible for high EC values in the region (Ramos Ramos et al., 2011). The high content of sulphate is probably due to the influence of the acid mine drainage.

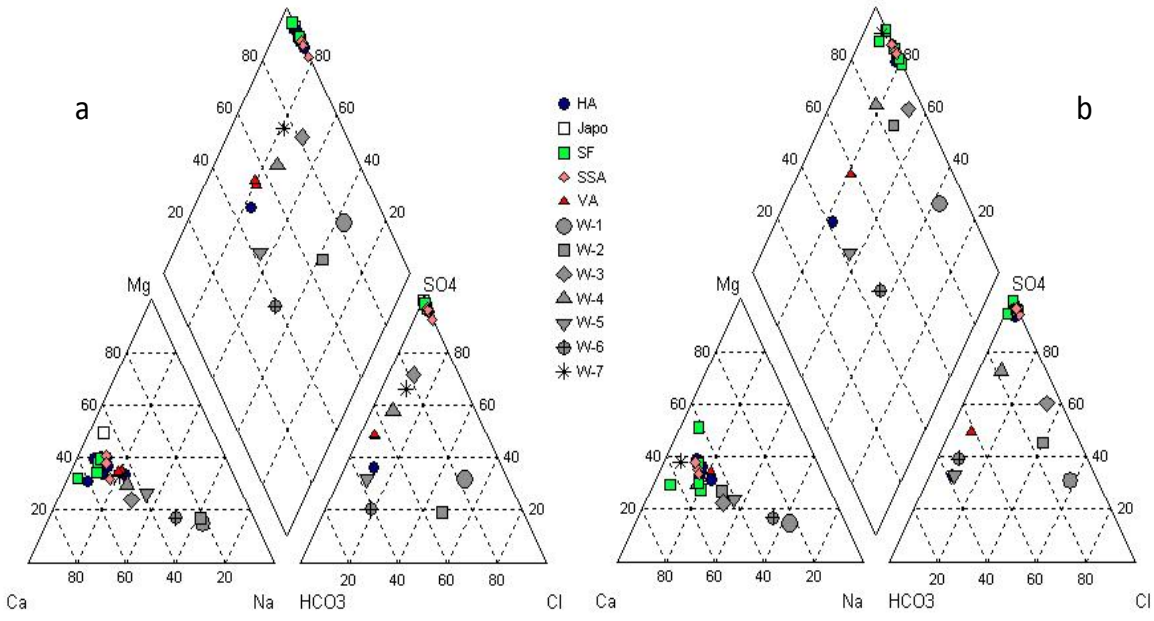

Figure 5: Major ions presented in terms of relative concentrations of the major ions in equivalent units trough Piper-type diagrams representing the dry season (a) and wet season (b) sampling campaign.

In order to better represent the water characteristics, its evolutions along the river flow and the variations related to the seasonality of the area, Stiff diagrams were plotted on the map (Figure 6). Ion concentrations in meq L^{-1} are plotted on the horizontal axis, cation are plotted to the left (Na, Ca, Fe and Zn) and anions (Cl, HCO_3^- and SO_4^{2-}) to the right of the vertical axes. Diagrams relative to the background area are represented separately (Figure 6c) with a lower scale (max 3meq L^{-1}) to highlight the sample composition, where HCO_3^- is the prevailing anion and Ca the cation and is representative for both the seasons.

In the Figure 6a, representing the dry season, the waters are characterized by high concentrations in sulphate, especially near the mine tailings output and by a progressive dilution along the river flow. During the wet season (Figure 6b) the concentrations of sulphates are lower in all the samples instead of Japo and SF-1, characterized by high concentrations of sulphate and iron. In both figures is important to note the particular composition of the W-3 with really high concentrations in SO_4^{2-} and Ca^{2+}.

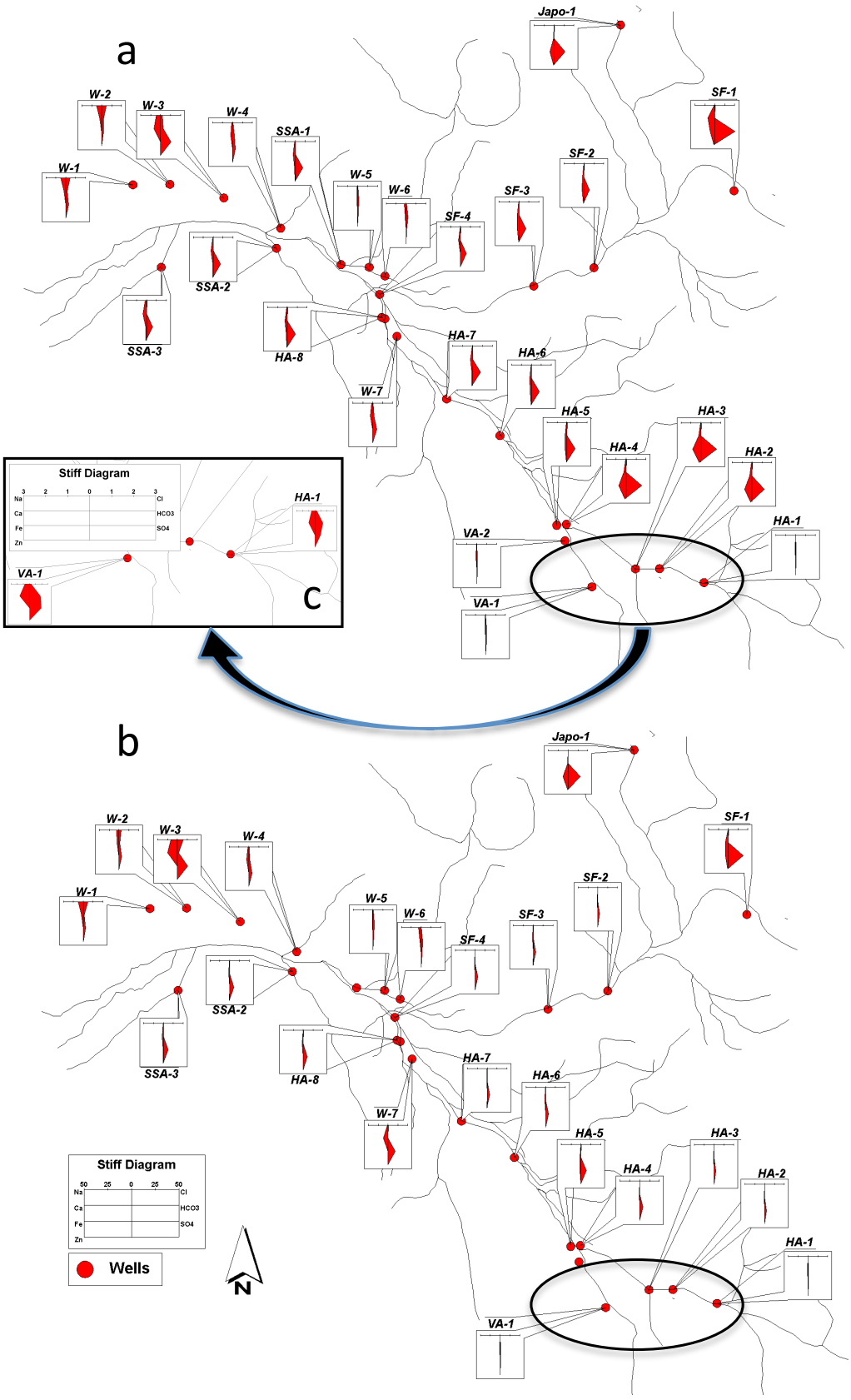

Figure 6: Stiff diagrams representing the dry season (a) and the wet season (b) and a zoom to the background area (c).

Seasonal variation of the mining related contaminants

Figure displays the seasonal variation of the mining related contaminants analysed as box-and-whisker plots. The length of the box represents the interquartile range, which contains 50% of the values, and the heavy horizontal line inside the box indicates the median. The whiskers are lines that extend from the box to the highest and lowest values excluding the outliers.

The **seasonal effects** are marked in the increase of pH values, the decrease in concentrations of all the considered elements in the wet season and its lower range. In particular the median of the pH values increase from 3.8 during the dry season to 4.9 in the wet season. Iron result the most sensible to this increase in pH and result almost completely depleted in the wet season.

In an area characterized by low precipitations distributed in few months (from December to March) most of the year the waters are characterized by high concentrations of contaminants.

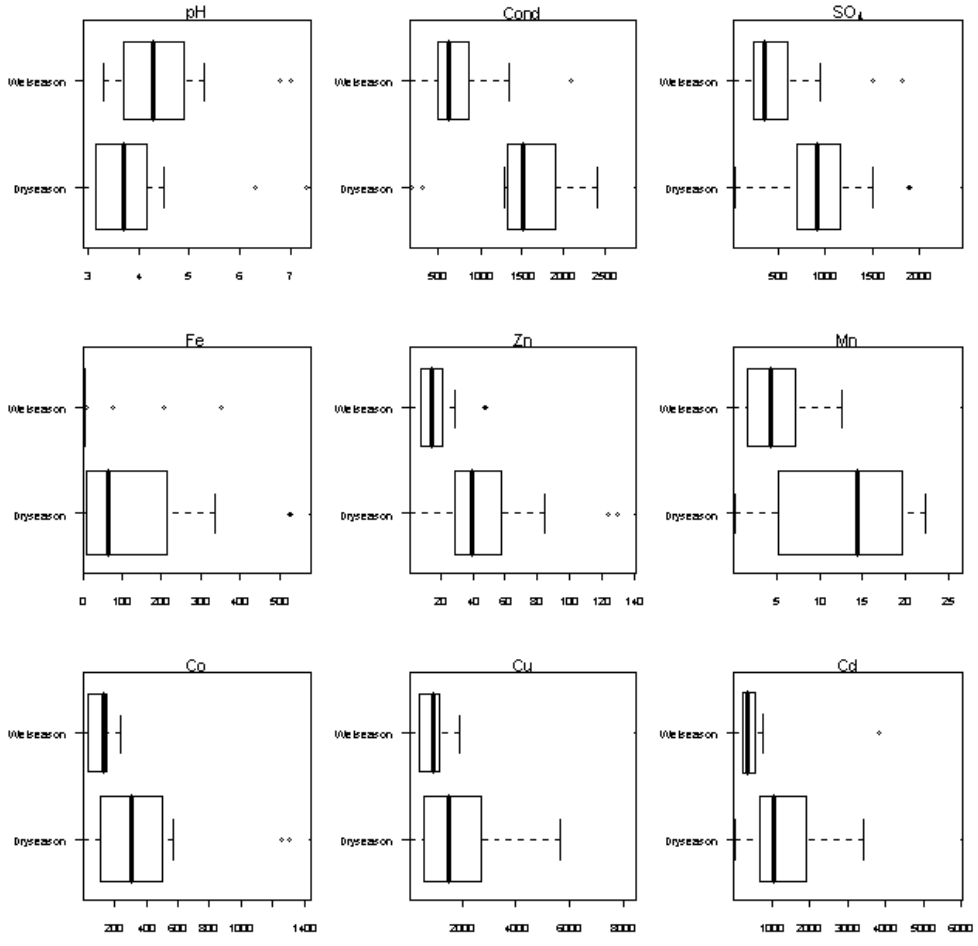

Figure 7: Seasonal variability of the mining related contaminants analysed as box-and-whisker plots. The length of the box represents the interquartile range, which contains 50% of the values, and the heavy horizontal line inside the box indicates the median. The whiskers are lines that extend from the box to the highest and lowest values excluding the outliers.

The relationships between variables typical of mining related contamination were analysed through a correlation matrix (Table 4) realized with the Paleontological Statistics Software Package for Education and Data Analysis (Hammer et al., 2001). The non-parametric Spearman correlation was used in order to analyse any monotonic relations, and not only linear relations (Pearson correlation method), and to minimize the effects of the outliers (Reimann et al., 2008). The significance of the correlation is interpreted in bold as very high significance ($p<0.001$), and italic as high significance ($0.001 \leq p < 0.01$).

The correlation matrix indicates that all the variables, instead of Pb during the DS, display a negative correlation with the pH, high correlation with sulphur, and in the DS with the conductivity. During the dry season few groups of variables, Fe, S, Zn; Cu, Cd and Co, Mn are tightly correlated (>0.81) with a very high significance ($p<0.001$); probably because these metals are strongly sorbed on Fe/Mn- oxides, although in acidic conditions are desorbed and stabile in solution. Pb shows weak correlations with all the elements (<0.4).

During the wet season overall heavy metals shows lower correlations each other and with sulphur instead of manganese and cadmium, which increase the correlation with the others heavy metals.

Table 4: Non- parametric Spearman correlation matrix between mining related contamination elements, in bold p<0.001 (very high significance), in italic (0.001 ≤ p <0.01) high significance.

Dry season

	pH	Cond	S	Fe	Zn	Mn	Co	Cu	Cd
pH									
Cond	-0.45								
S	-0.40	**0.72**							
Fe	-0.51	**0.74**	**0.91**						
Zn	-0.30	**0.70**	**0.93**	**0.90**					
Mn	-0.03	0.49	*0.54*	0.45	**0.67**				
Co	-0.11	*0.57*	*0.64*	**0.69**	0.81	**0.88**			
Cu	-0.31	0.54	**0.73**	0.82	0.77	*0.61*	0.76		
Cd	-0.45	0.51	**0.69**	0.81	**0.72**	0.51	**0.69**	**0.93**	
Pb	*0.64*	-0.02	0.25	0.22	0.38	0.31	0.39	0.29	0.17

Wet season

	pH	Cond	S	Fe	Zn	Mn	Co	Cu	Cd
pH									
Cond	-0.38								
S	**-0.74**	0.36							
Fe	*-0.69*	0.11	*0.70*						
Zn	-0.57	0.12	0.88	**0.76**					
Mn	-0.45	0.15	0.84	0.50	**0.78**				
Co	-0.39	-0.06	*0.62*	*0.70*	**0.70**	**0.79**			
Cu	-0.43	0.06	**0.79**	*0.63*	0.86	*0.92*	0.85		
Cd	-0.20	-0.28	0.53	0.44	**0.74**	**0.72**	0.81	0.82	
Pb	-0.53	0.12	0.23	0.50	0.11	0.13	0.28	0.20	0.05

Heavy metals

Heavy metals concentrations in the San Juan de Sora Sora basin indicate a huge break between surface and ground waters, and waters draining pristine and mining area. Most of the waters downstream the mine exceed the water guidelines proposed by the World Health Organization (WHO) (Table 3). Lead in the DS was the only element to exceed guidelines values also in the background samples. There is a general trend in the concentrations of the contaminants in the Huanuni River, with high values till the HA-4. The Ventaimedia River waters in the DS dilute significantly some contaminants like Zn, Mn, Fe and Co (HA-5). The SFA-2 sample is influenced by the Japo high concentrations for Mn, Co, Cu and Cd, showing the mixing of the two water bodies in the DS; along the Santa Fe River there is a dilution in concentrations for Zn, Fe and Pb.

In WS there is an anomaly in the samples HA-5 and SFA-3, with higher values, maybe because in the area there are some sediment re-modelling sites.

In the wet season most of the considered groundwaters are enriched in some heavy metals. Concentration of Zn is higher respect to the dry season and in the W-7 is above guideline limits, higher concentrations are detected in W-1, 2, 3 and 4 for Fe, and extremely high quantities of Cd in W-7 exceeding the guideline limits. The lead concentrations increase in W-1 and W-5 in the wet season, and in W-6 are considerably above permitted limits in both seasons.

In the dry season the concentration of Cd is exceeding WHO guidelines in the W-7 and concentration of Mn in the W-2 is close to the WHO water guideline.

Ficklin diagram

In Figure the sum of the base metals: zinc (Zn), cobalt (Co), copper (Cu), cadmium (Cd), lead (Pb) and nickel (Ni) is plotted against pH (Plumlee et al., 1994). The samples show a linear inverse distribution respect to the pH values; near neutral pH values are characterized by low heavy metal content (pristine and ground-waters) and acidic pH by high heavy metal content (mine polluted area). When plotted on Ficklin diagram all the stream waters in both the seasons are classified as high acidic waters with high heavy metal content, instead of the groundwaters, which are classified as near neutral waters with low heavy metal content.

Concentrations of Potentially harmful elements (PHEs) in the surface contaminated waters are at least three orders of magnitude higher than in the pristine- and ground-waters. A seasonal comparison of heavy metals concentrations reveals a significant hydrological influence in the polluted samples. This effect is marked at the Huanuni mine output where in the DS the concentrations can be up to two orders of magnitude higher than in the WS, probably because of the considerable difference in the river flow during the two seasons (Figure 8). The seasonal variations have an opposite influence on the heavy metal concentrations in groundwaters respect to the surface waters. During the wet season the heavy metals concentrations decrease in the surface waters,

but increase in the ground waters. The sample W-7 during the wet season collocates in the mixing line between the acid mine contaminated and the unpolluted samples.
The increase in element concentrations in groundwaters during the WS is probably provoked by fresh water inputs after rainfall which determine the dissolution of efflorescent sulphate previously formed during the dry period and could induce local increases of the SO4 and metal contents (Sánchez España et al., 2005).
In W-7 the increase in heavy metal concentrations (Figure 8), conductivity and sulphate and the lowering of pH, during the wet season could be a consequence of surface water infiltration. The calcite present in small amounts in the sediments probably dissolved and neutralizes the acid effect of the infiltrated waters, with a consequent enhance in Ca and Mg in the water and low alkalinity values (Morin and Cherry, 1986).

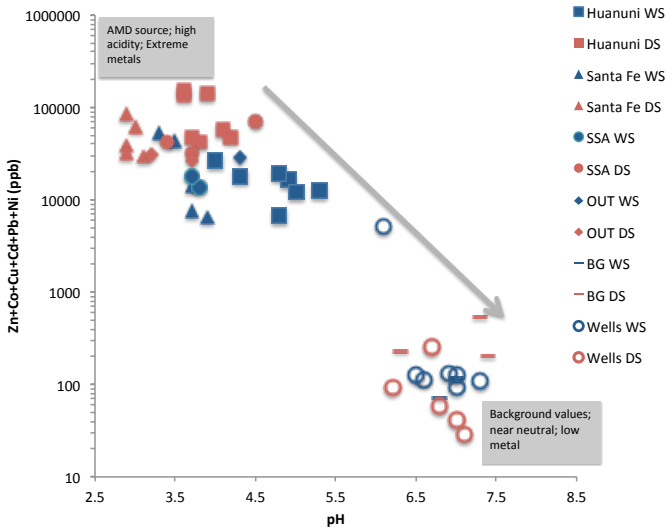

Figure 8: Ficklin diagram corresponding to water samples in dry season (red) and wet season (blue); SSA corresponds to San Juan de Sora Sora River, OUT are the outcrops and BG background values (VA-1-2, HA-1) (Plumlee et al., 1994).

The strong variance in the concentrations of the heavy metals used in the Ficklin diagram during the two seasons doesn't reflect on the proportions between the elements instead of for the background samples. In the upstream mine area during the dry season lead is the most concentrated ion (78-92%) and Zn is present in concentrations varying between 6 and 20%. During the wet season the ratio is inverted and Zn became the predominant ion (96%). Along the Huanuni and San Juan de Sora Sora rivers Zn is the main ion during both the seasons (>87%). Japo sample in the DS is dominated by Zn (81%) Cd (10%) and Cu (9%). The composition of this sample has a strong influence on the composition of the SF samples. During the WS there is a slight decrease in the Zn percentage and an increase of the Cu content (16%). HA-5 sample reflect an anomaly in both the seasons, with lower percentages of zinc and an increase in Cu, probably induced by the mixing with the waters of the Ventaimedia River.
Groundwaters are characterized by high Zn fraction (76-99%). W-6 has a 10-19% of Pb during DS and WS respectively, and W-5 a percentage of 22% of Cu during the DS.

Metal provenance and source detection

Through the analysis of the trace element concentrations it was possible to determine the different impacts generated by the three mines operating in the area. The Huanuni mine outputs generate waters that are highly polluted in zinc, lithium, nickel and uranium. Some of these trace elements were detected in concentrations that are consistently higher than the WHO guideline proposed limits. Uranium concentrations after the mine discharge is found in concentrations up to 500 ppb in the dry season and 100 ppb in the wet season, whereas the proposed limit is 30ppb. Also Ni, detected in concentrations up to 1200 ppb in the dry season exceeds the guideline (70 ppb).
Trace elements concentrations found in the first sample of the Santa Fe River (SF-1), represent the influence of the Morococala mine. This waters result particularly enriched in lithium, scandium, rubidium, strontium and cesium. Japo mine is characterized by scandium, chromium, copper, arsenic, cadmium and indium high concentrations. Presence of As, well-known for its harmful effects (Masotti et al., 2009; Sharma and Sohn, 2009) are detected in Japo sample at extremely high concentrations, up to 135 ppb and 69 ppb in wet and dry season respectively, and in SF-1 up to 93 ppb exceeding greatly the WHO guideline of 10ppb.

Pyrite oxidation

The reactions of acid generation are best illustrated by examining the oxidation of pyrite (FeS_2), which is one of the most common sulphide minerals. Oxidation of pyrite by atmospheric oxygen produces one mole of Fe^{2+}, two moles of SO_4^{2-} and two moles of H^+ for every mole of pyrite oxidized (Nordstrom, 1982):

$$FeS_2 + 7/2O_2 + H_2O \rightarrow Fe^{2+} + 2SO_4^{2-} + 2H^+ \qquad \text{Equation 1}$$

The dissolved $Fe2^+$, SO_4^{2-} and H^+ represent an increase in the total dissolved solids and acidity of the water and, unless neutralized, induce a decrease in pH. If the surrounding environment is sufficiently oxidizing (dependent on O2 concentration, pH and bacterial activity), much of the ferrous iron will oxidize to ferric iron, according to the following reaction:

$$Fe^{2+} + 1/4\ O_2 + H^+ \rightarrow Fe^{3+} + 1/2\ H_2O \qquad \text{Equation 2}$$

At pH values between 2.3 and 3.5, ferric iron precipitates as Fe(OH)3 and jarosite, leaving little Fe^{3+} in solution while simultaneously lowering pH:

$$Fe^{3+} + 3H_2O \rightarrow Fe(OH)_{3\ solid} + 3H^+ \qquad \text{Equation 3}$$

Any Fe^{3+} from Equation 2 that does not precipitate from solution through Equation 3 may be used to oxidize additional pyrite, according to the following:

$$FeS_2 + 14\ Fe^{3+} + 8H_2O \rightarrow 15Fe^{2+} + 2SO_4^{2-} + 16H^+ \qquad \text{Equation 4}$$

Based on these simplified basic reactions, acid generation that produces iron which

eventually precipitates as $Fe(OH)_3$ may be represented by a combination of Equations 1-3:

$$FeS_2 + 15/4O_2 + 7/2H^2O \rightarrow Fe(OH)^3 + 2SO_4^{2-} + 4H^+ \quad \text{Equation 5}$$

These overall reactions results in the release of 4 mol of H^+ for each mole of pyrite oxidized.
All the above equations, with the exception of Equations 2 and 3, assume that the oxidized mineral is pyrite and the oxidant is oxygen.

During the pyrite oxidation process, two moles of sulphate are produced for every mole of Fe, a relationship near this ratio indicates a composition closer to the leach products derived from the weathering of pyrite. As the relationship is lower, this indicates 'more evolved' water, where through mixing or mineral hydrolysis processes, it loses Fe, whilst the sulphate remains in solution (Olias et al., 2004), or enrichment in sulphate due to solubilisation of sulphate efflorescent salts (Nordstrom and Alpers, 1999). The oxidation of Fe (II) is very fast, and therefore the AMD waters evolve geochemically downstream in a short distance as they become equilibrated with atmospheric O_2. The hydrolysis of Fe (III) also occurs rapidly, and its precipitation could takes place at a few meters from the discharge points (España et al., 2005).

In Figure 9 is represented the distribution between iron and sulphate during the two seasons. During the dry season background samples are characterized by low concentrations similar to groundwater samples, the surface water samples have a linear distribution 1:2 typical of the dissolution of pyrite (Figure 9), instead of sample SF-1 which result enriched in sulphate, that reflect the strong correlation between the two elements (0.91 $p<0.001$). During the wet season the background samples maintain the same characteristics, all the surface water samples, instead of HA-5, SF-1 and Japo, results depleted in iron (Fig 6b), probably precipitated due to higher pH values validating the decrease relationship between the two elements. The groundwater samples results enriched in sulphate, in particular the wells W-6 and W-7.

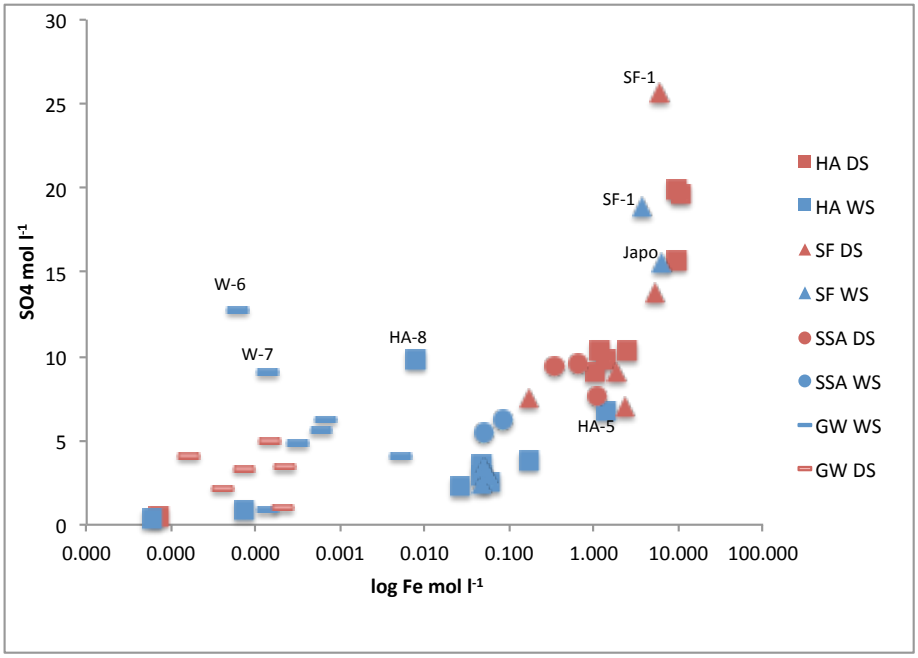

Figure 9: Molar ratio between Fe and SO4 during dry and wet season for surface and ground-waters.

Distance evolution graph

Distance evolution graphs have been plotted for the studied heavy metals (Figure 10) along the Huanuni River, establishing a comparison over the river flow and the evolution of the chemistry between the two sampling campaign. By studying the resulting graphs, the following can be deduced:

In dry season heavy metals behave similarly, with a strong increase in concentrations after the Huanuni mine discharge and a constant concentrations up to the Ventaimedia River confluence. At the confluence there is an increase in pH values and a marked decrease in concentrations for all the elements. After the confluence a group of elements (Cu, SO4, Al, Co, Ni, Zn, Cd and Mn) conserve the same concentrations or dilute slightly; Pb and Fe are characterized by a constant decrease in concentrations along the river flow. All the elements are characterized by an increase in concentrations in the last sampling point, especially Pb and Fe, which indicate the strong influence of the Machacamarca treatment plant.

During the wet season the concentrations of all the heavy metals increase strongly after the mine output like in the dry season. The increase in concentrations of iron is less marked than the others analysed elements, which indicate the strong influence of the pH on its abundance. At the input of the unpolluted waters of Ventaimedia river there is an anomaly. The pH in the waters decrease strongly and there is a heavy increase of the concentrations of all the elements. Probably this data doesn't reflect the real composition of the waters but are influenced by the numerous sediment-remodelling sites present in the area. The other sampling points along the river flow are characterized by dilution and another increase in concentrations before the Santa Fe river confluence. Lead and iron behaves differently with more marked changes.

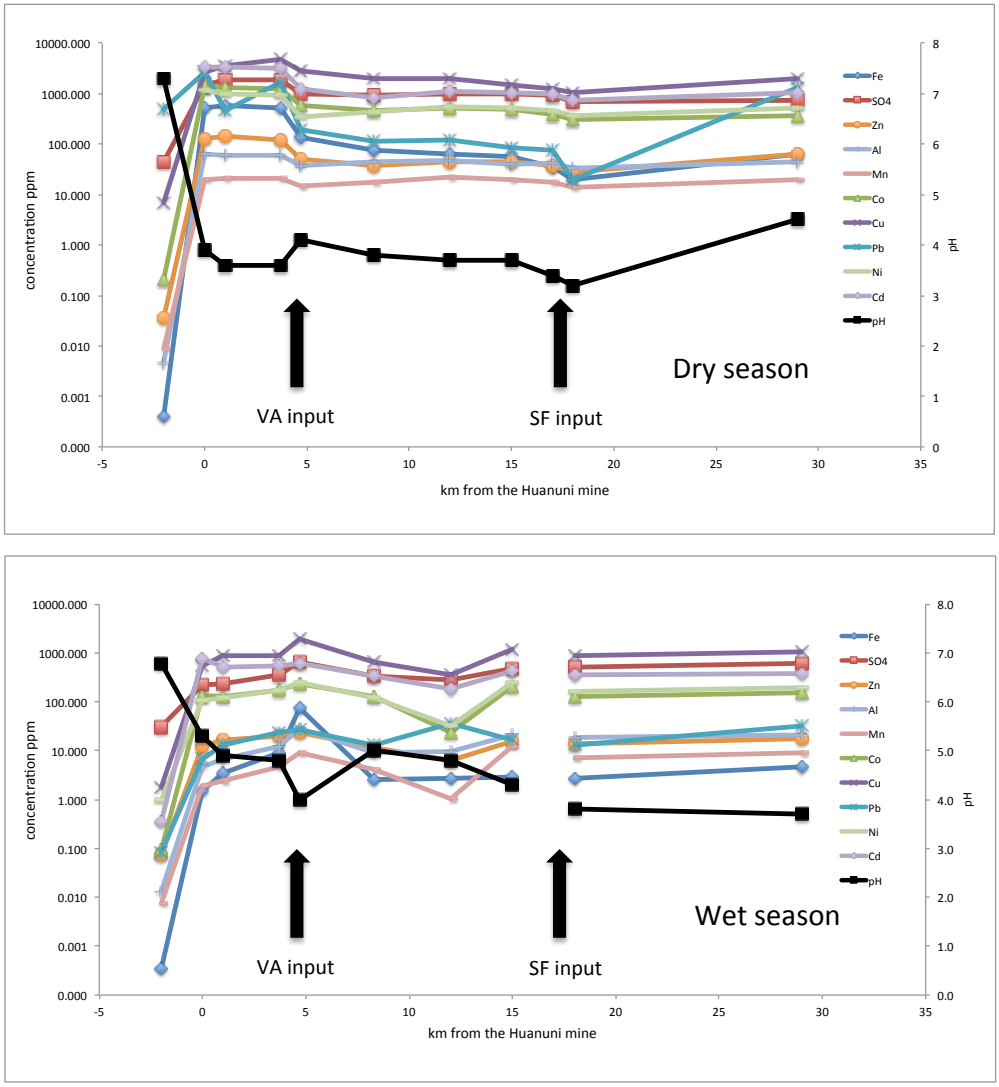

Figure 10: Distance evolution graph along the river stream, from the Huanuni mine up to the flow in the Uru Uru lake in the dry season and wet season.

Rare Earth Elements

REE analysis was performed only in the DS samples. In the upstream sampling points and in the groundwaters there is no evidence of REE elements. The total concentration of REEs (∑REE) in the AMD samples range from 56 ppb to 242 ppb and the concentrations increase along the river flow. It appears that concentration of SO_4^{2-} is not controlling the concentrations of REEs like found by (Zhao et al., 2007; Pérez-López et al., 2010).

REE elements in the San Juan de Sora Sora River behave as in the Huanuni River, which indicates a strong influence of the Huanuni mine. The Santa Fe River and Japo data indicate a different water composition characterizing the two mines in the area. The lack of data present in the SF-1 for Terbium (Tb) and Holmium (Ho) indicate that these two elements are typical of the Japo mine. Most of the others elements have higher concentrations in Japo than in Santa Fe, instead of Ce, La and Pr.

The normalization of REE concentrations to those in North American Shale Composite (NASC, Taylor and McLennan, 1985) can act as an indicator of REE enrichment (Table 5).

Figure 11 illustrates the NASC-normalized patterns of REE concentrations in the studied area. All samples are enriched in the middle rare earth elements (MREE) (Sm–Gd) over both light rare earth elements (LREE) and heavy rare earth elements (HREE) in comparison with NASC. Similar observations were also made elsewhere (Johannesson and Lyons, 1995; Elbaz-Poulichet and Dupuy, 1999; Johannesson and Zhou, 1999; Gimeno Serrano et al., 2000; Worrall and Pearson, 2001; Zhao et al., 2007; Sahoo et al. 2012) in areas affected by mine pollution.

The convex-up NASC- normalized REEs pattern of the samples, characteristic of acidic mine water, is probably produced due to acid leaching of Fe–Mn-oxides/oxyhydroxides (Johannesson and Zhou 1999).

However, the processes controlling MREE enrichment observed in acidic terrestrial waters are still not well understood and it is unclear whether observed distributions relate to the source or aqueous processes. Some particular behaviour are observed in the area: samples HA-7-8 result slightly enriched in Lanthanum, and HA-4 enriched and HA-5 depleted in Europium, Japo is particularly enriched in MREE and HREE, and SF-4 in LREE. The outcrop HA-8b is strongly depleted in Cerium, Neodymium and Europium respect to the other samples.

Table 5: Rare Earth Elements (REE) in the dry season sampling campaign and the North American Shale Composite (NASC, Taylor and McLennan, 1985) concentrations.

		Ventaimedia		Huanuni river								Snta Fe- Japo river					S. Juan de Sora Sora river			Outcrops		
(ppb)		VA-1	VA-2	HA-1	HA-2	HA-3	HA-4	HA-5	HA-6	HA-7	HA-8	JAPO-1	SFA-1	SFA-2	SFA-3	SFA-4	SSA-1	SSA-2	SSA-3	HA-8b	SSA-2b	NASC
La	DS	<0.2	<0.2	<0.2	8	8	10	11	14	21	19	4	6	7	5	24	19	28	21	16	17	32
Ce	DS	<0.2	<0.2	<0.2	19	22	26	30	38	46	42	13	16	20	15	65	45	71	50	17	41	73
Pr	DS	<0.2	<0.2	<0.2	3.4	3.7	4.8	5.2	7.1	10.1	8.3	2.7	3.1	3.8	3.2	12.4	8.5	13.5	9.3	5.0	7.7	7.9
Nd	DS	<0.2	<0.2	<0.2	15	17	21	23	31	43	34	14	13	18	15	51	36	57	39	20	31	33
Sm	DS	<0.2	<0.2	<0.2	5.3	5.3	7.0	6.8	9.6	13.2	10.6	7.5	4.0	7.2	5.4	14.2	10.5	16.8	11.4	5.7	9.2	5.7
Eu	DS	<0.2	<0.2	<0.2	2.4	2.5	2.9	2.3	2.8	4.0	3.2	2.8	1.5	2.3	1.7	3.7	3.1	4.3	3.3	1.7	2.5	1.2
Gd	DS	<0.2	<0.2	<0.2	6.7	6.9	9.2	8.9	12.5	17.4	15.7	10.6	5.4	9.3	6.9	18.1	14.8	21.4	15.4	10.2	12.1	5.2
Tb	DS	<0.2	<0.2	<0.2	<0.2	<0.2	1.20	1.12	1.47	2.09	1.86	1.56	<0.2	1.20	0.88	2.17	1.77	2.50	1.91	1.22	1.48	0.85
Dy	DS	<0.2	<0.2	<0.2	5.5	5.8	7.1	6.4	8.3	11.6	10.2	9.1	3.7	7.1	5.0	12.9	9.8	13.9	10.6	6.3	8.2	5.8
Ho	DS	<0.2	<0.2	<0.2	<0.2	<0.2	1.12	1.04	1.29	1.87	1.55	1.55	<0.2	1.17	<0.2	1.96	1.55	2.15	1.60	1.03	1.27	1.00
Er	DS	<0.2	<0.2	<0.2	2.6	2.8	3.1	2.6	3.3	4.5	3.6	3.9	1.5	3.0	2.0	5.0	3.9	5.6	4.2	2.4	3.3	3.4
Tm	DS	<0.2	<0.2	<0.2	<0.2	<0.2	<0.2	<0.2	<0.2	<0.2	<0.2	<0.2	<0.2	<0.2	<0.2	0.7	<0.2	0.7	<0.2	<0.2	<0.2	0.5
Yb	DS	<0.2	<0.2	<0.2	2.5	2.4	3.0	2.3	2.9	3.9	3.2	3.7	1.8	2.7	1.9	4.5	3.3	4.7	3.2	1.5	2.7	3.1
Lu	DS	<0.2	<0.2	<0.2	<0.2	<0.2	<0.2	<0.2	<0.2	<0.2	<0.2	<0.2	<0.2	<0.2	<0.2	<0.2	<0.2	<0.2	<0.2	<0.2	<0.2	0.48
ΣREE	DS				71	75	96	101	133	179	153	75	56	83	62	215	157	242	170	87	137	173

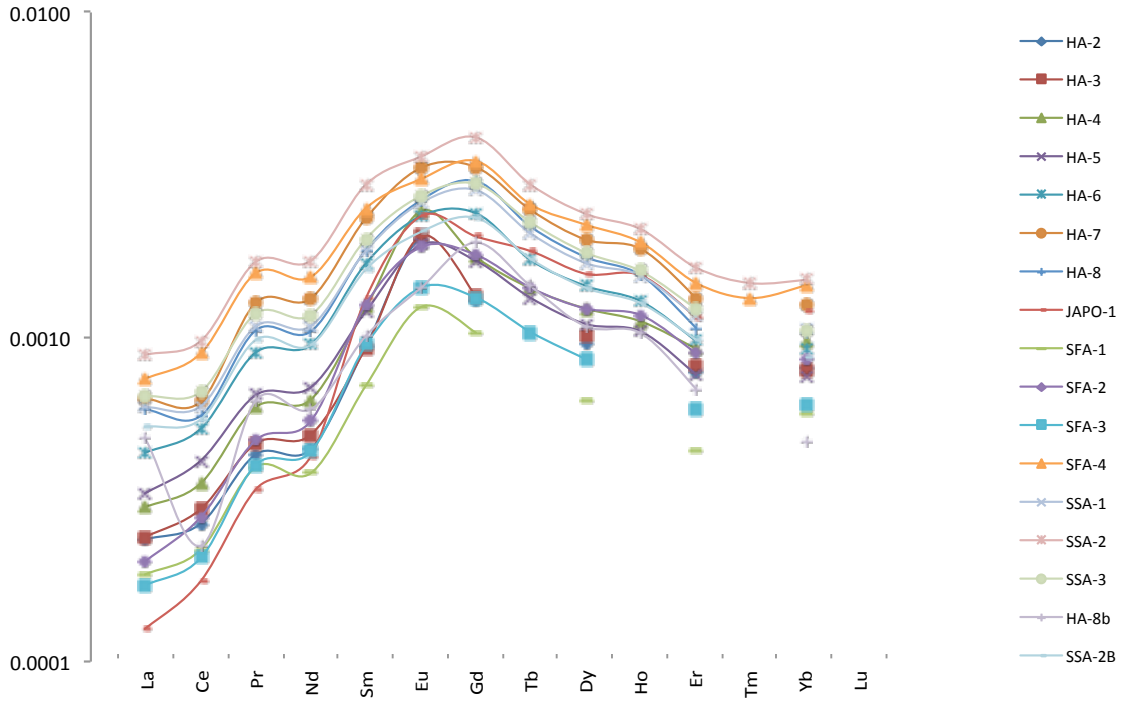

Figure 11: NASC-normalized patterns of the REE concentrations.

Surface and ground-water interactions

In a basin strongly influenced by seasonal variations in precipitations, there is usually a pattern in the stream water composition. During the dry season, dissolved concentrations increases due to strong evaporation, thus normally cause precipitation of secondary minerals in the river courses and mining areas. Dissolution of these salts is produced with the first rainfalls, when the highest contamination levels of the waters are reached. Once these salts are fully washed, contaminant concentration decrease during the wet season, due to the dilution caused by the highest river flow rates. (Blowes et al., 2003)

In the study area there was a similar behaviour of the contaminant concentrations. During the dry season there is an increase in contaminant concentrations, with the highest values at the mines inputs and a progressive dilution downstream. In the points where different kind of waters are mixing, i.e. HA-5, heavy polluted Huanuni mine and village waters and the unpolluted Ventaimedia waters, there is a high decrease in the concentrations of heavy metals, probably due to precipitations of secondary minerals. Distributions of REE differ completely, with an increase in concentrations along the river flow.

As concern the composition of the groundwaters it is possible to note a different effect of the seasonality. During the wet season in some sampling points the contaminant concentrations are higher than in the dry season. This behaviour probably is due to the dissolution of the salts precipitated in the dry season and the connection and interchange of waters with the rivers. As summarized by Sophocleous (2002) under

conditions of high precipitations, surface runoff and interflow gradually increase, leading to higher hydraulic pressures in the lower stream, which cause the river to change from effluent to influent condition, infiltrating its banks and recharging the aquifer and can occurs diffusely or at discrete locations. During the dry season occurs the opposite: the release of groundwater compensates for a decrease in stream discharge.

In the study area most of heavy metals (Zn, Fe, Cu, Pb and As) are present in groundwaters with higher concentrations during the wet season. This is particularly evident in the W-7 and could explain the composition of the Outcrop HA-8b, that was characterized by lower concentrations of contaminants (compared to the same river sampling point HA-8) in the dry season and higher in dry season, that indicate the interchange between surface and ground waters in both the seasons (Table 3).

Some examples are summarized in Figure 12 where seasonal changes in stream- and ground- waters for pH, Zn, Fe and SO_4^{2-} are represented. It is possible to note that in the wet season the variance in the elements concentration between the surface and ground waters are less pronounced than in the dry season for all the analysed elements. In particular iron and sulphate concentrations seems to trend to a homogenization between the two types of water that indicate the connection and the interchange between the surface- and ground- waters. This is more evident during the wet season, when the highly polluted surface waters infiltrate in the aquifer worsening the quality of the groundwaters.

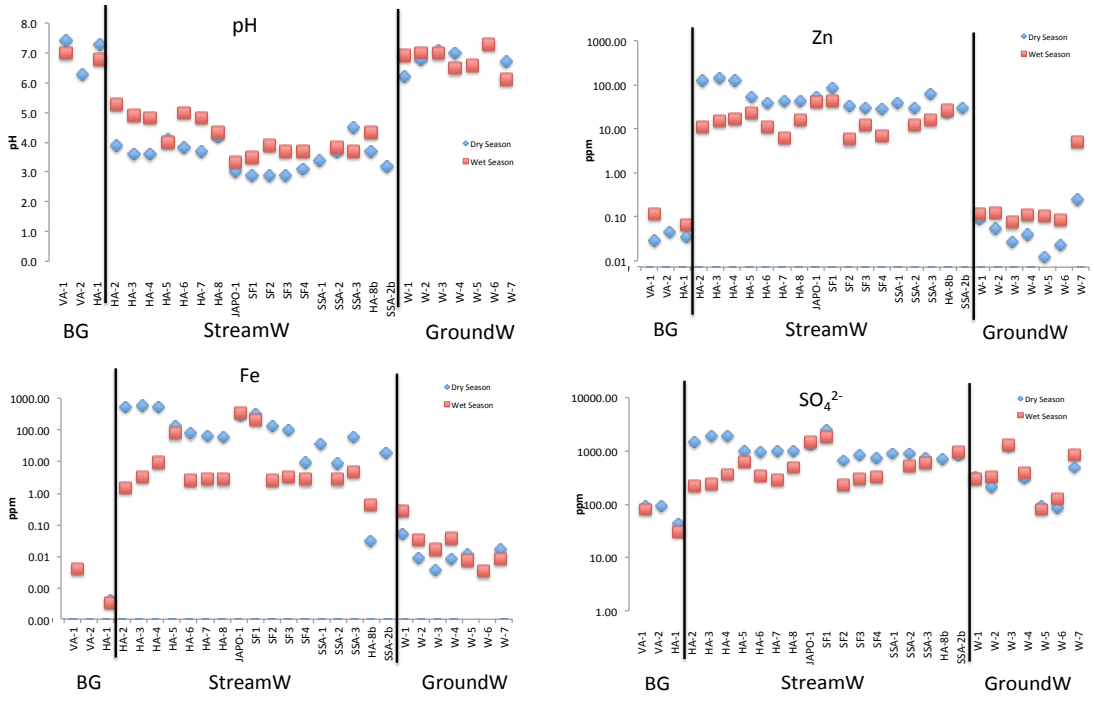

Figure 12: Seasonal changes in unpolluted waters (BG) stream- and ground- waters (W) for pH, Zn, Fe and SO_4^{2}.

Geochemical characterization of Sediments

Total sediment composition allowed a picture on the element concentrations, variations and correlations. In order to determine the contamination degree of the sediment, it was first necessary to define the background concentration and its natural variation respect to the average upper crust composition (UCC). The determination of the natural variability, detection and quantification of anthropogenic enrichment require a geochemical normalization, establishing mathematical correlations between metal concentrations and the concentration of a reference element in a reference material. The reference element must be of lithogenic origin, structurally linked to at least one of the main carriers of metals to the sediment, stable under geochemical conditions found in the sediment and its concentration must not be significantly influenced by anthropogenic inputs (Tapia et al., 2012; Varol, 2011; Loring, 1991; Kersten and Smedes, 2002). When geochemical normalization is conducted, it will help differentiate any potential site contaminant releases from background sources. Titanium was utilised in this study to normalize the data.

The environmental impact of metal pollution in soils depends not only on the total concentrations of the pollutants, but also on their mobility and availability, which influence their release and their interaction with other components of the ecosystem. Hence, it is possible for sediment to be metal-contaminated, with a metal content higher than the natural background, without the manifestation of any toxic effects.

Single and sequential extraction schemes are among the most widely used techniques for the selective extraction of trace elements from operationally defined sediment and soil solid fractions (Tessier et al., 1979; Meguellati et al., 1983; Sahuquillo et al., 2003; Morillo et al., 2002; Cappuyns et al., 2007;).

These techniques give information on the element distribution among the different phases of a soil and help to predict the potential effects of metal contamination in soils in changing environmental conditions, such as pH or redox potential. There are many criticisms of these procedures, being greatly influenced by experimental factors such as choice of reagents, extraction time, weight ratio of sample to volume of solution, lack of specificity of reagents, the possibility of re-adsorption of released metals to remaining fractions and the potential alteration of phases during extraction (Bermond and Yousfy, 1997; Gómez Ariza et al. 2000).

With the aim of harmonising all the extraction methodologies, the European Community Standards, Measurement and Testing Programme (formerly the Community Bureau of Reference (BCR)), developed an extraction scheme in which the metals are divided into i) exchangeable, water and acid-soluble, ii) reducible and iii) oxidisable fractions. The three-step scheme proposed by the BCR and the modified version (Sahuquillo et al., 1999) have become very popular during recent years and their application has increased lately. The reproducibility of the modified procedure and its applicability to soils has been tested through interlaboratory exercises, showing a good reproducibility for Cd, Cr, Cu, Ni, Pb, and Zn in the three steps and the suitability of the modified version of the BCR scheme for the analysis of contaminated soil samples (Pueyo et al., 2008).

The modified version of the three-step scheme proposed by the BCR was applied in this study to predict changes over time in the fate of the pollutants, in an area affected by mine contamination providing comparative information on trace-metal mobility.

Total sediment composition

A total of 21 samples was analysed for the total chemical composition, 19 bedload and 2 suspended sediments, indicated with the code 's', corresponding to the water sampling points (Figura 4). For the sample Japo there is no data about the trace element composition because there wasn't enough sample to perform the analysis. In the Table 3 the complete dataset of the trace elements is reported

Table 6 reports the bulk chemical composition of the sediment samples. The samples upstream of the mine area (VA-1-2 and HA-1) are characterized by SiO_2 (70%), Al_2O_3 (12-14%), Fe_2O_3 (6%), K_2O (2-3%), MgO (1%) and NaO (0.8%). Downstream the Huanuni mine discharges the percentage of Fe_2O_3 increases (up to 13.84%) while all the other major elements decrease. Sediment related to the Japo mine has high Fe_2O_3 (14.73%) and low Al_2O_3 (4.71%) content. Santa Fe River sediment near the mine (SF-1) is characterized by a high Fe_2O_3 (18.96%) content, low SiO_2 (52.31%) and Al_2O_3 (8.78%). Suspended sediments are characterized by higher Al2O3, K2O, lower Fe2O3, and similar MgO, MnO, SiO2 concentrations compared to the bedload sediment sampled in the same site.

Table 6: Main composition of bedload and suspended sediment samples.

	(%) Al2O3	(%) CaO	(%) Fe2O3	(%) K2O	(%) MgO	(%) MnO	(%) Na2O	(%) P2O5	(%) SiO2	(%) TiO2
Ventaimedia River										
VA-1	13.51	0.52	6.15	2.69	1.10	0.08	0.94	0.17	70.68	0.70
VA-2	12.31	0.39	5.82	2.51	0.98	0.08	0.79	0.12	73.58	0.65
Huanuni River										
HA-1	14.14	0.28	6.90	3.12	1.21	0.19	0.71	0.14	70.13	0.66
HA-2	7.95	0.20	13.84	0.42	0.97	0.05	-	0.10	64.69	0.46
HA-3	7.68	0.14	10.03	0.47	0.90	0.03	-	0.09	73.46	0.47
HA-4	9.98	0.15	8.05	0.91	1.04	0.05	-	0.14	70.44	0.50
HA-5	8.86	0.15	10.56	0.59	1.01	0.05	-	0.11	69.76	0.49
HA-6	8.93	0.15	8.81	0.59	1.01	0.04	-	0.12	71.34	0.49
HA-7	8.56	0.14	9.41	0.48	1.03	0.05	-	0.10	72.28	0.49
HA-8	8.84	0.26	12.40	0.53	1.11	0.07	1.46	0.13	66.62	0.53
Japo River										
Japo	4.71	0.06	14.73	1.06	0.35	0.01	-	0.14	70.09	0.61
Snta Fe River										
SF-1	8.78	0.26	18.96	1.69	0.44	0.00	-	0.33	52.31	0.70
SF-2	10.86	0.21	10.94	2.60	0.64	0.02	-	0.24	64.62	0.71
SF-3	11.09	0.25	14.37	2.76	0.62	0.02	0.51	0.30	58.20	0.63
SF-4	9.56	0.51	4.81	2.29	0.44	0.02	1.08	0.13	78.69	0.43
S. Juan de Sora Sora river										
SSA-1	12.71	0.16	9.23	1.60	1.10	0.05	-	0.17	64.58	0.55
SSA-3	9.48	0.14	6.57	0.82	1.01	0.04	-	0.12	73.94	0.46
Outcrops										
HA-8B	13.44	0.19	9.59	1.80	1.13	0.06	-	0.19	61.31	0.57
SSA-2B	8.23	0.13	7.84	0.49	0.98	0.04	-	0.10	74.48	0.44
Suspended										
HA-2 s	9.99	0.16	12.08	0.92	1.01	0.04	-	0.13	64.45	0.48
HA-3 s	11.16	0.19	10.74	1.19	1.05	0.05	-	0.16	62.31	0.51

Table 7: Heavy metals and trace element concentrations of bedload and suspended sediment samples. The elements with the star were analysed with a semi-quantitative method.

		Ventaimedia River		Huanuni River								Snta Fe River				S. Juan de Sora Sora River		Outcrops		Suspended	
		VA-1	VA-2	HA-1	HA-2	HA-3	HA-4	HA-5	HA-6	HA-7	HA-8	SF-1	SF-2	SF-3	SF-4	SSA-1	SSA-3	HA-8B	SSA-2B	HA-2 s	HA-3 s
(ppm)	As	54.5	36.0	33.3	1234.4	629.6	555.6	692.1	613.1	604.5	728.0	2278.7	1138.9	1726.7	344.3	620.6	605.0	882.2	433.7	998.0	989.5
(ppm)	Ba*	568	467	591	ND	ND	ND	ND	ND	ND	ND	29	189	269	437	ND	ND	ND	ND	ND	ND
(ppm)	Bi	2.0	0.4	0.8	151.9	68.0	118.0	99.5	100.9	90.6	89.0	93.3	78.4	80.6	6.9	162.0	85.1	245.3	69.4	219.0	263.5
(ppm)	Br*	2.8	1.3	1.2	0.3	ND	ND	0.5	0.3	0.5	0.3	ND	0.3	0.7	0.4	0.3	ND	0.9	0.0	0.3	0.3
(ppm)	Ce	64.7	67.8	70.5	36.6	38.4	44.6	41.4	48.0	41.0	52.7	124.5	94.2	86.8	55.0	54.3	36.3	66.7	34.6	55.3	58.0
(ppm)	Co*	12.9	11.5	13.6	14.6	10.1	8.9	9.6	8.1	9.1	9.6	ND	2.7	0.4	1.9	7.8	5.5	11.1	7.5	14.4	14.7
(ppm)	Cr	104	137	147	191	269	140	191	143	183	206	101	56	74	171	94	103	112	132	140	113
(ppm)	Cu	55	26	27	1309	695	731	752	758	759	823	46	127	104	18	802	631	1181	597	1318	1394
(ppm)	Ga	18.8	16.2	18.9	60.5	49.1	57.8	56.4	60.1	59.2	61.7	29.6	28.0	29.2	15.9	49.7	56.9	66.2	53.8	63.4	64.7
(ppm)	Ge*	2.1	1.3	1.5	20.4	18.6	19.0	20.6	19.6	20.5	23.7	3.1	0.8	0.4	2.0	14.5	16.8	18.7	18.5	19.3	19.0
(ppm)	Hf*	8.1	5.3	4.9	22.1	12.5	11.5	12.8	14.0	15.3	19.2	ND	4.4	1.4	2.9	9.4	12.6	15.3	11.2	18.7	18.6
(ppm)	La*	28.6	34.9	36.2	25.0	24.5	24.3	25.0	21.6	20.0	21.6	62.2	38.9	46.0	22.9	24.9	22.5	33.8	13.2	28.6	31.3
(ppm)	Mn*	616	570	986	448	296	360	420	357	419	568	84	188	166	123	287	299	444	341	366	430
(ppm)	Mo	0.4	0.1	0.2	1.4	0.9	1.4	1.4	0.6	1.0	0.9	2.3	1.9	1.4	0.1	2.0	0.8	3.9	0.6	2.3	3.0
(ppm)	Nb	15.5	13.7	14.8	11.2	10.8	11.8	11.5	11.4	11.5	12.7	16.5	16.5	14.7	12.1	10.4	11.0	13.8	10.8	11.7	12.3
(ppm)	Nd*	28.7	29.7	31.6	16.7	11.9	20.9	16.3	19.7	20.5	21.6	49.9	34.8	35.8	22.1	22.1	14.1	28.4	16.0	20.7	24.5
(ppm)	Ni	31.2	22.8	27.0	21.3	14.4	14.3	14.3	13.2	13.5	16.0	5.6	8.1	7.2	5.6	13.9	10.5	22.0	10.6	23.0	23.0
(ppm)	Pb*	56	40	48	174	92	167	132	141	120	140	2996	591	666	221	192	279	294	96	248	301
(ppm)	Rb	130	119	173	38	41	77	50	51	40	40	90	141	151	120	106	63	157	40	82	105
(ppm)	Sb*	19.8	12.0	8.4	ND	ND	2.6	ND	ND	ND	ND	149.6	10.5	22.5	18.2	7.6	208.4	15.8	ND	8.7	14.2
(ppm)	Sc*	13.6	12.8	15.6	ND	0.3	ND	ND	ND	ND	ND	ND	ND	ND	6.6	ND	3.3	ND	ND	ND	ND
(ppm)	Se*	0.6	0.0	0.2	4.2	2.1	2.0	2.8	2.2	2.5	3.2	12.1	6.0	6.0	1.5	2.2	2.9	3.0	2.1	4.0	3.9
(ppm)	Sm*	9.1	3.5	5.7	2.8	5.9	6.9	2.9	0.6	1.4	5.5	6.7	4.6	3.0	4.5	4.8	0.7	ND	2.2	2.7	7.1
(ppm)	Sn*	391	121	66	17149	7645	8070	10032	10510	10379	11965	10695	7982	6688	1179	5767	6091	10638	7162	11174	11956
(ppm)	Sr	102	78	61	49	43	67	53	57	54	58	289	130	149	165	71	64	98	50	69	79
(ppm)	Ta*	1.2	0.8	ND	3.7	2.8	2.5	3.3	2.3	3.7	4.5	0.5	0.5	2.1	0.9	2.5	2.8	4.1	3.3	4.3	4.8
(ppm)	Te*	2.0	ND	ND	ND	1.2	3.4	ND	0.8	ND	0.4	ND	0.3	2.5	0.1	3.7	1.9	0.6	1.7	ND	0.6
(ppm)	Th	10.2	8.4	10.2	11.0	7.8	10.4	10.1	9.0	9.5	9.7	12.2	14.2	13.5	6.9	9.8	8.0	16.6	8.3	13.3	15.1
(ppm)	Tl*	1.9	1.2	2.0	4.1	3.2	3.0	4.0	3.5	3.9	3.1	3.0	1.5	2.5	0.9	5.5	1.7	8.1	2.7	6.5	6.7
(ppm)	U*	2.5	1.1	2.2	1.1	1.4	2.5	2.0	2.5	1.6	1.6	1.2	2.5	1.9	1.8	2.9	1.6	5.6	0.6	3.8	5.5
(ppm)	V	100	99	115	81	68	85	78	80	76	82	111	94	104	59	82	76	111	70	92	96
(ppm)	W	8.3	4.2	5.6	113.2	57.2	72.1	73.7	82.9	79.3	91.2	52.9	38.4	35.8	8.6	75.2	55.6	107.5	57.0	90.9	97.6
(ppm)	Y	27.6	23.7	27.7	20.5	16.4	19.5	19.1	19.4	19.2	20.8	35.3	29.0	24.5	15.6	16.4	17.5	23.6	16.4	20.4	22.0
(ppm)	Yb*	4.1	3.9	2.7	ND	0.9	2.7	1.8	1.3	1.1	0.2	ND	2.2	ND	2.6	2.0	2.2	ND	3.2	ND	ND
(ppm)	Zn	351	209	237	1513	823	872	985	934	1009	1239	295	167	134	58	813	968	1269	815	1488	1645
(ppm)	Zr	236	215	180	269	220	166	223	193	216	309	304	234	189	176	113	131	137	164	176	162

Through the analysis of the trace element concentrations (Table 7) it is possible to observe the different sediment composition of the analysed areas. The Huanuni sediments are characterized by high Cu, Ga, Ge, Ta, Te, W and Zn content. Santa Fe River has high concentrations of As, Pb and Sr, which indicate a different ore composition. The sediments of Santa Fe are also characterized by high content of Ba, Sb and Se.
In Table 7 are presented the data of the main heavy metals content. The upstream samples VA (1-2) and HA-1 show the lower concentrations of the metals. A sharp increase in concentration occurs after the Huanuni mine discharge (HA-2). The change affects mainly Sn, the main product of the mine, which increases three orders of magnitude, important are the variations affecting As and Cu (two orders of magnitude) while Zn and Pb increase of one order of magnitude. These changes in concentrations are directly related to the mining activities. The decrease in concentrations downstream probably is due to dilution effect.

Enrichment factor

In the interpretation of geochemical data, choice of background values plays an essential role. Many authors have used the average shale values or the average crustal abundance data as reference baselines. The best alternative is to compare concentrations between contaminated and uncontaminated sediments that are mineralogically and texturally comparable. In our approach we will use the upper continental crust as a reference, but we will consider the sediments upstream the mine area (HA-1, VA-1, VA-2) as possible estimate of the local background. It is a rough estimate but permits interesting considerations.

As many different metallogenic belts surround the considered area, a Natural Enrichment Factor (EF) was computed in order to determine the geologic influence and the local enrichment compared to the upper continental crust (UCC). This natural background refers to the uncontaminated sediments of the study area.
Titanium was used to normalize the data, because of its conservative behaviour in rocks from Earth Crust, the constant concentrations in the studied area (c. 0.67%), similar to that of the Upper continental crust given by Rudnik and Gao, 2003 (0.64%).

Table 8: Recommended composition of the upper continental crust. Major elements in weight percent (Rudnik and Gao 2003).

Element	Units	Upper crust	1 Sigma	%	Element	Units	Upper crust	1 Sigma	%
SiO2	wt.%	66.6	1.18	2	**Ag**	ng/g	53	3	5
TiO2	”	0.64	0.08	13	**Cd**	mg/g	0.09	0.01	15
Al2O3	”	15.4	0.75	5	**In**	”	0.056	0.008	14
FeOT	”	5.04	0.53	10	**Sn**	”	2.1	0.5	26
MnO	”	0.1	0.01	13	**Sb**	”	0.4	0.1	28
MgO	”	2.48	0.35	14	**I**	”	1.4	50	5
CaO	”	3.59	0.2	6	**Cs**	”	4.9	1.5	31
Na2O	”	3.27	0.48	15	**Ba**	”	628	83	13
K2O	”	2.8	0.23	8	**La**	”	31	3	9
P2O5	”	0.15	0.02	15	**Ce**	”	63	4	6
Li	mg/g	24	5	21	**Pr**	”	7.1		
Be	”	2.1	0.9	41	**Nd**	”	27	2	8
B	”	17	8	50	**Sm**	”	4.7	0.3	6
N	”	83			**Eu**	”	1	0.1	14
F	”	557	56	10	**Gd**	”	4	0.3	7
S	”	62	33	53	**Tb**	”	0.7	0.1	21
Cl	”	370	382	103	**Dy**	”	3.9		
Sc	”	14	0.9	6	**Ho**	”	0.83		
V	”	97	11	11	**Er**	”	2.3		
Cr	”	92	17	19	**Tm**	”	0.3		
Co	”	17.3	0.6	3	**Yb**	”	1.96	0.4	18
Ni	”	47	11	24	**Lu**	”	0.31	0.05	17
Cu	”	28	4	14	**Hf**	”	5.3	0.7	14
Zn	”	67	6	9	**Ta**	”	0.9	0.1	13
Ga	”	17.5	0.7	4	**W**	”	1.9	1	54
Ge	”	1.4	0.1	9	**Re**	ng/g	0.198		
As	”	4.8	0.5	10	**Os**	”	0.031	0.009	29
Se	”	0.09	0.05	54	**Ir**	”	0.022	0.007	32
Br	”	1.6			**Pt**	”	0.5	0.5	95
Rb	”	84	17	20	**Au**	”	1.5	0.4	26
Sr	”	320	46	14	**Hg**	mg/g	0.05	0.04	76
Y	”	21	2	11	**Tl**	”	0.9	0.5	57
Zr	”	193	28	14	**Pb**	”	17	0.5	3
Nb	”	12	1	12	**Bi**	”	0.16	0.06	38
Mo	”	1.1	0.3	28	**Th**	”	10.5	1	10
Ru	ng/g	0.34	0.02	6	**U**	”	2.7	0.6	21
Pd	”	0.52	0.02	3					

The Natural EF for all the analysed elements was calculated through the Equation 6. The average of the concentrations measured in the mine upstream sites normalized to titanium was related to the average composition of the Upper continental Crust presented in Table 8 (Rudnik and Gao, 2003) normalized to titanium.

$$\text{Natural EF} = [M_b/Ti_b]/[M_{ucc}/Ti_{ucc}] \qquad \text{Equation 6}$$

In this equation M corresponds to the metal(loid) of interest, Ti to Titanium and subscript b indicates sediment concentration in the unpolluted upstream sediment samples, subscript UCC is for the Upper Continental Crust concentration.

The natural EF data are summarized in the Table 9 and are interpreted as suggested by Sakan (2009), where EF<1 indicates no enrichment; <3 is minor enrichment; 3-5 moderate enrichment; 5-10 moderately severe enrichment; 10-25 severe enrichment; 25-50 very severe enrichment; >50 extremely severe enrichment. It appears that even in the presumably less affected sites, there is unusual presence of elements as As, Bi, Sn. Tin is the main ore metal in the area, Sb is associated to the mineral deposits of the area. The moderate enrichment in Arsenic and Bismuth could be related to rich sulphide deposits (Merian et al., 2004). For these elements a local increased background is to be expected, likely due to the presence of diffused mineralization of minor economic importance in the catchment upstream.

Table 9: Natural EF of the studied area, elements with the star were calculated with a semi-quantitative method

Element	EF	*Element*	EF	*Element*	EF	*Element*	EF
As	8.2	*Ge**	1.1	*Sb**	31.8	*U**	0.7
*Ba**	0.8	*Hf**	1.1	*Sc**	0.9	*V*	1.0
Bi	6.4	*La**	1.0	*Se**	2.5	*W*	3.0
*Br**	1.0	*Mo*	0.2	*Sm**	1.2	*Y*	1.2
Ce	1.0	*Nb*	1.2	*Sn**	87.0	*Yb**	1.7
*Co**	0.7	*Nd**	1.1	*Sr*	0.2	*Zn*	3.8
Cr	1.3	*Ni*	0.5	*Ta**	0.6	*Zr*	1.0
Cu	1.2	*Pb**	2.7	*Th*	0.9		
Ga	1.0	*Rb*	1.6	*Tl**	1.8		

Then the EF has been calculated for the other samples following Equation 7 where metal concentration data are reported to the natural background values (subscript b).

$$EF = [M/Ti]/[M_b/Ti_b] \quad \text{Equation 7}$$

In Table 10 are presented the EF>5, showing the 'moderately severe' to 'extremely severe' enriched samples. The Bi is the most enriched element with the maximum EF (322) in the suspended sediments of the HA-3 sample and high values in all the Huanuni and San Juan de Sora Sora rivers samples with a minimum value in HA-3 (91). In the Santa Fe River the EF of Bi is lower, with values between 69 and 83 and a minimum in SF-4 (10). This element is typical of sulphide ore deposits associated with lead copper and tin oxides (Merian et al., 2004). High EF is detected for Sn in all the samples with the maximum in HA-2 (129) and the minimum in SF-4 (10). The EF of Cu, Ge and W indicate a strong enrichment in the Huanuni and San Juan de Sora Sora rivers sediments and a moderate enrichment for the Santa Fe River samples. Sediments are enriched in As principally at the mines discharges (HA-2, SF-1) and high values in SF-3 and in suspended sediments is detected. Ga and Zn are moderately- strongly enriched in the HA

an SSA samples and not in the SF samples. The behaviour of Pb and Sb is opposite, with enriched sediments in the Santa Fe River and normal concentrations in the Huanuni samples.

The calculation of the Enrichment Factor is an important tool to define the mine impact on the sediment composition. It is important to note that the natural EF was determined only on Huanuni and Ventaimedia mine upstream samples. It is possible that in the Morococala and Japo Mines, which influence the composition of Santa Fe River, the composition of sediments is different.

Table 10: Enrichment Factor >5 based on natural Enrichment factor of the studied area. Elements with the star were calculated with a semi-quantitative method

	As	Bi	Cu	Ga	Ge*	Mo	Pb*	Sb*	Se	Sn*	Ta*	W	Zn
Huanuni River													
HA-2	43	206	53	5	18	9	5	<5	26	129	5	27	8
HA-3	22	91	28	<5	17	6	<5	<5	13	57	<5	14	<5
HA-4	18	147	27	<5	16	8	5	<5	11	56	<5	16	<5
HA-5	23	126	28	<5	17	8	<5	<5	16	71	5	17	5
HA-6	20	129	29	5	17	<5	<5	<5	13	75	<5	19	5
HA-7	20	115	29	<5	17	6	<5	<5	14	74	5	18	5
HA-8	22	105	29	<5	19	5	<5	<5	17	78	6	19	6
Snta Fe River													
SF-1	53	83	<5	<5	<5	9	60	11	48	53	<5	8	<5
SF-2	26	69	<5	<5	<5	8	12	<5	24	39	<5	6	<5
SF-3	44	80	<5	<5	<5	6	15	<5	27	37	<5	6	<5
SF-4	13	10	<5	<5	<5	<5	7	<5	10	10	<5	<5	<5
S. Juan de Sora Sora river													
SSA-1	18	185	27	<5	11	11	5	<5	11	37	<5	15	<5
SSA-3	21	115	25	5	15	5	8	23	18	46	<5	13	5
Outcrops													
HA-8B	25	268	38	<5	14	20	7	<5	15	65	5	21	6
SSA-2B	16	98	25	5	17	<5	<5	<5	13	56	5	14	5
Suspended													
HA-2 s	34	284	51	5	17	13	7	<5	23	81	6	21	8
HA-3 s	31	322	51	5	15	17	8	<5	22	81	6	21	8

Relationships between the trace elements

The relationships of the analysed samples were explored through a Spearman correlation matrix, as for the water samples, in order to minimize the effects of the outliers. The obtained matrix is presented in the (Annex 2). The bold values indicate a correlation with a $p<0.001$. An excellent correlation is shown between Ga, Ge, Hf, Sn Ta, Tl, W, Yb and Zn with Bi and Cu. A second high correlated group is: Ce, La, Nb, Nd, Rb, Sr, Ti, V and Y. As is highly correlated (>0.9) with Fe and Se. Co, Mn and Ni are strongly correlated (>0.83)

Sequential extractions

The objective of the four-step sequential extraction procedure in this study was the evaluation of the mobility and retention behaviour of some elements of particular interest for the analysed area Ca, Mg, Cu, Mn, Zn, Fe, and S, in specific physical–chemical and mineral phases. The results for the four extractions steps are presented in the Annex 2.
The extractable fractions are presented as Steps (St):

- **Step 1 (St1)** represents the most labile portion, the water- acid- soluble, bound to the carbonate fraction.
- **Step 2 (St2)** represents the reducible portion ions bounded to Fe- Mn- oxides and hydroxides
- **Step 3 (St3)** represents the oxidisable part of the sediment, ions bounded to organic matter or sulphurs
- **Step 4 (St4)** mineralized portions, bounded to the crystalline structure of the mineral

An internal check was performed on the results of the sequential extraction by comparing the total amount of metals removed in the procedure with the results of the total concentrations values obtained with the XRF analysis; the extraction rates were extremely variable (Cu varies from 107 to 180%, 90-134% for Mn, 99-153% for Zn, 68-107& Pb, 81-108% Fe). Since no suitable certified reference materials were available to validate either the extraction or the aqua regia digestion, it was not possible to determine the source of the variability.

Samples for sequential chemical extraction analysis were selected in order to reasonably represent the three considered rivers, mines up- and down- stream and the type of sediment (suspended, bedload) and are presented in the Table 1 and shown in the Figure 4.

Bedload Sediment

In Table 11 are presented the extraction data in the four extraction steps for calcium, magnesium and sulphur. In Figure 13 a are shown the extraction percentage for calcium: in the first two sites (HA-1 VA-1), the 60% of Ca is bounded to the most labile portion of sediment, which represents the part bound to carbonates or in a sorbed-exchangeable position. 30% is bounded to the oxidized portion and 10% to the reduced and crystalline fraction of the sediment, that indicate a high mobility and a strong association with the fraction dissolved in acetic acid. Downstream, the exchangeable fraction decreases, a consequence of the contact with acidic waters that have a similar effect of the laboratory experiment. This is also reflected by the change in the recovery of Ca (Figure 13b). The sample SF-3 indicates a different composition of the River sediment, with the 40% of Ca linked to the residual fraction. Samples HA-5 and SSA-1

are characterized by low concentrations and all the Ca associated to the redicible fraction.

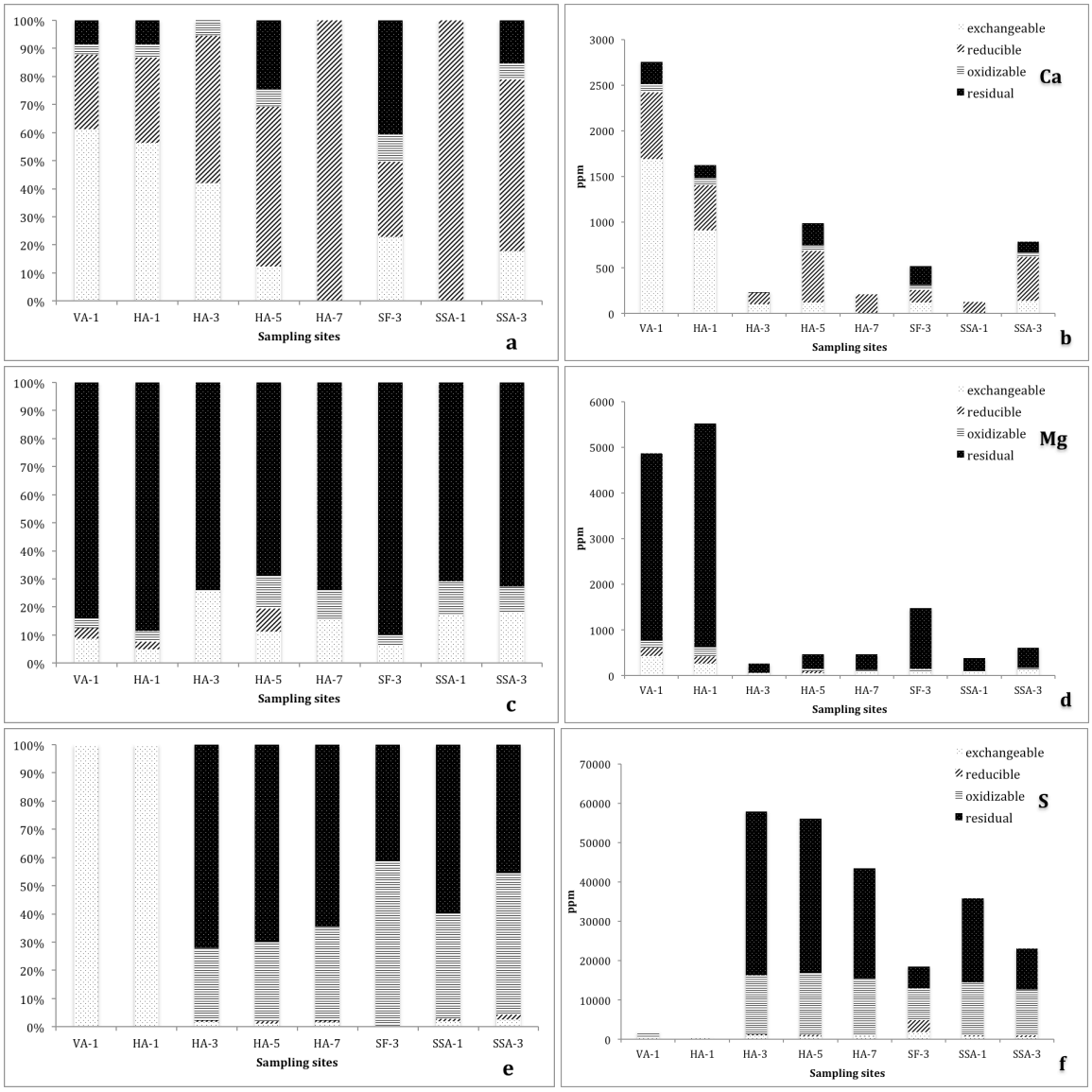

Figure 13: Mobility of Ca (a-b), Mg (c-d) and S (e-f) from sediments given as percentage of pseudototal metal concentrations (a-c) and the recovery (b-d).

Figure 13c-d represents the Magnesium partitioning: more than 70% of Mg in all the samples is bounded with the crystalline structure. The XRF total concentrations indicate a homogeneous distribution of Mg along the Huanuni River (c. 6000 ppm) with the exception of the Santa Fe River (c. 3700 ppm). The recovery varies greatly between the upstream samples (VS-1 and HS-1) with high extraction rates (75%) and lower rates downstream (5-39%), which indicate a strong link with the silica crystalline structure.
The speciation of Sulphur (Figure 13e-f) indicates that in the mine upstream the entire S is easily exchangeable and that the concentrations are really low. Downstream the mine there is a high increase of the concentrations and S is bounded for 40-60% to the mineral part and 39-60% the oxidizable fraction. The decrease downstream of the recovery is probably due to the dilution effect. In particular the concentrations of the residual portion is decreasing and the oxidizable increasing.

Table 11: Concentration at each step of the BCR sequential extraction procedure for Ca, Mg, and S.

	Ca				Mg				S			
	exchangeable	reducible	oxidizable	residual	exchangeable	reducible	oxidizable	residual	exchangeable	reducible	oxidizable	residual
Venteimedia River												
VA-1	1690	733	97	238	426	182	162	4093	668	DL	1227	DL
Huanuni River												
HA-1	913	494	78	142	267	152	211	4897	327	DL	DL	DL
HA-3	100	125	13	DL	67	DL	DL	191	974	314	14933	41761
HA-5	121	563	60	244	53	39	56	325	682	420	15830	39223
HA-7	DL	211	DL	DL	70	DL	50	343	683	235	14556	28007
Snta Fe River												
SF-3	118	140	50	211	89	DL	57	1329	1808	3128	8003	5605
S. Juan de Sora Sora river												
SSA-1	DL	128	DL	DL	68	DL	45	273	671	324	13473	21312
SSA-3	139	480	49	118	112	DL	55	445	613	376	11647	10444

The fingerprint of the mine discharge was evident for Fe, which acted as a marker of the pollution source (Figure 14). In the upstream-unpolluted samples, the 90% is linked to the residual fraction, sonly a small fraction of Fe (10%) was solubilized by reduction and no extraction was observed at the oxidation step. After the mine discharge Fe was partially solubilized in the oxidizable step (>30%), with the rest remaining in the residual fraction, linked to more resistant mineralogical phases, such as crystalline Fe oxides and residual silicate phases. The SF-3 sample is characterized by a 30% of reducible fraction, which indicate the presence of Fe- oxi-hydroxide.

The distribution obtained for Manganese (Figure 14c) showed a high extractability, being the sum of the Mn extracted in the three steps up to 90%. In the upstream sites Manganese is mainly bound to the reducible part of sediments, indicating that it is mainly associated with Mn oxides (Zhang et al. 1998, Maiz et al. 2000). In the dowstream sites increase the link with the oxidizable fraction, and the portion extracted with acetic acid. This fact indicates that Mn in highly contaminated soils was also associated with fractions such as sulfides of Mn(II) (da Silva et al. 2002) . Manganese also decreases in concentrations after the mine discharge (Figure 14d), probabily due to the solubilization of secondary minerals. The total concentration indicates high concentrations in the background area, and a reduction in concentrations mine downstream and the vanishing of the reducible fraction.

Table 12: Concentration at each step of the BCR sequential extraction procedure for Fe, Mn, Cu and Zn.

	Fe				Mn				Cu				Zn			
	exchangeable	reducible	oxidizable	residual	exchangeable	reducible	oxidizable	residual	exchangeable	reducible	oxidizable	residual	exchangeable	reducible	oxidizable	residual
Venteimedia River																
VA-1	201	2099	722	38244	264	240	30	236	5	16	19	41	207	103	65	160
Huanuni River																
HA-1	5	1406	275	43922	109	629	42	332	DL	5	DL	41	26	36	39	192
HA-3	1659	1454	21528	50923	93	28	55	130	51	18	520	660	DL	DL	660	513
HA-5	1187	3004	23728	47783	72	47	117	221	29	25	521	600	43	22	716	588
HA-7	1593	2179	21020	38700	109	51	105	182	32	14	595	445	18	DL	744	378
Snta Fe River																
SF-3	1100	26999	8101	68567	24	45	14	140	13	30	23	78	37	8	48	68
S. Juan de Sora Sora river																
SSA-1	1368	1772	20288	30968	106	33	87	113	29	16	520	292	DL	DL	666	244
SSA-3	614	3666	12935	20031	120	50	82	55	25	15	561	175	58	30	768	223

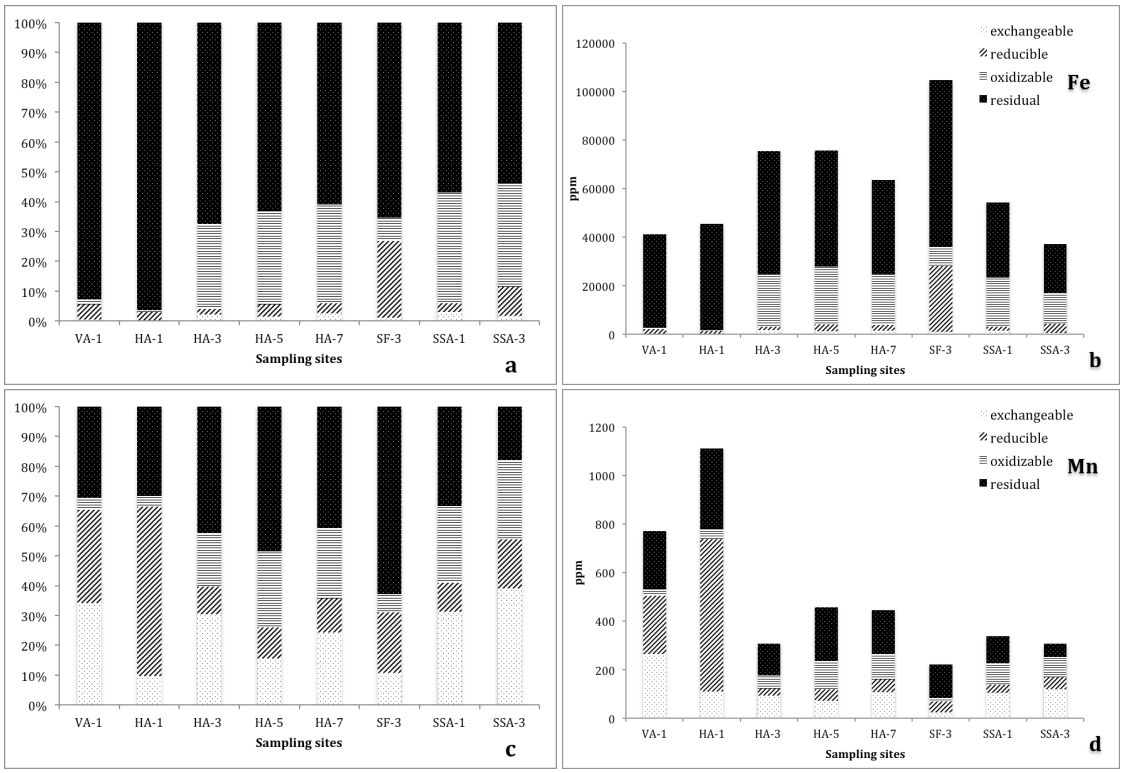

Figure 14: Mobility of Fe (a-b) and Mn (c-d) from sediments given as percentage of pseudototal metal concentrations (a-c) and the recovery (b-d).

The extractability of Copper, shown in Figure 15a, indicate that in almost all the samples have a good association with the residual fraction (c. 50%) although in sample HA-1 up to 90% of the Cu is in the residual fraction, while in SSA-1-3 only the 34%. Sediments of the VA-1 and SF-3 samples have the same composition, with about 20% of reducible Cu and 20% oxidisable, which indicates that the Santa Fe river has a copper distribution similar to that of the background area. This two samples and the HA-1 reflects the affinity of Copper to be adsorbed and co-precipitated with Fe oxy-hydroxides (Adriano, 2001; James and Barrow, 1981). The Huanuni dowstream sediments indicate significant concentrations of Cu in the oxidizable fraction (42-72%) which increase along the stream flow associated to the decrease in the residual fraction and almost the depletion of the reducible. The recovery data (Figures 15b) confirm low data upstream the mine (VA-1 and HA-1) and in Santa Fe River sample, indicates that the sample with the higher concentration (HA-3 1249ppm) is influenced by Huanuni mine discharges, the other sample concentrations indicate a progressive dilution along the river flow.

In the upstream sampling sites Zinc (Figure 15c) is distributed through the different phases, with predominance of the exchangeable portion in VA-1 (39%) and of the mineral phase in HA-1 (66%). The SF-3 sample has similar characteristics of the upstream samples with a high association to the exchangeable phase (23%). The samples dowstream the mine are characterized by an increase in the oxidizable portion (52-73%) and the disappearance of the reducible and exchangeable fractions.

Association to ore minerals (sulphides) could be the likely explanation. The recovery (Figures 15d) increase significantly after Huanuni mine discharge, with the maximum extraction in HA3 (1368ppm) and a progressive dilution along the river flow.
Comparing the distribution pattern for Cu, Zn an increase in the extraction rates after sludge discharge and the decrease in the exchangeable fraction (first step), with the others two fractions (second and third step) is observed. The oxidation of the sludge leads to the formation of soluble weathering products that can be solubilized due to washing processes as documented by Pueyo et al. (2008). This implies a decrease in the trace elements concentrations immediately after mine discharge as indicated by the concentrations of these two elements in the Table 7.

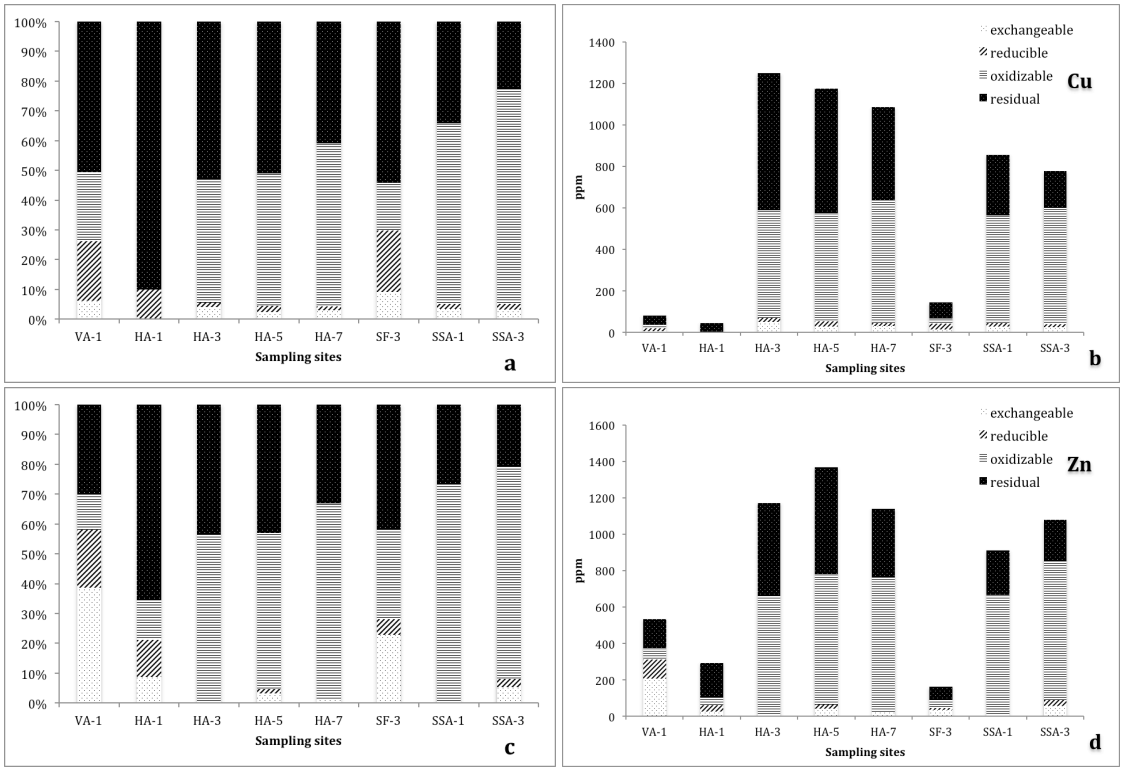

Figure 15: Mobility of Cu (a-b) and Zn (c-d) from sediments given as percentage of pseudototal metal concentrations (a-c) and the recovery (b-d).

Suspended Sediment

The characteristics of suspended sediments were determinate with the application of sequential extractions to three samples. HA-3s sample represent the discharges of the Huanuni mine, HA-5s the confluence with the Ventaimedia River waters and the SSA-1s the mixing with the Santa Fe River waters (Table 1). The data are compared with the bedload sediment sequential extractions data (Figures 16-17). The recovery of all the analysed elements instead of Fe and S is higher in the suspended sediments than in the bedload. These elements are characterized by the increase in the extractable fraction and the decrease of the residual fraction for Cu, Zn and Mn. Fe and S behave differently and are characterized by lower recovery in the suspended sediment. Fe is characterized by the increase of the reducible fraction, which indicates the presence of secondary iron-oxi-hydroxides (Blowes and Ptacek, 2003).

The sample with the greater differences between the suspended and the bedload sediment is the HA-3s, resulting easy extractable for hazardous elements such Cu and Zn.

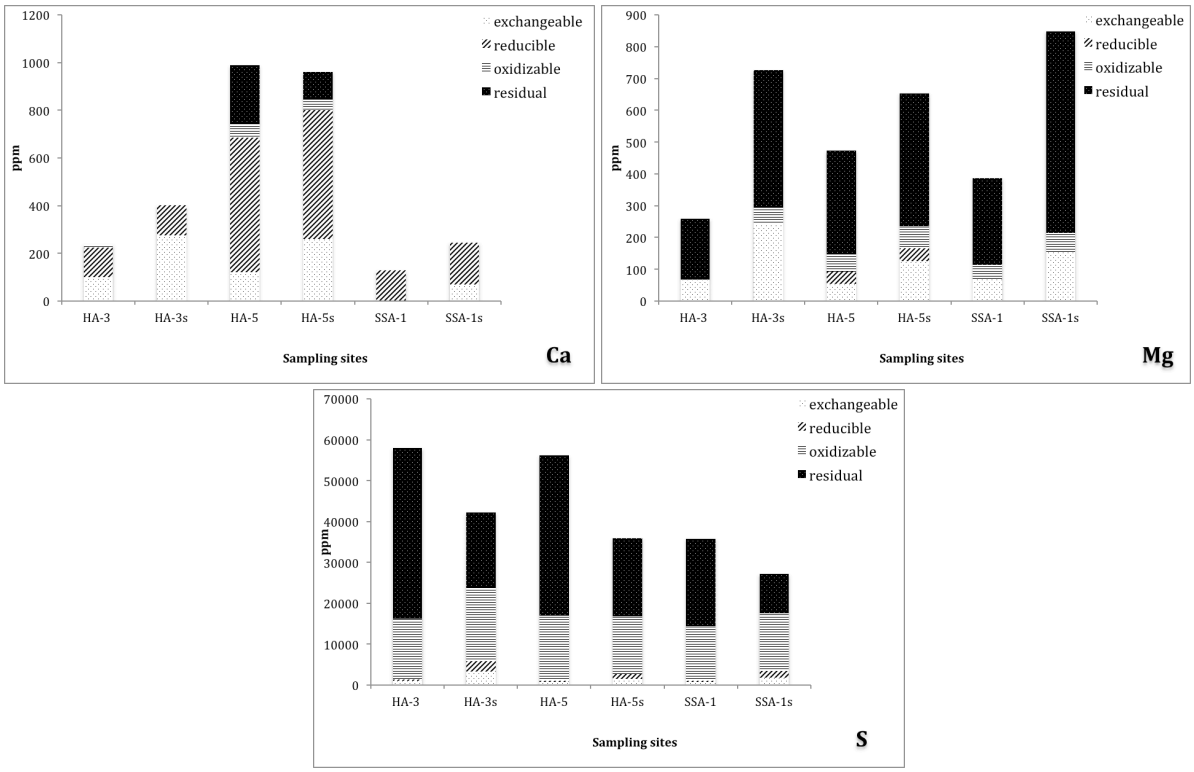

Figure 16: Recovery for Ca, Mg, and S in suspended and bedload sediments.

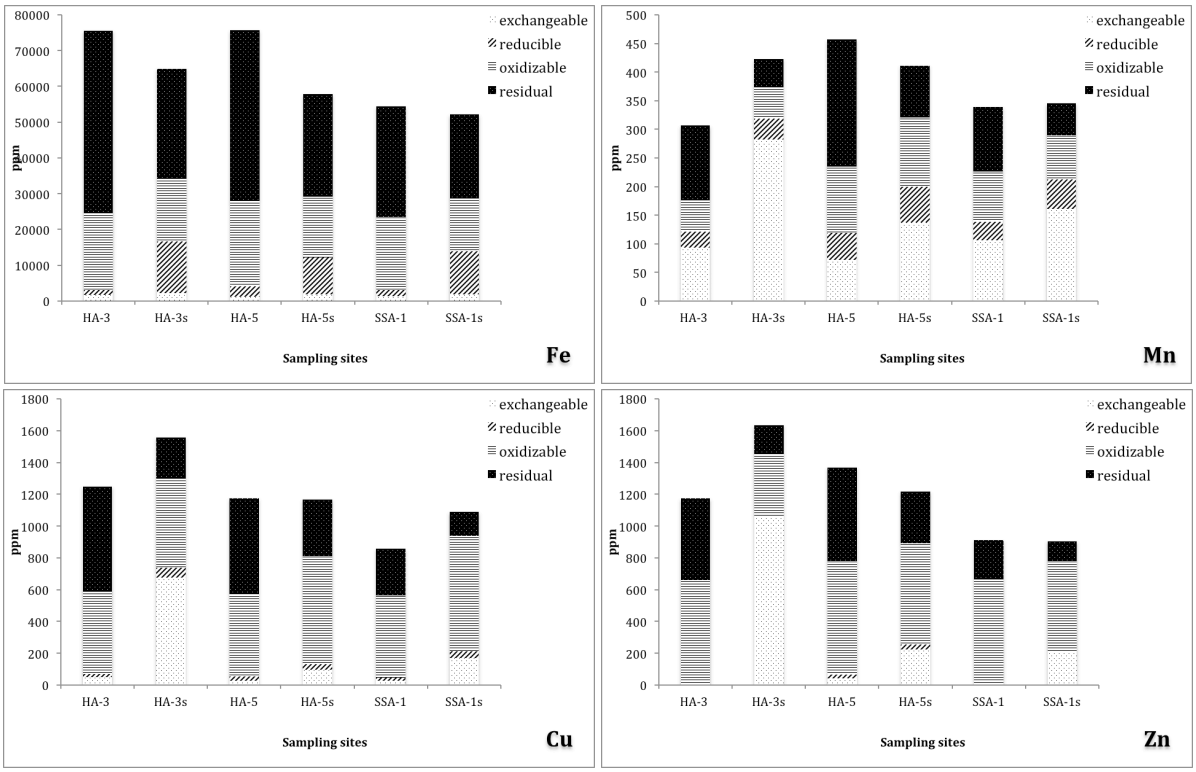

Figure 17: Recovery for Fe, Mn, Cu and Zn in suspended and bedload sediments.

From data obtained in the *first extraction step*, Ca and Mn and to a lesser extent Mg were the most mobile elements. Cu and Zn were significantly leached in the first step, especially in suspended sediment samples. The relative mobility of Cu and Zn in the suspended sediment, however differ completely from that in the bedload sediment. This highlights the active role of the suspended sediment in the trace element interaction in the contaminated sediments.
Extraction yields in the *second extraction step* were high for Ca, especially in contaminated soils, Fe extraction rates were high in suspended sediment. In the sample SF-3, that differs from the others, Cu, Fe and Mn have the higher extraction rates.
The greater extractions in the *third extraction step* were for the Cu, Fe, Zn and S, displaying a strong connection between the trace element and sulphur.

Water - Sediment Interactions

In order to analyse the water-sediment interactions will be considered the Huanuni area since the dataset is complete with background values during the dry season.
Calcium is a key factor in an environment affected by acidification because of its buffer effect in the dissolution of carbonate and aluminosilicate. In the Huanuni area the interaction between the sediment and water components is highly connected. Mine upstream the 0.2% of total sediment content is CaO and the sequential extractions demonstrate a high extractability (60%) in the first step, which indicates the high mobility of this element. Analysing the data after mine discharge there is a decrease in the total sediment content (0.15%) and an increase in the water content as a result of the dissolution of Ca-bearing minerals as for example carbonate, plagioclase, smectite, amphibole and piroxene.
Concentrations of **Magnesium** increase in water content after mine discharge and the content in the sediments decrease. The concentration of this element as for Calcium is strongly dependent by the dissolution of aluminosilitate minerals, which, in contact with acid waters dissolve and contribute to acid-neutralization of the waters. The high residual fraction (up to 90%) obtained by the sequential extraction and the strong decrease in recovery after the mine discharge confirm the link with the most common Mg-bearing minerals associated with sulphide rich tailing as for example chlorite, smectite, biotite, amphibole and piroxene.
Sulphur data in the total sediment composition are not available. The concentrations in water after mine discharge rise up to 600 ppm and decrease to 300ppm at the inflow of the Ventaimedia River and remain constant along the river flow. Sequential extractions indicate that the concentrations increase after mine discharge; the 70% is bound to the residual fraction and 30% could be released in an oxidizable environment. The bedload sediment carries out more sulphate than the suspended but result less extractable.
Iron in upstream waters wasn't detected, in sediment formed the 7% (expresses as Fe_2O_3) of the total content and the sequential extractions indicate that is bounded for 95% to the residual fraction. After the mine, concentrations increased to 14%, (Fe_2O_3) with a 30% bounded to oxidizable fraction (sulphur) of the sediments and in waters the

concentrations increase up to 500 ppm. Mine discharges could be considered the input in to the waters and sediments of iron in solution; its occurrence is connected to the oxidation of pyrite as demonstrate by the strong connection with the sulphates (AMD process). The increase in concentrations in sediments could be related to the crystallization of secondary minerals as iron-sulphate of the type $Fe^{2+}SO_4$*n H_2O and iron oxides and –oxihydroxides in the suspended sediments.

Manganese content in total sediments decrease from 0.19% to 0.05% after the mine discharge and its link to the sediment varies greatly. In the HA-1 site the 60% of the manganese is bound to the reducible portion (Mn-hydroxides), after the discharge 30% is easy extractable 10% reducible and 20% oxidizable; in the waters increase from 0 to 20 ppm. The discharges of the mines produce the release of this element in waters due to the dissolution of aluminosilicate and the decrease in the sediment content. The data of the suspended sediment (67% extracted in the step 1) confirm the high mobility of this element due to the mine sludge.

Copper is present in the background area in water in low concentrations, don't exceed the WHO limits and isn't enriched in the sediment compared to the upper continental crust. Sequential extractions indicate that in these conditions 90% is bound to the residual fraction. After the mine discharge, the content in sediment increase two orders of magnitude, only 50% is bound to the residual fraction and 40% to the sulphur and organic matter. The suspended sediment extraction data shows that the 43% is easy extractable, that confirm the high values (up to three orders of magnitude higher than in background) in the water concentration. It is important to note that the concentrations in water increase downstream, and the total sediment content of Copper decrease probably due to the high mobility in the suspended sediment and its release along the river flow.

Zinc as Cu in the background area doesn't exceed WHO limits in the waters. Its concentrations in the sediment indicate that the area is moderately enriched referring to the UCC with a 60% bound to the residual part. After the mine discharge the total sediment content increase up to one order of magnitude, only 40% is linked to the residual part, and the 60% is bound to the sulphate. The suspended sediment analysis demonstrate that 65% is easy exchangeable, that confirm the increase in concentrations in waters and a progressive decrease in the total content.

Conclusions

For the first time, mining related contamination in the San Juan de Sora Sora basin in Bolivia was investigated using a geochemical approach. Surface waters were identified as the vector for the contaminants, which can cause multiple and serious effect on the environment and furthermore to the human health.

This study highlight that the oxidation of sulphide minerals released from the mine activities of the three mines Huanuni, Morococala and Japo strongly influence the quality of waters and sediments of the area with an increase in the acidity of the waters containing high concentrations of SO_4^{2-}, Fe and other metals.

The pH value and the redox conditions of the waters are a good instrument to define the pollution intensity and a good tool to identify most of the processes controlling the precipitation and/or dissolution of minerals.

Throughout the analysis of the surface water is possible make a distinction between unpolluted waters, characterized by high pH 6.3-5.3 and defined as Ca-Mg-Na-HCO3-SO4 type and mine-contaminated waters classified as Ca-Mg-SO4 type characterized by low pH (2.9-5.3). The pH values and the composition of these two types of water are strongly dependent on the seasonal variation of the precipitations and to the distance from the mine spill.

Most of the mine contaminated waters were exceeded the water guidelines proposed by the World Health Organization (WHO) for the heavy metal content. The highest concentrations of pollutants were found at the mines discharge during the dry season. In the unpolluted waters only lead, in the dry season, exceeded the guidelines, which could be a natural enrichment due to the mineralogical composition of the area characterized by Galena minerals.

The waters of the three studied rivers differ in heavy metal composition as index of different ore composition of the area. Huanuni River waters were characterized by high contents of almost all the heavy metals, in particular Zn, Fe, Co, Cu, Cd and Pb; Japo River waters have extremely high concentrations of Cu, Cd, and As and Santa Fe River waters are characterized by high Zn and Fe content. Considering the evolution along the river flow it is evident the mixing of different kind of waters in samples taken after the confluence of two rivers (HA-5, SF-2 and SSA-1) and the dilution effect.

Seasonal effects are evident in the decrease of the concentrations of all the considered elements and in the distinctive behaviour pattern of iron. During the wet season iron result almost completely depleted as result of the increase in pH and the consequent precipitation of secondary minerals. The presence of high concentrations of aluminium indicates that the waters are in a range of pH where occur the dissolution of Al-hydrite and not the dissolution of iron, typical of lower pH values.

The detection of the Rare Earth Element only in the acidic waters and the convex-up NASC- normalized REEs pattern of the samples indicate its strong dependence with the mine discharges.

Groundwaters can be distinguished in Chlorine, enriched in sulphate and alkaline-sulphate waters. High concentrations in Cl^- are linked to salt deposit of palaeolakes present in the region, while the increase in content of sulphate and heavy metals (Cu, Zn,

Pb and As) during the wet season are related to aquifer recharge by the highly polluted surface waters.

The values of the total metal content in the sediment show that the three mines have different patterns on the river sediment quality. Huanuni area is enriched in Fe, Mn, Cr, Cu, Sn, Zn and Santa Fe River is characterized by extremely high values of Fe, As, Pb Sn and Sr.

Through the comparison between the observed concentrations in the unpolluted samples and the mean composition of the upper continental crust (UCC), the area result enriched in As, Bi, Sb, and Sn. This reflects the particular mineralogy in the area characterized by the Tin Belt, the Gold-Antimony Belt and the Lead-Zinc Belt.

From the comparison of the mine affected samples and the background area, result that the Huanuni and Morococala mines affect the river sediments in different ways: the Huanuni River sediments resulted enriched in As, Bi, Cu, Ge, Mo, Se, Sn, and W; Santa Fe River sediments resulted enriched in As, Bi, Pb, Se and Sn this indicate the different ore composition of the two areas.

Sediment speciation analysis indicates that Ca and Mg bearing minerals are strongly affected by the increased acidity of the waters after the mine spills. The concentrations decrease strongly in the mine-polluted samples. This is confirmed by high concentrations of Ca and Mg in the mine downstream sampled waters and could be ascribed to calcite and aluminosilicate mineral dissolution. The decrease in manganese extraction rates after the mine spill indicates its natural association with oxides and its solubilisation after the mine discharge, supported by the increase of its concentration in downstream waters. The other analysed elements (Fe, Cu, Zn, and S) are characterized by low concentrations in the background area and their increase after the mine spill, by the decrease of the reducible fraction and the increase in the oxidizable fraction and indicate the presence of secondary minerals.

All the analysed elements results enriched in suspended sediments instead of iron and sulphide, which are characterized by higher recovery in the bedload sediment instead of the suspended sediments. The suspended sediments are characterized by a higher reducible fraction than the bedload sediment, which indicate that these sediments are less evolved and the heavy metals more easily extracted.

All the analysed elements results enriched in suspended sediments instead of iron and sulphide, which are characterized by higher recovery in the bedload sediment instead of the suspended sediments. The suspended sediments are characterized by a higher reducible fraction than the bedload sediment, which indicate that these sediments are less evolved and the heavy metals more easily extracted.

General conclusions

The present study investigates the effect of two different kind of water pollution caused by human activities.

In the first part, the salt water intrusion in the shallow aquifer of Ravenna (Italy) was analysed. The depth specific sampling method allows a detailed characterization of the geochemical processes affecting the area. Salinization and freshening of the area are correlated to the precipitation rates and the agriculture activities, which are strongly dependent on the seasons. Ion exchange, mineral dissolution and precipitation could be defined as the most important factors resulting from the salinization/freshening of the area. High concentrations of arsenic observed in the area correlate with the peat layers characteristics of the studied aquifer.

The second part focused on the heavy metal pollution affecting the basin of the San Juan de Sora Sora River, Bolivia, due to the acid mine drainage. Water and sediment analysis allows us to define the impact of mine extraction and the influence of the ore geology on the contamination. The marked periodicity of the precipitations is a key factor for the multiple processes occurring in the river waters and sediments, and for the hydraulic connection between surface- and ground- waters. Selective extractions results to be a good tool to delineate the behaviour of some heavy metals in environments seriously contaminated by acid mine drainage.

The analysis of this two case studies emphasize the significance of considering also the seasonality effects for water pollution studies, together with the importance of waters/sediments interactions in stress conditions, to understand the release of pollutants in the water system.

References

Abbott, M.B., and A.P. Wolfe. (2003). Intensive pre-Incan metallurgy recorded by lake sediments from the Bolivian Andes. *Science 301*, 1893–1895.

Adriano, D. (2001) *Trace Elements in Terrestrial Environments*. Biogeochemistry, Bioavailability and Risks of Metals, Springer, New York.

Alpers, C.N., Nordstrom, D.K., Spitzley, J., (2003). *Extreme acid mine drainage from a pyritic massive sulfide deposit: the Iron Mountain end-member*. In: Jambor, J.L., Blowes, D.W., Ritchie, A.I.M. (Eds.), Environmental Aspects of Mine Wastes. Mineralogical Association of Canada, Vancouver, 407–430.

Arce Burgoa, O. R. (2009). *Metalliferous Ore Deposits of Bolivia*, SPC Impresores S.A., pp 233, La Paz, Bolivia Economic Geology, vol 104 n 7,1081-1082.

Audry, S., Blanc, G., & Schafer, J. (2005). The impact of sulphide oxidation on dissolved metal (Cd, Zn, Cu, Cr, Co, Ni, U) inputs into the Lot-Garonne fluvial system (France). *Applied Geochemistry 20*, 919–931.

Banks, D., Marklandc, H., Smithd, P.V., Mendezc, C., Rodriguezc, J., Huertac, A., & Sæthere, O.M. (2004), Distribution, salinity and pH dependence of elements in surface waters of the catchment areas of the Salars of Coipasa and Uyuni, Bolivian Altiplano. *Journal of Geochemical Exploration 84*, 141–166.

Bermond, A. P., & Yousfi, I. (1997). Reliability of comparisons based on sequential extraction procedures applied to soil samples: The thermodynamic point of view. *Environmental technology, 18 (2)*, 219-224.

Bervoets, L., Solis, D., Romero, A.M., Damme, P.A.V., & Ollevier, F. (1998). Trace metal levels in chironomid larvae and sediments from a Bolivian river: impact of mining activities. *Ecotoxicology and Environmental Safety 41*, 275–283.

Binford M. W., Kolata A. L., Brenner M., Janusek J. W., Seddon M.T. Abbott M., & Curtis J. H. (1997). Climate Variation and the Rise and Fall of an Andean Civilization, Quaternary research 47, 235–248.

Blowes, D.W., Ptacek, C.J., Jambor, J.L. & Weisener, C.G., (2003). The geochemistry of acid mine drainage, In *Environmental Geochemistry (ed. Lollar, B.S.) Vol. 9 of Treatise on Geochemistry (eds. Holland, H.D.; Turekian, K.K.), Vol. 9,* Elsevier-Pergamon, Oxford, pp. 149-204.

Cáceres, L. F., Choque, R. R., Ramos, O., & Choque, R. (2004). Trace elements specification on sediments of the Poopó Lake (Especiación de elementos traza en sedimentos del Lago Poopó). *Revista Boliviana de Química 21*, 42–48.

Cappuyns, V., Swennen, R., & Niclaes, M. (2007). Application of the BCR sequential extraction scheme to dredged pond sediments contaminated by pb-zn mining: A combined geochemical and mineralogical approach. *Journal of Geochemical Exploration, 93*(2), 78-90.

Chatelain, D., & Wittinton, H.M., (1992). Evaluación de los Recursos Hídricos en Bolivia, Sur América. In: Ricaldi, V., Flores, C., Anaya, L. (Eds.), Seminario de los Recursos H ídricos en Bolivia y su Dimensión Ambiental. Cochabamba, 133–136.

Cunningham, C., McNamee, J., Pinto, J. & Ericksen, G. 1991. A model of volcanic dome-hosted precious metal deposits in Bolivia. *Economic Geology, 86*, 415-421.

da Silva, I. S., Abate, G., Lichtig, J., & Masini, J. C. (2002). Heavy metal distribution in recent sediments of the Tietê-Pinheiros river system in São Paulo state, Brazil. *Applied Geochemistry 178(2),*105–116.

Dittmar, T., (2004). Hydrochemical processes controlling arsenic and heavy metal contamination in the Elqui river system (Chile). *Science of Total Environment 325*, 193–207.

Dold, B., & Fontbote, L. (2002). A mineralogical and geochemical study of element mobility in sulfide mine tailings of Fe oxide Cu–Au deposits from the Punta del Cobre belt, northern Chile. *Chemical Geology 189*, 135–163.

Elbaz-Poulichet, F., & Dupuy, C. (1999). Behaviour of rare earth elements at the freshwater-seawater interface of two acid mine rivers: The Tinto and Odiel (Andalucia, Spain). *Applied Geochemistry, 14*(8), 1063-1072.

España, J. S., Pamo, E. L., Santofimia, E., Aduvire, O., Reyes, J., & Barettino, D. (2005). Acid mine drainage in the Iberian pyrite belt (Odiel river watershed, Huelva, SW Spain): Geochemistry, mineralogy and environmental implications. *Applied Geochemistry, 20*(7), 1320-1356.

Espi, E., Boutron, C.F., Hong, S., Pourchet, M., Ferrari, C., Shotyk, W., & Charlet, L. (1997). Changing concentrations of Cu, Zn, Cd and Pb in a high altitude peat bog from Bolivia during the past three centuries. *Water Air and Soil Pollution 100*, 289–296.

Garreaud, R. (1999). Multiscale analysis of the summertime precipitation over the Central Andes. *Monthly Weather Review* 127, 901–921.

GEOBOL 1992a. Carta Geológica de Bolivia, Hoja Oruro, 6140. Escala 1:100.000. Publicación SGB Serie I-CGB-11, 1 mapa.

GEOBOL, SGAB 1995b. Mapas tema´ticos de recursos minerales de Bolivia. SF 19-10 y SF 19-11: Hojas Corque y Nevados Payachata, Escala 1:250,0000, Mapa Geolo´ gico. Servicio Geolo ´gico de Bolivia/Swedish Geological AB.

GEOBOL, SGAB, 1995a. Mapas tema´ticos de recursos minerales e Bolivia. SF 19-15: Hoja Salinas de Garci Mendoza, Escala 1:250,0000, Mapa Geolo´ gico. Servicio Geolo´gico de Bolivia/ Swedish Geological AB.

Gimeno Serrano, M. J., Auqué Sanz, L. F., & Nordstrom, D. K. (2000). REE speciation in low-temperature acidic waters and the competitive effects of aluminum. *Chemical Geology, 165*(3-4), 167-180.

Gómez Ariza, J.L, Giráldez, I., Sánchez-Rodas, D., & Morales, E. (2000). Selectivity assessment of a sequential extraction procedure for metal mobility characterization using model phases. *Talanta, 52 (3)*, 545–554.

Grant, J.N., Halls, C., Sheppard, S.M.F. & Avila, W., (1980). *Evolution of the Porphyry Tin Deposits of Bolivia*; In Granitic Magmatism and Related Mineralization, Ishihara, S. and Takenouchi, S., Editors; The Society of Mining Geologists of Japan, Mining Geology Special Issue, No. 8, 151-173.

Hammer, Ø., Harper, D.A.T., Ryan, P. D., (2001). PAST: Paleontological Statistics Software Package for Education and Data Analysis. *Palaeontologia Electronic,a 4(1*), 9pp. http://palaeo-electronica.org/2001_1/past/issue1_01.htm

Hudson Edwards, K. A., Macklinb, M. G., Millerc, J. M.,& Lechlerd, M. P., (2001). Distribution and storage of heavy metals in the Rio Pilcomayo, Bolivia. *Journal of Geochemical Exploration 72*, 229-250.

James, R.O. & Barrow, N.J. (1981). *Copper reactions with inorganic components of soils including uptake by oxide and silicate minerals*, J. Loneragan, A. Robson, R. Graham, Editors , *Copper in Soils and Plants*, Academic Press, New York, 47–68.

Johannesson, K. H., & Lyons, W. B. (1995). Rare-earth element geochemistry of colour lake, an acidic freshwater lake on Axel Heiberg island, northwest territories, Canada. *Chemical Geology, 119*(1-4), 209-223.

Johannesson, K. H., & Zhou, X. (1999). Origin of middle rare earth element enrichments in acid waters of a canadian high arctic lake. *Geochimica Et Cosmochimica Acta, 63(1)*, 153-165.

Kersten, M., Smedes, F. (2002). Normalization procedures for sediment contaminants in spatial and temporal trend monitoring. *Journal of Environmental Monitoring, 4(1)*, 109–15.

Lacal, J., Da Silva, M. P., García, R., Sevilla, M. T., Procopio, J. R., & Hernández, L. (2003). Study of fractionation and potential mobility of metal in sludge from pyrite mining and affected river sediments: Changes in mobility over time and use of artificial ageing as a tool in environmental impact assessment. *Environmental Pollution, 124*(2), 291-305.

Lilja, A., & Linde, G. (2006). Occurrence and distribution of heavy metalsin three rivers on the Bolivian high plateau. Lund Institute of technology, Lund University, Lund

Linton, T.K., M.A.W. Pacheco, D.O. McIntyre, W.H. Clement, and J. Goodrich- Mahoney. (2007). Development of bioassessment-based benchmarks for iron. *Environmental Toxicology and Chemistry,* 26(6), 1291-1298.

Lodenius, M., & Malm, O., (1998). Mercury in the Amazon. *Reviews of Environmental Contamination And Toxicology 157*, 25–52.

López, E., Cuenca, Á., Lafuente, S., Madrid, E. & Molina P. (2010), *El costo ecológico de la política minera en Huanuni y Bolívar*, Ed. Monserrat Fernández.

Loring, DH. (1991). Normalization of heavy-metal data from estuarine and coastal sediments. *ICES Journal of Marine Science, 48*, 101–15.

Maiz, I., Arambarri, I., Garcia, R., Millán, E., 2000. Evaluation of heavy metal availability in polluted soils by two sequential extraction procedures using factor analysis. *Environmental Pollution 110*, 3-9.

Markgraf V., 2001, Interhemispheric climate linkages, Academic Press, p96-97

Masotti, A., Da Sacco, L., Bottazzo, GF., & Sturchio, E. (2009). Risk assessment of inorganic arsenic pollution on human health. *Environmental Polluion. 157,* 1771-2.

Maurice-Bourgoin, L., Alanoca, L., Fraizy, P., & Vauchel, P., (2003). Sources of mercury in surface waters of the upper Madeira erosive basins, Bolivia. *Journal of Physics IV 107*, 855–858.

Meguellati, N., Robbe, D., Marchandise, P., & Astruc, M. (1983). New chemical extraction procedure in the fractionation of heavy metals in sediments - interpretation. *Proceedings of the international conference Heavy metals in the Environment*. 1090-1093.

Merian, E., Anke, M., Ihnat, M., & Stoeppler, M. (2004). *Elements and Their Compounds in the Environment: Occurrence, Analysis and Biological Relevance*, WILEY-VCH Verlag GmbH & Co. KGaA, Weinheim: D

Mikaelsson A. Ny C. Ground Water and Surface Water Influence on the Water Quality in the Antequera River basin, Bolivia, A minor field study

Miller, J.R., Hudson-Edwards, K.A., Lechler, P.J., Preston, D., & Macklin, M.G. (2004). Heavy metal contamination of water, soil and produce within riverine communities of the Rio Pilcomayo basin, Bolivia. *Science of Total Environment 320*, 189–209.

Montes de Oca, I., 1982. *Geografía y Recursos Naturales de Bolivia*. Bancos Central de Bolivia y Cochabamba, La Paz.

Morillo, J., Usero, J., & Gracia, I. (2002). Partitioning of metals in sediments from the Odiel river (Spain). *Environment International, 28*(4), 263-271.

Morin, K. A., & Cherry, J. A. (1986). Trace amounts of siderite near a uranium-tailings impoundment, Elliot Lake, Ontario, Canada, and its implication in controlling contaminant migration in a sand aquifer. *Chemical Geology, 56*(1-2), 117-134.

Müller B, Frischknecht R, Seward TM, (2001). A fluid inclusion reconnaissance study of the Huanuni tin deposit (Bolivia), using LA-ICP-MS micro-analysis. Miner Deposita 36, 680-688.

Nordstrom, D.K. (1982). Aqueous pyrite oxidation and the consequent formation of secondary iron minerals, *In: Kittrick, J.A., Fanning, D.S. and Hossner, L.R., eds. Acid sulfate weathering. Soil Science Society of America*, 37-63.

Nordstrom, D.K., & Alpers, C.N. (1999). Negative pH, efflorescent mineralogy, and consequences for environmental restoration at the Iron Mountain Superfund site, California. Proc. Natl. Acad. Sci. USA 96, 3455–3462.

Nordstrom, D.K., & Alpers, C.N., (1999a). Geochemistry of Acid Mine Waters, In*: Plumlee, G.S., and Logsdon, M.J. (eds.), The Environmental Geochemistry of Mineral Deposits. Part A. Processes, Methods, and Health Issues,* Society of Economic Geologists, Reviews in Economic Geology, v. 6A, chapter 6, 133-160.

Nordstrom, & D.K., Alpers, C.N., (2000). Negative pH and Extremely AcidicMine Waters from Iron Mountain, California. *Environmental Science & Technology 34*, 254-258.

Ny, C., Mikaelsson, A. (2009). Ground Water and Surface Water Influence on the Water Quality in the Antequera River basin, Bolivia : A Minor Field Study. University essay from Lunds universitet.

NYSDEC. (1986). Water Quality Regulations: surface and groundwater classifications and standards. In*: New York State codes, rules and regulations*. (Title 6, Chapter X, pp 700-705). NY State Department of Conservation.

Olías, M., Nieto, J. M., Sarmiento, A. M., Cerón, J. C., & Cánovas, C. R. (2004). Seasonal water quality variations in a river affected by acid mine drainage: The odiel river (south west spain). *Science of the Total Environment, 333*(1-3), 267-281.

Oporto, C., Vandecasteele, C., & Smolders, E., (2007). Elevated cadmium concentrations in potato tubers due to irrigation with river water contaminated by mining in Potosi, Bolivia. *Journal of Environmental Quality 36*, 1181–1186.

Oyarzun, R., Lillo, J., Higueras, P., Oyarzun, J., Maturana, H. (2004). Strongarsenic enrichment insediments fromtheElquiwatershed, Northern Chile: industrial (gold mining at El Indio-Tambo district) vs. geologic processes. *Journal of Geochemical Exploration 84*, 53–64.

Pérez-López R., Delgado J., Nieto J. M., Márquez-García B. (2010). Rare earth element geochemistry of sulphide weathering in the São Domingos mine area (Iberian Pyrite Belt): A proxy for fluid–rock interaction and ancient mining pollution. *Chemical Geology 276, 29–40*

Pfeiffer, W.C., Lacerda, L.D., Salomons, W., & Malm, O., (1993). Environmental fate of mercury from gold mining in the Brazilian Amazon. *Environmental Review 1*, 26–37.

Pillco R. y A. Calizaya. 2008. "Hidrología y recursos hídricos en la cuenca de los lagos Poopó y Uru Uru". En: Rocha, O.O. y S. Aguilar (ed.). Bases técnicas para el plan de manejo del Sitio Ramsar Lagos Poopó y Uru Uru. Pp. 9-27. Oruro, Bolivia.

Pillco Zolá, R. & Bengtsson L. (2006). Long-term and extreme water level variations of the shallow Lake Poopó, Bolivia, *Hydrological Sciences Journal, 51*, 98-114.

Plumlee, G. S., Smith, K. S., & Ficklin, W. H., (1994). Geoenvironmental models of mineral deposits, and geology-based mineral-environmental assessments of public lands: *U.S. Geol. Survey Open File Report, v. 94*, 203.

PPO 1993-1996. Proyecto Piloto Oruro. Ministerio de Desarrollo Sostenible y MedioAmbiente Secretaría Nacional de Minería, Swedish Geological AB.

Pueyo, M., Mateu, J., Rigol, A., Vidal, M., López-Sánchez, J. F., & Rauret, G. (2008). Use of the modified BCR three-step sequential extraction procedure for the study of trace element dynamics in contaminated soils. *Environmental Pollution, 152*(2), 330-341.

Pueyo, M., Sastre, J., Hernández, E., Vidal, M., López-Sánchez, J. F., & Rauret, G. (2003). Heavy metals in the environment: Prediction of trace element mobility in contaminated soils by sequential extraction. *Journal of Environmental Quality, 32*(6), 2054-2066.

Quino, I. (2006). Groundwater quality determination on the North and East regions of the Poopó Lake, (Determinación de la calidad deaguas subterráneas en la región norte y este del lago Poopó),Thesis, UMSA, La Paz, Bolivia

Ramos Ramos, O. E., Cáceres, L. F., Ormachea Muñoz, M. R., Bhattacharya, P., Quino, I., & Quintanilla, J., (2011). Sources and behaviour of arsenic and trace elements in

groundwater and surface water in the Poopó lake basin, Bolivian Altiplano. *Environmental Earth Sciences*, 1-15.

Reimann, R. C., Filzmoser, P., Garrett, R. G., Dutter, R., (2008). *Statistical data Analysis Explained: Applied Environmental Statistics with R*, Chichester, UK: John Wiley & Sons, Ltd.

Risacher, F. & Fritz, B. (1991). Quaternary geochemical evolution of the salars of Uyuni and Coipasa, central Altiplano, Bolivia. *Chemical Geology 90*, 211-231.

Rocha, O. O. (2002), Diagnóstico de los recursos naturales y culturales de los Lagos Poopó y Uru Uru, Oruro – Bolivia

Roche, M. A., Bourges, J., Cortez, J. & Mattos, R. (1992) Climatology and hydrology of the Lake Titicaca basin. In: Lake In Lake Titicaca: A Synthesis of Limnological Knowledge, edited by C. Dejoux and A. Iltis, pp. 63-88. Monographiae Biologicae. vol. 68, H. J. Dumont and M. J. A. Werger, general editor. Kluwer Academic Publishers, Boston.

Rojas, J.C., Vandecasteele, C. (2007). Influence of Mining Activities in the North of Potosi, Bolivia on the Water Quality of the Chayanta River, and its Consequences. *Environmental Monitoring and Assessment 132*, 321–330.

Romero, L., Alonso, H., Campano, P., Fanfani, L., Cidu, R., Dadea, C., Keegan, T., Thornton, I., Farago, M., (2003). Arsenic enrichment in waters and sediments of the Rio Loa (Second Region, Chile). *Applied Geochemistry 18*, 1399–1416.

Rosenberg, M., Stålhammar, K. (2010). Evaluation of Heavy Metals in Waters Influenced by Mining in the Poopó and Antequera River Basins, Oruro – Bolivia. University essay from Lunds universitet.

Rudnik, R. L., & Gao, S. (2003). Composition of the continental crust. In *The crust (ed. Rudnik, L.R.) Vol. 3 of Treatise on Geochemistry (eds. Holland, H.D.; Turekian, K.K.), Vol. 9,* Elsevier-Pergamon, Oxford

Sahoo, P. K., Tripathy, S., Equeenuddin, S. M., & Panigrahi, M. K. (2012). Geochemical characteristics of coal mine discharge vis-à-vis behaviour of rare earth elements at jaintia hills coalfield, northeastern India. *Journal of Geochemical Exploration, 112*, 235-243.

Sahuquillo, A., & Rauret, G. (2003). Overview of the use of leaching/extraction tests for risk assessment of trace metals in contaminated soils and sediments. *Trends in Analytical Chemistry 22,* 152-159

Sahuquillo, A., López-Sánchez, J. F., Rubio, R., Rauret, G., Thomas, R. P., Davidson, C. M., et al. (1999). Use of a certified reference material for extractable trace metals to assess sources of uncertainty in the BCR three-stage sequential extraction procedure. *Analytica Chimica Acta, 382*(3), 317-327.

Sakan, S. M., Dordević, D. S., Manojlović, D. D., & Predrag, P. S. (2009). Assessment of heavy metal pollutants accumulation in the tisza river sediments. *Journal of Environmental Management, 90*(11), 3382-3390.

Salvarredy-Aranguren, M. M. (2008), Contamination of surface waters by mining wastes in the Milluni Valley (Cordillera Real, Bolivia): Mineralogical and hydrological influences *Applied Geochemistry 23*,1299–1324

Sanchez España, J., Lopez Pamo, E., Santofimia, E., Aduvire, O., Reyes, J., Barettino, D., (2005). Acid mine drainage in the Iberian Pyrite Belt (Odiel river watershed, Huelva, SW Spain): geochemistry, mineralogy and environmental implications.Appl. Geochem. 20, 1320–1356.

Sánchez España, J., López Pamo, E., & Santofimia Pastor, E. (2007). The oxidation of ferrous iron in acidic mine effluents from the Iberian pyrite belt (Odiel basin, Huelva, Spain): Field and laboratory rates. *Journal of Geochemical Exploration, 92*(2-3), 120-132.

Selander, L., & Svan, P. (2007). *Occurrence and distribution of heavy metals in lake Poopó, Bolivia*. Department of Chemical and Water Resources Engineering, Lund University, Lund.

SENAMHI, 2011. SisMeteBase de datos oficial del Servicio Nacional de Meteorología e Hidrología. accessed 21.04.11. Servicio Nacional de Meteorología e Hidrología, La Paz. http://www.senamhi.gob.bo/sismet/index.php.

Sharma, V. K., & Sohn, M. (2009). Aquatic arsenic: Toxicity, speciation, transformations, and remediation. *Environmental International 35,* 743–759.

Smedley, P.L., & Kinniburgh, D.G. (2002). A review of the source, behaviour and distribution of arsenic in natural waters. *Applied Geochemistry 17*, 517–568.

Smolders A.J.P., Lock, R. A. C., Van der Velde, G., Medina Hoyos, R. I., & Roelofs, J. G. M. (2003) Effects of Mining Activities on Heavy Metal Concentrations in Water, Sediment, and Macroinvertebrates in Different Reaches of the Pilcomayo River, South America, *Archives of Environmental Health 44*, 314–323.

Smolders, A.J.P., Hudson-Edwards, K.A., Van der Velde, G., Roelofs, J.G.M., (2004). Controls on water chemistry of the Pilcomayo River (Bolivia, South-America). *Applied Geochemistry 19*, 1745–1758.

Sophocleous, M. (2002). Interactions between groundwater and surface water: The state of the science. *Hydrogeology Journal, 10*(1), 52-67.

Strosnider, W. H. J., Llanos López, F. S., Nairn, R. W.,(2011). Acid mine drainage at Cerro Rico de Potosí I: unabated high-strength discharges reflect a five century legacy of mining, Environmental Earth Science 64, 911–923.

Swedlund, P. J., & Webster, J. G. (2001). Cu and zn ternary surface complex formation with so4 on ferrihydrite and schwertmannite. Applied Geochemistry, 16(5), 503-511.

Tapia, J. Audry, S., Townley, B. & Dupley J.L. (2012). Geochemical background, baseline and origin of contaminants from sediments in the mining-impacted Altiplano and Eastern Cordillera of Oruro, Bolivia. *Geochemistry: Eploration, Environment, Analysis 12*, 3-20.

Taylor, S. R. and McLennan, S. H. (1985) *The Continental Crust: Its Composition and Evolution.* Blackwell Scientific, Oxford, 311.

Tessier, A., Campbell, P. G. C., Bisson, M. (1979). Sequential extractions procedure for speciation of particulate trace metals. *Anal. Chem*., 51, 844-851.

Troëng, B., Riera-Kilibarda, C., 1996a. Mapas temáticos de recursos minerales de Bolivia, Hoja Salinas de Garci Mendoza, Memoria Explicativa. Boletı´n del Servicio Geolo´gico de Bolivia 9.

Troëng, B., Riera-Kilibarda, C., 1996b. Mapas temáticos de recursos minerales de Bolivia, Hojas Corque y Nevados Payachata. Memoria Explicativa. Boletín del Servicio Geológico de Bolivia 11.

Troëng, B., Riera-Kilibarda, C., 1998. Mapas temáticos de recursos minerales de Bolivia, Hoja Uyuni, Memoria Explicativa. SERGEOMIN Boletı´n 18.

Varol, M., (2011). Assessment of heavy metal contamination in sediments of the Tigris River (Turkey) using pollution indices and multivariate statistical techniques. *Journal of Hazardous Materials 195,* 355–364.

Villaroel, L. F., Miller, J. R., LechlerP. J., & Germanoski, D. (2006). Lead, zinc, and antimony contamination of the Rio Chilco-Rio Tupiza drainage system, Southern Bolivia, *Environmental Geology 51*, 283–299.

Vuille, M., Amman, C. (1997). Regional snowfall patterns in the high, arid Andes. *Climatic Change 36,* 413–423.

Wasserman, J.C., Hacon, S., & Wasserman, M.A. (2003). Biogeochemistry of mercury in the Amazonian environment. *AMBIO 32*, 336–342.

WHO (2011) *Guidelines for drinking-water quality, 4th edition*, Geneva, Switzerland, WHO press

Worrall, F., & Pearson, D. G. (2001). Water-rock interaction in an acidic mine discharge as indicated by rare earth element patterns. *Geochimica Et Cosmochimica Acta, 65*(18), 3027-3040.

Zhang, T., Shan, X., Ling, F., 1998. Comparison of two sequential extraction procedures for speciation analysis of metals in soils and plant availabil- ity. Communications in Soil Science and Plant Analysis 29 (7e8), 1023e1034.

Zhao, F., Cong, Z., Sun, H., & Ren, D. (2007). The geochemistry of rare earth elements (REE) in acid mine drainage from the Sitai coal mine, Shanxi province, north China. *International Journal of Coal Geology, 70*(1-3 SPEC. ISS.), 184-19

Ringraziamenti

Vorrei ringraziare il mio tutor, Prof. Enrico Dinelli, per i suoi preziosi insegnamenti in questi anni di dottorato e per aver capito e appoggiato le mie decisioni incoerenti.
Sarò per sempre grata al Dr. Massimo Marchesi per aver reso possibile questa impresa, per la sua amicizia, per gli incoraggiamenti, per dare sempre il meglio.
Grazie alla mia famiglia in ordine di età nonna Ivanka, papà Ladi, mamma Daniela, Caterina Nicola e Chiara per il loro eterno amore e appoggio.
Un particolare ringraziamento ai miei amici, che hanno accettato la mia presenza a intervalli e per aver reso ogni momento prezioso, in particolare Manuela, splendida per la sua insostituibile capacità di farmi ragionare e farmi sentire un eterno viaggiatore e Gelsomina per farmi sentire a casa, ovunque sia.
Grazie a tutti i miei colleghi del gruppo IGRG, per il loro aiuto nel campionamento e per i bei momenti passati all'Università, un particolare ringraziamento va al Dr. Mario Laghi e Nicolas Greggio per la loro impareggiabile capacità di tirarmi fuori dai guai.
Quiero agradecer Silvana Lafuente y Felipe Coronado por su ayuda en el campo y para introducirme en la cultura y las traiciones de los bolivianos y para compartir momentos preciosos de mi breve pero inolvidable estancia en Bolivia.
Un particolare ringraziamento ai colleghi dell'Istituto OGS, per avermi dato l'opportunità di dedicarmi alla stesura della tesi e in particolare a Cinzia DV e Michele per avermi spronato a non mollare.

Annex I

Physical and chemical data of the spring sampling campaign, ND (not detected).

Wells	W.table	Sampling depth	Temperature	pH	Eh	EC	S2-	Fe2+	Fe tot	NO_2^-	NO_3^-	PO_4^{3-}	NH3-N	Na^+	K^+	Ca^{2+}	Mg^{2+}	HCO_3^{2-}	Cl	Br	SO_4^{2-}
	(m)	(m)	[°C]		[mV]	[mS/cm]	[mg/l]	[mg/l]	[mg/l]	[mg/l]	[mg/l]	[mg/l]	[mg/l]	ppm	ppm	ppm	ppm	ppm	ppm	ppm	ppm
PZSV17a	0.76	-0.30	19.2	7.03	-137.60	3.8	0.00	ND	ND	0.13	5.30	0.16	ND	442	54	140	92	772	751	4	11
PZSV17b	0.76	-2.24	17.5	7.12	-152.20	7.7	0.00	ND	ND	0.04	5.20	0.08	ND	1036	67	134	159	748	1959	3	248
PZSV17c	0.76	-3.79	17.3	7.42	-168.90	19.8	0.03	ND	ND	0.09	3.70	0.18	ND	3385	105	145	472	1140	6265	31	613
PZSV18a	0.53	-0.28	24.0	7.32	-80.50	2.3	0.00	ND	ND	0.00	2.20	0.44	ND	284	26	107	62	680	352	3	77
PZSV18b	0.53	-2.43	17.7	7.09	-136.90	3.1	0.00	ND	ND	0.03	6.20	0.96	ND	385	32	105	74	616	640	4	41
PZSV18c	0.53	-4.77	20.4	7.05	-158.60	11.8	ND	ND	ND	0.16	5.90	0.83	ND	1672	80	127	215	536	3161	9	392
PZSV13a	-0.19	-1.45	20.0	7.08	-58.80	2.0	ND	ND	ND	0.01	2.10	0.20	0.40	183	5	162	49	480	229	3	256
PZSV13b	-0.19	-2.11	18.8	7.06	-87.00	2.0	ND	ND	ND	0.01	3.30	0.10	0.50	187	10	221	58	492	257	0	262
PZSV13c	-0.19	-3.79	17.5	7.09	-103.90	2.2	ND	ND	ND	0.02	3.70	0.56	0.95	189	7	165	52	480	272	0	256
PZSV14a	-0.52	-1.00	16.9	6.87	-150.80	25.0	0.06	>30	ND	0.06	4.80	2.59	ND	3994	75	707	710	520	8116	6	189
PZSV14b	-0.52	-2.50	16.5	6.95	-159.00	30.0	0.04	28.80	ND	0.15	6.50	0.76	ND	4949	112	524	820	712	9704	7	210
PZSV14c	-0.52	-4.50	16.3	7.18	-142.70	37.6	0.03	12.60	ND	0.11	8.80	0.24	ND	6781	201	337	982	1028	12738	41	1825
PZSVS23a	-1.29	-1.46	15.8	7.46	165.40	2.2	0.00	0.00	0.09	0.00	2.70	2.20	1.5	363	34	50	61	276	667	19	51
PZSVS23b	-1.29	-4.35	14.8	7.60	-127.90	3.3	0.01	0.53	0.62	0.00	1.50	1.30	2.2	437	64	49	90	308	685	4	181
PZSVS23c	-1.29	-6.35	15.9	7.63	-135.00	4.0	0.01	0.58	0.83	0.00	1.00	1.70	1.7	562	81	37	107	312	963	6	189
PZSVS23d	-1.29	-8.35	16.0	7.70	-158.60	6.1	0.03	0.24	0.91	0.00	0.80	11.30	3.2	965	102	43	119	296	1532	6	271
PZSVS23e	-1.29	-10.10	15.5	7.37	-152.20	37.8	0.05	3.80	8.50	0.01	1.40	3.80	22	7215	289	232	828	336	13772	60	1846
PZSVS30a	-0.24	-0.41	15.6	7.10	-5.30	34.5	0.01	1.35	1.51	0.00	1.40	4.40	ND	7040	135	772	787	180	12823	52	1864
PZSVS30b	-0.24	-5.02	15.7	7.10	-111.50	59.0	0.00	4.80	13.35	0.02	3.40	19.30	ND	12423	372	331	1533	504	22911	93	2259
PZSVS30c	-0.24	-14.02	16.0	7.45	-110.00	62.6	0.01	3.50	6.70	0.01	2.40	0.30	ND	13433	434	318	1605	540	24311	79	2734
PZSVS26a	-0.23	-1.33	17.3	7.28	-89.20	1.5	0.00	0.89	2.15	0.01	3.30	0.41	ND	92	10	200	97	512	147	0	424
PZSVS26b	-0.23	-5.68	17.3	7.32	-135.00	10.0	0.01	1.73	7.55	0.01	1.60	0.07	ND	2138	58	168	280	872	3994	9	517
PZSVS26c	-0.23	-6.68	16.8	7.17	-152.50	16.3	0.00	2.95	13.75	0.01	4.00	0.13	ND	3331	102	242	418	924	6379	21	7
PZSVS26d	-0.23	-8.18	17.8	7.29	-77.90	23.3	0.01	0.60	8.15	0.01	1.90	0.36	ND	4946	154	246	575	972	9578	31	87
PMSV7a	-0.29	-0.95	20.2	7.63	54.50	3.8	0.01	0.09	0.36	0.01	0.80	4.40	ND	560	35	68	110	488	845	0	167
PMSV7b	-0.29	-4.29	18.2	7.66	68.40	15.2	0.02	0.32	1.85	0.01	0.80	3.80	ND	2594	124	78	298	396	4650	10	572
PMSV7c	-0.29	-6.29	18.8	6.70	-7.00	47.7	0.05	1.56	ND	0.01	1.10	2.70	ND	9255	355	299	974	448	16671	80	2088
PMSV7d	-0.29	-12.89	18.6	7.56	-146.70	48.1	0.12	2.30	5.62	0.01	1.50	2.90	ND	9283	365	306	971	372	16728	60	1996
PMSV7p a	-0.24	-15.76	17.6	7.55	-172.20	34.8	0.02	0.09	9.60	0.02	2.60	8.00	ND	6630	166	144	756	900	12382	44	0
PZSV37a	-1.20	-1.20	18.4	7.46	-161.40	18.0	0.36	0.39	0.58	0.01	2.20	17.10	ND	3855	102	198	535	408	7261	28	546
PZSV37b	-1.20	-2.70	19.0	7.43	-182.40	23.7	0.35	0.45	0.76	0.01	2.90	32.00	ND	6011	163	184	770	518	10898	19	255
PZSV37c	-1.20	-3.70	17.4	7.46	-134.00	27.5	0.04	0.69	0.96	0.01	3.60	18.10	ND	5186	131	188	651	486	10082	33	177
PZSV37d	-1.20	-10.70	17.0	7.44	-146.70	28.9	0.03	0.80	0.93	0.02	2.60	21.00	ND	6920	178	184	815	542	12086	42	285
PMSV 6	-0.30	-	15.9	7.20	-113.80	36.9	ND	ND	ND	ND	ND	0.87	12	6630	308	781	868	416	11700	40	2368
PMSV 6p	-0.35	-15.95	15.0	7.56	-166.00	36.4	0.193	ND	ND	ND	ND	13.20	14	7309	222	93	716	828	12857	49	348
PMSV 6p	-0.35	-24.85	15.9	7.50	-133.50	38.3	0.007	0.02	ND	ND	ND	6.20	51	7378	225	114	831	312	13459	53	77
PMSV 8p	-0.25	-21.75	15.6	7.41	-118.80	48.3	0.003	0.01	0.06	ND	3	12.35	48	9330	33	88	1147	908	17628	70	19
PMSV 8p	-0.25	-26.25	15.1	7.40	-133.20	48.3	0.017	0.00	0.04	ND	2.6	13.15	54	9908	353	85	1035	916	17661	75	51
PMSV8a	-0.34	-0.34	18.9	7.67	35.30	8.9	0.01	0.13	0.76	0.01	0.80	2.20	ND	1536	83	60	77	668	2377	14	181
PMSV8b	-0.34	-2.00	17.2	7.45	-100.20	15.7	0.03	2.03	3.21	0.01	1.50	0.28	ND	4515	138	100	460	508	7748	20	631
PMSV8c	-0.34	-7.00	17.0	7.25	-103.70	44.3	0.06	9.80	19.40	0.05	6.50	0.99	ND	8565	368	316	1013	380	15361	54	1723
PMSV8d	-0.34	-9.50	16.3	7.22	-94.00	64.2	0.06	10.50	30.00	0.03	8.20	0.25	ND	12428	505	382	1598	544	23152	66	2631
PMSV 8	-0.23	ND	14.6	7.15	-109.20	31.4	ND	ND	ND	ND	4.1	0.22	54	6122	259	261	1601	532	13308	38	1302
Sea Water	ND	0.00	ND	8.23	95.00	45.5	ND	ND	ND	0.01	4.20	0.26	ND	9004	383	325	1095	128	15558	43	2494

Physical and chemical data of the summer sampling campaign, ND (not detected).

Wells	W.table	mpling dep	emperatur	pH	Eh	EC	S2-	Fe2+	Fe tot	NO_2^-	NO_3^-	PO_4^{3-}	NH3-N	Na^+	K^+	Ca^{2+}	Mg^{2+}	HCO_3^{2-}	Cl	Br	SO_4^{2-}
	(m)	(m)	[°C]		[mV]	[mS/cm]	[mg/l]	[mg/l]	[mg/l]	[mg/l]	[mg/l]	[mg/l]	[mg/l]	ppm	ppm	ppm	ppm	ppm	ppm	ppm	ppm
PZSV26a	-0.95	-1.85	17.70	7.30	-49.70	2.13	ND	1.71	4.3	0.01	0.9	10.4	3.1	179	13.77	179	79	528	273	0	314
PZSV26b	-0.95	-6.55	15.50	7.25	-101.50	10.24	0.01	4.5	30	0.01	2.1	2.2	>50	1504	49	138	189	848	2864	10	12
PZSV26 c	-0.95	-7.55	16.40	7.39	-104.50	21.90	0.03	4.7	12.2	0.01	2.1	0.51	44	3423	103	224	428	948	7125	24.3	108
PZSV23a	-1.45	-1.35	20.50	7.53	123.30	2.30	0.03	0.29	0.57	0.01	1.7	0.24	0.6	283	37	67	70	284	650	0	36
PZSV23 b	-1.45	-6.05	18.10	7.46	60.00	3.97	0.04	0.21	0.98	0.00	3	1.53	0.6	635	94	93	130	304	1250	5.02	226
PZSV23c	-1.45	-7.05	17.40	7.38	-66.00	11.60	0.03	1.15	2.34	0.01	2.1	1.37	1.6	2066	146	91	244	294	4190	13.9	195
PZSV23d	-1.45	-9.18	16.90	7.15	-102.10	35.40	ND	0.75	0.56	0.01	2.6	0.8	4.6	8035	291	299	784	428	14324	63.7	693
PMSV7a	-0.21	-1.29	23.90	7.80	76.00	4.33	0.01	0.15	0.72	0.01	1	1.82	ND	637	46	22	81	540	964	0	121
PMSV7b	-0.21	-2.79	21.70	7.89	17.00	7.70	0.04	0.37	1.14	0.00	1	2.11	ND	1275	44	17	158	532	2254	0	350
PMSV7c	-0.21	-4.79	19.80	7.53	-98.00	36.90	0.05	1.6	7.9	0.00	0.9	0.09	ND	6963	292	254	711	296	13137	28	1775
PMSV7d	-0.21	-11.79	16.80	7.49	-144.00	45.50	0.13	6.5	9	0.01	2.9	1.55	ND	9098	311	335	864	316	16247	50.92	2759
PMSV7p	-0.39	-19.37	17.30	7.33	-145.00	34.40	0.11	4.1	9.5	0.01	1.9	0.45	ND	6773	156	146	618	900	12800	28.27	140
PZSV30a	-1.01	0.24	19.10	7.23	-31.70	36.20	0.01	4.85	6	0.03	4.1	0.1	4.3	6270	95	942	657	700	12175	42.23	1723
PZSV30b	-1.01	-3.99	14.90	6.95	-93.10	60.40	0.01	8.05	11.4	0.06	5.9	0.58	OR	11850	387	379	1235	536	21580	69.97	2539
PZSV30c	-1.01	-5.99	13.90	7.05	-80.70	62.40	0.04	2.85	6.6	0.01	3.6	0.21	51	12540	439	324	1340	544	23279	109.51	2030

Physical and chemical data of the autumn sampling campaign, ND (not detected); OR (over range); UR (under range).

Wells	W.table	mpling dep	emperatur	pH	Eh	EC	S2-	Fe2+	Fe tot	NO_2^-	NO_3^-	PO_4^{3-}	NH3-N	Na^+	K^+	Ca^{2+}	Mg^{2+}	HCO_3^{2-}	Cl	Br	SO_4^{2-}
	(m)	(m)	[°C]		[mV]	[mS/cm]	[mg/l]	[mg/l]	[mg/l]	[mg/l]	[mg/l]	[mg/l]	[mg/l]	ppm	ppm	ppm	ppm	ppm	ppm	ppm	ppm
PZSV23a	-1.27	-1.87	13.50	7.50	-29.40	2.80	0.00	0.06	0.15	0.02	4.9	0.17	0.8	341	40	71	101	410	596	ND	162
PZSV23b	-1.27	-6.27	13.30	7.66	-111.10	3.25	0.01	0.41	0.45	0.02	4.5	1.14	0.8	393	55	61	123	410	665	ND	189
PZSV23c	-1.27	-12.27	13.00	7.73	-194.30	9.00	0.01	1.96	1.72	UR	0.7	1.63	0.9	1377	105	101	189	380	2413	ND	168
PZSV30a	-0.25	-1.35	13.80	6.80	4.60	30.72	0.00	1	2.3	0.03	0.2	0	3.4	5413	53	929	627	445	10339	ND	1624
PZSV30b	-0.25	-3.25	13.50	6.98	-45.30	53.37	0.00	6.15	18.2	ND	ND	ND	OR	10308	298	569	1180	585	18095	ND	1850
PZSV30c	-0.25	-5.75	13.30	7.03	-106.00	59.32	0.00	12.95	17.3	ND	ND	ND	OR	11425	380	423	1294	648	20246	ND	2168
PZPM7p	-0.46	-16.46	14.20	7.71	-156.70	36.55	0.03	1.59	1.66	0.00	3.1	2.33	OR	6545	203	191	787	1055	12080	ND	424
PZSV26a	-0.57	-1.57	15.40	7.70	-86.70	2.65	0.01	0.9	2	UR	2.3	1.09	OR	373	17	128	139	513	591	ND	158
PZSV26b	-0.57	-5.07	15.50	7.85	-160.00	7.28	0.01	4.25	5.2	UR	UR	2.06	OR	1296	46	138	171	893	2170	ND	114
PZSV26c	-0.57	-6.57	15.20	7.71	-152.00	15.95	UR	15	28.75	ND	ND	2.19	OR	2564	76	199	475	1120	4987	ND	21
PZSV26d	-0.57	-10.07	14.80	7.59	-150.00	28.17	0.00	3.25	7.6	UR	UR	5.04	OR	4678	137	282	570	1230	9583	ND	62
PZPM7a	-0.30	-1.30	12.50	7.97	-53.50	4.55	0.12	0.65	0.69	0.01	8.2	1.18	0.06	866	38	154	82	435	1109	ND	233
PZPM7b	-0.30	-2.80	13.70	7.71	-98.80	26.53	0.19	1.6	3.38	0.00	3	0.67	ND	4979	200	254	707	495	8115	ND	1267
PZPM7c	-0.30	-11.30	13.90	7.78	-105.70	47.58	0.08	4.35	4.75	UR	UR	1.96	OR	9408	368	393	1342	640	16426	ND	2034
PZSV17a	0.52	-0.12	15.70	7.45	-17.90	4.98	0.31	26.5	OR	0.00	UR	UR	OR	632	63	156	99	880	1320	ND	48
PZSV17b	0.52	-1.62	16.20	7.32	-10.00	5.46	0.11	20.75	25.1	0.08	UR	UR	OR	885	73	177	122	920	1460	ND	44
PZSV17c	0.52	-3.12	15.20	7.46	-18.40	17.35	0.04	10.25	19.7	UR	UR	UR	OR	2073	115	208	390	1270	4396	ND	12
PZSV14a	-0.03	-0.53	14.20	7.24	-5.10	25.76	0.02	27.00	OR	UR	UR	n.d	OR	3980	81	757	602	720	7534	ND	127
PZSV14b	-0.03	-2.03	14.20	7.22	-4.00	26.86	0.05	57.75	OR	UR	UR	n.d	OR	4131	87	724	603	740	7584	ND	114
PZSV14c	-0.03	-4.03	14.20	7.34	-12.00	34.98	0.01	20.75	OR	UR	UR	n.d	OR	5785	160	466	980	1220	11131	ND	39
PZSV18a	0.29	-0.61	14.80	7.35	-15.00	2.17	0.23	6	11	ND	ND	0.04	0.46	230	22	124	60	875	314	ND	82
PZSV18b	0.29	-2.21	15.20	7.46	-18.70	2.29	0.38	8.5	11.9	ND	ND	ND	0.9	249	23	131	64	910	325	ND	280
PZSV18c	0.29	-4.21	15.30	7.46	-17.20	5.30	0.34	77.25	ND	ND	ND	ND	1.2	640	37	126	103	755	1200	ND	294
PZSV13a	0.04	-0.21	14.50	7.41	-13.40	2.22	0.05	2.25	11.4	ND	ND	ND	ND	0.4	195	7	223	54	318	ND	34
PZSV13c	0.04	-3.96	14.70	7.53	-20.50	2.37	0.71	16	27.5	ND	ND	ND	ND	0.68	196	9	226	57	333	ND	23
PMSV6a	-0.18	-0.53	14.10	7.00	-119.10	24.20	ND	ND	ND	ND	ND	ND	ND	3722	84	853	510	640	6865	1	1475
PMSV6b	-0.18	-4.53	13.80	7.20	-156.00	43.50	ND	ND	ND	ND	ND	ND	ND	7830	294	438	1005	351	13340	1	1749
PMSV6c	-0.18	-7.53	13.10	7.40	-157.50	49.30	ND	ND	ND	ND	ND	ND	ND	8173	277	366	1047	421	14395	1	1746
PMSV6d	-0.18	-12.03	13.10	7.40	-147.30	49.70	ND	ND	ND	ND	ND	ND	ND	8964	287	390	1166	470	15308	1	1548
PMSV6p	-0.38	-14.88	13.30	7.70	-148.00	42.90	ND	ND	ND	ND	ND	ND	ND	7867	228	142	911	1111	14981	1	3
PMSV8p	-0.05	-20.15	14.30	7.60	-145.20	49.60	ND	ND	ND	ND	ND	ND	ND	9759	334	89	1009	1052	16834	1	7
PMSV8 a	0.10	-0.20	13.00	7.70	-90.00	8.90	ND	ND	ND	ND	ND	ND	ND	1213	53	69	70	1037	1857	1	1
PMSV8b	0.10	-4.20	13.80	7.70	-162.00	16.60	ND	ND	ND	ND	ND	ND	ND	2593	112	89	218	601	4110	1	78
PMSV8c	0.10	-7.20	13.30	7.40	-155.50	47.40	ND	ND	ND	ND	ND	ND	ND	8574	348	391	1014	436	14514	1	411
PMSV8d	0.10	-13.20	13.40	7.50	-165.00	71.30	ND	ND	ND	ND	ND	ND	ND	14470	564	513	1698	659	24600	1	2235
PZSV37a	-0.58	-2.08	12.00	8.00	-223.70	6.70	ND	ND	ND	ND	ND	ND	ND	686	18	91	156	547	1229	1	118
PZSV37b	-0.58	-5.58	12.40	7.80	-235.00	36.00	ND	ND	ND	ND	ND	ND	ND	5561	120	198	763	1262	9694	1	5
PZSV37c	-0.58	-9.58	12.20	7.90	-219.40	37.60	ND	ND	ND	ND	ND	ND	ND	5762	128	206	782	1300	10432	1	6
PZSV30a	0.05	-1.05	12.10	6.90	-19.60	27.20	ND	ND	ND	ND	ND	ND	ND	3430	23	899	425	512	6493	1	1355
PZSV30b	0.05	-4.25	12.20	7.50	-152.20	62.70	ND	ND	ND	ND	ND	ND	ND	11495	338	415	1391	597	19059	1	1865
PZSV30c	0.05	-8.25	12.20	7.20	-140.20	65.70	ND	ND	ND	ND	ND	ND	ND	11050	256	537	1393	639	20222	172	1514
PZSV30d	0.05	-12.25	12.60	7.40	-158.70	66.30	ND	ND	ND	ND	ND	ND	ND	12410	362	418	1554	679	20749	170	1629

Calculated sea water fraction for individual observation wells, mixing (mix) and reacting (react) concentrations expected according to a theoretical seawater/freshwater mixing model in the three sampling campaign, Saturation index SI for calcite, dolomite and Gypsum calculated with PHREEQC, Water Type obtained by Stuyfzand method

Season		% Sw fraction	meq Na^+ Mix	meq Na^+ react	meq Ca^{2+} mix	meq Ca^{2+} react	meq Mg^{2+} mix	meq Mg^{2+} react	meq K^+ mix	meq K^+ react	meq HCO_3^- mix	meq HCO_3^- react	meq SO_4^{2-} mix	meq SO_4^{2-} react	SI Calcite	SI Dolomite	SI Gypsum	Water Type
	Northern Transect																	
Spring	**PZSV 18a**	2.3	8.9	3.5	0.4	5.0	2.0	3.0	0.2	0.4	0.0	11.1	1.2	0.4	0.49	1.03	-1.78	B4NaMix+
Spring	**PZSV 18b**	4.1	16.1	0.7	0.7	4.6	3.7	2.4	0.4	0.4	0.1	10.0	2.1	-1.3	0.16	0.44	-2.09	B4NaCl+
Spring	**PZSV 18c**	20.3	79.6	-6.8	3.3	3.0	18.3	-0.6	2.0	0.1	0.4	8.4	10.6	-2.4	-0.05	0.42	-1.37	b4NaCl
Spring	**PZSV 17a**	4.8	18.9	0.3	0.8	6.2	4.4	3.2	0.5	0.9	0.1	12.6	2.5	-2.3	0.54	1.84	-1.33	B4NaCl+
Spring	**PZSV 17b**	12.6	49.3	-4.2	2.0	4.6	11.3	1.8	1.2	0.5	0.3	12.0	6.5	-1.4	0.27	0.58	-2.58	b4NaCl
Spring	**PZSV 17c**	40.3	157.7	-10.5	6.5	0.7	36.3	2.6	3.9	-1.3	0.8	17.8	20.9	-8.2	0.20	0.69	-1.42	b5NaCl
Spring	**PZSV 13a**	1.5	5.8	2.2	0.2	7.8	1.3	2.7	0.1	0.0	0.0	7.8	0.8	4.6	0.23	0.19	-1.08	f3CaMix+
Spring	**PZSV 13b**	1.7	6.5	1.7	0.3	10.8	1.5	3.3	0.2	0.1	0.0	8.0	0.9	4.6	0.28	0.19	-0.97	f3CaMixo
Spring	**PZSV 13c**	1.7	6.8	1.4	0.3	8.0	1.6	2.7	0.2	0.0	0.0	7.8	0.9	4.4	0.22	0.16	-1.08	f4CaMix+
Spring	**PZSV 14a**	52.2	204.3	-31.0	8.5	26.8	47.0	11.4	5.1	-3.2	1.1	7.4	27.1	-23.1	0.34	0.99	-1.29	b4NaCl-
Spring	**PZSV 14b**	62.4	244.3	-29.0	10.1	16.0	56.2	11.3	6.1	-3.2	1.3	10.4	32.4	-28.0	0.38	1.24	-1.40	b4NaCl-
Spring	**PZSV 14c**	81.9	320.7	-25.8	13.3	3.5	73.8	7.0	8.0	-2.9	1.7	15.1	42.5	-4.5	0.51	1.76	-0.75	S5NaCl
	Central transect																	
Spring	**PZSV26a**	0.9	3.7	0.3	0.2	9.8	0.9	7.1	0.1	0.2	0.0	8.4	0.5	8.3	0.58	1.08	-0.85	F4CaMix+
Spring	**PZSV26b**	25.7	100.5	-7.2	4.2	4.2	23.1	-0.1	2.5	-1.0	0.5	13.8	13.3	-2.6	0.22	0.89	-1.19	b4NaCl-
Spring	**PZSV26c**	41.0	160.6	-15.7	6.7	5.4	36.9	-2.6	4.0	-1.4	0.9	14.3	21.3	-21.1	0.08	0.65	-3.01	b3NaCl-
Spring	**PZSV26d**	61.6	241.1	-26.0	10.0	2.3	55.5	-8.2	6.0	-2.1	1.3	14.6	32.0	-30.2	0.30	1.22	-2.03	b4NaCl-
Spring	**PZSV23a**	4.3	16.8	-1.0	0.7	1.8	3.9	1.2	0.4	0.4	0.1	4.4	2.2	-1.2	0.12	0.56	-2.26	B4NaCl+
Spring	**PZSV23b**	4.4	17.2	1.8	0.7	1.7	4.0	3.4	0.4	1.2	0.1	5.0	2.3	1.5	0.40	1.28	-1.80	B4NaCl+
Spring	**PZSV23c**	6.2	24.2	0.2	1.0	0.8	5.6	3.2	0.6	1.5	0.1	5.0	3.2	0.7	0.34	1.38	-1.96	B4NaCl+
Spring	**PZSV23d**	9.8	38.6	3.4	1.6	0.5	8.9	0.9	1.0	1.6	0.2	4.6	5.1	0.5	0.45	1.62	-1.84	b4NaCl+
Spring	**PZSV23e**	88.5	346.7	-32.9	14.4	-2.8	79.8	-11.6	8.7	-1.3	1.9	3.6	46.0	-7.5	0.72	2.28	-0.90	S3NaCl
Spring	**PMSV7a**	5.4	21.3	15.2	0.9	2.5	4.9	4.2	0.5	0.4	0.1	7.9	2.8	0.6	0.16	0.75	-1.71	B3NaCl+
Spring	**PMSV7b**	29.9	117.1	-4.2	4.8	-1.0	26.9	-2.9	2.9	0.2	0.6	5.9	15.5	-3.6	-0.22	0.41	-1.51	b2NaCl
Spring	**PMSV7c**	107.2	419.7	-17.1	17.4	-2.5	96.6	-16.6	10.5	-1.4	2.2	5.1	55.6	-12.2	-0.34	0.12	-0.79	S4NaCl
Spring	**PMSV7d**	107.5	421.1	-17.3	17.4	-2.2	96.9	-17.9	10.5	-1.2	2.3	3.8	55.8	-14.3	0.54	1.86	-0.80	S4NaClo
Spring	**PMSV7 p**	79.6	311.7	-23.3	12.9	-5.7	71.7	-9.5	7.8	-3.6	1.7	13.1	41.3	-41.3	0.25	1.51		S3NaCl-
Spring	**PZSV30a**	82.4	322.8	-16.6	13.4	25.2	74.3	-9.5	8.1	-4.6	1.7	1.2	42.8	-4.0	0.58	1.54	-0.41	S4NaCl-
Spring	**PZSV30b**	147.3	576.8	-36.4	23.9	-7.4	132.7	-6.5	14.4	-4.9	3.1	5.2	76.5	-29.4	0.02	1.02	-0.81	H3NaCl-
Spring	**PZSV30c**	156.3	612.0	-27.7	25.3	-9.5	140.8	-8.7	15.3	-4.2	3.3	5.6	81.1	-24.2	0.45	1.96	-0.78	H4NaCl
	Southern transect																	
Spring	**PZSV37a**	46.7	182.8	-15.1	7.6	2.3	42.1	2.0	4.6	-2.0	1.0	5.7	24.2	-12.9	0.22	1.12	-1.28	b3NaCl-
Spring	**PZSV37b**	64.8	253.8	-28.8	10.5	-1.3	58.4	5.0	6.3	-2.2	1.4	7.1	33.7	-28.3	0.16	1.21	-1.76	S3NaCl
Spring	**PZSV37c**	70.0	274.3	-13.3	11.4	-2.0	63.1	-9.5	6.9	-3.5	1.5	6.5	36.4	-32.7	0.29	1.37	-1.86	S4NaCl-
Spring	**PZSV37d**	90.5	354.6	-10.1	14.7	-5.5	81.6	-14.5	8.9	-4.3	1.9	7.0	47.0	-41.1	0.27	1.48	-1.76	S4NaCl
Spring	**PZSV6 p a**	82.6	323.7	-5.7	13.4	-8.8	74.5	-15.5	8.1	-2.4	1.7	11.8	42.9	-35.7	0.30	1.79	-1.97	S4NaCl
Spring	**PMSV6 p b**	86.5	338.8	-17.9	14.0	-8.3	77.9	-9.6	8.5	-2.7	1.8	3.3	44.9	-43.3	-0.12	0.90	-2.53	S3NaCl-
Spring	**PMSV8a**	15.3	59.8	7.0	2.5	0.5	13.8	-7.4	1.5	0.6	0.3	10.6	7.9	-4.2	0.39	1.18	-1.90	b4NaCl+
Spring	**PMSV8b**	49.8	195.1	1.3	8.1	-3.1	44.9	-7.0	4.9	-1.3	1.0	7.3	25.9	-12.7	0.10	1.18	-1.53	b4NaClo
Spring	**PMSV8c**	98.7	386.7	-14.2	16.0	-0.2	89.0	-5.6	9.7	-0.3	2.1	4.2	51.3	-15.4	0.10	0.98	-0.83	S3NaClo
Spring	**PMSV8d**	148.8	582.8	-42.2	24.1	-5.1	134.1	-2.6	14.6	-1.7	3.1	5.8	77.3	-22.5	0.26	1.43	-0.69	H4NaClo
Spring	**PMSV8 p a**	113.3	443.8	-37.9	18.4	-14.0	102.1	-7.7	11.1	-10.3	2.4	12.5	58.8	-58.4	0.21	1.96	-3.39	S4NaCl-
	Central transect																	
Summer	**PZSV26 a**	1.8	6.9	0.9	0.3	8.6	1.6	4.9	0.2	0.2	0.0	8.6	0.9	5.6	0.5	0.9	-1.01	f4CaMix+
Summer	**PZSV26 b**	18.4	72.1	-6.7	3.0	3.9	16.6	-1.1	1.8	-0.6	0.4	14.1	9.6	-9.3	0.38	1.12	-2.78	b4NaCl
Summer	**PZSV26 c**	45.8	179.4	-30.5	7.4	3.8	41.3	-6.0	4.5	-1.8	1.0	14.6	23.8	-21.5	0.65	1.83	-1.89	b4NaClo
Summer	**PZSV23 a**	4.2	16.4	-4.0	0.7	2.7	3.8	2.0	0.4	0.5	0.1	4.6	2.2	-1.4	0.14	0.6	-2.28	B3NaCl
Summer	**PZSV23 b**	8.0	31.5	-3.8	1.3	3.4	7.2	3.4	0.8	1.6	0.2	4.8	4.2	0.5	0.1	0.61	-1.52	b3NaCl+
Summer	**PZSV23 c**	26.9	105.5	-15.6	4.4	0.2	24.3	-4.2	2.6	1.1	0.6	4.3	14.0	-9.9	-0.15	0.4	-1.84	b3NaClo
Summer	**PZSV23 d**	92.1	360.6	-11.1	14.9	0.0	83.0	-18.5	9.0	-1.6	1.9	5.1	47.8	-33.4	0.08	0.86	-1.19	S3NaCl-
Summer	**PMSV7a**	6.2	24.3	3.1	1.0	0.1	5.6	1.1	0.6	0.6	0.1	8.7	3.2	-0.7	0.17	1.26	-2.34	B4NaCl+
Summer	**PMSV7b**	14.5	56.7	-1.3	2.3	-1.5	13.1	-0.1	1.4	-0.3	0.3	8.4	7.5	-0.2	0	1.28	-2.19	b4NaCl
Summer	**PMSV7c**	84.4	330.7	-36.6	13.7	-1.0	76.1	-17.8	8.3	-0.8	1.8	3.1	43.8	-6.9	0.25	1.27	-0.85	S3NaCl
Summer	**PMSV7d**	104.4	409.0	-13.3	16.9	-0.2	94.1	-23.0	10.2	-2.3	2.2	3.0	54.2	3.2	0.28	1.25	-0.61	S3NaCl
Summer	**PMSV7p a**	82.3	322.2	-27.6	13.3	-6.1	74.1	-23.3	8.1	-4.1	1.7	13.0	42.7	-39.8	0.31	1.53	-2.13	S4NaCl-
Summer	**PZSV30 a**	78.3	306.5	-33.8	12.7	34.3	70.5	-16.5	7.7	-5.2	1.6	9.8	40.6	-4.8	0.88	1.91	-0.32	S4NaCl-
Summer	**PZSV30 b**	138.7	543.3	-27.8	22.5	-3.6	125.0	-23.4	13.6	-3.7	2.9	5.9	72.0	-19.2	-0.02	0.73	-0.66	H4NaClo
Summer	**PZSV30 c**	149.6	586.0	-40.6	24.3	-8.1	134.8	-24.6	14.7	-3.4	3.1	5.8	77.7	-35.4	-0.07	0.63	-0.8	H4NaClo
	Northern Transect																	
Autumn	**PZSV18a**	2.02	7.91	2.08	0.33	5.87	1.82	3.12	0.20	0.37	0.04	14.30	1.05	-0.35	0.58	1.06	-1.17	B4CaHCO3+
Autumn	**PZSV18b**	2.09	8.18	2.66	0.34	6.20	1.88	3.36	0.20	0.39	0.04	14.87	1.08	-0.61	0.63	1.39	-1.29	B4CaHCO3+
Autumn	**PZSV18c**	7.71	30.20	-2.36	1.25	5.04	6.95	1.51	0.76	0.19	0.16	12.21	4.00	-2.29	0.58	1.3	-1.61	b4NaCl
Autumn	**PZSV17a**	8.48	33.22	-5.74	1.38	6.43	7.64	0.50	0.83	0.79	0.18	8.18	4.40	-3.41	0.77	1.6	-2	b4NaCl
Autumn	**PZSV17b**	9.38	36.74	1.75	1.52	7.33	8.45	1.59	0.92	0.95	0.20	14.23	4.87	-3.95	0.59	1.69	-2.76	b4NaCl+
Autumn	**PZSV17c**	28.26	110.67	-20.49	4.58	5.80	25.46	6.63	2.77	0.18	0.59	14.49	14.67	-14.42	1.29	2.72	-1.41	b5NaCl
Autumn	**PZSV13a**	2.05	8.01	0.45	0.33	8.81	1.84	2.62	0.20	-0.03	0.04	19.95	1.06	4.77	0.75	1.11	-2	B4CaHCO3
Autumn	**PZSV13b**	2.14	8.37	0.16	0.35	10.94	1.93	2.78	0.21	0.02	0.04	12.57	1.11	5.00	0.72	1.34	-1.67	B4CaHCO3o
Autumn	**PZSV14a**	48.42	189.65	-16.53	7.85	29.92	43.63	5.94	4.74	-2.68	1.02	19.80	25.15	-22.50	0.81	1.76	-1.46	b4NaCl
Autumn	**PZSV14b**	48.75	190.92	-11.22	7.91	28.22	43.92	5.68	4.78	-2.55	1.02	10.78	25.31	-22.93	0.56	1.68	-2.2	b4NaCl
Autumn	**PZSV14c**	71.55	280.22	-28.59	11.60	11.66	64.47	16.17	7.01	-2.91	1.50	10.63	37.15	-36.33	0.96	1.5	-1.87	S5NaCl
	Central transect																	
Autumn	**PZSV26a**	3.80	14.87	1.35	0.62	6.43	3.42	8.02	0.37	0.07	0.08	17.21	1.97	1.32	0.63	1.58	-1.76	B4MgCl+
Autumn	**PZSV26b**	13.95	54.63	1.73	2.26	4.65	12.57	1.52	1.37	-0.19	0.29	8.11	7.24	-4.86	1.03	2.69	-2.59	b4NaCl+
Autumn	**PZSV26c**	32.06	125.55	-14.04	5.20	4.71	28.89	10.20	3.14	-1.19	0.67	13.95	16.65	-16.21	1.05	2.66	-2.12	b5NaClo
Autumn	**PZSV26d**	61.60	241.25	-37.79	9.99	4.06	55.50	-8.60	6.03	-2.53	1.29	17.06	31.99	-30.69	0.96	1.85	-1.33	b5NaCl-
Autumn	**PZSV23a**	3.83	14.99	-0.18	0.62	2.92	3.45	4.8617	0.38	0.64	0.08	6.64	1.99	-3.95	0.15	0.64	-1.65	B3NaCl+
Autumn	**PZSV23b**	4.28	16.75	0.35	0.69	2.33	3.85	6.2679	0.42	0.98	0.09	6.63	2.22	-12.75	0.22	0.93	-1.68	B3NaCl+
Autumn	**PZSV23c**	15.51	60.75	-0.84	2.52	2.50	13.98	1.577	1.52	1.16	0.33	5.90	8.05	-22.50	0.35	1.16	-1.73	b3NaCl
Autumn	**PZPM7a**	7.13	27.92	9.73	1.16	6.53	6.42	0.32	0.70	0.29	0.15	20.01	3.70	1.14	0.79	2.22	-0.88	b3NaCl
Autumn	**PZPM7b**	52.16	204.29	12.27	8.46	4.20	47.00	11.18	5.11	0.01	1.09	6.04	27.09	-0.72	0.7	2.17	-0.7	b4NaCl
Autumn	**PZPM7c**	105.58	413.51	-4.31	17.12	2.50	95.13	15.30	10.34	-0.93	2.21	5.90	54.83	-12.49	0.91	1.81	-1.95	S4NaCl
Autumn	**PZPM7p**	77.65	304.10	-19.41	12.59	-3.07	69.96	-5.20	7.61	-2.42	1.63	15.66	40.32	-31.49	0.97	2.18	-1.51	S5NaCl-
Autumn	**PZSV30a**	66.46	260.28	-24.83	10.78	35.56	59.88	-8.29	6.51	-5.16	1.39	5.90	34.51	-0.70	0.19	0.44	-0.29	S3NaCl-
Autumn	**PZSV30b**	116.31	455.53	-7.16	18.86	9.55	104.80	-7.70	11.39	-3.76	2.44	7.15	60.40	-21.87	0.21	0.98	-0.59	S4NaCl
Autumn	**PZSV30c**	130.14	509.67	-12.72	21.11	0.00	117.26	-10.78	12.75	-3.04	2.73	7.88	67.58	-22.43	0.16	1.05	-0.67	H4NaClo
	Southern transect																	
Autumn	**PZSV37a**	7.8994	30.938	-1.10	1.28	3.27	7.12	5.70	0.77	-0.32	0.17	8.80	4.10	-1.64	0.78	1.96	-1.8	b4NaCl+
Autumn	**PZSV37b**	62.309	244.03	-2.15	10.11	-0.22	56.14	6.67	6.10	-3.04	1.31	19.38	32.36	-32.25	0.99	2.76	-3.39	b5NaCl
Autumn	**PZSV37c**	67.054	262.61	-11.98	10.88	-0.58	60.42	3.95	6.57	-3.28	1.41	19.90	34.82	-34.70	1.1	2.98	-3.35	S5NaCl
Autumn	**PZPM6a**	44.126	172.82	-10.92	7.16	35.41	39.76	2.24	4.32	-2.18	0.93	9.56	22.91	7.79	0.56	1.11	-0.29	b4NaCl
Autumn	**PZPM6b**	85.748	335.83	-5.83	13.91	7.97	77.26	5.44	8.40	-0.87	1.80	3.95	44.53	-8.11	0.13	0.85	-0.66	S3NaCl
Autumn	**PZPM6c**	92.525	362.37	-7.22	15.01	3.25	83.37	2.76	9.06	-1.97	1.94	4.96	48.05	-11.70	0.32	1.31	-0.73	S3NaCl
Autumn	**PZPM6d**	98.395	385.36	-4.10	15.96	3.51	88.66	7.29	9.64	-2.31	2.06	5.64	51.10	-18.88	0.38	1.47	-0.79	S3NaCl
Autumn	**PZPM6 p**	96.294	377.14	-34.94	15.62	-8.55	86.77	-11.83	9.43	-3.60	2.02	16.19	50.00	-49.95	0.66	2.35	-3.88	S5NaCl-
Autumn	**PMSV8a**	11.934	46.738	6.03	1.94	1.52	10.75	-4.98	1.17	0.18	0.25	16.75	6.20	-6.17	0.63	1.46	-3.91	b5NaCl+
Autumn	**PMSV8b**	26.415	103.45	9.32	4.28	0.15	23.80	-5.84	2.59	0.27	0.55	9.30	13.72	-12.10	0.41	1.41	-2.25	b4NaCl
Autumn	**PMSV8c**	93.289	365.37	7.49	15.13	4.39	84.06	-0.62	9.14	-0.25	1.96	5.19	48.44	-39.89	0.39	1.42	-1.31	S3NaCl
Autumn	**PMSV8d**	158.12	619.29	10.11	25.65	-0.07	142.48	-2.75	15.49	-1.05	3.32	7.48	82.11	-35.58	0.7	2.16	-0.64	H4NaCl
Autumn	**PMSV8 p**	108.2	423.77	0.71	17.55	-13.09	97.50	-14.47	10.60	-2.06	2.27	14.97	56.19	-56.04	0.33	1.97	-3.73	S5NaCl

Annex II

Water samples in dry season (Part I).

	sample	VA-1	VA-2	HA-1	HA-2	HA-3	HA-4	HA-5	HA-6	HA-7	HA-8	JAPO-1	SFA-1	SFA-2	SFA-3	SFA-4	SSA-1	SSA-2	SSA-3	HA-8b	SSA-2B	P-1	P-2	P-3	P-4	P-5	P-6	P-7
	pH	7.4	6.3	7.3	3.9	3.6	3.6	4.1	3.8	3.7	3.7	3	2.9	2.9	2.9	3.1	3.4	3.7	4.5	4.2	3.2	6.2	6.8	7.1	7	-	-	6.7
	T (°C)	11.3	12.3	7.1	10.6	11.6	12.9	13.2	13.2	12.6	12.2	10.6	15.5	7.9	8.2	11.4	11	11.1	12.9	12.8	8.5	10.5		10	10	-	-	-
	Cond (µS)	318	320	187	2290	2367	2405	1532	1438	1535	1471	1800	2865	1481	1425	1310	1306	1545	1385	1524	2010	1726	948	2330	841	-	-	958
	TDS	158	162	93	1120	1200	1242	1544	720	760	730	897	1434	759	726	663	659	675	697	760	1035	862	545	1150	419	-		469
ppm	Cl	9.1	8.7	10.7	13.7	22.3	33.2	22.4	16.9	16.1	33.7	19.6	29.3	19.8	19.8	9.6	29.3	22.0	75.9	23.1	20.3	383.8	396.1	135.0	36.1	24.0	56.9	54.3
ppm	NO2	<0.1	<0.1	<0.1	<0.1	<0.1	<0.1	<0.1	<0.1	<0.1	<0.1	<0.1	<0.1	<0.1	<0.1	<0.1	<0.1	<0.1	<0.1	<0.1	<0.1	<0.1	<0.1	<0.1	<0.1	<0.1	<0.1	<0.1
ppm	NO3	<0.1	<0.1	<0.1	29.7	25.9	<0.1	<0.1	<0.1	<0.1	<0.1	<0.1	<0.1	<0.1	<0.1	<0.1	<0.1	<0.1	<0.1	<0.1	<0.1	<0.1	<0.1	<0.1	<0.1	<0.1	<0.1	<0.1
ppm	PO4	<5	<5	<5	<5	<5	<5	<5	<5	<5	<5	<5	<5	<5	<5	<5	<5	<5	<5	<5	<5	<5	<5	<5	<5	<5	<5	<5
ppm	SO4	92	94	44	1509	1889	1907	991	948	992	995	1326	2460	673	875	720	913	908	738	875	689	325	212	1252	317	91	85	478
ppm	Na	17	16	12	19	28	36	28	26	24	38	4	27	13	17	20	34	30	71	32	26	287	312	250	59	43	93	65
ppm	Ca	32	33	20	110	114	127	94	89	110	118	27	344	62	74	89	114	107	180	207	85	86	96	334	91	41	50	125
ppm	K	3	4	2	12	14	14	7	5	6	7	3	13	2	2	3	6	3	10	11	5	25	19	15	14	9	13	9
ppm	S	30	29	14	634	668	650	349	333	358	337	483	851	363	311	307	314	294	430	311	239	103	104	434	107	28	26	151
ppm	Fe	0.0	0.0	0.0	525.5	580.0	527.0	135.5	76.5	65.5	58.0	293.3	335.8	133.2	101.7	9.4	36.0	8.6	62.3	0.0	19.6	0.1	0.0	0.0	0.0	0.0	0.0	0.0
ppm	Al	0.0	0.0	0.0	62.8	61.1	61.6	38.0	45.5	48.5	39.6	82.6	76.2	60.7	45.7	80.8	41.3	51.7	44.3	10.9	32.9	0.0	0.0	0.1	0.0	0.0	0.0	0.0
ppm	Zn	0.0	0.0	0.0	129.2	141.2	123.8	51.7	38.6	43.7	44.2	51.2	84.7	33.1	29.6	28.0	38.6	29.1	63.8	24.6	28.8	0.1	0.1	0.0	0.0	0.0	0.0	0.2
ppm	Mg	15.4	15.2	9.5	34.5	47.7	49.4	39.2	45.3	53.4	52.8	18.4	105.2	27.6	28.1	42.0	52.3	55.5	68.2	92.8	39.3	36.2	44.9	105.2	36.2	17.0	16.3	53.6
ppm	Si	5.7	7.3	4.4	20.4	19.9	22.8	22.0	27.0	30.6	27.8	22.6	33.9	31.5	28.7	62.6	32.5	37.3	35.2	34.8	25.6	15.3	14.1	18.2	17.9	12.2	9.9	16.4
ppm	Mn	0.0	0.0	0.0	19.6	20.4	21.4	15.0	17.5	22.4	19.8	5.7	4.9	5.6	3.7	7.2	18.0	19.2	19.6	12.6	13.9	0.0	0.5	0.0	0.0	0.0	0.0	0.0
ppb	Li	24.0	19.3	16.9	246.1	256.0	274.8	249.4	374.9	488.7	482.8	113.3	280.4	182.9	148.9	504.8	547.4	605.6	823.2	887.2	429.7	952.8	867.3	424.2	262.6	60.4	245.4	457.6
ppb	Be	-	-	-	-	-	-	-	-	9.70	-	-	-	-	-	12.81	9.11	9.99	-	7.59	6.07	-	-	-	-	-	-	-
ppb	B	-	-	-	-	-	-	-	-	-	-	-	-	-	-	-	-	-	-	-	-	-	-	-	-	-	438.63	-
ppb	Sc	-	-	-	-	-	-	-	-	-	-	10.75	13.49	10.14	8.87	11.71	-	-	-	-	-	-	-	-	-	2.12	-	-
ppb	Ti	-	-	2.18	-	-	-	-	-	-	-	-	-	-	-	9.61	11.50	6.56	-	7.84	6.53	-	-	8.25	-	2.68	-	-
ppb	Cr	-	-	-	-	-	-	-	-	-	-	48.58	-	-	-	-	-	-	-	-	-	-	-	-	-	-	-	-
ppb	Co	0.32	0.34	0.21	1441.9	1299.8	1258.8	569.9	453.4	520.9	486.8	254.0	120.1	162.3	99.3	153.7	398.9	294.6	360.5	6.3	312.4	-	-	-	-	-	-	-
ppb	Ni	-	-	-	1213.6	992.2	939.7	339.2	448.6	555.0	525.8	-	-	19.3	-	228.3	470.5	395.4	512.4	547.5	377.8	-	-	-	-	-	-	8.40
ppb	Cu	5.70	2.66	6.73	2645.6	3479.1	4888.7	2896.5	1949.7	2022.0	1453.0	5652.7	259.6	2639.6	1460.4	761.1	1271.5	1198.5	2038.0	329.2	1040.5	-	-	-	-	3.54	-	-
ppb	Ga	-	-	-	-	-	-	-	-	-	-	6.9	6.8	4.1	4.6	-	-	-	-	-	-	-	-	-	-	-	-	-

Water samples in dry season (Part II).

	sample	VA-1	VA-2	HA-1	HA-2	HA-3	HA-4	HA-5	HA-6	HA-7	HA-8	JAPO-1	SFA-1	SFA-2	SFA-3	SFA-4	SSA-1	SSA-2	SSA-3	HA-8b	SSA-2B	P-1	P-2	P-3	P-4	P-5	P-6	P-7
ppb	As	-	-	-	-	-	-	-	-	-	-	69.4	-	-	-	-	-	-	-	-	-	-	-	-	-	-	-	-
ppb	Rb	1.29	-	1.27	87.7	83.3	79.3	31.3	21.9	24.3	25.5	22.4	178.0	19.6	21.9	5.3	20.4	9.3	37.6	10.3	17.2	22.46	9.12	6.00	2.78	2.58	2.64	8.02
ppb	Sr	173.60	173.64	99.67	268.9	297.0	298.3	247.7	255.1	363.0	396.1	80.8	4090.2	441.5	566.6	479.3	439.7	421.3	648.5	1011.4	328.0	593.5	589.0	1276.6	400.5	341.5	392.9	618.8
ppb	Y	-	-	-	38.4	41.1	46.7	39.4	50.4	71.6	66.3	53.0	23.2	42.4	28.9	73.8	64.1	86.1	66.2	53.0	52.2	-	-	-	-	-	-	-
ppb	Mo	0.23	0.21	0.36	-	-	-	-	-	-	-	-	-	-	-	-	-	-	-	-	-	-	-	0.84	-	0.89	1.01	-
ppb	Ag	-	-	-	-	-	-	-	-	-	-	1.1	-	1.1	-	-	-	-	-	-	-	-	-	-	-	-	-	-
ppb	Cd	0.49	0.56	-	3402.3	3348.9	3219.0	1272.7	812.0	1085.7	1068.4	6032.4	307.4	2500.5	1305.1	977.5	963.0	659.1	1057.7	588.5	721.8	1.29	1.69	0.90	-	-	-	4.62
ppb	In	-	-	-	8.8	11.7	7.9	3.7	2.7	4.8	-	111.5	24.6	47.4	30.4	4.2	1.9	-	13.3	-	1.3	-	-	-	-	-	-	-
ppb	Sb	1.66	2.41	2.28	-	-	-	-	-	-	-	-	-	-	-	1.1	-	-	-	0.6	-	-	1.67	1.26	0.50	0.82	0.53	0.83
ppb	Cs	-	-	0.40	100.5	128.1	93.7	39.5	27.0	26.7	29.9	5.5	436.6	25.8	38.0	0.8	20.7	1.3	58.2	11.8	15.5	1.03	-	-	-	1.36	-	6.20
ppb	Ba	30.35	31.47	30.01	20.7	34.4	23.7	23.7	24.0	34.8	34.5	18.2	37.7	9.9	13.1	8.3	24.8	12.0	28.5	24.0	16.2	51.95	78.23	22.63	23.80	29.55	75.14	36.75
ppb	La	-	-	-	7.6	7.7	9.5	10.6	14.0	20.6	19.1	4.0	5.9	6.5	5.5	23.7	19.5	28.2	21.1	15.8	16.9	-	-	-	-	-	-	-
ppb	Ce	-	-	-	19.4	21.6	25.9	30.4	38.1	46.2	41.7	12.9	16.2	20.4	15.2	65.1	44.7	71.0	49.5	16.6	40.7	-	-	-	-	-	-	-
ppb	Pr	-	-	-	3.4	3.7	4.8	5.2	7.1	10.1	8.3	2.7	3.1	3.8	3.2	12.4	8.5	13.5	9.3	5.0	7.7	-	-	-	-	-	-	-
ppb	Nd	-	-	-	14.9	16.5	21.2	23.1	31.3	43.4	34.4	14.2	12.6	18.2	14.6	50.5	35.7	56.7	38.6	19.7	31.2	-	-	-	-	-	-	-
ppb	Sm	-	-	-	5.3	5.3	7.0	6.8	9.6	13.2	10.6	7.5	4.0	7.2	5.4	14.2	10.5	16.8	11.4	5.7	9.2	-	-	-	-	-	-	-
ppb	Eu	-	-	-	2.4	2.5	2.9	2.3	2.8	4.0	3.2	2.8	1.5	2.3	1.7	3.7	3.1	4.3	3.3	1.7	2.5	-	-	-	-	-	-	-
ppb	Gd	-	-	-	6.7	6.9	9.2	8.9	12.5	17.4	15.7	10.6	5.4	9.3	6.9	18.1	14.8	21.4	15.4	10.2	12.1	-	-	-	-	-	-	-
ppb	Tb	-	-	-	-	-	1.2	1.1	1.5	2.1	1.9	1.6	-	1.2	0.9	2.2	1.8	2.5	1.9	1.2	1.5	-	-	-	-	-	-	-
ppb	Dy	-	-	-	5.5	5.8	7.1	6.4	8.3	11.6	10.2	9.1	3.7	7.1	5.0	12.9	9.8	13.9	10.6	6.3	8.2	-	-	-	-	-	-	-
ppb	Ho	-	-	-	-	-	1.1	1.0	1.3	1.9	1.6	1.5	-	1.2	-	2.0	1.5	2.1	1.6	1.0	1.3	-	-	-	-	-	-	-
ppb	Er	-	-	-	2.6	2.8	3.1	2.6	3.3	4.5	3.6	3.9	1.5	3.0	2.0	5.0	3.9	5.6	4.2	2.4	3.3	-	-	-	-	-	-	-
ppb	Tm	-	-	-	-	-	-	-	-	-	-	-	-	-	-	0.7	-	0.7	-	-	-	-	-	-	-	-	-	-
ppb	Yb	-	-	-	2.5	2.4	3.0	2.3	2.9	3.9	3.2	3.7	1.8	2.7	1.9	4.5	3.3	4.7	3.2	1.5	2.7	-	-	-	-	-	-	-
ppb	Lu	-	-	-	-	-	-	-	-	-	-	-	-	-	-	-	-	-	-	-	-	-	-	-	-	-	-	-
ppb	Hg	-	-	5.15	-	-	-	-	-	-	-	-	-	-	-	-	-	-	-	-	-	-	-	-	-	-	-	-
ppb	Tl	-	-	-	15.6	18.4	23.8	10.0	6.0	6.6	5.8	3.6	4.7	1.2	0.9	-	4.7	0.7	6.1	-	3.8	-	-	-	-	-	-	-
ppb	Pb	169.45	181.71	488.28	2629.4	459.0	1633.6	196.1	111.5	117.9	84.3	43.9	21.0	19.3	34.0	5.3	77.6	12.0	1310.8	44.0	19.7	1.67	2.62	-	0.52	0.21	2.61	1.48
ppb	Yh	-	-	-	5.7	8.7	5.1	2.1	1.0	1.8	-	21.0	3.0	14.5	10.3	1.5	0.8	-	3.1	-	0.6	-	-	-	-	-	-	-
ppb	U	0.42	0.39	0.50	542.8	534.3	499.0	211.2	150.1	174.7	139.9	11.1	10.1	13.7	12.9	17.4	106.4	24.4	93.7	1.6	72.8	-	3.20	4.07	0.94	1.89	4.46	1.20

Water samples in wet season.

Wet		VA-1	HA-1	HA-2	HA-3	HA-4	HA-5	HA-6	HA-7	HA-8	JAPO-1	SFA-1	SFA-2	SFA-3	SFA-4	SSA-2	SSA-3	HA-8B	P-1	P-2	P-3	P-4	P-5	P-6	P-7
	pH	7.0	6.8	5.3	4.9	4.8	4.0	5.0	4.8	4.3	3.8	3.7	4.3	3.3	3.5	3.9	3.7	3.7	6.9	7.0	7.0	6.5	6.6	7.3	6.1
	T (°C)	12	17	13	10	12	16	12	10	19	15	13	11	13	15	15	15	16	16	15	17	-	15	18	15
	Cond (µS)	870	234	156	366	460	649	1000	502	793	1324	751	608	620	1355	2087	530	548	1751	872	3618	488	428	970	1355
	TDS	435	116	78	188	228	324	499	252	392	655	374	300	311	685	1026	264	276	875	434	1827	253	214	486	685
ppm	Cl	7.72	5.46	5.73	5.99	8.56	9.49	8.51	8.14	31.16	10.44	9.10	6.94	9.01	8.02	12.66	21.28	12.70	415.70	214.85	519.17	37.30	17.93	21.65	54.23
ppm	NO2	0.25	0.25	<0.1	<0.1	<0.1	<0.1	<0.1	<0.1	<0.1	<0.1	<0.1	<0.1	<0.1	<0.1	<0.1	<0.1	<0.1	<0.1	<0.1	<0.1	<0.1	<0.1	<0.1	-
ppm	NO3	0.12	1.74	<0.1	4.32	3.09	2.84	2.98	2.34	5.51	1.63	5.50	1.91	2.98	2.02	3.35	3.06	3.98	<0.1	72.89	<0.1	<0.1	<0.1	3.29	-
ppm	SO4	78.6	31.2	221.1	240.3	361.3	642.9	345.0	283.9	948.5	1499.3	1809.6	233.0	295.2	335.4	526.8	600.7	493.5	387.6	536.9	465.9	601.9	87.1	1222.7	-
ppm	Ca	22.8	16.2	24.5	25.2	32.9	44.2	32.6	26.5	138.7	33.7	146.9	26.0	40.8	30.4	49.5	63.8	60.4	88.0	92.7	486.8	126.1	41.1	65.0	224.8
ppm	Fe	0.00	0.00	1.48	3.37	9.28	76.24	2.59	2.69	0.42	352.30	204.64	2.59	3.18	2.79	2.79	4.65	2.81	0.29	0.03	0.02	0.04	0.01	0.00	0.01
ppm	K	3.37	2.56	3.56	3.82	4.25	4.35	3.72	3.58	9.23	5.21	7.69	3.57	3.72	3.21	4.26	5.01	4.92	22.62	13.70	18.82	9.48	6.00	10.95	12.08
ppm	S	19.4	8.7	53.6	67.1	98.9	194.2	81.7	68.4	270.0	501.6	438.2	66.5	103.5	79.9	117.1	148.6	148.0	100.7	110.4	418.9	130.6	26.3	42.8	291.2
ppm	Na	12.2	9.1	9.7	10.0	13.2	13.7	13.3	11.7	42.9	7.2	19.0	11.7	14.0	12.4	17.9	24.2	18.1	278.0	70.0	389.1	50.1	41.4	144.4	32.7
ppm	Mg	10.6	6.7	8.9	9.8	13.7	21.8	15.1	8.6	64.4	25.4	41.0	8.3	19.1	10.6	21.3	25.9	28.0	34.7	34.1	144.1	43.5	14.7	23.2	94.1
ppm	Ba	0.03	0.02	0.03	0.03	0.03	0.03	0.04	0.02	0.02	0.01	0.03	0.03	0.03	0.02	0.03	0.04	0.04	0.08	0.03	0.05	0.03	0.06	0.04	0.03
ppm	Mn	0.00	0.01	1.91	2.40	4.58	9.19	4.18	1.06	26.73	7.20	2.66	0.99	6.32	1.52	7.14	8.92	12.65	0.01	0.00	0.00	0.09	0.00	0.01	0.01
ppm	Sr	0.13	0.08	0.10	0.10	0.12	0.14	0.14	0.24	0.59	0.12	1.60	0.24	0.17	0.25	0.25	0.30	0.25	0.65	0.45	1.93	0.69	0.29	0.51	1.02
ppm	B	0.30	0.20	0.26	0.26	0.26	0.19	0.31	0.24	0.50	-0.57	-0.08	0.25	0.32	0.25	0.32	0.38	0.36	1.44	1.32	2.17	0.81	0.87	1.56	0.49
ppm	Si	7.93	5.90	6.83	7.29	9.84	14.14	10.60	13.93	33.84	25.43	23.65	13.54	12.97	18.57	17.60	20.49	18.01	14.44	17.97	19.02	10.11	12.60	14.44	34.67
ppm	Zn	0.11	0.07	11.13	14.84	17.37	23.73	10.86	6.05	26.34	41.42	43.10	5.95	12.61	7.01	12.18	16.28	15.35	0.12	0.12	0.08	0.11	0.10	0.09	4.97
ppm	Li	0.02	0.01	0.03	0.03	0.07	0.16	0.08	0.05	0.79	0.20	0.14	0.04	0.12	0.07	0.17	0.24	0.24	0.88	0.26	0.53	0.14	0.05	0.64	0.91
ppm	P	0.00	0.03	0.02	0.01	0.07	0.25	0.08	0.04	0.44	0.43	0.87	0.08	0.14	0.09	0.16	0.15	0.23	0.15	0.21	1.12	0.19	0.12	0.20	0.53
ppb	Ba	27.15	21.85	26.11	30.09	29.86	28.14	34.36	22.04	16.97	14.40	22.13	27.44	33.22	23.16	33.00	36.49	35.03	86.36	32.25	55.24	34.99	56.67	37.19	32.93
ppb	Li	17.38	7.36	30.72	34.25	71.25	147.26	77.60	45.24	762.26	201.04	122.87	42.09	117.08	68.21	172.31	234.14	228.55	908.29	266.89	557.78	148.11	53.04	663.54	916.82
ppb	Mn	2.90	7.20	1776	2255	4443	7829	3953	965	24755	6746	2504	932	5993	1408	6946	8338	11535	5.94	0.92	4.14	91.93	2.21	1.01	1.69
ppb	Zn	125.19	71.62	12385	16790	20197	23767	11916	6408	28437	46982	46522	6492	13877	7533	14005	17626	15801	130.36	139.07	82.25	123.57	117.09	93.72	5042.23
ppb	Al	10.92	13.23	4701	6899	12169	27746	9124	9417	35937	92347	46663	9260	13976	12816	18304	21312	21515	17.76	1.83	5.23	7.62	113.93	1.78	13.21
ppb	Se	0.96	0.96	1.16	1.47	2.34	3.26	1.40	0.76	6.69	6.76	16.93	0.90	1.82	1.30	2.32	3.72	3.33	4.21	3.15	9.33	1.27	1.04	2.71	1.90
ppb	As	1.50	1.06	0.12	0.28	0.62	0.70	0.36	0.27	1.35	135.06	93.47	0.43	0.48	0.30	0.47	0.56	0.59	4.30	0.82	14.05	1.63	3.22	6.79	2.59
ppb	Cr	-0.07	-0.31	-0.21	0.35	1.60	6.68	0.06	2.91	-0.42	76.77	38.44	3.18	0.62	3.57	1.74	3.08	0.07	-1.43	-0.57	-0.72	-0.02	-0.14	-0.06	-0.79
ppb	Pb	0.17	0.08	6.84	13.34	23.98	26.85	13.00	35.62	2.40	25.99	13.01	34.20	16.46	28.23	13.33	31.76	16.61	7.22	0.12	0.29	0.13	6.49	21.00	0.26
ppb	Cu	1.52	1.79	551.8	900.0	880.7	1873.0	648.2	354.7	1348.1	8454.2	616.5	377.4	875.8	376.6	880.6	1089.4	1198.3	4.62	2.25	5.31	2.52	1.33	1.60	1.34
ppb	U	0.08	0.13	100.4	83.1	79.8	77.4	42.9	2.1	3.1	7.0	7.6	2.7	42.1	2.5	29.1	28.7	39.3	0.47	0.78	3.95	0.64	1.21	1.84	0.01
ppb	Cd	0.64	0.35	759.48	528.02	544.59	623.43	331.84	183.04	668.23	3802.99	205.81	178.60	355.75	218.40	356.80	391.45	427.32	0.76	0.08	0.12	0.86	0.05	0.14	56.95
ppb	V	-0.03	-0.22	-0.26	-0.23	-0.11	-0.58	-0.24	-0.11	-0.18	6.58	7.69	0.04	-0.11	-0.10	-0.12	-0.36	-0.59	5.15	1.34	12.00	1.23	1.40	4.76	1.48
ppb	Ni	1.38	0.98	108.67	119.12	169.42	255.67	123.98	31.38	582.40	271.21	120.58	32.61	168.85	45.79	167.27	197.69	243.07	1.80	1.91	8.50	11.88	0.97	1.41	209.35
ppb	Co	0.07	0.09	132.78	130.02	178.93	240.28	126.06	23.37	114.00	233.42	68.60	24.13	150.39	32.78	131.50	152.03	207.21	0.40	0.18	0.86	1.27	0.27	0.31	0.44
ppb	Hg	-0.01	-0.01	0.02	0.02	0.00	0.03	0.00	0.02	0.10	0.07	0.02	0.06	0.08	0.02	0.00	0.02	0.06	0.12	0.00	0.29	0.01	0.03	0.12	-0.01

Major and trace element sediment composition.

	Sample	VA-1	VA-2	HA-1	HA-2	HA-3	HA-4	HA-5	HA-6	HA-7	HA-8	JAPO-1	SF-1	SF-2	SF-3	SF-4	SSA-1	SSA-3	HA-8B	SSA-2B	HA-2s	HA-3s
(%)	Al2O3	13.5	12.3	14.1	7.9	7.7	10.0	8.9	8.9	8.6	8.8	4.7	8.8	10.9	11.1	9.6	12.7	9.5	13.4	8.2	10.0	11.2
(%)	CaO	0.5	0.4	0.3	0.2	0.1	0.2	0.1	0.1	0.1	0.3	0.1	0.3	0.2	0.2	0.5	0.2	0.1	0.2	0.1	0.2	0.2
(%)	Fe2O3	6.2	5.8	6.9	13.8	10.0	8.1	10.6	8.8	9.4	12.4	14.7	19.0	10.9	14.4	4.8	9.2	6.6	9.6	7.8	12.1	10.7
(%)	K2O	2.7	2.5	3.1	0.4	0.5	0.9	0.6	0.6	0.5	0.5	1.1	1.7	2.6	2.8	2.3	1.6	0.8	1.8	0.5	0.9	1.2
(%)	MgO	1.1	1.0	1.2	1.0	0.9	1.0	1.0	1.0	1.0	1.1	0.3	0.4	0.6	0.6	0.4	1.1	1.0	1.1	1.0	1.0	1.1
(%)	MnO	0.1	0.1	0.2	0.1	0.0	0.0	0.1	0.0	0.1	0.1	0.0	0.0	0.0	0.0	0.0	0.1	0.0	0.1	0.0	0.0	0.1
(%)	Na2O	0.9	0.8	0.7	<	<	<	<	<	<	1.5	<	<	<	0.5	1.1	<	<	<	<	<	<
(%)	P2O5	0.2	0.1	0.1	0.1	0.1	0.1	0.1	0.1	0.1	0.1	0.1	0.3	0.2	0.3	0.1	0.2	0.1	0.2	0.1	0.1	0.2
(%)	SiO2	70.7	73.6	70.1	64.7	73.5	70.4	69.8	71.3	72.3	66.6	70.1	52.3	64.6	58.2	78.7	64.6	73.9	61.3	74.5	64.5	62.3
(%)	TiO2	0.7	0.6	0.7	0.5	0.5	0.5	0.5	0.5	0.5	0.5	0.6	0.7	0.7	0.6	0.4	0.5	0.5	0.6	0.4	0.5	0.5
(ppm)	As	54	36	33	1234	630	556	692	613	604	728	ND	2279	1139	1727	344	621	605	882	434	998	990
(ppm)	Ba*	568	467	591	ND	ND	ND	ND	ND	ND	ND	ND	29	189	269	437	ND	ND	ND	ND	ND	ND
(ppm)	Bi	2.0	0.4	0.8	151.9	68.0	118.0	99.5	100.9	90.6	89.0	ND	93.3	78.4	80.6	6.9	162.0	85.1	245.3	69.4	219.0	263.5
(ppm)	Br*	2.8	1.3	1.2	0.3	ND	ND	0.5	0.3	0.5	0.3	ND	-0.9	0.3	0.7	0.4	0.3	ND	0.9	ND	0.3	0.3
(ppm)	Ce	65	68	71	37	38	45	41	48	41	53	ND	124	94	87	55	54	36	67	35	55	58
(ppm)	Co*	12.9	11.5	13.6	14.6	10.1	8.9	9.6	8.1	9.1	9.6	ND	-1.4	2.7	0.4	1.9	7.8	5.5	11.1	7.5	14.4	14.7
(ppm)	Cr	104	137	147	191	269	140	191	143	183	206	ND	101	56	74	171	94	103	112	132	140	113
(ppm)	Cu	55	26	27	1309	695	731	752	758	759	823	ND	46	127	104	18	802	631	1181	597	1318	1394
(ppm)	Ga	19	16	19	60	49	58	56	60	59	62	ND	30	28	29	16	50	57	66	54	63	65
(ppm)	Ge*	2	1	2	20	19	19	21	20	21	24	ND	3	1	0	2	15	17	19	18	19	19
(ppm)	Hf*	8	5	5	22	12	12	13	14	15	19	ND	-1	4	1	3	9	13	15	11	19	19
(ppm)	La*	29	35	36	25	25	24	25	22	20	22	ND	62	39	46	23	25	22	34	13	29	31
(ppm)	Mn*	616	570	986	448	296	360	420	357	419	568	ND	84	188	166	123	287	299	444	341	366	430
(ppm)	Mo	0.4	0.1	0.2	1.4	0.9	1.4	1.4	0.6	1.0	0.9	ND	2.3	1.9	1.4	0.1	2.0	0.8	3.9	0.6	2.3	3.0
(ppm)	Nb	15.5	13.7	14.8	11.2	10.8	11.8	11.5	11.4	11.5	12.7	ND	16.5	16.5	14.7	12.1	10.4	11.0	13.8	10.8	11.7	12.3
(ppm)	Nd*	28.7	29.7	31.6	16.7	11.9	20.9	16.3	19.7	20.5	21.6	ND	49.9	34.8	35.8	22.1	22.1	14.1	28.4	16.0	20.7	24.5
(ppm)	Ni	31.2	22.8	27.0	21.3	14.4	14.3	14.3	13.2	13.5	16.0	ND	5.6	8.1	7.2	5.6	13.9	10.5	22.0	10.6	23.0	23.0
(ppm)	Pb*	56	40	48	174	92	167	132	141	120	140	ND	2996	591	666	221	192	279	294	96	248	301
(ppm)	Rb	130	119	173	38	41	77	50	51	40	40	ND	90	141	151	120	106	63	157	40	82	105
(ppm)	Sb*	19.8	12.0	8.4	ND	ND	2.6	ND	ND	ND	ND	ND	149.6	10.5	22.5	18.2	7.6	208.4	15.8	ND	8.7	14.2
(ppm)	Sc*	13.6	12.8	15.6	ND	0.3	ND	ND	ND	ND	ND	ND	ND	ND	ND	6.6	ND	3.3	ND	ND	ND	ND
(ppm)	Se*	0.6	0.0	0.2	4.2	2.1	2.0	2.8	2.2	2.5	3.2	ND	12.1	6.0	6.0	1.5	2.2	2.9	3.0	2.1	4.0	3.9
(ppm)	Sm*	9.1	3.5	5.7	2.8	5.9	6.9	2.9	0.6	1.4	5.5	ND	6.7	4.6	3.0	4.5	4.8	0.7	ND	2.2	2.7	7.1
(ppm)	Sn*	391	121	66	17149	7645	8070	10032	10510	10379	11965	ND	10695	7982	6688	1179	5767	6091	10638	7162	11174	11956
(ppm)	Sr	102	78	61	49	43	67	53	57	54	58	ND	289	130	149	165	71	64	98	50	69	79
(ppm)	Ta*	1.2	0.8	ND	3.7	2.8	2.5	3.3	2.3	3.7	4.5	ND	0.5	0.5	2.1	0.9	2.5	2.8	4.1	3.3	4.3	4.8
(ppm)	Te*	2.0	ND	ND	ND	1.2	3.4	ND	0.8	ND	0.4	ND	-4.3	0.3	2.5	0.1	3.7	1.9	0.6	1.7	-4.7	0.6
(ppm)	Th	10	8	10	11	8	10	10	9	9	10	ND	12	14	14	7	10	8	17	8	13	15
(%)	TiO2	0.7	0.6	0.7	0.5	0.4	0.5	0.5	0.5	0.5	0.6	ND	0.8	0.7	0.7	0.4	0.4	0.4	0.6	0.4	0.5	0.5
(ppm)	Tl*	1.9	1.2	2.0	4.1	3.2	3.0	4.0	3.5	3.9	3.1	ND	3.0	1.5	2.5	0.9	5.5	1.7	8.1	2.7	6.5	6.7
(ppm)	U*	2.5	1.1	2.2	1.1	1.4	2.5	2.0	2.5	1.6	1.6	ND	1.2	2.5	1.9	1.8	2.9	1.6	5.6	0.6	3.8	5.5
(ppm)	V	100	99	115	81	68	85	78	80	76	82	ND	111	94	104	59	82	76	111	70	92	96
(ppm)	W	8	4	6	113	57	72	74	83	79	91	ND	53	38	36	9	75	56	108	57	91	98
(ppm)	Y	28	24	28	21	16	20	19	19	19	21	ND	35	29	25	16	16	17	24	16	20	22
(ppm)	Yb*	4.1	3.9	2.7	ND	0.9	2.7	1.8	1.3	1.1	0.2	ND	ND	2.2	ND	2.6	2.0	2.2	ND	3.2	ND	ND
(ppm)	Zn	351	209	237	1513	823	872	985	934	1009	1239	ND	295	167	134	58	813	968	1269	815	1488	1645

Sequential extraction data (Part I).

	Ca	Mg	Ba	Cd	Co	Cu	Mn	Pb	Sr	Zn	K	Al	Be	Fe	Li	Mo	Ni	Sb	Ti	Tl	V	Na	As	B	Cr	P	S	Se	Si
VA1 -St1	1690	426	12	DL	DL	5	264	DL	12	207	232	DL	DL	201	DL	DL	DL	DL	DL	DL	DL	DL	DL	DL	DL	DL	668	DL	222
VA1 -St2	733	182	75	DL	DL	16	240	DL	6	103	DL	797	DL	2099	DL	DL	DL	DL	DL	DL	DL	DL	DL	DL	DL	DL	DL	DL	434
VA1 -St3	97	162	8	DL	DL	19	30	DL	DL	65	DL	450	DL	722	DL	DL	DL	DL	DL	DL	DL	DL	DL	DL	DL	DL	1227	DL	470
VA1 -St4	238	4093	86	DL	DL	41	236	DL	14	160	3160	16798	DL	38244	DL	DL	DL	DL	161	DL	DL	DL	DL	DL	19	DL	DL	DL	DL
SF3 -St1	118	89	DL	DL	DL	13	24	DL	DL	37	DL	107	DL	1100	DL	DL	DL	DL	DL	DL	DL	DL	DL	DL	DL	DL	1808	DL	DL
SF3 -St2	140	DL	7	DL	DL	30	45	DL	DL	8	DL	368	DL	26999	DL	DL	DL	DL	DL	DL	DL	DL	DL	DL	DL	DL	3128	DL	193
SF3 -St3	50	57	DL	DL	DL	23	14	DL	DL	48	DL	261	DL	8101	DL	DL	DL	DL	DL	DL	DL	DL	DL	DL	DL	DL	8003	DL	257
SF3 -St4	211	1329	162	DL	DL	78	140	710	70	68	3360	8472	DL	68567	DL	DL	DL	DL	139	DL	DL	DL	1480	DL	12	1290	5605	DL	DL
HA5 -St1	121	53	DL	DL	DL	29	72	DL	DL	43	DL	DL	DL	1187	DL	DL	DL	DL	DL	DL	DL	DL	DL	DL	DL	DL	682	DL	DL
HA5 -St2	563	39	DL	DL	DL	25	47	DL	DL	22	DL	DL	DL	3004	DL	DL	DL	DL	DL	DL	DL	DL	DL	DL	DL	DL	420	DL	DL
HA5 -St3	60	56	DL	8	6	521	117	DL	DL	716	DL	DL	DL	23728	DL	DL	DL	DL	DL	DL	DL	DL	DL	DL	DL	DL	15830	DL	DL
HA5 -St4	244	325	40	DL	DL	600	221	DL	25	588	635	1813	DL	47783	DL	DL	DL	DL	DL	DL	DL	DL	723	DL	DL	DL	39223	DL	DL
SSA -St1	137	113	DL	DL	DL	28	118	DL	DL	59	DL	DL	DL	640	DL	DL	DL	DL	DL	DL	DL	DL	DL	DL	DL	DL	639	DL	DL
SSA -St2	502	DL	5	DL	DL	15	51	DL	DL	33	DL	118	DL	3721	DL	DL	DL	DL	DL	DL	DL	DL	DL	DL	4	DL	397	DL	DL
SSA -St3	49	58	DL	7	DL	575	83	DL	DL	775	DL	DL	DL	13131	DL	DL	DL	DL	DL	DL	DL	DL	DL	DL	DL	DL	11914	DL	DL
SSA -St4	107	465	63	DL	DL	170	57	205	36	200	1298	3658	DL	20002	DL	DL	DL	DL	24	DL	DL	DL	DL	DL	9	DL	10580	DL	DL
AH1 -St1	902	259	11	DL	DL	DL	116	DL	6	27	DL	DL	DL	5	DL	DL	DL	DL	DL	DL	DL	DL	DL	DL	DL	DL	332	DL	98
AH1 -St2	504	151	63	DL	6	5	600	DL	DL	36	DL	676	DL	1416	DL	DL	DL	DL	DL	DL	DL	DL	DL	DL	DL	DL	DL	DL	300
AH1 -St3	71	206	DL	DL	DL	DL	44	DL	DL	40	DL	405	DL	292	DL	DL	DL	DL	DL	DL	DL	DL	DL	DL	DL	DL	DL	DL	397
AH1 -St4	142	5086	30	DL	DL	39	348	DL	DL	197	2404	17023	DL	45379	DL	DL	DL	DL	63	DL	DL	DL	DL	DL	20	DL	DL	DL	DL
AH1 -St1	925	275	11	DL	DL	DL	103	DL	6	24	DL	DL	DL	5	DL	DL	DL	DL	DL	DL	DL	DL	DL	DL	DL	DL	321	DL	104
AH1 -St2	483	153	59	DL	4	4	659	DL	DL	35	DL	709	DL	1396	DL	DL	DL	DL	DL	DL	DL	DL	DL	DL	DL	DL	DL	DL	311
AH1 -St3	85	216	DL	DL	DL	DL	40	DL	DL	38	DL	425	DL	257	DL	DL	DL	DL	DL	DL	DL	DL	DL	DL	DL	DL	DL	DL	409
AH1 -St4	DL	4709	31	DL	DL	42	316	DL	DL	188	2179	16049	DL	42464	DL	DL	DL	DL	63	DL	DL	DL	DL	DL	18	DL	DL	DL	DL
SSA3 -St1	141	110	DL	DL	DL	22	123	DL	DL	57	DL	DL	DL	589	DL	DL	DL	DL	DL	DL	DL	DL	DL	DL	DL	DL	588	DL	DL
SSA3 -St2	457	DL	4	DL	DL	14	49	DL	DL	26	DL	116	DL	3611	DL	DL	DL	DL	DL	DL	DL	DL	DL	DL	DL	DL	355	DL	DL
SSA3 -St3	DL	52	DL	7	DL	548	82	DL	DL	761	DL	DL	DL	12740	DL	DL	DL	DL	DL	DL	DL	DL	DL	DL	DL	DL	11381	DL	DL
SSA3 -St4	128	425	59	DL	DL	181	53	191	35	246	1108	3433	DL	20060	DL	DL	DL	DL	22	DL	DL	DL	DL	DL	10	DL	10308	DL	DL
HA5 -St1s	261	126	DL	9	5	97	137	DL	DL	225	DL	159	DL	1952	DL	DL	DL	DL	DL	DL	DL	DL	DL	DL	DL	DL	1526	DL	DL
HA5 -St2 s	541	40	5	DL	DL	32	62	DL	DL	29	DL	231	DL	10171	DL	DL	DL	DL	DL	DL	DL	DL	DL	DL	12	DL	1188	DL	125
HA5 -St3 s	45	70	DL	7	DL	683	122	DL	DL	637	DL	DL	DL	17068	DL	DL	DL	DL	DL	DL	DL	DL	DL	DL	DL	DL	14169	DL	98
HA5-St4 s	115	418	72	DL	DL	354	90	106	41	327	1432	4227	DL	28678	DL	DL	DL	DL	20	DL	DL	DL	480	DL	13	DL	19053	DL	DL

Sequential extraction data (Part II).

	Ca	Mg	Ba	Cd	Co	Cu	Mn	Pb	Sr	Zn	K	Al	Be	Fe	Li	Mo	Ni	Sb	Ti	Tl	V	Na	As	B	Cr	P	S	Se	Si
HA3 -St1	100	67	DL	7	DL	51	93	DL	DL	DL	DL	DL	DL	1659	DL	DL	DL	DL	DL	DL	DL	DL	DL	DL	DL	DL	974	DL	DL
HA3 -St2	125	DL	DL	DL	DL	18	28	DL	DL	DL	DL	DL	DL	1454	DL	DL	DL	DL	DL	DL	DL	DL	DL	DL	DL	DL	314	DL	DL
HA3 -St3	13	DL	DL	8	5	520	55	DL	DL	660	DL	DL	DL	21528	DL	DL	DL	DL	DL	DL	DL	DL	DL	DL	DL	DL	14933	DL	DL
HA3 -St4	DL	191	30	11	DL	660	130	DL	20	513	DL	1497	DL	50923	DL	DL	DL	DL	DL	DL	DL	DL	794	DL	DL	DL	41761	DL	229
HA3 -St1 s	275	253	DL	28	13	701	294	DL	DL	1096	DL	345	DL	2084	DL	DL	DL	DL	DL	DL	DL	DL	DL	DL	DL	DL	3329	DL	DL
HA3 -St2 s	136	DL	DL	DL	DL	60	35	DL	DL	DL	DL	197	DL	13422	DL	DL	DL	DL	DL	DL	DL	DL	DL	DL	12	DL	2368	DL	97
HA3 -St3 s	DL	49	DL	6	DL	570	58	DL	DL	389	DL	137	DL	18196	DL	DL	DL	DL	DL	DL	DL	DL	DL	DL	DL	DL	18301	DL	120
HA3 -St4 s	DL	419	89	DL	DL	245	47	205	51	170	2073	5999	DL	30219	DL	DL	DL	DL	26	DL	DL	DL	639	DL	19	DL	17192	DL	DL
HA3 -St1 s	274	234	DL	26	DL	654	271	DL	DL	1026	DL	315	DL	2385	DL	DL	DL	DL	DL	DL	DL	DL	DL	DL	DL	DL	3229	DL	DL
HA3 -St2 s	116	DL	DL	4	DL	61	37	DL	DL	DL	DL	222	DL	15491	DL	DL	DL	DL	DL	DL	DL	DL	DL	DL	14	DL	2755	DL	121
HA3 -St3 s	DL	53	DL	6	DL	557	55	DL	DL	403	DL	117	DL	17184	DL	DL	DL	DL	DL	DL	DL	DL	DL	DL	DL	DL	17654	DL	106
HA3 -St4 s	DL	443	90	DL	DL	269	49	204	53	187	2129	6072	DL	30949	DL	DL	DL	DL	24	DL	DL	DL	615	DL	19	DL	19503	DL	DL
HA7 -St1	DL	70	DL	DL	DL	32	109	DL	DL	18	DL	DL	DL	1593	DL	DL	DL	DL	DL	DL	DL	DL	DL	DL	DL	DL	683	DL	DL
HA7 -St2	211	DL	DL	DL	DL	14	51	DL	DL	DL	DL	DL	DL	2179	DL	DL	DL	DL	DL	DL	DL	DL	DL	DL	DL	DL	235	DL	DL
HA7 -St3	DL	50	DL	9	7	595	105	DL	DL	744	DL	DL	DL	21020	DL	DL	DL	DL	DL	DL	DL	DL	DL	DL	DL	DL	14556	DL	DL
HA7 -St4	DL	343	46	DL	DL	445	182	DL	27	378	765	2289	DL	38700	DL	DL	DL	DL	17	DL	DL	DL	527	DL	DL	DL	28007	DL	197
SSA1 -St1	DL	68	DL	DL	DL	29	106	DL	DL	DL	DL	DL	DL	1368	DL	DL	DL	DL	DL	DL	DL	DL	DL	DL	DL	DL	671	DL	DL
SSA1 -St2	128	DL	DL	DL	DL	16	33	DL	DL	DL	DL	DL	DL	1772	DL	DL	DL	DL	DL	DL	DL	DL	DL	DL	DL	DL	324	DL	DL
SSA1 -St3	DL	45	DL	8	DL	520	87	DL	DL	666	DL	DL	DL	20288	DL	DL	DL	DL	DL	DL	DL	DL	DL	DL	DL	DL	13473	DL	DL
SSA1 -St4	DL	273	38	DL	DL	292	113	DL	21	244	614	1823	DL	30968	DL	DL	DL	DL	DL	DL	DL	DL	DL	DL	DL	DL	21312	DL	DL
SSA1 -St1 s	68	155	DL	8	6	165	162	DL	DL	207	DL	242	DL	1884	DL	DL	DL	DL	DL	DL	DL	DL	DL	DL	DL	DL	1806	DL	DL
SSA1 -St2 s	170	DL	8	DL	DL	43	50	DL	DL	DL	DL	368	DL	11943	DL	DL	DL	DL	DL	DL	DL	DL	DL	DL	20	DL	1616	DL	122
SSA1 -St3 s	DL	61	12	6	DL	718	78	DL	DL	582	DL	167	DL	14932	DL	DL	DL	DL	DL	DL	DL	DL	DL	DL	DL	DL	14151	DL	150
SSA1 -St4 s	DL	612	109	DL	DL	153	55	170	61	122	2594	7668	DL	23428	DL	DL	DL	DL	31	DL	DL	DL	DL	DL	21	DL	9543	DL	DL
SSA1 -St1 s	69	154	DL	8	6	172	160	DL	DL	199	DL	252	DL	1821	DL	DL	DL	DL	DL	DL	DL	DL	DL	DL	DL	DL	1757	DL	DL
SSA1 -St2 s	184	DL	9	DL	DL	45	53	DL	DL	DL	DL	380	DL	12201	DL	DL	DL	DL	DL	DL	DL	DL	DL	DL	20	DL	1648	DL	127
SSA1 -St3 s	DL	59	DL	6	DL	731	77	DL	DL	575	DL	151	DL	14567	DL	DL	DL	DL	DL	DL	DL	DL	DL	DL	DL	DL	14242	DL	144
SSA1 -St4 s	DL	655	112	DL	DL	148	57	174	61	124	2860	8281	DL	23450	DL	DL	DL	DL	31	DL	DL	DL	DL	DL	23	DL	9510	DL	DL

Spearman correlation matrix, in bulk values with p<0.01 (Partl)

	Al2O3	CaO	Fe2O3	K2O	MgO	MnO	P2O5	SiO2	TiO2	As	Bi	Br*	Ce	Co*	Cr	Cu	Ga	Ge*	Hf*	La*	Mn*	Mo
Al2O3	0.00																					
CaO	0.52	0.00																				
Fe2O3	-0.32	-0.04	0.00																			
K2O	**0.85**	**0.70**	-0.21	0.00																		
MgO	0.49	-0.01	-0.25	0.06	0.00																	
MnO	0.44	0.24	-0.31	0.08	**0.80**	0.00																
P2O5	0.66	0.54	**0.26**	0.78	0.11	-0.09	0.00															
SiO2	-0.28	-0.22	**-0.78**	-0.28	-0.09	0.06	**-0.70**	0.00														
TiO2	0.61	0.56	0.18	**0.70**	0.23	0.26	0.77	**-0.54**	0.00													
As	-0.25	-0.05	**0.94**	-0.13	-0.35	-0.46	0.34	**-0.79**	0.12	0.00												
Bi	-0.05	-0.37	0.50	-0.34	0.25	-0.03	0.14	-0.60	-0.15	0.58	0.00											
Br*	**0.66**	0.54	-0.26	0.56	0.38	0.64	0.23	-0.10	0.42	-0.31	-0.22	0.00										
Ce	0.65	**0.72**	0.20	**0.86**	-0.04	-0.01	**0.84**	-0.58	**0.83**	0.22	-0.13	0.44	0.00									
Co*	0.22	0.11	-0.02	-0.13	0.51	**0.71**	-0.25	-0.08	-0.01	-0.12	0.21	0.36	-0.09	0.00								
Cr	-0.52	-0.15	-0.05	-0.61	0.09	0.27	**-0.75**	0.41	-0.52	-0.24	-0.06	-0.01	-0.53	0.41	0.00							
Cu	-0.17	-0.44	0.47	-0.56	0.40	0.20	-0.16	-0.40	-0.28	0.46	**0.86**	-0.16	-0.36	0.48	0.21	0.00						
Ga	-0.23	-0.49	0.43	-0.57	0.40	0.15	-0.16	-0.35	-0.31	0.43	**0.84**	-0.25	-0.36	0.38	0.22	**0.93**	0.00					
Ge*	-0.52	-0.49	0.29	**-0.80**	0.32	0.23	-0.52	-0.02	-0.47	0.18	0.60	-0.21	-0.61	0.38	0.64	**0.77**	**0.80**	0.00				
Hf*	-0.29	-0.40	0.25	**-0.68**	0.43	0.37	-0.46	-0.07	-0.44	0.20	0.62	-0.11	-0.54	0.62	0.50	**0.89**	**0.88**	**0.87**	0.00			
La*	0.54	0.59	0.34	**0.73**	-0.15	-0.01	**0.72**	-0.66	**0.75**	0.38	-0.06	0.35	**0.86**	0.09	-0.50	-0.27	-0.31	-0.57	-0.45	0.00		
Mn*	0.31	0.24	-0.20	0.00	**0.69**	**0.93**	-0.18	0.06	0.18	-0.36	-0.04	0.54	-0.03	**0.83**	0.38	0.23	0.24	0.32	0.48	0.02	0.00	
Mo	0.05	-0.20	**0.70**	-0.04	0.04	-0.24	0.48	**-0.83**	0.22	**0.78**	**0.82**	-0.23	0.23	0.03	-0.36	0.61	0.57	0.22	0.25	0.36	-0.25	0.00
Nb	0.50	**0.74**	0.16	**0.75**	0.00	0.08	**0.73**	-0.43	**0.79**	0.14	-0.25	0.40	**0.87**	-0.05	-0.37	-0.41	-0.32	-0.47	-0.45	**0.73**	0.15	0.09
Nd*	0.64	**0.77**	0.14	**0.86**	-0.02	0.04	**0.85**	-0.53	**0.84**	0.15	-0.18	0.46	**0.96**	-0.15	-0.57	-0.41	-0.41	-0.64	-0.59	**0.80**	-0.02	0.17
Ni	0.42	0.22	-0.11	0.07	0.65	**0.80**	-0.05	-0.11	0.20	-0.23	0.10	0.45	0.06	**0.94**	0.26	0.34	0.26	0.23	0.46	0.17	**0.87**	-0.02
Pb*	0.05	0.02	0.56	0.20	-0.32	-0.61	0.60	-0.65	0.11	**0.76**	0.53	-0.30	0.35	-0.42	-0.57	0.22	0.26	-0.13	-0.09	0.36	-0.60	**0.73**
Rb	**0.87**	0.61	-0.20	**0.96**	0.13	0.08	**0.77**	-0.33	0.64	-0.08	-0.21	0.54	**0.83**	-0.07	-0.59	-0.43	-0.44	**-0.75**	-0.58	**0.72**	-0.01	0.08
Sb*	0.55	0.47	-0.11	**0.72**	-0.12	-0.18	0.70	-0.27	0.39	0.10	-0.10	0.23	0.60	-0.28	**-0.72**	-0.39	-0.31	-0.63	-0.49	0.56	-0.22	0.13
Se*	-0.25	-0.09	**0.88**	-0.11	-0.31	-0.46	0.35	**-0.73**	0.11	**0.95**	0.54	-0.32	0.20	-0.20	-0.31	0.43	0.45	0.18	0.21	0.31	-0.35	**0.72**
Sm*	0.23	0.50	0.04	0.32	0.07	0.09	0.38	-0.17	0.45	-0.06	-0.21	0.02	0.36	0.12	-0.05	-0.25	-0.37	-0.26	-0.34	0.35	0.06	0.04
Sn*	-0.46	-0.24	**0.74**	-0.56	0.00	-0.11	-0.07	-0.50	-0.18	**0.71**	**0.74**	-0.37	-0.16	0.23	0.25	**0.77**	**0.82**	**0.74**	0.70	-0.11	0.05	0.62
Sr	0.58	0.63	0.02	**0.81**	-0.18	-0.25	**0.85**	-0.41	0.56	0.18	-0.05	0.28	**0.81**	-0.36	-0.70	**-0.38**	**-0.37**	**-0.64**	**-0.59**	0.63	-0.32	0.25
Ta*	-0.30	-0.45	0.35	-0.64	0.32	0.22	-0.35	-0.16	-0.47	0.32	0.65	-0.11	-0.52	0.46	0.36	0.89	0.86	0.79	0.90	-0.42	0.28	0.40
Te*	0.16	-0.26	-0.16	0.03	0.20	-0.17	0.22	0.02	-0.05	-0.06	0.11	-0.22	-0.20	-0.32	-0.39	0.06	0.03	-0.16	-0.12	-0.24	-0.31	0.11
Th	0.42	0.24	0.60	0.37	0.16	0.05	**0.69**	**-0.88**	0.56	0.63	0.54	0.17	0.58	0.24	-0.45	0.37	0.35	-0.04	0.10	**0.68**	0.12	**0.77**
TiO2	0.41	0.63	0.34	0.60	0.07	0.18	0.66	-0.55	**0.86**	0.25	-0.17	0.40	**0.80**	0.04	-0.32	-0.27	-0.20	-0.33	-0.32	**0.74**	0.26	0.14
Tl*	-0.12	-0.40	0.50	-0.45	0.35	0.18	-0.07	-0.53	-0.16	0.47	**0.86**	-0.04	-0.20	0.46	0.19	**0.89**	**0.82**	**0.69**	**0.71**	-0.08	0.18	**0.69**
U*	0.62	0.04	0.06	0.34	0.52	0.15	0.50	-0.48	0.26	0.14	0.57	0.24	0.33	0.24	-0.26	0.44	0.37	0.09	0.20	0.20	0.09	0.53
V	**0.71**	0.56	0.22	**0.72**	0.30	0.31	**0.79**	**-0.68**	**0.84**	0.20	0.07	0.44	**0.83**	0.21	-0.52	-0.11	-0.07	-0.41	-0.26	**0.83**	0.31	0.34
W	-0.32	-0.43	0.49	-0.64	0.30	0.11	-0.21	-0.36	-0.36	0.49	**0.86**	-0.24	-0.40	0.37	0.30	**0.96**	**0.94**	**0.83**	**0.88**	-0.34	0.16	0.58
Y	0.43	0.60	0.35	0.58	0.07	0.18	0.65	-0.57	**0.83**	0.29	-0.12	0.30	**0.79**	0.15	-0.39	-0.20	-0.14	-0.36	-0.26	**0.80**	0.29	0.21
Yb*	0.26	0.12	**-0.85**	0.26	0.14	0.27	-0.17	**0.72**	0.05	**-0.87**	**-0.68**	0.16	-0.11	-0.10	-0.03	-0.62	-0.63	-0.39	-0.43	-0.22	0.18	**-0.73**
Zn	-0.27	-0.45	0.34	-0.64	0.42	0.31	-0.33	-0.22	-0.36	0.31	0.74	-0.17	-0.47	0.59	0.37	**0.91**	**0.93**	**0.86**	**0.95**	-0.33	0.42	0.43
Zr	-0.39	0.38	0.40	-0.13	-0.30	0.00	-0.07	-0.08	0.29	0.24	-0.31	0.03	0.16	0.03	0.33	-0.18	-0.21	0.14	-0.04	0.17	0.15	-0.17

Spearman correlation matrix, in bulk values with p<0.01 (PartII)

	Nb	Nd*	Ni	Pb*	Rb	Sb*	Se*	Sm*	Sn*	Sr	Ta*	Te*	Th	TiO2	Tl*	U*	V	W	Y	Yb*	Zn	Zr
Al2O3																						
CaO																						
Fe2O3																						
K2O																						
MgO																						
MnO																						
P2O5																						
SiO2																						
TiO2																						
As																						
Bi																						
Br*																						
Ce																						
Co*																						
Cr																						
Cu																						
Ga																						
Ge*																						
Hf*																						
La*																						
Mn*																						
Mo																						
Nb	0.00																					
Nd*	**0.89**	0.00																				
Ni	0.10	0.01	0.00																			
Pb*	0.24	0.33	-0.48	0.00																		
Rb	**0.67**	**0.79**	0.11	0.25	0.00																	
Sb*	0.57	0.62	-0.16	0.54	**0.68**	0.00																
Se*	0.18	0.16	-0.31	**0.80**	-0.11	0.19	0.00															
Sm*	0.37	0.40	0.25	-0.08	0.25	0.13	-0.18	0.00														
Sn*	-0.07	-0.21	0.06	0.41	-0.50	-0.29	**0.70**	-0.16	0.00													
Sr	**0.72**	**0.83**	-0.22	0.58	**0.77**	**0.85**	0.21	0.30	-0.21	0.00												
Ta*	-0.46	-0.54	0.32	0.08	-0.54	-0.38	0.31	-0.28	**0.69**	-0.45	0.00											
Te*	-0.27	-0.13	-0.18	0.16	0.10	0.11	-0.09	0.15	-0.22	0.07	0.03	0.00										
Th	0.55	0.55	0.26	0.57	0.42	0.31	0.61	0.16	0.44	0.43	0.15	-0.03	0.00									
TiO2	**0.91**	**0.81**	0.19	0.14	0.51	0.38	0.28	0.29	0.04	0.49	-0.40	-0.28	0.61	0.00								
Tl*	-0.34	-0.28	0.34	0.20	-0.30	-0.36	0.38	-0.20	**0.70**	-0.31	**0.75**	-0.02	0.42	-0.18	0.00							
U*	0.17	0.23	0.31	0.34	0.48	0.16	0.10	0.09	0.15	0.32	0.20	0.29	0.57	0.11	0.45	0.00						
V	**0.77**	**0.82**	0.39	0.23	**0.71**	0.52	0.19	0.30	-0.04	0.57	-0.29	-0.09	**0.74**	**0.83**	0.04	0.38	0.00					
W	-0.41	-0.44	0.20	0.25	-0.50	-0.43	0.46	-0.32	**0.85**	-0.40	**0.86**	0.01	0.30	-0.28	**0.88**	0.34	-0.18	0.00				
Y	**0.88**	**0.78**	0.28	0.20	0.52	0.42	0.32	0.33	0.08	0.49	-0.35	-0.28	**0.68**	**0.96**	-0.15	0.12	**0.87**	-0.24	0.00			
Yb*	-0.02	-0.03	0.05	-0.63	0.16	0.01	**-0.81**	0.17	**-0.79**	-0.04	-0.53	0.15	-0.53	-0.12	**-0.69**	-0.21	-0.15	**-0.68**	-0.15	0.00		
Zn	-0.38	-0.52	0.44	0.06	-0.54	-0.36	0.32	-0.27	**0.77**	-0.49	**0.89**	-0.11	0.24	-0.26	**0.80**	0.25	-0.14	**0.89**	-0.17	-0.53	0.00	
Zr	0.37	0.16	0.00	-0.19	-0.26	-0.23	0.21	0.27	0.26	-0.09	-0.17	-0.44	0.03	0.52	-0.18	-0.43	0.04	-0.10	0.43	-0.11	-0.09	0.00